

**Synthesis and Properties of New Luminescent
Iridium and Platinum Complexes**

**Thesis Submitted for the Degree of
Doctor of Philosophy**

By

Noreldin S. Y. Abdolla

at the University of Leicester

Chemistry Department

June 2018

Title: Synthesis and Properties of New Luminescent Iridium and Platinum Complexes

Author: Noreldin Abdolla

ABSTRACT

A range of luminescent Ir(III) complexes $[\text{Ir}(\text{C}^{\wedge}\text{N})_2(\text{N}^{\wedge}\text{N})]^{n+}$ ($n = 0, 1$) and Pt(II) complexes $[\text{Pt}(\text{C}^{\wedge}\text{N})(\text{N}^{\wedge}\text{N})]^+$ and $[\text{Pt}(\text{C}^{\wedge}\text{N})(\text{O}^{\wedge}\text{O})]$ containing different cyclometallated ($\text{C}^{\wedge}\text{N}$) and ancillary ($\text{X}^{\wedge}\text{Y}$) ligands has been synthesised. All new compounds were fully characterised by ^1H and ^{13}C NMR spectroscopy, mass spectrometry and most compounds were structurally characterised by X-ray crystallography.

Chapter one provides an introduction to luminescent transition metal complexes, in particular Ru(II) and Ir(III) and Pt(II) complexes and gives an overview of the factors controlling the emission wavelengths of cyclometallated Ru(II) and Ir(III) and Pt(II) complexes and their applications, particularly as sensors and probes. Chapter two discusses the synthesis and properties of $[\text{Ir}(\text{C}^{\wedge}\text{N})_2(\text{N}^{\wedge}\text{N})]^{n+}$ ($n = 0, 1$) and shows that that pH responsive Ir(III) bis cyclometallated complexes can be designed to have a $\text{p}K_{\text{a}}$ in the range which is relevant for biological imaging. Chapter three covers the synthesis and characterisation of cationic Ir(III) complexes $[\text{Ir}(\text{ppz})_2(\text{N}^{\wedge}\text{N})][\text{PF}_6]$ ($\text{N}^{\wedge}\text{N}$ = bidentate PYE ligands) an investigation of the donor properties and resonance structures of the ligands and on photophysical properties of the ligands and complexes. The study shows that there was no clear evidence from NMR spectroscopy that more polar solvents lead to an increase in the zwitterionic resonance structure for the complexed PYE ligands. In Chapter four the synthesis and characterisation of cyclometallated Pt(II) complexes $[\text{Pt}(\text{C}^{\wedge}\text{N})(\text{X}^{\wedge}\text{Y})]^{n+}$ ($n = 0, 1$) with extra substituents that are free to rotate in solution to show EPESS activity is discussed. Chapter five describes the synthetic methodology and characterisation of a series of ligand and complexes.

Acknowledgements

First of all, I would like to thank my supervisor Prof. **David L. Davies** for giving me the opportunity to carry out this project in his group and in helping, advising and supporting me when needed. Without his guidance and extreme patience, I would never have been able to complete this first hurdle.

Thanks to Higher Education Commission of **Libya** for providing me financial assistance in the form of Doctoral Scholarship and to the Chemistry Department of The University of **Omar Al-Mukhtar** for providing me research resources.

I am truly indebted and thankful to Dr **Barbara Villa-Marcos** and Dr **Charles Ellul** for their advice and support. Their kindness and understanding made this project a pleasant experience.

I would like to thank all the people who have been involved in this project, Dr. **Mark P. Lowe** for the use of the fluorimeter, Dr. **G. A. Griffith** for the NMR spectra and Mr **K. Singh** for the X-ray structure determinations and Mr **Mick Lee** for the mass spectra analysis.

A special thanks to Mrs **Raissa Patia** and, **Neringa Tamosiunaite** for her friendship and assistance in the preparation of this report, without her help, understanding and excellent salads I never would have been able to finish.

I am thankful to all my lab colleagues who have helped make my learning experience an enjoyable and stimulating one, especially to **Raid, Adil** and **Vicki**

Lastly, this PhD was the dream of my late father. I will never forget his support and encouragement that came from him. It is because of his faith in me that I thank him. I am obliged to my family members who supported me throughout my academic journey. My Mum and wife for being a great strength and allowed to me carry on with my studies even after our struggles and my sisters and brothers for being a great support. Many apologies to my sweet kids **Al-Batool, Aoun** and **Saada** for not spending enough time due to my study.

Statement

This thesis is based on work conducted by the author, in the Department of Chemistry of the University of Leicester, during the period between September 2014 and June 2018. Except where specific reference has been made to other sources, the work in this thesis is the original work of the author. It has not been submitted for any other degree and The results have not been published yet.

Signed: _____ Date: _____

Noreldin S. Y. Abdolla

Abbreviations:

NMR			
bd	Broad Doublet	td	Triplet Of Doublets
bs	Broad Singlet	tt	Riplet Of Triplets
d	Doublet	COSY	Correlated Spectroscopy
dd	Doublet Of Doublets	HMBC	Heteronuclear Multiple Bond Coherence
ddd	Doublet Of Doublet Of Doublets	HSQC	Heteronuclear Single Quantum Correlation
dt	Doublet Of Triplets	NMR	Nuclear Magnetic Resonance
m	Multiplet	NOE	Nuclear Overhauser Effect
q	Quartet	NOESY	Nuclear Overhauser effect Spectroscopy
qd	Quartet of doublets	TOCSY	Total Correlation Spectroscopy
s	Singlet	ppm	Parts Per Million
t	Triplet	δ	Delta (NMR Chemical Shift)
Other Techniques			
ASAP	Atmospheric solids analysis probe (Mass Spectrometry)		
ES-MS	Electrospray mass spectrometry		
FAB-MS	Fast atom bombardment mass spectrometry		
IR	Infrared		
HRMS	High resolution mass spectrometry		
MW	Microwave		
Others			
DFT	density functional theory	sh	Shoulder
HOMO	Highest Occupied Molecular Orbital	($^{\circ}$)	Bond Angle
LC	Ligand Centred	Å	Angstrom
LECs	Light-Emitting Electrochemical Cells	λ	Wavelength (nm)
LLCT	Ligand To Ligand Charge Transfer	LUMO	Lowest Unoccupied Molecular Orbital

MC	Metal Centred	MP	Melting Point
mg	Mailgram	nm	Nanometre
min	Minute	OLED	Organic Light Emitting Diode
ml	Millilitre	pK _a	Acid dissociation constant
MLCT	Metal To Ligand Charge Transfer	H.B	Hydrogen bonds
MLLCT	Metal Ligand To Ligand Charge Transfer	sh	Shoulder
MO	Molecular Orbital		
Chemical			
DCM	Dichloromethane	Phen	1,10-Phenanthroline
DMF	Dimethylformamide	bpy	2,2'-Bipyridyl
DMSO	Dimethyl sulfoxide	ppy	2-Phenylpyridine
dpm	Dipivolylmethanoate	ppz	1-Phenylpyrazole
EtOH	Ethanol	PrOH	Propan-2-ol
Et ₂ O	Diethyl ether	PYE	pyridylideneamine
en	ethylenediamine	tBu	t-butyl
MeCN	Acetonitrile		
MeOH	Methanol		
Ph	Phenyle		

List of contents

Chapter 1 General Introduction	1
1.1 Luminescence	2
1.2 Luminescent transition metal complexes	3
1.2.1 Luminescence properties of Ru(II) complexes	5
1.2.2 Luminescence properties of Ir(III) complexes	7
1.2.2.1 Tuning of luminescent wavelength by variation of X ^Y ligands	10
1.2.2.2 Tuning of luminescent wavelength by variation of C ^N ligands	12
1.2.2.3 Effect of conjugation	14
1.2.2.4 Tuning of emission by varying substituents	15
1.2.3 Luminescence properties of Pt(II) complexes.	17
1.2.3.1 Pt complexes with bidentate ligands.	19
1.2.3.2 Pt complexes with tri-dentate cyclometallated ligands	20
1.3 Applications of luminescent metal complexes	21
1.3.1 Transition Metal Complexes in Displays, OLEDs/LECS.	22
1.3.2 Transition Metal complexes as Photocatalysts and Photoredox Catalysis.	24
1.3.3 Transition Metal complexes as sensors.	25
1.3.4 Transition Metal complexes for bioimaging applications	29
1.4 Aims of the Project	32
Bibliography	33
Chapter 2 Synthesis and characterisation of cyclometallated Ir(III) complexes [Ir(C^NN)₂(N^NN)]^{m+} (N^NN = 2 pyrazolylpyridine; n = 0, 1) for use as pH sensors	43
2.1 Introduction	44
2.2 Results and Discussion	51
2.2.1 Synthesis of N ^N Ligands	51
2.2.2 Synthesis of C ^N Ligands	51
2.2.3 Synthesis of cyclometallated Ir(III) dichloro-bridged dimers	52

2.2.4	Synthesis and Characterisation of Cationic Phenylpyrazole Iridium(III) Complexes	53
2.2.5	Synthesis and Characterisation of Neutral Phenylpyrazole Iridium(III) Complexes	58
2.2.6	Synthesis and Characterisation of Cationic Phenylpyridine Iridium(III) Complexes.	63
2.2.7	Synthesis and Characterisation of Neutral Phenylpyridine Iridium(III) Complexes.	66
2.3	Photophysical properties	70
2.3.1	Photophysical properties of Phenylpyrazole Ir(III) Complexes (2.16aHL ₁₋₃ , 2.17aL ₁₋₃ and 2.17bL ₁₋₃).	71
2.3.2	Photophysical properties of Phenylpyridine Ir(III) Complexes (2.16cHL ₁₋₃ , 2.17cL ₁₋₃ and 2.17dL ₂).	75
2.4	pH Titration Studies	78
2.4.1	pH Titrations of Phenylpyrazole Ir(III) Complexes 2.17aL ₁₋₃ .	79
2.4.2	pH Titrations of Phenylpyridine Ir(III) Complexes 2.17cL ₁₋₃ .	82
2.4.3	pH Titrations of CF ₃ Phenylpyrazole Ir(III) Complex 2.17bL ₁₋₃	85
2.4.4	pH Titrations of CF ₃ Phenylpyridine Ir(III) Complex 2.17dL ₂	87
2.5	Conclusion and future work	88
	Bibliography	91
	Chapter 3 Synthesis and Characterisation of Ir(III) pyridylideneamine (PYE) Complexes [Ir(C[^]N)₂(PYE)][PF₆]	94
3.1	Introduction	95
3.2	Results and Discussion	104
3.2.1	Synthesis of [<i>p</i> -H _n PYE ₁₋₃] I _n (n = 1, 2).	104
3.2.2	Synthesis of <i>o</i> -PYE ligands	107
3.2.3	Attempts to synthesise <i>m</i> -PYE ligands	111
3.2.4	Synthesis and characterisation of <i>para</i> -PYE Ir(III) complexes	111
3.2.5	Synthesis and characterisation of <i>ortho</i> -PYE Ir(III) complexes	118
3.3	Photophysical properties	124
3.3.1	Photophysical properties of [<i>p</i> -H ₂ PYE ₁] I ₂ , [<i>p</i> -H ₂ PYE ₂] I ₂ and [<i>p</i> -HPYE ₃] I	124
3.3.2	Photophysical properties of ligands <i>o</i> -PYE ₁ , <i>o</i> -PYE ₂ and <i>o</i> -PYE ₃	125
3.3.3	Photophysical properties of complexes <i>p</i> -3.30, <i>p</i> -3.31 and <i>p</i> -3.32	127

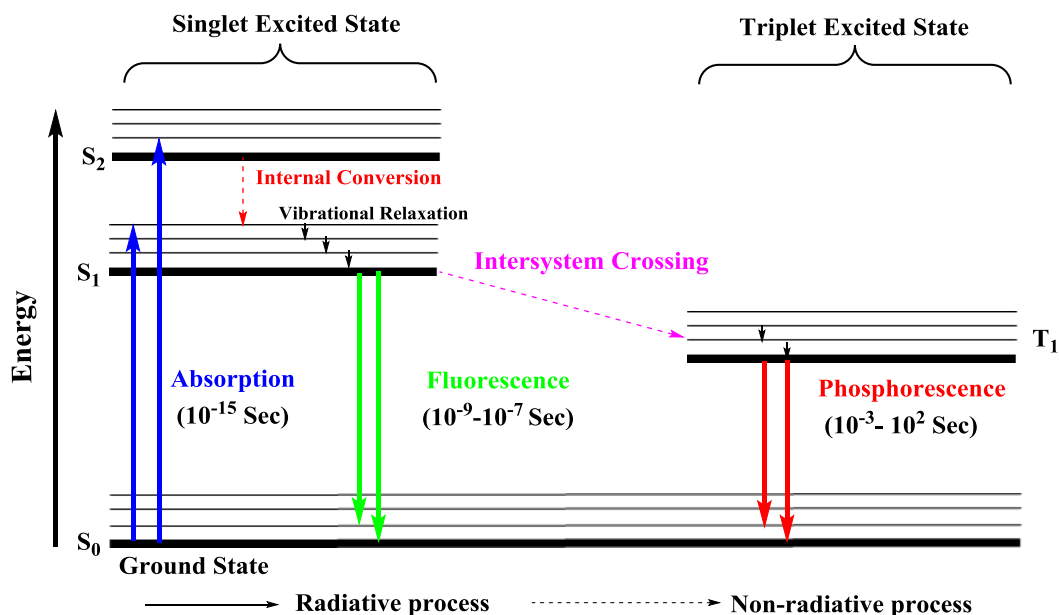
3.3.4	Photophysical properties of complexes <i>o</i>-3.30, <i>o</i>-3.31 and <i>o</i>-3.32	129
3.4	Conclusion and future work	130
	Bibliography	132
Chapter 4	Enhanced Phosphorescence Emission in the Solid State (EPESS) of cyclometalated Pt(II) Complexes	133
4.1	Introduction	134
4.1.1	Aggregation-induced Emission	134
4.1.2	Aggregation-induced Emission in Transition Metal complexes	135
4.2	Results and Discussion	139
4.2.1	Synthesis of C ^N ligands	139
4.2.2	Synthesis of Pt(II)- μ -dichloro-bridged dimers	140
4.2.3	Synthesis and characterisation of [Pt(C ^N)(en)]PF ₆ complexes	143
4.2.4	Synthesis and characterisation of [Pt(C ^N)(dpm)] complexes	145
4.3	Photophysical properties	147
4.3.1	Photophysical properties of cationic Pt complexes 4.16a-c and 4.17a-b	147
4.3.2	Photophysical properties of neutral Pt complexes 4.18a-c and 2.19a-b	150
4.4	Conclusions and future work	154
	Bibliography	156
Chapter 5	Experimental.	157
	Bibliography	192
	Appendix	194

Chapter One
General Introduction

1. Introduction:

1.1. Luminescence:

When a molecule absorbs energy in the form of electromagnetic radiation, an electron is excited to a higher energy level (S_1 or S_2), it can return to the ground state (S_0) by a number of routes with emission of light. This process is known as luminescence and a typical Jablonski diagram (Scheme 1.1) can be used to explain this phenomenon.^{1,2}



Scheme 1.1: Jablonski energy diagram.³

Fluorescence is observed when the electron decays immediately from the first excited state S_1 to the ground state S_0 . An electron in S_1 is paired anti-parallel with the electron in S_0 thus this transition is spin allowed and therefore the emission of a photon is very fast, in the region between 10^{-9} - 10^{-7} sec. Generally, emission from most organic molecules occurs from singlet excited states. On the other hand, phosphorescence is emission from a triplet excited state and unlike fluorescence, it does not occur immediately after the absorption of radiation. Phosphorescence occurs when the electron in the excited state S_1 undergoes a spin conversion and jumps to a forbidden triplet excited state T_1 (intersystem crossing) then the emission from the excited triplet state occurs with lower energy (longer wavelength) relative to fluorescence. It is a forbidden transition hence the time scale is longer as compared to fluorescence (10^{-3} - 10^2 sec for organic molecules). Additionally, non-radiative processes can occur (Scheme 1.1) which include:

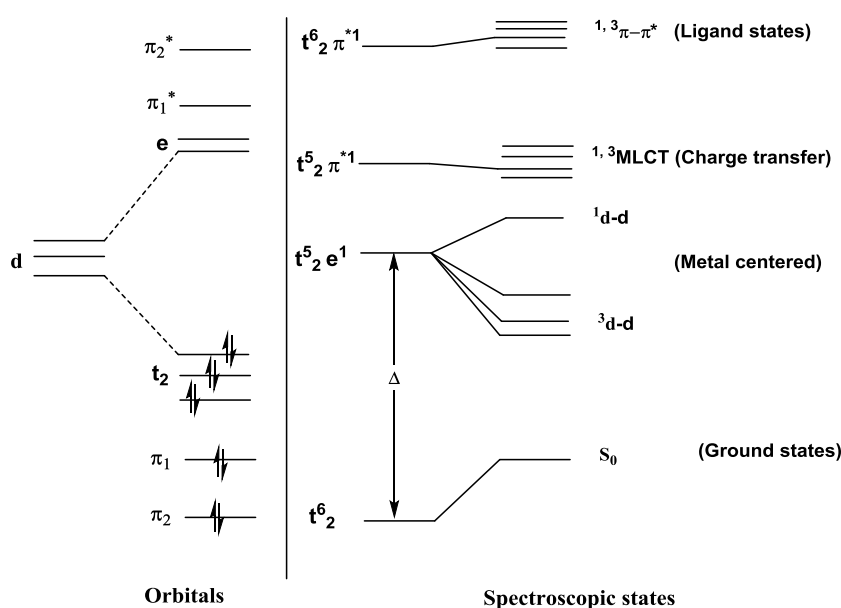
- 1- **Internal Conversion (IC):** an intramolecular process in which a molecule goes to a lower energy electronic state without emission of radiation. If vibrational energy levels strongly overlap electronic energy levels, a possibility exists that the excited

molecule can transition from a vibrational level in one electronic state to another vibrational level in a lower electronic state. This process is a result of the overlap of vibrational and electronic energy states.

- 2- **Vibrational Relaxation (VR)**: typically can occur if excess vibrational energy is lost due to collisions between excited state molecules and solvent molecules. This process can be extremely rapid thus, it is likely to happen immediately after absorption leaving the molecule in the lowest vibrational level of S_1 . In general, this relaxation occurs through vibrational levels so, the movement of electrons from one electronic level to another will not occur through this process.
- 3- **Intersystem Crossing (ISC)**: this occurs when the spin of the excited electron changes direction and the spin multiplicity changes from an excited singlet state to an excited triplet state and it is a forbidden transition.

1.2 Luminescent transition metal complexes

The luminescence of d^6 transition metal complexes, is best understood through consideration of the molecular orbitals involved. Scheme 1.2 shows the molecular orbitals and spectroscopic states diagram for a low spin d^6 octahedral complex (ML_6).⁴⁻⁷ In an octahedral crystal field, there are six ligands attached to the transition metal and the d-orbitals divide into two different levels. The triply degenerate t_{2g} level with lower energy and a doubly degenerate e_g^* level with higher energy and both the field strength of the ligands and the nature of the metal ion and its oxidation state affect the magnitude of the splitting (Δ).^{5, 6}



Scheme 1.2: Simplified molecular orbital and state diagrams for a d^6 metal in an octahedral environment.⁵

The ground state configuration is t_{2g}^6 and so all spins are paired thus the ground state has singlet character. The lowest excited states are attained by raising an electron to one of the unoccupied orbitals. In principle, the excited states are divided into three types.⁵⁻⁷

- (i) Metal centred (MC) d-d excited states arise from promoting a bonding electron from the t_{2g} level to the e_g^* level and give rise to weak absorption bands and therefore have small extinction coefficients. The d-d emission is characterised by long radiative lifetimes and negligible quantum yields.
- (ii) Ligand centred (LC) $\pi-\pi^*$ states derive from promoting a bonding π -electron to an antibonding π^* level. These transitions are highly intense and are localised on the ligands.
- (iii) Metal-to-ligand-charge transfer (MLCT) states involves promoting an electron from a metal orbital to a ligand orbital (e.g. π^*) or ligand to metal charge transfer (LMCT) which involves promoting an electron from a ligand to a metal orbital. These transitions have significant absorptions in the visible with high extinction coefficients.

There are some essential criteria for a metal complex to be luminescent. To avoid photochemical instability which is related with unstable d-d excited states, the lowest excited state must be either ligand $\pi-\pi^*$ or a charge transfer (CT). Spin-orbit coupling should be high to enhance the emission to be more allowed and permit radiative decay to compete more effectively with non-radiative decay. Furthermore, the crystal field should be strong enough to raise the d-d state above the MLCT state, to avoid their thermal population.

Over the last decade there has been a rapid increase in papers regarding luminescent metal complexes, for example, Re(I), Ru(II), Pt(II) and Ir(III) complexes.⁸⁻¹¹ These second and third row transition metal ions have ideal characteristics for luminescence. For instance, they have high photoluminescence quantum yields, high spin-orbit coupling, good stability and the emission wavelength can be tuned by synthetic modifications¹²⁻¹⁴ and often have a considerable Stokes shift.^{15, 16} Due to their ideal characteristics, second and third row transition metal complexes are attractive for use in several applications, such as, dye sensitised solar cells (DSSCs),¹⁷⁻¹⁹ electroluminescent devices,²⁰⁻²² cell imaging,^{8, 23, 24} emissive dopants in organic light emitting devices,^{25, 26} sensors^{4, 27-30} and in photocatalysis.³¹⁻³³ Certain of these applications will be discussed in more detail in Section 1.3.

In the next section a general overview of the luminescence properties of Ru(II), Ir(III) and Pt(II) complexes is given, with some selected examples, especially tuning their photophysical properties by modification of the ligands and/or by the effect of changing substituents on the ligands.

1.2.1 Luminescence properties of Ru(II) complexes

Ru(II) complexes have a low spin d^6 electronic structure and usually form octahedral complexes. $[\text{Ru}(\text{bpy})_3]^{2+}$ (**1.1**) and its derivatives are the most widely studied luminescent ruthenium complexes,³⁴⁻³⁷ indeed they are some of the most widely studied luminescent metal complexes due to their straightforward synthesis and interesting photophysical properties.

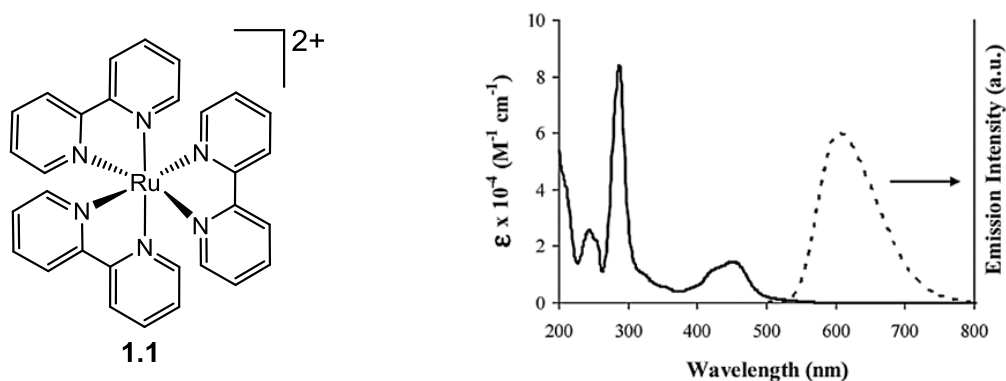


Figure 1.1: Absorption and emission for $[\text{Ru}(\text{bpy})_3]^{2+}$.³⁸

The main absorption band of complex **1.1** between 270 and 300 nm has been assigned to ligand-centred ($\pi \rightarrow \pi^*$) transitions, while the band at 450 nm is assigned to $^1\text{MLCT}$ ($d \rightarrow \pi^*$) transitions (**Fig 1.1**).^{38,39} The excitation of the complex in any of the absorption bands in solution results in a luminescence emission centred around 620 nm at room temperature with typical quantum yields in deaerated solutions in the order of 0.062 and a lifetime of 860 ns. The lowest emitting state is usually considered to be a $^3\text{MLCT}$ level transition.⁴⁰

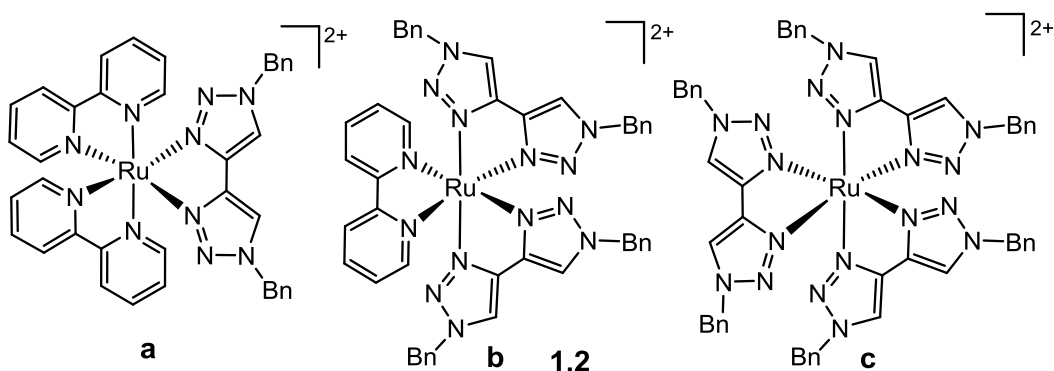


Figure 1.2: Structure of the Ru(II) complexes showing the effect of changing the ligands.

The luminescence properties of Ru(II) complexes can be tuned to some extent by altering the ligands (**Fig. 1.2**). Complexes **1.2a-c** show how changing the ligands changes the energy levels and hence the absorption and emission.⁴¹ There is a blue-shift in ¹MLCT absorption bands as the number of triazole ligands increases. Complexes **1.2a-b** exhibit MLCT absorption bands at 446 and 425 nm respectively showing a progressive blue-shift in the absorption on increasing the btz (4,4'-bi-1,2,3-triazolyl) ligand content when compared to [Ru(bpy)₃]Cl₂ which has an absorption band at 455 nm. Complex **1.2c** exhibits a heavily blue-shifted absorption spectrum (λ_{abs} 300 nm) with respect to those of [Ru(bpy)₃]Cl₂ and **1.2a-b**, indicating that the LUMO of the latter are bpy-centred with little or no btz contribution whereas that of **1.2c** is necessarily btz-centred. The final replacement of bpy by btz in **1.2c** reflecting the higher energy (~ 1 eV) of the (btz) LUMO compared to that of bpy. DFT studies on this series suggest that whilst the T₁ states of **1.2a** and **1.2b** are of ³MLCT character, the lowest energy triplet state of **1.2c** is ³MC in nature. As a result for **1.2c** thermal population of the ³MC state quenches emission and promotes photochemical ligand ejection.⁴¹

The addition of substituents to ligands can also alter the photophysical properties (**Fig. 1.3**). Thus, Ru(II) complexes **1.3a-c** containing covalently attached arenes were described by Mau *et al.*⁴² The group used three different aryl units for the purpose of tuning the energy level of their lowest lying triplet state. They found that, the photophysics of the bichromophoric system is completely dictated by the relative energy of the lowest aromatic triplet state with respect to the ³MLCT state of the metal complex. The study demonstrated that the energy transfer to the ruthenium trisbipyridine unit occurs only when the aryl triplet state lies at a higher energy, compared with the emitting ³MLCT state. Whilst, the ³MLCT emission was completely quenched when the aryl triplet state lies below the ³MLCT state. However, when the aryl triplet and the ³MLCT states are isoenergetic, establishment of a rapid equilibrium between the two states produces a long-lived emission which is the same as the ³MLCT emission from the unsubstituted metal complex.

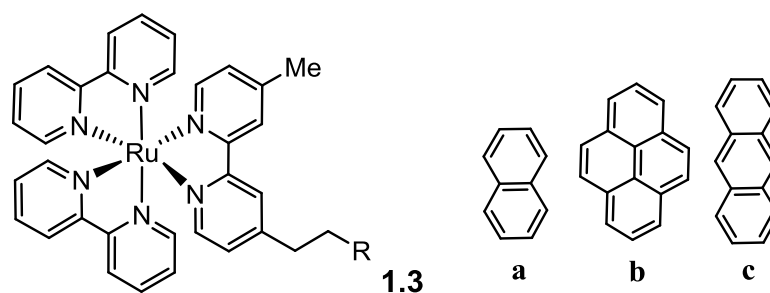


Figure 1.3: Structure of the Ru(II) complexes showing the effect of changing the substituents on the N^N ligand.

1.2.2 Luminescence properties of Ir(III) complexes

The luminescent complex *fac*-Ir(ppy)₃ (1.4) was first reported by Watts and co-workers in 1985,⁴³ however it was the publications of Thompson *et al.*,^{44, 45} that showed their applications in OLEDs and led to a surge in interest in luminescent iridium(III) complexes since then. There are three main types of luminescent cyclometalated Ir(III) complexes with bidentate ligands reported in the literature; homoleptic [Ir(C^N)₃], and heteroleptic [Ir(C^N)₂(X^Y)]ⁿ⁺ and [Ir(C^N)(X^Y)₂]ⁿ⁺ all of which have attractive photophysical and photochemical properties. The spin-orbit coupling in Ir(III) complexes allows mixing of singlet and triplet excited states removing the spin-forbidden nature of the phosphorescent transitions so they often show intense phosphorescence at room temperature with emission quantum yields close to unity in deaerated solutions. The excited states of the complexes are often a combination of singlet and triplet states so emission lifetimes vary from hundreds of nanoseconds to several microseconds.^{5, 9, 15}

Complexes [Ir(C^N)₃] can exist as two different geometrical isomers facial (*fac*) and meridional (*mer*) as shown in **Fig. 1.4**. The two isomers show considerable differences in photophysical properties. In particular, the *mer* excited state can give rise to an efficient bond breaking process, and isomerisation to the *fac* form.⁴⁶

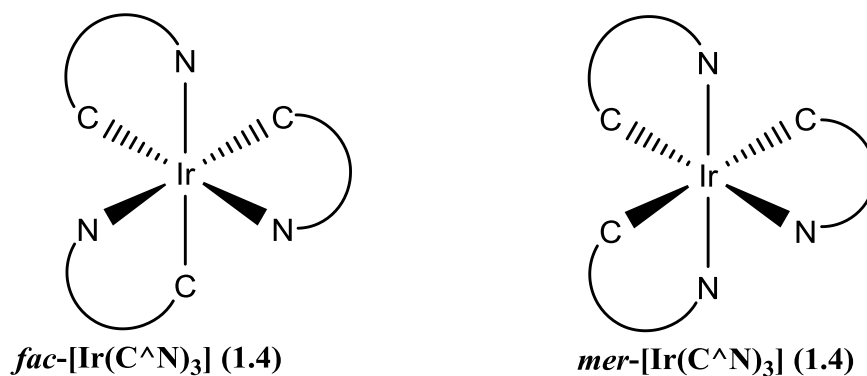


Figure 1.4: Facial (*fac*) and meridional (*mer*) isomers of Ir(C^N)₃.

Complexes with general formal $[\text{Ir}(\text{C}^{\wedge}\text{N})_2(\text{X}^{\wedge}\text{Y})]^{n+}$ ($n = 0, 1$) usually have *cis* carbon atoms and *trans* nitrogen atoms of the cyclometallated ligands^{47, 48, 49} (as in *mer*- $[\text{Ir}(\text{C}^{\wedge}\text{N})_3]$) and are commonly a racemic mixture (**Fig. 1.5**). Note throughout the thesis only one enantiomer will be drawn however in all cases the complexes are racemates

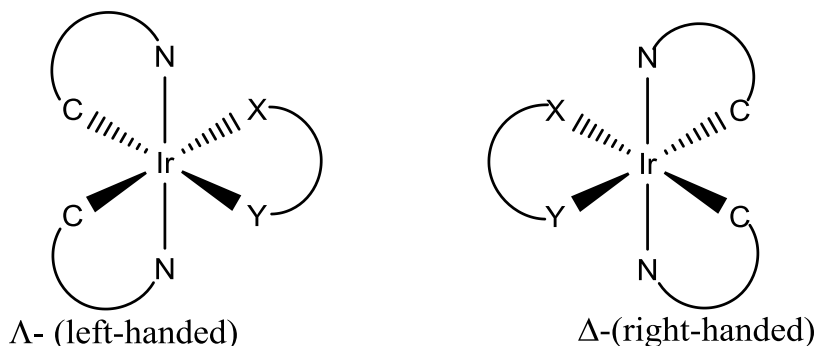


Figure 1.5: Left and right-handed enantiomers of $[\text{Ir}(\text{C}^{\wedge}\text{N})_2(\text{X}^{\wedge}\text{Y})]$.

As mentioned earlier $[\text{Ir}(\text{ppy})_3]$ exists as two isomers, *fac* and *mer*, which have different photophysical properties.⁴⁶ The photophysical properties of the *fac* isomer **1.4** (**Fig. 1.6**) have been extensively studied by several groups.^{43, 46, 49, 50} The π - π^* absorption (^1LC band) falls in the range 250–320 nm, whilst the band between 320–420 nm has been assigned to $^1\text{MLCT}$ transitions⁵⁰ and the weak shoulders between ca. 420 and 500 nm to spin forbidden $^3\text{MLCT}$ transitions. The $^3\text{MLCT}$ transitions become partly allowed because of the large spin-orbit coupling induced by the Ir(III) center.^{51–52} At room temperature complex *fac*- $[\text{Ir}(\text{C}^{\wedge}\text{N})_3]$ **1.4** showed emission centred at ~ 520 nm, with a quantum yield of 0.4 and lifetime of 1.9 μs in degassed DCM at room temperature. The emissive state is considered to be a mixture of ^3LC and $^3\text{MLCT}$ levels.^{46, 53, 54} In contrast, the quantum yield 0.036 and emission lifetime 0.15 μs of the *mer* isomer are significantly lower. This large difference between the two isomers has been explained by an efficient bond breaking process for the *mer* excited state, acting as an effective quenching pathway and giving subsequent isomerisation to the *fac* form.⁴⁶

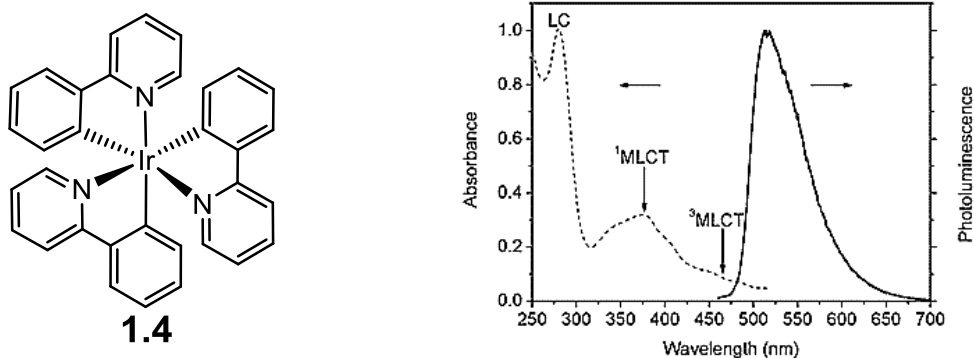


Figure 1.6: Absorption and emission spectra for *fac* $\text{Ir}(\text{ppy})_3$.⁵¹

The luminescent property of both *fac* and *mer* isomers of some complexes have been reported (Fig. 1.7, Table 1.1).^{46, 54} Adding electron-donating or electron withdrawing substituents on the C[^]N ligands can tune the emission wavelength. In general emission λ_{max} of the *mer* complexes are red-shifted compared to the *fac* complexes.^{46, 54}

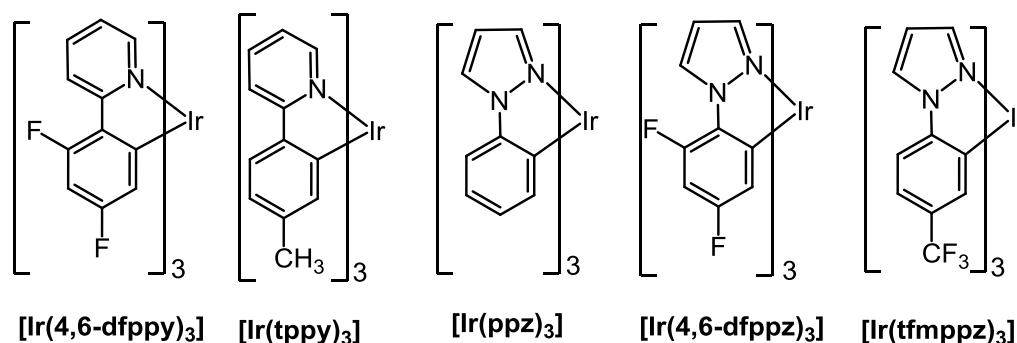


Figure 1.7: *Mer* and *fac* isomers of Ir(C[^]N)₃ with different cyclometalating ligands and different substituents.⁴⁶

Table 1.1. Photophysical Properties of Ir(C[^]N)₃ Complexes.⁴⁶

Ir(C [^] N) ₃ Complexes		Emission at 77 K	Emission at 298 K
[Ir(4,6-dfppy)₃]	<i>fac</i>	450	468
	<i>mer</i>	460	482
[Ir(tppy)₃]	<i>fac</i>	492	510
	<i>mer</i>	530	550
[Ir(ppz)₃]	<i>fac</i>	414	-
	<i>mer</i>	427	-
[Ir(4,6-dfppz)₃]	<i>fac</i>	390	-
	<i>mer</i>	402	-
[Ir(tfmppz)₃]	<i>fac</i>	422	428
	<i>mer</i>	430	-

Several different bidentate (X[^]Y) ligands and cyclometalated (C[^]N) ligands have been utilized for the synthesis of heteroleptic complexes [Ir(C[^]N)₂(X[^]Y)]ⁿ⁺ (n = 0, 1). Use of anionic X[^]Y ligands gives neutral complexes which can often be sublimed under vacuum and are miscible in organic materials which make them suitable for the fabrication of OLEDs using direct vacuum deposition.^{55, 56} Alternatively neutral X[^]Y ligands give

cationic complexes which makes them suitable for different applications. For instance, cationic iridium(III) complexes are more suitable for use as LECs, in which they require an excess of mobile ions in the emissive layer.^{49, 57, 58}

In general, for cationic complexes with X⁺Y is a bpy type ligand the HOMO is located on the iridium atom and on the phenyl part of the cyclometallating C⁺N ligands, whereas the LUMO is usually centered on the bpy ligand e.g. (N⁺N) (**Fig.1.8**).^{26, 59, 60} For neutral complexes the situation is rather more complicated and the HOMO and LUMO can be located in different parts of the complex depending on the actual ligands involved. To blue shift the emission, requires an increase in the band gap between the HOMO and LUMO, which means either that the HOMO needs to be stabilized, (i.e. lower energy), and/or the LUMO needs to be destabilized (increased energy) whilst the opposite is true for a red-shift. The use of different ligands can allow the emission of the complexes to be tuned over the whole visible spectrum from blue to red and even infrared and selected examples are discussed in the next sections.^{59, 61-65}

Stabilization of the HOMO, can be achieved by attaching electron-withdrawing substituents such as F or CF₃ on the phenyl part of the cyclometallated ligands. Whilst, destabilization of the LUMO, needs electron-donating substituents such as N(CH₃)₂ to be attached to the ancillary ligand. Both strategies have been widely used to increase the HOMO-LUMO band gap to give rise to a blue emission.^{60, 65-72}

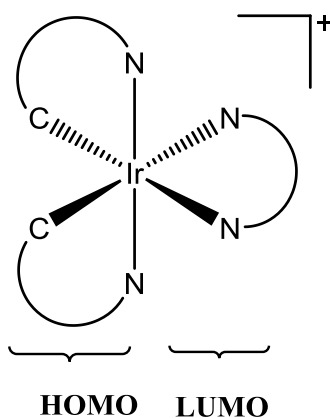


Figure 1.8: Location of the HOMO and LUMO in cationic $[\text{Ir}(\text{C}^+\text{N})_2(\text{X}^+\text{Y})]^+$ (N⁺N = bpy or related ligand).

1.2.2.1 Tuning of luminescent wavelength by variation of X⁺Y ligands

The effect of changing the X⁺Y ligand on the emission wavelength and electrochemical properties can be illustrated by complexes **1.5a-g** (**Fig. 1.9**). The oxidation potentials (**Table 1.2**) range from 0.85 to 1.19 V for the neutral complexes and between 1.25 and

1.45 V for the cationic ones, giving a full range of *ca.* 0.6 V with the cationic complexes being harder to oxidise as expected. The oxidation is mainly metal based, Ir^{III}→Ir^{IV} with some contribution from the Ir-C σ -bond consistent with the localisation of the HOMO as determined by DFT calculations. In comparison the reduction potentials span a wider range of 0.9 V from -1.42 to -2.28 V. The wider range reflects the fact that the reduction can be on the C^N ligand or on the X^Y ligand in some cases. The easiest complex to reduce is the cationic complex [Ir(ppy)₂(bpy)]⁺ **1.5a** and reduction occurs on the bpy. DFT calculations confirm that the LUMO is mainly on the diimine and partly on the pyridyl ring of the C^N ligand (ppy).

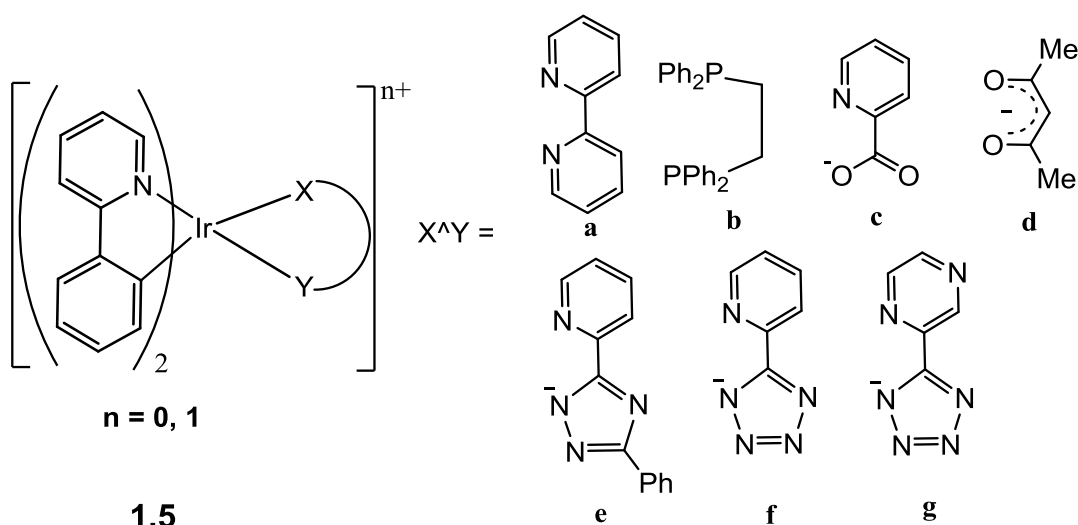


Figure 1.9: Selected examples of Ir(III) complexes with different X^Y ligands.

Table 1.2: Emission wavelength and redox properties of [Ir(C^N)₂(X^Y)]ⁿ (n = 0, +1).

Entry	complex	λ_{em} (nm)	$E^{1/2}_{ox}$	$E^{1/2}_{red}$	$\Delta E^{1/2}$	References
1	[1.5a] ⁺	580	1.25	-1.42	2.67	73-75
2	[1.5b] ⁺	458	1.45	-2.04	3.49	76
3	1.5c	505	0.99	-1.94	2.93	73, 77
4	1.5d	516	0.85	-2.10	2.95	73, 78
5	1.5e	489, 517	1.06	-2.11	3.17	79
6	1.5f	418, 510	1.13	-2.00	3.13	80
7	1.5g	601	1.19	-1.47, -2.28	2.66, 3.47	80

^aThe potentials are given vs SCE. ^b* - C^N ligand has a methyl substituent on the phenyl ring *para* to the pyridine.

Substituting the conjugated bipy in **1.5a** with a saturated diphosphine ligand (dppe) in **1.5b** has more effect on the LUMO hence affects the reduction potential (change of 0.62 V) more than the oxidation potential (change of 0.20 V) (**Table 1.2**, entries **1**, **2**). Hence, in $[\text{Ir}(\text{ppy})_2(\text{dppe})]^+$, the LUMO resides mainly on the pyridyl rings of the C^N ligands. Moreover, the higher HOMO-LUMO gap for **1.5b** is consistent with the observed blue shift of emission.

The neutral complexes (**1.5c-f**) have a larger $\Delta E^{1/2}$ than cationic complex **1.5a** mainly due to a more negative reduction, *i.e.* raised LUMO (**Table 1.2**, entries **1**, **3-6**), which leads to a blue shift in emission. Substituting the pyridine ring of the X^Y ligand in **1.5f** with a pyrazine ring in **1.5g** (**Table 1.2**, entries **6** and **7**) has very little effect on the oxidation potentials, however, since pyrazine is much easier to reduce than pyridine this causes a red shift in the emission. DFT calculations confirm that the excited states vary according to the nature of the X^Y ligand. For X^Y ligands containing a pyridine **1.5c** and **1.5e-g** the LUMO resides mainly on the X^Y ligand and partially on the pyridyl ring of the ppy.⁸⁰⁻⁸³ In contrast, when X^Y = acac (**1.5d**), the LUMO is mostly localised on the pyridyl ring of ppy.^{81, 83, 84}

1.2.2.2 Tuning of luminescent wavelength by variation of C^N ligands

As mentioned earlier in (**Table 1.1**) changing the C^N ligand in $[\text{Ir}(\text{C}^{\text{N}})_3]$ can affect the emission wavelength. The same is true for heteroleptic complexes $[\text{Ir}(\text{C}^{\text{N}})_2(\text{X}^{\text{Y}})]^{n+}$ ($n = 0, 1$), see **Figure 1.10**. For example, in cationic complexes $[\text{Ir}(\text{C}^{\text{N}})_2(\text{bpy})]^+$, replacement of 2-phenyl pyridine in (**1.6a**) with 2-phenyl pyrazole in (**1.6b**) mainly affects the HOMO. Pyrazole is less electron donating than pyridine, therefore it lowers the HOMO causing a blue shift. Alternatively, increasing the number of nitrogen atoms of the C^N ligand (**1.6b-d**) leads to a blue shift in the emission wavelength. In addition, the position of the nitrogen atoms in the azole ring also plays an important role in determining the emission wavelength. Complexes with phenyl-azole C^N ligands (**1.6b-d**) bearing a nitrogen in the azole position to which the phenyl is linked show a markedly blue-shifted emission compared to complexes with the same number of nitrogen atoms in the azole ring and bearing a carbon atom in that position (**1.6e-g**).⁵⁹

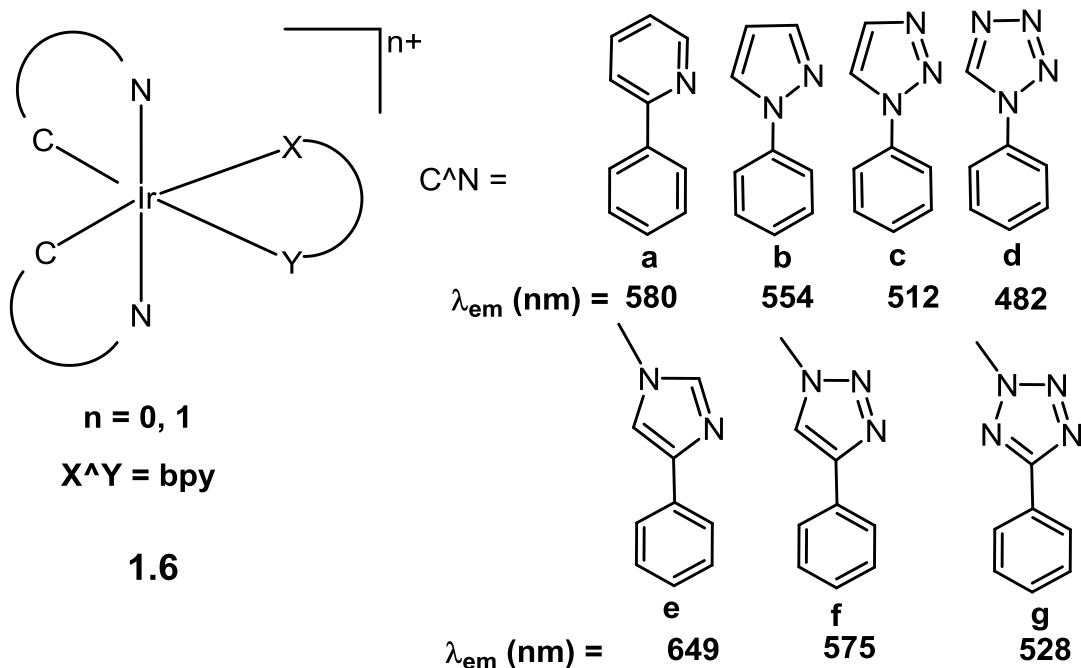


Figure 1.10: Effect of number and position of N atoms in C^N ligand on emission.

In contrast to cationic complexes in **Fig. 1.10**, for neutral complexes $[\text{Ir}(C^N)_2(\text{acac})]$ **1.7a,b**, substituting the pyridine ring of **1.7a** with a pyrazole ring **1.7b** causes a slight red shift (**Fig 1.11**).

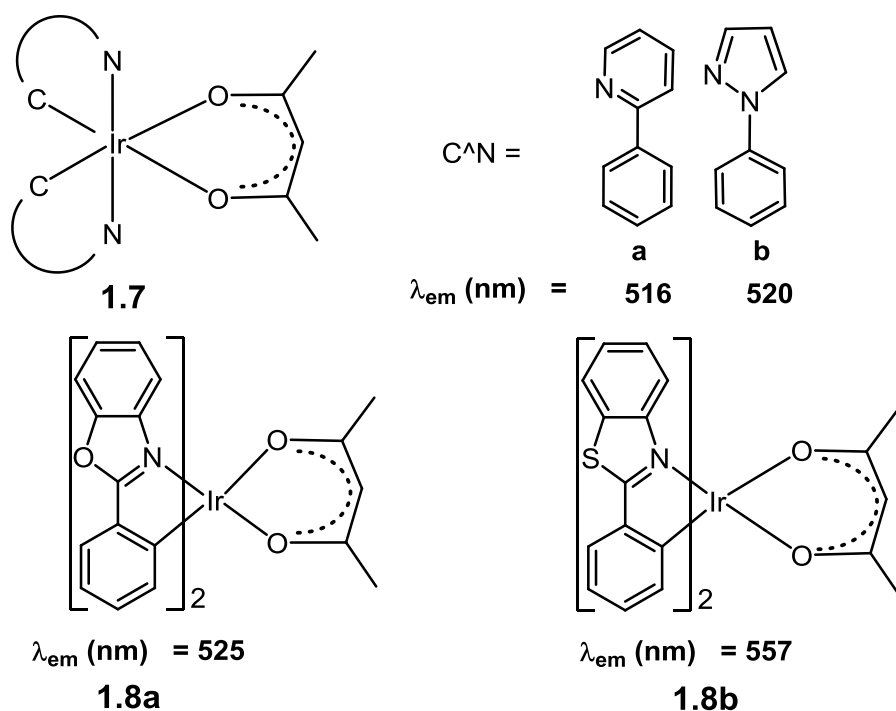


Figure 1.11: Selected examples of neutral Ir(III) complexes with different C^N ligands.

In these neutral complexes the HOMO and LUMO can be on the same ligand leading to a π - π^* transition (ILCT). For example, complexes **1.8a-b** containing different C^N ligands⁸⁵ show a moderate difference in wavelength of emission (**Fig 1.11**). The higher

polarizability and delocalization for the less electronegative heteroatom, S in **1.8b** led to a 30 nm red shift in the emission compared to the O-containing ligand in **1.8a**.

1.2.2.3 Effect of conjugation

Increasing the conjugation of the X^Y or C^N ligand can also affect the emission wavelength. For example, Zhao co-workers synthesised a series of complexes [Ir(piq)₂(X^Y)]PF₆ (**1.9a-d**) (**Fig. 1.12**) and showed that the emission wavelength of the complexes varies from 586 to 659 nm, **1.9a** to **1.9d**, respectively.⁴⁸ Hence, they concluded that increasing the π -conjugation of the X^Y ligand leads to a red shift in emission consistent with DFT calculations which showed the LUMO being centred on the X^Y ligand.⁴⁸

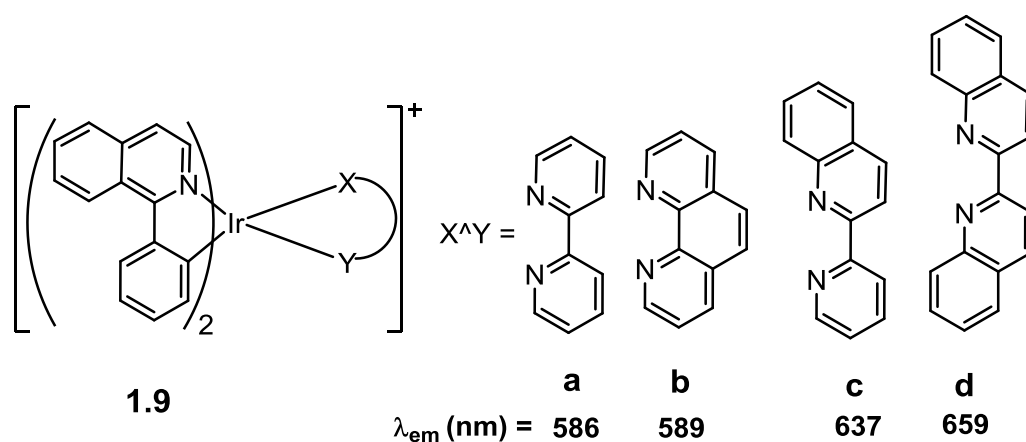


Figure 1.12: Selected examples of cationic Ir(III) complexes showing the effect of conjugation in the X^Y ligand on emission wavelength.

In neutral complexes, both the HOMO and the LUMO involve the C^N ligand, hence it is difficult to adjust the energy of just one without having any effect on the other, due to conjugation in the C^N ligand. To overcome this intrinsic problem, in 2008, Y. Chi and co-workers reported **1.10** with a non-conjugated C^N ligand in which the two chromophores were linked with a methylene spacer.⁸⁶ This destabilizes the π^* orbitals of the non-conjugated C^N ligand, causing a blue shift in emission for **1.10**,⁸⁶ (λ_{em} = 437, 460 (sh) nm) compared with **1.11**⁸⁷ (λ_{em} = 457 nm) with a conjugated C^N ligand.

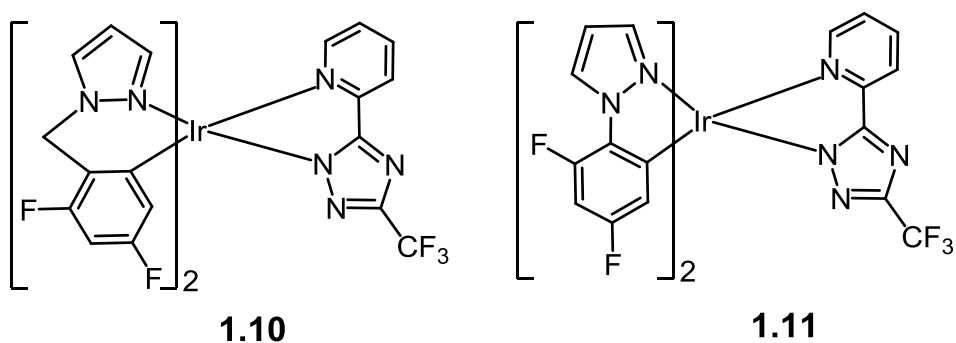
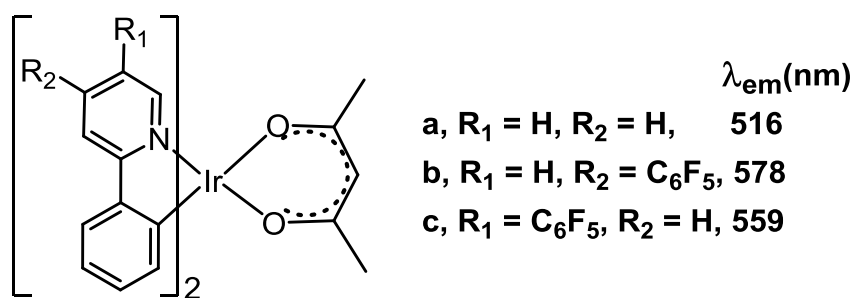


Figure 1.13: Examples of neutral Ir(III) complexes showing the effect of conjugation in the C[^]N ligand.

1.2.2.4 Tuning of emission by varying substituents

As discussed in section 1.2.2.3, for complexes $[\text{Ir}(\text{C}^{\wedge}\text{N})_2(\text{X}^{\wedge}\text{Y})]^{n+}$ ($n = 0, 1$) the HOMO mainly resides on the d-orbitals of Ir and partly over the phenyl ring of the C[^]N ligand. Therefore, putting substituents on the phenyl ring of the C[^]N ligand will mostly affect the HOMO. The situation is more complicated for the LUMO since it may be primarily on the X[^]Y ligand or on the heterocyclic part of the C[^]N hence the effect of substituents on the X[^]Y ligand or the heterocyclic part of C[^]N is more difficult to predict. Indeed, in some cases the effect of substituents can be sufficient to shift the LUMO from the C[^]N to the X[^]Y ligand or vice versa.

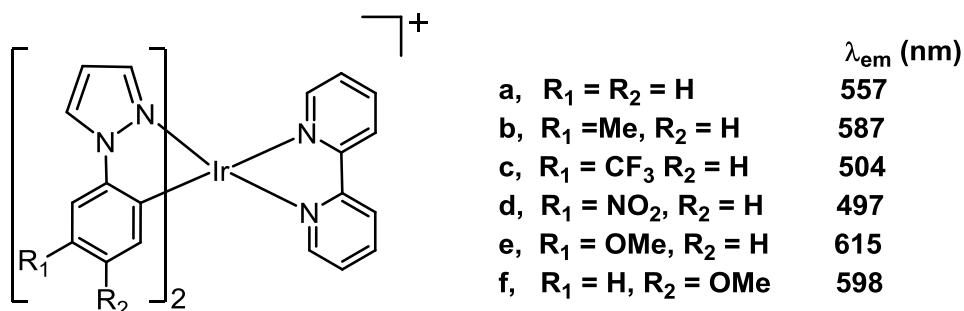
Some examples of the effect of substituents in tris-cyclometallated complexes $[\text{Ir}(\text{C}^{\wedge}\text{N})_3]$ were shown in Fig 1.7 (Table 1.1).⁴⁶ In complexes 1.12 (Fig. 1.14) the LUMO resides on the pyridyl ring, therefore, electron withdrawing substituents on the pyridine cause a red shift. Tsuzuki *et. al.*, showed that the position of the substituent also effects the emission wavelength.⁸⁸ Thus, the C₆F₅ substituted complexes 1.12b and 1.12c show a red shift of emission with respect to the unsubstituted complex 1.12a. DFT calculations suggest that the increased shift for 1.12b compared with 1.12c is because the LUMO is more concentrated on the *para* position with respect to N, therefore, substitution on this position has a greater effect. This indicates that the emission wavelength is tunable according to the position as well as the electronic properties of the substituent.



1.12

Figure 1.14: Examples of neutral Ir(III) complexes showing the effect of substituents on the C^N ligand on emission.

Changing the position of the substituent on the phenyl of the C^N ligand also effects the emission wavelength. For instance, Davies and co-workers⁶⁵ showed that changing the R group *para* to the metal in complexes **1.13** had a larger influence on emission and redox potentials than the same substituents at the *meta* position (**1.13**). The study showed that a large variation in emission wavelength (118 nm) is observed upon changing the substituent on the phenyl ring from NO₂ to OMe. Substituting H by Me or OMe lowers the $\Delta E^{1/2}$ causing a red shift in emission (from 557 nm in **1.13a** to 615 nm in **1.13a**). Conversely, replacing H with electron-withdrawing groups (CF₃ and NO₂) causes a significant blue shift (*ca.* 50–60 nm) with respect to **1.13a**. In addition, the electrochemistry and emission of complexes **1.13e, f** show that substituents on the cyclometallated phenyl *para* to the metal have a larger impact than those at the *meta* position and hence enable tuning of emission over a wider range from the same substituent. This is consistent with DFT calculations which showed the *para* position having a larger contribution to the HOMO



1.13

Figure 1.15: Examples of cationic Ir(III) complexes showing the effect of substituent and position of the substituent in C^N ligand on emission.

The overall effect of changing substituents on the HOMO and LUMO to effect the emission in cationic iridium complexes can be illustrated by considering the complexes in **1.14a-c**. (Table 1.2). Complex **1.14a** is easiest to oxidise due to the donor strength of 4,4'- dimethylamino substituent.^{66, 89} but is correspondingly more difficult to reduce compared to **1.14b**. Hence, destabilization of the LUMO orbitals of **1.14a** is greater than the destabilization of the HOMO orbitals leading to an increase in the HOMO LUMO gap of **1.14a** compared to that of complex **1.14b**. This leads to shorter wavelength emission for **1.14a**. Complex **1.14c** is more difficult to oxidise than **1.14b** due to the F substituents on the phenyl. The reduction potential of **1.14c** is almost the same as that of **1.14a** hence overall HOMO/LUMO gap for **1.14c** is larger than for **1.14a** hence the emission is blue shifted relative to **1.14a**.⁸⁹

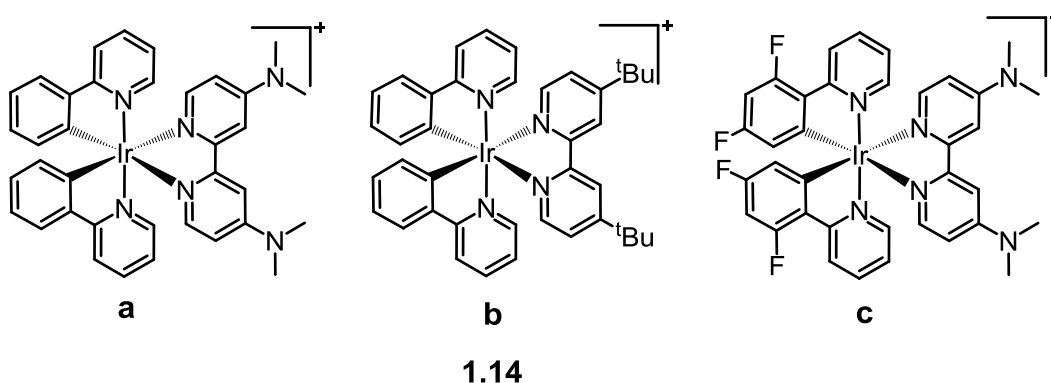


Figure 1.16: Examples of cationic Ir(III) complexes showing the the effect of changing of the substituent in C^N and N^N ligand on the emission.

Table 1.3:. Emission, and electrochemical properties of the selected cationic iridium(III) complexes.

Complex	Emission ^a λ_{\max} (nm)	Electrochemical data V vs. Fc ^b		References
		$E^{1/2}_{\text{ox}}$	$E^{1/2}_{\text{red}}$	
1.14a	491, 520	0.72	- 2.17,- 2.61,- 2.87	66, 89
1.14b	581	0.83	- 1.88	66, 67, 89
1.14c	463, 493	1.0	- 2.13,- 2.49, - 2.77	55, 89

^aEmission data were collected at 298K by exciting at 380 nm. ^bElectrochemical measurements were carried out in acetonitrile solution and the potentials are V vs. ferrocinium/ferrocene (Fc⁺/Fc).

1.2.3 Luminescence properties of Platinum(II) complexes.

Pt(II) complexes are d⁸ metal ions and adopt a square planar geometry as opposed to the distorted octahedral complexes of the d⁶ metal ions. A range of platinum(II) complexes, with bi- and tri-dentate ligands such as **1.15** and **1.16**, are usually either non-emissive or

only very weakly luminescent at room temperature. This is attributed to the presence of low-lying MC (d–d) excited states, occupation of which leads to efficient non-radiative decay.⁹⁰

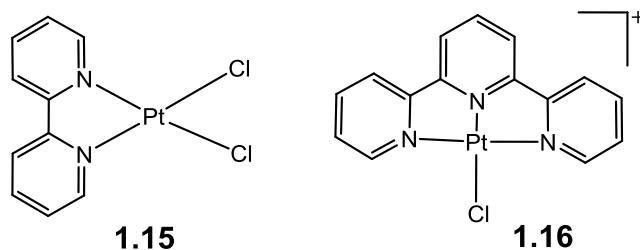


Figure 1.17: Examples of bidentate and tri-dentate Pt(II) complexes.

Replacement of the chloride in **1.17a** with the strong field acetylide in **1.17b** raises the energy of the d-d states, thereby reducing non-radiative decay pathways and giving an increase in quantum yields.⁹¹ A red shift is also observed in **1.17b** with respect to **1.17a**.

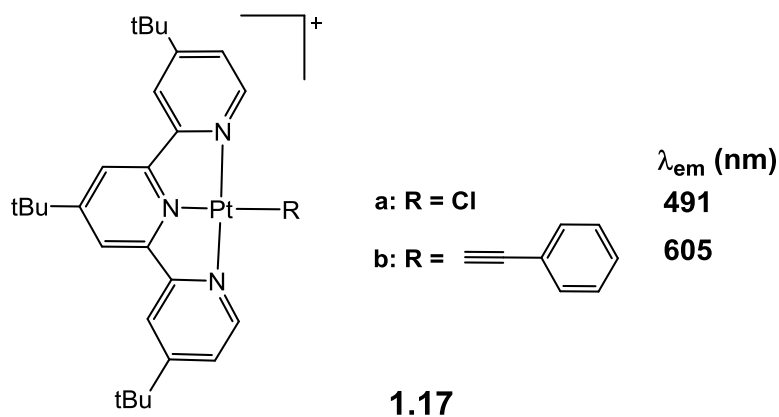


Figure 1.18: Tridentate Pt(II) complexes showing effect of R-group on emission.

An alternative to adding a strong field ligand as an ancillary ligand is to incorporate a strong donor atom into the bi or tridentate ligand. Hence, cyclometallated complexes offer certain advantages; firstly, the strong σ -donating character of the metallated aryl ring helps to raise the energy of the metal-centred deactivating d–d states so they have less contribution to the excited state. Secondly, it helps promote ISC and hence the radiative rate constants are increased.⁹⁰ Indeed, Pt(II) complexes with cyclometalating ligands $[\text{Pt}(\text{C}^{\wedge}\text{N})(\text{X}^{\wedge}\text{Y})]^{n+}$ ($n = 0, 1$), show strong emissions in the fluid and solid states and have attracted a great deal of fundamental interest in many application such as chemosensors,⁹² colorimetric oxygen sensors,⁹³ photovoltaics^{94, 95} and electrophosphorescent devices.⁹⁶ For most of such complexes, the emission profile at room temperature is highly structured with relatively long lifetimes. Hence, the origin of emission is considered to be predominantly from a ^3LC excited state.⁹⁷ The luminescence properties of cyclometallated Pt complexes are discussed below.

1.2.3.1 Cyclometallated Pt complexes with bidentate ligands.

Thompson *et. al.*,⁶² have reported several neutral cyclometallated Pt(II) complexes [Pt(C[^]N)(O[^]O)], (**1.18**) where (O[^]O) is a β -diketonate ligand. As for the Ir complexes discussed above, the emission of these complexes could be tuned over a wide range of the visible spectrum, either by changing the nature of cyclometallated ligand or by modifying the 2-phenylpyridyl ligand with electron donating or electron withdrawing substituents. All of these complexes are strongly emissive with λ_{max} values ranging from 456 to 600 nm. They show well-resolved vibronic fine structure (at room temperature and 77 K). Strong spin-orbit coupling of the Pt atom allows for the formally forbidden mixing of the ¹MLCT with the ³MCLT and ³ π - π^* states. This mixing leads to high emission quantum efficiencies (0.02-0.25) and lifetimes on the order of microseconds.

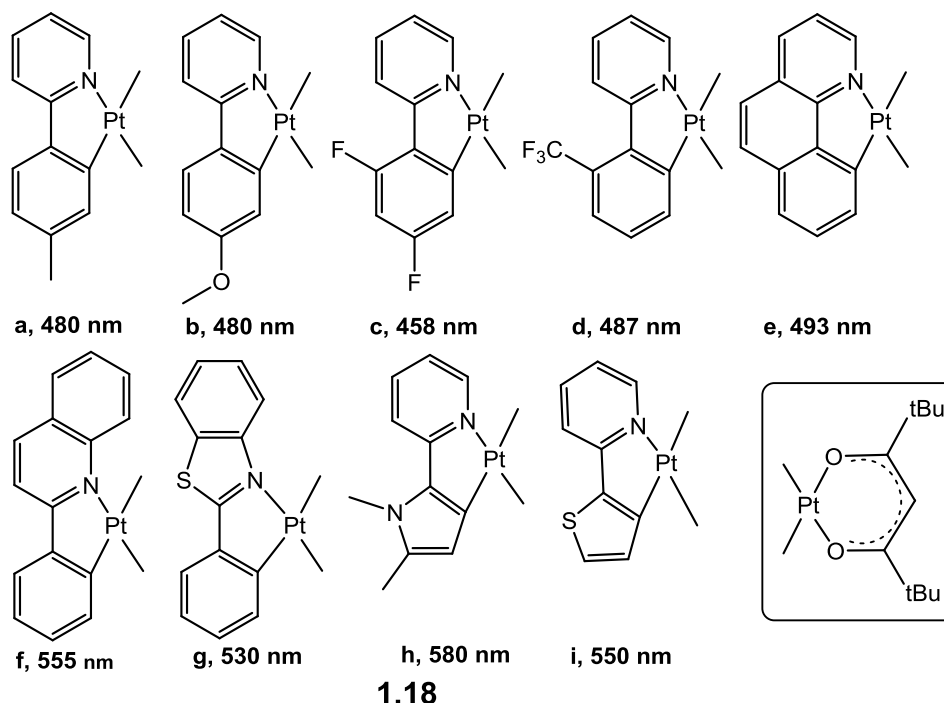


Figure 1.19: Selected examples of neutral Pt complexes [Pt(C[^]N)(O[^]O)].

Most of these complexes show a single reversible reduction wave between -1.9 and -2.6 V (*vs* Cp₂Fe/Cp₂Fe⁺), assigned to largely C[^]N ligand based reduction, and an irreversible oxidation, assigned to predominantly Pt based oxidation. DFT calculations showed that The HOMO levels are a mixture of Pt and ligand orbitals, while the LUMO is predominantly C[^]N ligand based.

Laskar and co-workers⁹⁸ investigated the photophysical properties of highly water soluble cationic Pt(II) complex (**1.19**). The complex exhibits a green emission in solution (λ_{max} 510 nm) but bright yellow emission (λ_{max} 553 nm) in the solid state. The X-ray structure

of **1.19** clearly indicates the presence of π - π stacking between the phenyl rings of consecutive molecules, the authors suggested that a new excited state i.e., $^3\text{MLLCT}$ is formed in the solid state leading to the change in emission.

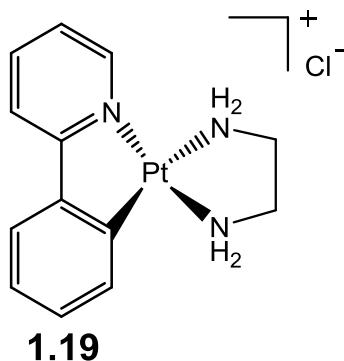


Figure 1.20: Example of cationic cyclometallated Pt complexes with N^N ligand.

1.2.3.2 Pt complexes with tri-dentate cyclometallated ligands

Complex **1.20**, incorporating a strong field tridentate cyclometallated ligand was reported by several authors.⁹⁹⁻¹⁰¹ The complex was intensely luminescent in fluid solution at room temperature, at 480 nm and has a luminescence quantum yield of 0.6 in degassed DCM solution, remarkably high for platinum chromophores. NIR two photon excitation has been employed for these complexes due to their low absorption in the visible region. The emission quantum yields of up to 70% and long lifetime (100 μs) of the excited state of the complexes allowed them to be used with time-gated technique time-resolved emission imaging microscopy (TREM) to eliminate background fluorescence.

Changing the position of the cyclometallated ring from a central to a lateral position led to different spectroscopic properties as cited in the literature.^{11, 102, 103} For example in 2009, Lam and co-workers reported complex **1.21** containing C^N^N tridentate cyclometallating ligand.¹⁰⁴ Complex **1.21** shows intense green emission (500-520 nm) under ambient conditions with a quantum yield of 0.09 and emission lifetime of 0.57 μs . in DMF. Complex **1.21** also shows two photon-induced luminescence and has potential as a luminescent probe for in vitro bioimaging.

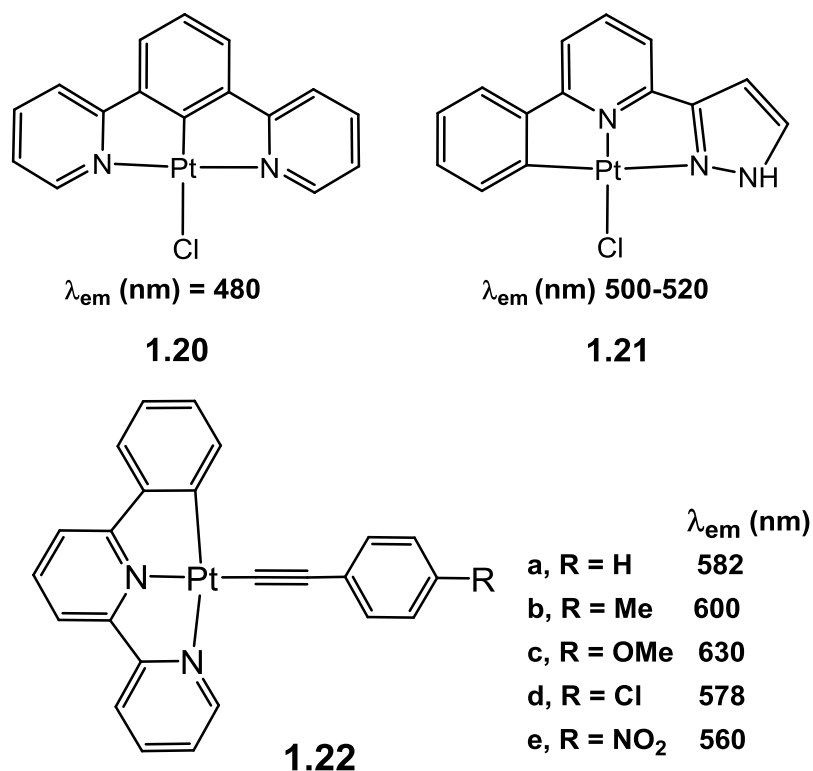


Figure 1.21: Selected examples of cyclometallated Pt complexes with tri-dentate ligands.

Cyclometallated Pt(II) complexes **1.22a-e** have better emissive properties compared to the terpy analogs *i.e.* these complexes show intense emission and have higher quantum yields.¹⁰⁵ All complexes **1.22a-e** show long lived yellow to red emission, which can be ³MLCT, ³ $\pi\pi^*$ (alkynyl) and/or ³ $\pi\pi^*$ (cyclometallating ligand) emission depending on the relative energies of the Pt d-orbitals and the $\pi\text{-}\pi^*$ orbitals of the ligands. Electron withdrawing substituents such as Cl, NO₂ on the phenyl of the alkyne increase the HOMO-LUMO gap and cause a blue shift in emission, while electron donating substituents (*i.e.* CH₃, OCH₃) cause a red shift.

1.3 Applications of luminescent metal complexes

Luminescent transition metal complexes have become widely used in several fields as a result of their advantageous photophysical properties.⁴ The effectiveness and performance of these complexes is determined by their excited state properties which, as described in sections **1.2.1-3**, can be controlled through synthetic modifications.¹⁴ Early studies mostly focused on Ru(II) tris-diimine complexes, however, these offer limited colour tuning capability due to thermal population of a nonemissive metal-centered (³MC) state. The thermal population of their ³MC state is not all that related to their limited colour tuning. This primarily affects photoluminescent quantum yield. The limited colour

tuning stems from the fact that the HOMO is not easily tunable due its being more or less pure Ru d-orbital character. Ir(III) complexes have increased ligand-field stabilization energy thus, the 3MC state is less accessible compared with Ru(II) complexes. In addition, Ir(III) complexes, enable broader ligand tuning possibilities, particularly heteroleptic complexes $[\text{Ir}(\text{C}^{\wedge}\text{N})_2(\text{X}^{\wedge}\text{Y})]^{n+}$ ($n = 0, 1$). These factors and their robust nature make Ir(III) complexes more attractive in several applications. As mentioned in sections 1.2.3 heteroleptic Pt(II) complexes $[\text{Pt}(\text{C}^{\wedge}\text{N})(\text{X}^{\wedge}\text{Y})]^{n+}$ ($n = 0, 1$) have also got useful luminescent properties and high thermal stability. The applications of luminescent metal complexes are discussed in sections 1.3.1-4, examples are chosen from Ru(II) since these were often the first ones studied, and Ir(III) and Pt(II) since these are discussed further in later Chapters.

1.3.1 Transition Metal Complexes in Displays, OLEDs/LECS

As mentioned in sections 1.3 since 2000 there has been a huge upsurge in interest in the use of Ir(III) and Pt(II) cyclometallated complexes as emissive materials in displays. While exciton-based electroluminescence from small fluorophors has a maximum quantum yield of 25% (according to spin statistics), however, due to spin-orbit coupling phosphorescent complexes can also provide emission from triplet excitons and hence theoretically can achieve quantum yields up to 100%. The requirements of metal complexes for use in an devices can be listed as following:⁵⁶

- They should be highly emissive, with high phosphorescence quantum yields at ambient temperature and the lifetime should be around 1 μs or less, to avoid competition from triplet-triplet annihilation at high currents.
- For OLEDs the compounds should be charge neutral, in order to avoid migration under the influence of the applied electric field
- It should be possible to obtain efficient red, blue and green emitters by making small changes to the structure of the complexes, without fundamentally altering their chemistry or other properties.
- Complexes which have reversible oxidation and reduction processes at accessible potentials are attractive in that they can act as charge carriers and sites for exciton formation, rather than serving simply as acceptors of excited state energy from excitons localised on the host molecules
- They should normally not be susceptible to aggregation or segregation within the host material, as this frequently leads to self-quenching of the emission

Combining phosphorescent emitters with proper host materials and optimized device set ups can result in highly efficient light-emitting devices.^{55, 106-108} As mentioned above tuning of the C^N, and X^Y ligands and substituents has allowed preparation of materials that can emit a full range of colours.^{9, 55, 56} A light-emitting electrochemical cell (LEC) can be defined as a solid-state device which can produce light from an electric current. LECs consist of two metal electrodes linked by an organic semiconductor containing mobile ions. LECs may provide an alternative kind of light emitting device to OLEDs.¹⁰⁹ LECs have certain beneficial characteristics over OLEDs, particularly light emission with low threshold voltages.¹¹⁰ Early examples of metal containing LECs used Ru(II) e.g. [Ru(bpy)₃]²⁺, due to the high stability of the reduced and oxidized species enabling annihilation efficiencies close to 100%.¹¹¹ However, recently, there has been growing interest of Ir(III) complexes due to their high efficiencies and also more easily tunable emission colours.

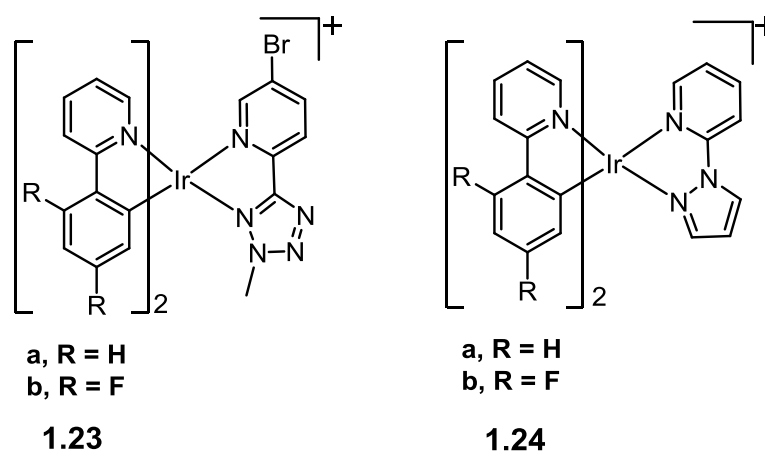


Figure 1.22: Selected examples of cyclometallated Ir(III) complexes used in LECs.

Complexes **1.23** are examples of Ir(III) complexes which have been used for the fabrication of LEC devices (**Fig. 1.22**). A LEC based on **1.23a** resulted in orange light emission (576 nm) with the Commission Internationale de l'Eclairage (CIE) coordinates of (0.45, 0.49), whilst **1.23b** has green emission at (518 nm) electroluminescence with the CIE coordinates of (0.33, 0.49).²¹

Two blue-emitting cationic Ir(III) complexes **1.24a-b** have been reported by Qiu and co-workers (**Fig. 1.22**).¹¹² LECs based on **1.24a** gave green-blue electroluminescence (486 nm) and had a relatively high efficiency of 4.3 cd A⁻¹ when an ionic liquid 1-butyl-3-methylimidazolium hexafluorophosphate was added into the light-emitting layer. LECs based on **1.24b** gave blue-shifted electroluminescence (460 nm) with CIE (Commission

Internationale de l'Eclairage) coordinates of (0.20, 0.28). The authors suggest that the obtained blue light emission LECs also pave the way for realizing highly efficient, single-layer white light-emitting electrochemical cells.

1.3.2 Transition Metal complexes as Photocatalysts and Photoredox Catalysis

Photocatalytic hydrogen evolution from water splitting under visible light irradiation has been an important goal for many scientists. Intensive efforts have been directed towards a solar-driven water splitting reaction using semiconductor-based photocatalysts,^{31, 113} or transition metal complexes as a chromophore/catalyst for photochemical hydrogen and oxygen generation.^{14, 31} Complexes of Ru(II)¹¹⁴ platinum(II)¹¹⁵ and iridium(III)¹¹⁶ have been used as photocatalysts for hydrogen evolution.¹¹⁷ In this context, Du *et al.*¹¹⁵ reported the photocatalytic generation of H₂ from H₂O using complex **1.25**, (**Fig. 1.23**) as a sensitizer, MV²⁺, as an acceptor, triethanolamine (TEOA), as a donor, and colloidal Pt (5-7 nm size stabilized by sodium polyacrylate), as a catalyst. The complex exhibits a strong photoluminescence in the range of 500-800 nm with λ_{max} at 605 nm and an emission quantum yield Φ of 0.025 based on [Ru(bpy)₃]PF₆ in degassed MeCN as the reference ($\Phi = 0.062$). In addition, the rate of H₂ evolution was found to depend on both solution pH and the concentration of MV²⁺. The amounts of H₂ produced as each of these parameters is varied. At pH 7, the maximum rate for H₂ generation is observed, while significant amounts of H₂ are also measured at pH 5 and 9.

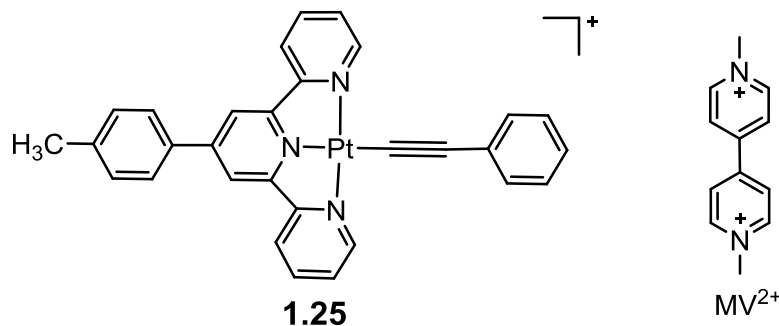
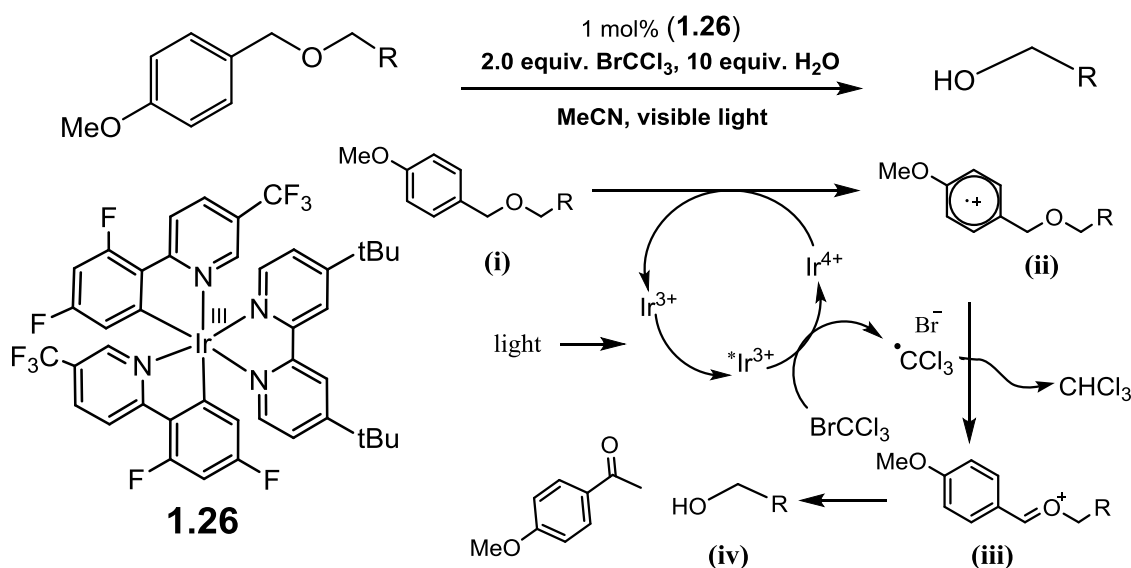


Figure 1.23: Example of Pt(II) complex for photocatalytic generation of H₂ from H₂O.

Recently, transition metal complexes have been being used as photoredox catalysts.^{118, 119} In this field, Stephenson and co-workers reported that the Ir(III) photocatalyst (**1.26**) is an effective catalyst for the deprotection of *para*-methoxybenzyl ethers (PMB) using BrCCl₃ as the stoichiometric oxidant.¹²⁰ Photoexcitation of the heteroleptic iridium complex provides a species that is sufficiently reducing ($E_{1/2}^{\text{IV}^*/\text{III}} = -0.89$ V vs SCE) to transfer an electron to BrCCl₃ ($E_{1/2}^{\text{red}} = -0.18$ V vs SCE) (**Scheme 1.3**). Reduction of BrCCl₃ gives bromide and trichloromethyl radical, while oxidation of the photoexcited

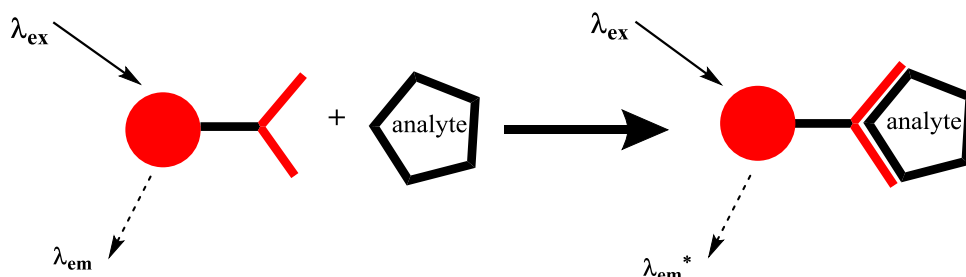
Ir(III) species gives an Ir(IV) intermediate. This Ir(IV) species is very strongly oxidizing ($E_{1/2}^{\text{IV/III}} = +1.69 \text{ V vs SCE}$) and, as in the oxidation of benzylic alcohols may oxidize the electron-rich aromatic ring of the PMB ether (i) to give radical cation (ii). The trichloromethyl radical may then abstract a hydrogen atom from the benzylic position of (ii), producing chloroform and oxocarbenium ion (iii). Hydrolysis of (iii) releases deprotected alcohol (iv) as well as the byproduct 4-methoxybenzaldehyde. The study showed that photoredox catalysts, via the oxidative quenching of the visible light induced excited state Ir(III), may promote the generation of valuable oxocarbenium intermediates under mild conditions by the oxidation of benzylic ethers



Scheme 1.3: Proposed mechanism of oxidative cleavage of PMB ethers mediated by Ir(III) photoredox catalysts.

1.3.3 Transition Metal Complexes as Sensors

A sensor can be defined as a compound that can detect an analyte by invoking a change in one or more properties of the system. Hence a molecular sensor needs to incorporate a recognition site for an analyte and produce a measurable output in response. A luminescent sensor is a system in which the reporter is a light-emitting group and where the binding of the analyte leads to some changes in the emission (**Scheme 1.4**).



Scheme 1.4: Schematic representation of a luminescent molecular sensor.

The use of luminescent transition metal complexes as sensors continues to attract considerable interest due to their significant Stokes shifts for easy separation of excitation and emission, shifts in emission wavelength with changes in the local environment, and relatively long lifetimes compared to their purely organic counterparts.^{4, 28} Luminescent transition metal complexes have been applied as chemosensors^{121, 122} for anions,¹²³⁻¹²⁵ metal ions,¹²⁶⁻¹²⁹ oxygen,^{130, 131} and protons¹³²⁻¹³⁴ and a number of comprehensive reviews have been published.^{135, 136} Some of these are discussed in this section, pH sensors will be discussed in detail in chapter two.

Zheng and co-workers¹³⁷ reported Ru(II) polypyridyl complex **1.27** which is sensitive to different anions. At room temperature, complex **1.27** showed a broad emission band centred at 608 nm in MeCN, which in the presence of H₂PO₄⁻ showed a 3-fold enhancement in luminescence, whilst with other anions, such as F⁻ or CH₃COO⁻, underwent quenching of the emission to *ca.* 89 and 83% (“switched off”) respectively. The study showed that, the presence of other anions (Cl⁻, Br⁻, I⁻, NO₃⁻, and ClO₄⁻) had almost no affect on the absorption or luminescence spectra of **1.27** in aqueous MeCN solution. This finding clearly demonstrates the ability of **1.27** to function as a highly selective “turn on” type of luminescence sensor for H₂PO₄⁻.

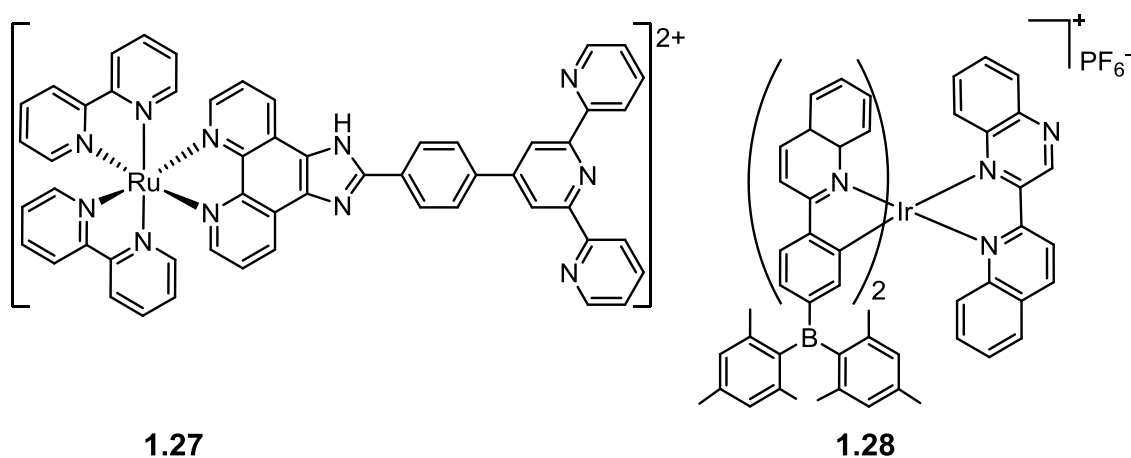


Figure 1.24: Selected examples of cyclometallated Ru(II) and Ir(III) complexes as chemosensor for anions.

A near-infrared phosphorescent probe for F⁻ based on a cationic Ir(III) complex **1.28** has been reported by Wei *et. al.*¹³⁸ The complex shows NIR phosphorescent emission around 680 nm. Interestingly, the complex can be excited with long wavelength light, around 610 nm. Such long-wavelength excitation can reduce the background emission interference and improve the signal-to-noise ratio. The study showed that upon addition of F⁻ to the DCM solution of **1.28**, the emission intensity around 680 nm decreased gradually until it

was completely quenched. Hence, **1.28** is an on-off-type NIR phosphorescent sensor for F^- .

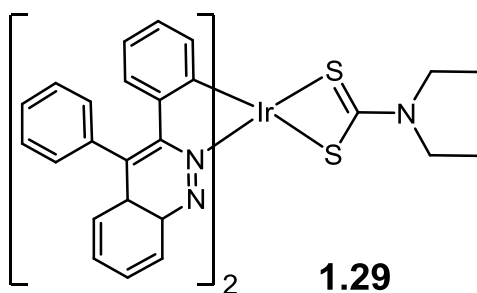


Figure 1.25: Example of cyclometallated Ir(III) complex as chemosensor for mercury(II) cation.

Hg(II) ions are considered one of the most serious problems in both health and the environment even at low levels; therefore a number of chemosensors for detecting Hg(II) ions have been studied utilizing chromogenic, fluorogenic and electrochemical sensors. In this context, a highly selective chemosensor for Hg(II) cations based on cyclometalated Ir(III) complex **1.29** has been prepared by Lu *et al.* (**Fig. 1.25**).¹³⁹ This complex showed an emission maximum at 686 nm with a lifetime of 0.77 μs . The emission titration of **1.29** with Hg^{2+} showed that the emission increases continuously until the addition of 1 equiv. of Hg^{2+} and the luminescence intensity had increased to *ca.* 474%, with a blue shift to 670 nm. Further addition induces only very minor change, which was consistent with the UV-Vis absorption result. Notably, no discernible change is observed for other metal ions, such as Ag^+ , Cu^{2+} , Fe^{2+} , Co^{2+} , Ni^{2+} .

The amount of O_2 is critical in cell metabolism, and the monitoring of O_2 quantity in cell biology is of great importance not only in living cells but also in the environment and in the food industry. Thus, several phosphorescent transition metal based O_2 sensors have been developed for the measurement of cellular O_2 levels and/or the imaging of hypoxic tumours and so on.

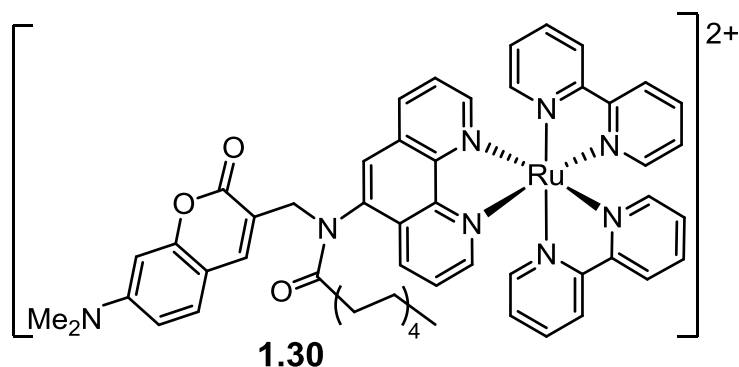


Figure 1.26: Example of Ru(II) complex for oxygen sensors.

Tanabe and co-workers reported the use of Ru complex **1.30** for ratiometric sensing of O₂ levels in living cells.¹⁴⁰ Under, anoxic conditions (0% O₂) the complex **1.30** showed two emissions band at 467 and 611 nm, which are assigned to the fluorescence of the coumarin unit (467 nm) and the ³MLCT phosphorescence of the ruthenium complex (611 nm). Increasing the O₂ concentration caused a decrease in phosphorescence intensity at 611 nm due to the quenching effect of oxygen, whilst, the fluorescence intensity at 467 nm was unaffected. Notably, the quenched phosphorescence emission of **1.30** under aerobic conditions was recovered to the intrinsic level after degassing with argon. Hence, the phosphorescence emission of **1.30** was regulated reversibly according to changes in the O₂ concentration, while its fluorescence is oxygen-independent.

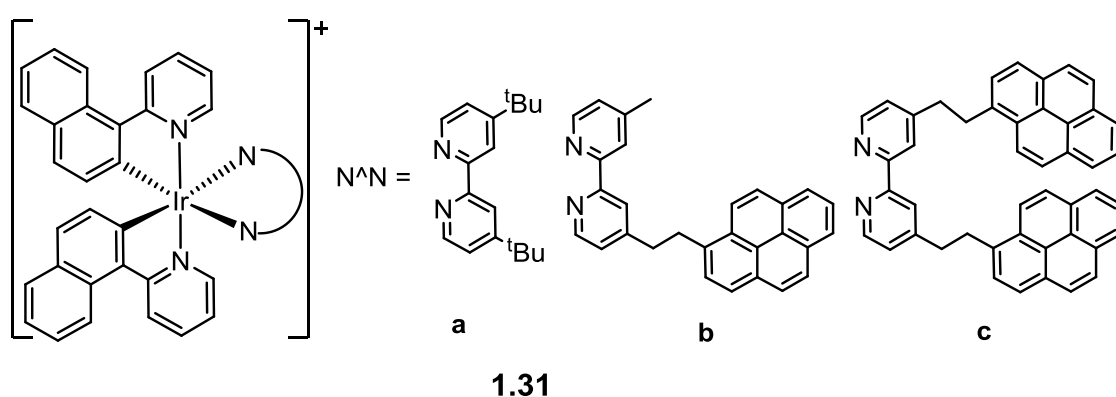
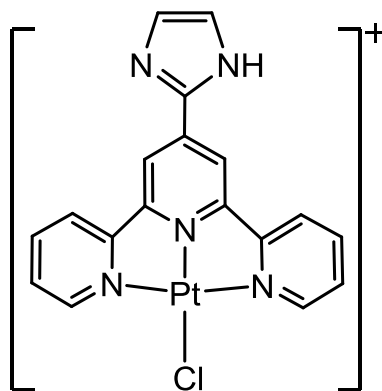


Figure 1.27: Example of bis-cyclometallated Ir(III) complex for oxygen sensing.

In 2016, Fernández-Sánchez and co-workers¹⁴¹ reported the use of bis-cyclometallated Ir(III) complexes **1.31** for luminescence oxygen sensing (**Fig. 1.27**). They showed that the phosphorescence was MLCT-based red emission for the complexes **1.31a**, **1.31b** and **1.31c** with emission maxima at *ca.* 625 nm, each with similar quantum yields ($\Phi_{\text{degas}} = 0.1$) and lifetimes of 8.3, 225 and 480 μs respectively in degassed MeCN. A higher oxygen sensitivity in dilute solution was noticed for **1.31c** compared to **1.31b** and parent **1.31a**. Whilst the latter molecule shows a $\Phi_{\text{degas}}/\Phi_{\text{air}}$ ratio of 26, a much higher value of 190 was obtained with **1.31b** and 950 with **1.31c**, which was consistent with much longer excited-state lifetimes on successive introduction of pyrene chromophores.

Metal complexes have also been used as sensors of biomolecules e.g. Nair and co-workers¹⁴² reported Pt(II) complex **1.32** for staining DNA (**Fig. 1.28**). They found that, the complex showed weak emission at 460 nm as well as at 533 nm and the emission band at 460 nm was assigned as ³ILCT transition. Upon addition of DNA, a 21-fold increase in the emission intensity of complex **1.32** was observed whilst there was no change in emission maxima with serum albumin. The complex **1.32** stains the nuclear DNA

specifically without addition of any external fluorophore. The study demonstrates the **1.32** can be used for staining DNA in gel electrophoresis as effectively as highly mutagenic ethidium bromide and it is at a non-toxic concentration. Further examples of sensing of biomolecules in cells are discussed below.



1.32

Figure 1.28: Example of Pt(II) complex used for staining DNA.

1.3.4 Transition Metal complexes for bioimaging applications.

The development of fluorescent and luminescent biological probes has relied mainly on organic dyes¹⁴³⁻¹⁴⁵ and lanthanide complexes.¹⁴⁶ Recently, luminescent transition metal complexes have emerged as attractive candidates for biological probes owing to their attractive photophysical attributes and the field has been reviewed.^{99, 147} As explained previously transition metal complexes can have a number of advantages for imaging. Long emission lifetimes (compared to fluorescent molecules), allows the application of time-resolved detection^{100, 148} and fluorescence lifetime imaging microscopy^{149, 150} that offer enhanced sensitivity. In addition, owing to their large Stokes shifts, transition metal complexes rarely suffer from self-quenching and homo-fluorescence resonance energy transfer (FRET), which usually confront fluorescent organic dyes. Moreover, the high photostability of many transition metal complexes permits continuous monitoring of biological events by fluorescence spectroscopy and microscopy. Lastly, as illustrated above (Section 1.2.1-3) the emission properties of transition metal complexes can be readily tuned by using a wide range of ligands. Tuning the emission wavelength into the near-infrared region is desirable because infrared light can penetrate tissue more than visible light which may be desirable in imaging or possibly in phototherapeutic applications.

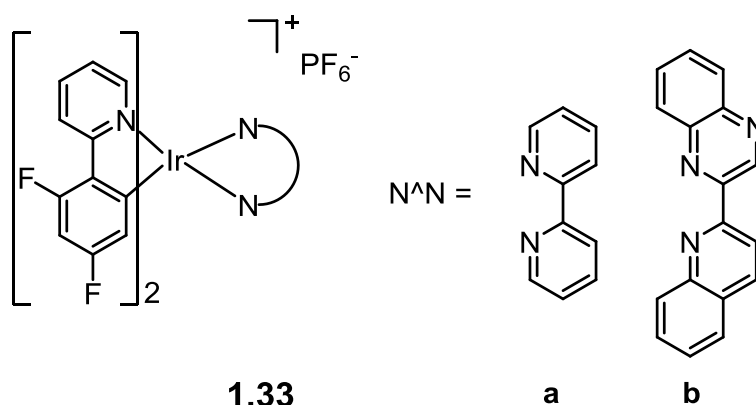


Figure 1.29: Example of bis-cyclometallated Ir(III) complex for for living cell imaging.

Li *et. al.* have reported simple cyclometallated species of Ir(III) **1.33a-b** as phosphorescent dyes for living cell imaging (HeLa cells).¹⁵¹ Complexes **1.33a,b** show intense green ($\lambda_{\text{max}} = 517 \text{ nm}$, $t = 0.9 \mu\text{s}$) and red ($\lambda_{\text{max}} = 623 \text{ nm}$, $t = 1.1 \mu\text{s}$) luminescence, respectively. The complexes localised in the cytoplasmic region of the cells, with emission maxima inside the cell (intracellular) are 512 nm and 617 nm for **1.33a,b** respectively. Furthermore, cytotoxicity studies showed staining in cytoplasm is relatively low toxicity ($\geq 100 \mu\text{M}$) and considerably higher photostability compared to organic dyes. Based on these results, the two complexes render them appealing for the design of particular phosphorescence bioimaging agents.

Chao and co-workers¹⁵² reported four cyclometalated Ir(III) complexes, **1.34a-d** which were utilized as color-tunable phosphorescent agents for mitochondrial imaging. All of the complexes exhibited intense photoluminescence emissions with quantum efficiencies of 0.049-0.957 and emission lifetimes of 195-463 ns, which can be mainly attributed to $d\pi(\text{Ir}) \rightarrow \pi^*(\text{N}-\text{N})$ ³MLCT transitions and $\pi(\text{C}-\text{N}) \rightarrow \pi^*(\text{N}-\text{N})$ ³LLCT transitions. The emission color was tuned from green-yellow to fuchsia 528 to 589 nm for **1.34a-1.34d**. The complexes possess high mitochondrial specificity, good photostability, low cytotoxicity at the imaging concentrations, high resistance to the loss of mitochondrial membrane potential as well as appreciable tolerance to environmental changes, hence are well-suited for use as imaging agents for mitochondria.

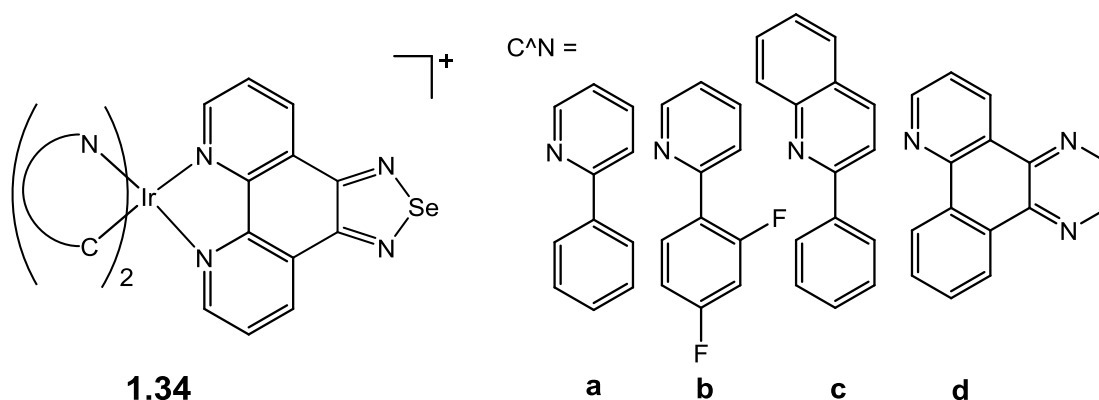


Figure 1.30: Example of cyclometallated Ir(III) complex as multicolor probes for specific mitochondrial imaging and tracking.

Thiol-containing amino acids, homocysteine (Hcy) and cysteine (Cys), play many crucial roles in biological systems. For example, elevated levels of Hcy in blood plasma (about 6 $\mu\text{mol/L}$) are risk factors for thrombosis and cardiovascular diseases. Li *et al.*, reported a cationic Ir(III) complex **1.35** containing aldehyde groups as a Hcy/Cys selective probe for ratiometric phosphorescence imaging in living cells.¹⁵³ They found that, in the presence of Cys or Hcy, the aldehyde groups of **1.32** reacts to form the thiazolidine **1.35a** or thiazinane **1.35b**, which converts the lowest excited state of the complex from ^3IL to a mixed $^3\text{MLCT}$ and $^3\text{LLCT}$ state. As a result, upon addition of Hcy or Cys, the emission band progressively shifted from *ca.* 546 to 586 nm with a decrease in intensity by factor *ca.* 1.6, resulting in a red-shift of ~ 40 nm and a change in colour from yellow to red. Cell imaging experiments demonstrated that the probe is membrane permeable and can monitor the changes of Hcy/Cys within living cells.

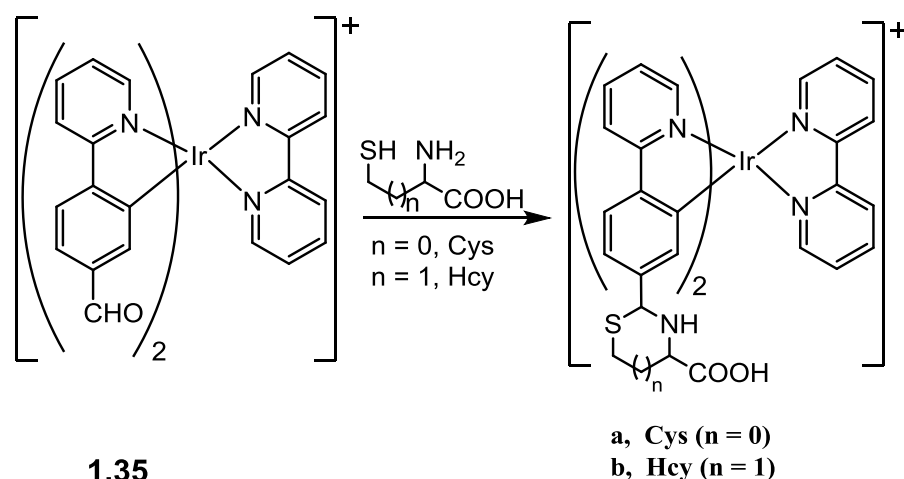


Figure 1.31: Example of cyclometallated Ir(III) complex as a ratiometric phosphorescence probe for amino acids.

In summary, it is clear that the luminescent transition metal complexes are currently revolutionizing many areas of photochemistry and photophysics. In particular, they are proving useful as molecular probes and sensors. As discussed earlier in **Section 1.5** there has been an explosion of interest in the photoluminescence properties of Ru(II), Ir(III) and Pt(II) complexes and they are amenable to the rational design of sensors.

1.4 Aims of the project

The overall aims of this research project are:

- The synthesis and characterisation of luminescent Ir(III) bis-cyclometallated complexes $[\text{Ir}(\text{C}^{\wedge}\text{N})_2(\text{N}^{\wedge}\text{N})]^{n+}$ ($n = 0, 1$). The potential use of these complexes as pH sensors will be investigated, including the effect of changing the heterocycle of the $\text{C}^{\wedge}\text{N}$ and the R groups on subsequent pK_a .
- The synthesis and characterisation of cationic Ir(III) complexes $[\text{Ir}(\text{ppz})_2(\text{N}^{\wedge}\text{N})]^+$ ($\text{N}^{\wedge}\text{N}$ = bidentate PYE ligands) and to further investigate the donor properties and resonance structures of the ligands and the photophysical properties of the ligands and complexes.
- The synthesis and characterisation of bidentate Pt(II) complexes $[\text{Pt}(\text{C}^{\wedge}\text{N})(\text{X}^{\wedge}\text{Y})]^{n+}$ ($n = 0, 1$) with additional substituents that are free to rotate in solution, and the evaluation of whether these complexes can be designed to show EPSS and hence whether they have any potential for application as viscosity sensors.

Bibliography

1. E. N. Harvey, *A history of luminescence from the earliest times until 1900*, American Philosophical Society, Philadelphia, 1957.
2. J. Zimmermann, A. Zeug and B. Roder, *Phys. Chem. Chem. Phys.*, 2003, **5**, 2964-2969.
3. J. Lakowicz, *Principles of Fluorescence Spectroscopy, Chapter 6, 2010, 205-235*, Springer, Boston, MA, University of Maryland School of Medicine. Baltimore, USA, Third Edition edn., 2010.
4. J. N. Demas and B. A. DeGraff, *Coord. Chem. Rev.*, 2001, **211**, 317-351.
5. J. N. Demas and B. A. DeGraff, *Anal. Chem.*, 1991, **63**, 829A-837A.
6. R. H. Crabtree, in *The Organometallic Chemistry of the Transition Metals*, John Wiley & Sons, Inc., Fourth Edition edn., 2005, pp. 1-28.
7. J. N. Demas and B. A. DeGraff, *J. Chem. Educ.*, 1997, **74**, 690-695.
8. V. Fernandez-Moreira, F. L. Thorp Greenwood and M. P. Coogan, *Chem. Commun.*, 2010, **46**, 186-202.
9. C. Ulbricht, B. Beyer, C. Friebe, A. Winter and U. S. Schubert, *Adv. Mater.*, 2009, **21**, 4418-4441.
10. V. W. W. Yam, V. K. M. Au and S. Y. L. Leung, *Chem. Rev.*, 2015, **115**, 7589-7728.
11. J. A. G. Williams, S. Develay, D. L. Rochester and L. Murphy, *Coord. Chem. Rev.*, 2008, **252**, 2596-2611.
12. I. M. Dixon, J. P. Collin, J.-P. Sauvage, L. Flamigni, S. Encinas and F. Barigelletti, *Chem. Soc. Rev.*, 2000, **29**, 385-391.
13. R. J. Watts, *Comments Inorg. Chem.*, 1991, **11**, 303-337.
14. M. S. Lowry and S. Bernhard, *Chem. Eur. J.*, 2006, **12**, 7970-7977.
15. Q. Zhao, M. Yu, L. Shi, S. Liu, C. Li, M. Shi, Z. Zhou, C. Huang and F. Li, *Organometallics*, 2010, **29**, 1085-1091.
16. Y. Yang, Q. Zhao, W. Feng and F. Li, *Chem. Rev.*, 2013, **113**, 192-270.
17. T. Bessho, E. Yoneda, J. H. Yum, M. Guglielmi, I. Tavernelli, H. Imai, U. Rothlisberger, M. K. Nazeeruddin and M. Grätzel, *J. Am. Chem. Soc.*, 2009, **131**, 5930-5934.
18. D. Wang, H. Dong, Y. Wu, Y. Yu, G. Zhou, L. Li, Z. Wu, M. Gao and G. Wang, *J. Organomet. Chem.*, 2015, **775**, 55-59.

19. M. Gennari, F. Légalité, L. Zhang, Y. Pellegrin, E. Blart, J. Fortage, A. M. Brown, A. Deronzier, M. N. Collomb, M. Boujtita, D. Jacquemin, L. Hammarström and F. Odobel, *J. Phys. Chem. Lett.*, 2014, **5**, 2254-2258.
20. J. Slinker, D. Bernards, P. L. Houston, H. D. Abruna, S. Bernhard and G. G. Malliaras, *Chem. Commun.*, 2003, 2392-2399.
21. Y. Kwon and Y. Choe, *J. Solution Chem.*, 2014, **43**, 1710-1721.
22. T. Li, M. Cui, G. Ran and Q. Song, *Dyes and Pigments*, 2015, **112**, 1-7.
23. D. L. Ma, H. J. Zhong, W. C. Fu, D. S. H. Chan, H. Y. Kwan, W. F. Fong, L. H. Chung, C. Y. Wong and C. H. Leung, *Plos One*, 2013, **8**, 55751-55757.
24. K. K. Yu, J. T. Hou, K. Li, Q. Yao, J. Yang, M. Y. Wu, Y. M. Xie and X. Q. Yu, *Scientific Reports*, 2015, **5**, 1-10.
25. J. Jayabharathi, V. Thanikachalam and R. Sathishkumar, *New J. Chem.*, 2015, **39**, 235-245.
26. J. B. Kim, S. H. Han, K. Yang, S. K. Kwon, J. J. Kim and Y. H. Kim, *Chem. Commun.*, 2015, **51**, 58-61.
27. M. C. DeRosa, D. J. Hodgson, G. D. Enright, B. Dawson, C. E. B. Evans and R. J. Crutchley, *J. Am. Chem. Soc.*, 2004, **126**, 7619-7626.
28. B. Higgins, B. A. DeGraff and J. N. Demas, *Inorg. Chem.*, 2005, **44**, 6662-6669.
29. Q. Zhao, F. Li and C. Huang, *Chem. Soc. Rev.*, 2010, **39**, 3007-3030.
30. M. Bar, D. Maity, S. Deb, S. Das and S. Baitalik, *Dalton Trans.*, 2017, **46**, 12950-12963.
31. G. J. Zhang, X. Gan, Q. Q. Xu, Y. Chen, X. J. Zhao, B. Qin, X. J. Lv, S. W. Lai, W. F. Fu and C. M. Che, *Dalton Trans.*, 2012, **41**, 8421-8429.
32. K. Teegardin, J. I. Day, J. Chan and J. Weaver, *Org. Process Res. Dev.*, 2016, **20**, 1156-1163.
33. I. Corbucci, K. Ellingwood, L. Fagiolari, C. Zuccaccia, F. Elisei, P. L. Gentili and A. Macchioni, *Catalysis Today*, 2017, **290**, 10-18.
34. J. P. Paris and W. W. Brandt, *J. Am. Chem. Soc.*, 1959, **81**, 5001-5002.
35. V. Balzani, A. deMeijere, K. N. Houk, H. Kessler, J. M. Lehn, S. V. Ley, S. L. Schreiber, J. Thiem, B. M. Trost, F. Vögtle and H. Yamamoto, *Photochemistry and Photophysics of Coordination Compounds I*, 2007.
36. Y. Qin and Q. Peng, *Int. J. Photoenergy*, 2012, **2012**, 1-22.
37. F. Heinemann, J. Karges and G. Gasser, *Acc. Chem. Res.*, 2017, **50**, 2727-2736.

38. K. Rangan, S. M. Arachchige, J. R. Brown and K. J. Brewer, *Energy Environ. Sci.*, 2009, **2**, 410-419.
39. A. Juris, V. Balzani, F. Barigelletti, S. Campagna, P. Belser and A. von Zelewsky, *Coord. Chem. Rev.*, 1988, **84**, 85-277.
40. J. M. Calvert, J. V. Caspar, R. A. Binstead, T. D. Westmoreland and T. J. Meyer, *J. Am. Chem. Soc.*, 1982, **104**, 6620-6627.
41. C. E. Welby, S. Grkinic, A. Zahid, B. S. Uppal, E. A. Gibson, C. R. Rice and P. I. P. Elliott, *Dalton Trans.*, 2012, **41**, 7637-7646.
42. G. J. Wilson, W. H. F. Sasse and A. W. H. Mau, *Chem. Phys. Lett.*, 1996, **250**, 583-588.
43. K. A. King, P. J. Spellane and R. J. Watts, *J. Am. Chem. Soc.*, 1985, **107**, 1431-1432.
44. S. Lamansky, P. Djurovich, D. Murphy, F. Abdel-Razzaq, R. Kwong, I. Tsyba, M. Bortz, B. Mui, R. Bau and M. E. Thompson, *Inorg. Chem.*, 2001, **40**, 1704-1711.
45. M. A. Baldo, S. Lamansky, P. E. Burrows, M. E. Thompson and S. R. Forrest, *Appl. Phys. Lett.*, 1999, **75**, 4-6.
46. A. B. Tamayo, B. D. Alleyne, P. I. Djurovich, S. Lamansky, I. Tsyba, N. N. Ho, R. Bau and M. E. Thompson, *J. Am. Chem. Soc.*, 2003, **125**, 7377-7387.
47. F. Neve, M. La Deda, A. Crispini, A. Bellusci, F. Puntoriero and S. Campagna, *Organometallics*, 2004, **23**, 5856-5863.
48. Q. Zhao, S. Liu, M. Shi, C. Wang, M. Yu, L. Li, F. Li, T. Yi and C. Huang, *Inorg. Chem.*, 2006, **45**, 6152-6160.
49. A. B. Tamayo, S. Garon, T. Sajoto, P. I. Djurovich, I. M. Tsyba, R. Bau and M. E. Thompson, *Inorg. Chem.*, 2005, **44**, 8723-8732.
50. V. Balzani, A. d. Meijere, K. N. Houk, H. Kessler, J. M. Lehn, S. V. Ley, S. L. Schreiber, J. Thiem, B. M. Trost, F. Vögtle and H. Yamamoto, *Photochemistry and Photophysics of Coordination Compounds II*, 2007.
51. H. Wang, Q. Liao, H. Fu, Y. Zeng, Z. Jiang, J. Ma and J. Yao, *J. Mater. Chem.*, 2009, **19**, 89-96.
52. W. Holzer, A. Penzkofer and T. Tsuboi, *Chem. Phys.*, 2005, **308**, 93-102.
53. M. G. Colombo, T. C. Brunold, T. Riedener, H. U. Guedel, M. Fortsch and H.-B. Büergi, *Inorg. Chem.*, 1994, **33**, 545-550.
54. T. Hofbeck and H. Yersin, *Inorg. Chem.*, 2010, **49**, 9290-9299.

55. M. K. Nazeeruddin, C. Klein, M. Grätzel, L. Zuppiroli and D. Berner, in *Highly Efficient OLEDs with Phosphorescent Materials*, Wiley-VCH Verlag GmbH & Co. KGaA, 2008, DOI: 10.1002/9783527621309.ch11, pp. 363-390.
56. L. F. Gildea and J. A. G. Williams, in *Organic Light-Emitting Diodes (OLEDs)*, Woodhead Publishing, 2013, ch. 3, pp. 77-113.
57. C. E. Housecroft and E. C. Constable, *Coord. Chem. Rev.*, 2017, **350**, 155-177.
58. C. E. Housecroft and E. C. Constable, in *Light-Emitting Electrochemical Cells: Concepts, Advances and Challenges*, ed. R. D. Costa, Springer International Publishing, Cham, 2017, ch. 7, pp. 167-202.
59. P. Pla, J. M. Junquera-Hernandez, H. J. Bolink and E. Orti, *Dalton Trans.*, 2015, **44**, 8497-8505.
60. C. H. Hsieh, F. I. Wu, C. H. Fan, M. J. Huang, K. Y. Lu, P. Y. Chou, Y. H. O. Yang, S. H. Wu, I. C. Chen, S. H. Chou, K. T. Wong and C. H. Cheng, *Chem. Eur. J.*, 2011, **17**, 9180-9187.
61. M. K. Nazeeruddin, R. Humphry-Baker, D. Berner, S. Rivier, L. Zuppiroli and M. Graetzel, *J. Am. Chem. Soc.*, 2003, **125**, 8790-8797.
62. J. Brooks, Y. Babayan, S. Lamansky, P. I. Djurovich, I. Tsyba, R. Bau and M. E. Thompson, *Inorg. Chem.*, 2002, **41**, 3055-3066.
63. W. J. Finkenzeller and H. Yersin, *Chem. Phys. Lett.*, 2003, **377**, 299-305.
64. W. J. Finkenzeller, P. Stößel and H. Yersin, *Chem. Phys. Lett.*, 2004, **397**, 289-295.
65. D. L. Davies, M. P. Lowe, K. S. Ryder, K. Singh and S. Singh, *Dalton Trans.*, 2011, **40**, 1028-1030.
66. M. K. Nazeeruddin, R. T. Wegh, Z. Zhou, C. Klein, Q. Wang, F. De Angelis, S. Fantacci and M. Grätzel, *Inorg. Chem.*, 2006, **45**, 9245-9250.
67. J. D. Slinker, A. A. Gorodetsky, M. S. Lowry, J. Wang, S. Parker, R. Rohl, S. Bernhard and G. G. Malliaras, *J. Am. Chem. Soc.*, 2004, **126**, 2763-2767.
68. M. S. Lowry, J. I. Goldsmith, J. D. Slinker, R. Rohl, R. A. Pascal, G. G. Malliaras and S. Bernhard, *Chem. Mater.*, 2005, **17**, 5712-5719.
69. I. Avilov, P. Minoofar, J. Cornil and L. De Cola, *J. Am. Chem. Soc.*, 2007, **129**, 8247-8258.
70. L. He, J. Qiao, L. Duan, G. Dong, D. Zhang, L. Wang and Y. Qiu, *Adv. Funct. Mater.*, 2009, **19**, 2950-2960.

71. D. Tordera, A. M. Bünzli, A. Pertegás, J. M. Junquera-Hernández, E. C. Constable, J. A. Zampese, C. E. Housecroft, E. Ortí and H. J. Bolink, *Chem. Eur. J.*, 2013, **19**, 8597-8609.
72. R. D. Costa, F. J. Cespedes-Guirao, E. Orti, H. J. Bolink, J. Gierschner, F. Fernandez-Lazaro and A. Sastre-Santos, *Chem. Commun.*, 2009, 3886-3888.
73. B. Beyer, C. Ulbricht, D. Escudero, C. Friebe, A. Winter, L. González and U. S. Schubert, *Organometallics*, 2009, **28**, 5478-5488.
74. J. I. Goldsmith, W. R. Hudson, M. S. Lowry, T. H. Anderson and S. Bernhard, *J. Am. Chem. Soc.*, 2005, **127**, 7502-7510.
75. F. Neve, M. L. Deda, F. Puntoriero and S. Campagna, *Inorg. Chim. Acta*, 2006, **359**, 1666-1672.
76. J. Li, P. I. Djurovich, B. D. Alleyne, M. Yousufuddin, N. N. Ho, J. C. Thomas, J. C. Peters, R. Bau and M. E. Thompson, *Inorg. Chem.*, 2005, **44**, 1713-1727.
77. A. R. McDonald, D. Mores, C. de Mello Donegá, C. A. van Walree, R. J. M. Klein Gebbink, M. Lutz, A. L. Spek, A. Meijerink, G. P. M. van Klink and G. van Koten, *Organometallics*, 2009, **28**, 1082-1092.
78. N. Jun-ichi, E. Hidenori, I. Takeshi and Y. Yoshiro, *Chem. Lett.*, 2005, **34**, 1378-1379.
79. P. Coppo, E. A. Plummer and L. De Cola, *Chem. Commun.*, 2004, 1774-1775.
80. S. Stagni, S. Colella, A. Palazzi, G. Valenti, S. Zacchini, F. Paolucci, M. Marcaccio, R. Q. Albuquerque and L. De Cola, *Inorg. Chem.*, 2008, **47**, 10509-10521.
81. T. Fei, X. Gu, M. Zhang, C. Wang, M. Hanif, H. Zhang and Y. Ma, *Synth. Met.*, 2009, **159**, 113-118.
82. M. Xu, R. Zhou, G. Wang, Q. Xiao, W. Du and G. Che, *Inorg. Chim. Acta*, 2008, **361**, 2407-2412.
83. H. Jang, C. H. Shin, N. G. Kim, K. Y. Hwang and Y. Do, *Synth. Met.*, 2005, **154**, 157-160.
84. L. Zhang, B. Li, L. Shi and W. Li, *Opt. Mater.*, 2009, **31**, 905-911.
85. S. Lamansky, P. Djurovich, D. Murphy, F. Abdel Razzaq, H. E. Lee, C. Adachi, P. E. Burrows, S. R. Forrest and M. E. Thompson, *J. Am. Chem. Soc.*, 2001, **123**, 4304-4312.

86. S. Yi-Hwa, C. Yuan-Chieh, C. Yun, C. Yi-Ming, L. Cheng-Hsuan, C. Pi-Tai, W. Ken-Tsung, T. Ming-Han and W. Chung-Chih, *Chem. Eur. J.*, 2008, **14**, 5423-5434.
87. C. H. Yang, S. W. Li, Y. Chi, Y. M. Cheng, Y. S. Yeh, P. T. Chou, G. H. Lee, C. H. Wang and C. F. Shu, *Inorg. Chem.*, 2005, **44**, 7770-7780.
88. T. T., S. N., S. T. and T. S., *Adv. Mater.*, 2003, **15**, 1455-1458.
89. F. De Angelis, S. Fantacci, N. Evans, C. Klein, S. M. Zakeeruddin, J.-E. Moser, K. Kalyanasundaram, H. J. Bolink, M. Grätzel and M. K. Nazeeruddin, *Inorg. Chem.*, 2007, **46**, 5989-6001.
90. J. A. G. Williams, in *Photochemistry and Photophysics of Coordination Compounds II*, eds. V. Balzani and S. Campagna, Springer Berlin Heidelberg, Berlin, Heidelberg, 2007, pp. 205-268.
91. B. Ventura, A. Barbieri, A. Zanelli, F. Barigelletti, J. B. Seneclauze, S. Diring and R. Ziessel, *Inorg. Chem.*, 2009, **48**, 6409-6416.
92. K. M. C. Wong, W. S. Tang, X. X. Lu, N. Zhu and V. W. W. Yam, *Inorg. Chem.*, 2005, **44**, 1492-1498.
93. R. C. Evans, P. Douglas, J. A. G. Williams and D. L. Rochester, *J Fluoresc*, 2006, **16**, 201-206.
94. J. E. McGarrah, Y.-J. Kim, M. Hissler and R. Eisenberg, *Inorg. Chem.*, 2001, **40**, 4510-4511.
95. A. Islam, H. Sugihara, K. Hara, L. P. Singh, R. Katoh, M. Yanagida, Y. Takahashi, S. Murata, H. Arakawa and G. Fujihashi, *Inorg. Chem.*, 2001, **40**, 5371-5380.
96. C. C. Kwok, H. M. Y. Ngai, S. C. Chan, I. H. T. Sham, C. M. Che and N. Zhu, *Inorg. Chem.*, 2005, **44**, 4442-4444.
97. K. P. Balashev, M. V. Puzyk, V. S. Kotlyar and M. V. Kulikova, *Coord. Chem. Rev.*, 1997, **159**, 109-120.
98. S. S. Pasha, P. Das, N. P. Rath, D. Bandyopadhyay, N. R. Jana and I. R. Laskar, *Inorg. Chem. Commun.*, 2016, **67**, 107-111.
99. E. Baggaley, J. A. Weinstein and J. A. G. Williams, *Coord. Chem. Rev.*, 2012, **256**, 1762-1785.
100. S. W. Botchway, M. Charnley, J. W. Haycock, A. W. Parker, D. L. Rochester, J. A. Weinstein and J. A. G. Williams, *Proc. Natl. Acad. Sci.*, 2008, **105**, 16071-16076.

101. W. A. Tarran, G. R. Freeman, L. Murphy, A. M. Benham, R. Katakya and J. A. G. Williams, *Inorg. Chem.*, 2014, **53**, 5738-5749.
102. R. McGuire, M. C. McGuire and D. R. McMillin, *Coord. Chem. Rev.*, 2010, **254**, 2574-2583.
103. G. S. M. Tong and C. M. Che, *Chem. Eur. J.*, 2009, **15**, 7225-7237.
104. C. K. Koo, K. L. Wong, C. W. Y. Man, Y. W. Lam, L. K. Y. So, H. L. Tam, S. W. Tsao, K. W. Cheah, K. C. Lau, Y. Y. Yang, J. C. Chen and M. H. W. Lam, *Inorg. Chem.*, 2009, **48**, 872-878.
105. W. Lu, B. X. Mi, M. C. W. Chan, Z. Hui, C. M. Che, N. Zhu and S. T. Lee, *J. Am. Chem. Soc.*, 2004, **126**, 4958-4971.
106. H. E., L. B. M. W. and S. U. S., *Adv. Mater.*, 2005, **17**, 1109-1121.
107. Y. Kawamura, K. Goushi, J. Brooks, J. J. Brown, H. Sasabe and C. Adachi, *Appl. Phys. Lett.*, 2005, **86**, 071104.
108. H. Yersin, in *Transition Metal and Rare Earth Compounds: Excited States, Transitions, Interactions III*, Springer Berlin Heidelberg, Berlin, Heidelberg, 2004, pp. 1-26.
109. F. C. Chen, Y. Yang and Q. Pei, *Appl. Phys. Lett.*, 2002, **81**, 4278-4280.
110. T. Hu, L. He, L. Duan and Y. Qiu, *J. Mater. Chem.*, 2012, **22**, 4206-4215.
111. W. L. Wallace and A. J. Bard, *J Phys Chem*, 1979, **83**, 1350-1357.
112. H. Lei, D. Lian, Q. Juan, W. Ruji, W. Peng, W. Liduo and Q. Yong, *Adv. Funct. Mater.*, 2008, **18**, 2123-2131.
113. K. Maeda, A. Xiong, T. Yoshinaga, T. Ikeda, N. Sakamoto, T. Hisatomi, M. Takashima, D. Lu, M. Kanehara, T. Setoyama, T. Teranishi and K. Domen, *Angew. Chem.*, 2010, **122**, 4190-4193.
114. K. Maeda, G. Sahara, M. Eguchi and O. Ishitani, *ACS Catalysis*, 2015, **5**, 1700-1707.
115. P. Du, J. Schneider, P. Jarosz and R. Eisenberg, *J. Am. Chem. Soc.*, 2006, **128**, 7726-7727.
116. A. Singh, K. Teegardin, M. Kelly, K. S. Prasad, S. Krishnan and J. D. Weaver, *J. Organomet. Chem.*, 2015, **776**, 51-59.
117. Y. J. Yuan, Z. T. Yu, D. Q. Chen and Z. G. Zou, *Chem. Soc. Rev.*, 2017, **46**, 603-631.
118. D. Ravelli, S. Protti and M. Fagnoni, *Chem. Rev.*, 2016, **116**, 9850-9913.

119. C. K. Prier, D. A. Rankic and D. W. C. MacMillan, *Chem. Rev.*, 2013, **113**, 5322-5363.
120. J. W. Tucker, J. M. R. Narayanam, P. S. Shah and C. R. J. Stephenson, *Chem. Commun.*, 2011, **47**, 5040-5042.
121. D. L. Ma, W. L. Wong, W. H. Chung, F. Y. Chan, P. K. So, T. S. Lai, Z. Y. Zhou, Y. C. Leung and K. Y. Wong, *Angew. Chem., Int. Ed.*, 2008, **47**, 3735-3739.
122. H. Chen, Q. Zhao, Y. Wu, F. Li, H. Yang, T. Yi and C. Huang, *Inorg. Chem.*, 2007, **46**, 11075-11081.
123. K. K. W. Lo, J. S. Y. Lau, D. K. K. Lo and L. T. L. Lo, *Eur. J. Inorg. Chem.*, 2006, **2006**, 4054-4062.
124. Q. Zhao, F. Li, S. Liu, M. Yu, Z. Liu, T. Yi and C. Huang, *Inorg. Chem.*, 2008, **47**, 9256-9264.
125. C. Wu, K. Vellaisamy, G. Yang, Z. Z. Dong, C. H. Leung, J. B. Liu and D. L. Ma, *Dalton Trans.*, 2017, **46**, 6677-6682.
126. M. L. Ho, Y. M. Cheng, L. C. Wu, P. T. Chou, G. H. Lee, F. C. Hsu and Y. Chi, *Polyhedron*, 2007, **26**, 4886-4892.
127. M. Schmittel and H. Lin, *Inorg. Chem.*, 2007, **46**, 9139-9145.
128. J. C. Araya, J. Gajardo, S. A. Moya, P. Aguirre, L. Toupet, J. A. G. Williams, M. Escadeillas, H. Le Bozec and V. Guerchais, *New J. Chem.*, 2010, **34**, 21-24.
129. Z. Chen, G. Meng, H. Tang, Y. Ye, R. Sun, M. Chen and K. M. Wang, *New J. Chem.*, 2017, **41**, 8312-8319.
130. G. Di Marco, M. Lanza, A. Mamo, I. Stefio, C. Di Pietro, G. Romeo and S. Campagna, *Anal. Chem.*, 1998, **70**, 5019-5023.
131. Y. Mao, Q. Zhao, T. Pan, J. Shi, S. Jiang, M. Chen, B. Zhou and Y. Tian, *New J. Chem.*, 2017, **41**, 5429-5435.
132. M. Licini and J. A. Gareth Williams, *Chem. Commun.*, 1999, 1943-1944.
133. C. Y. S. Chung, S. P. Y. Li, M. W. Louie, K. K. W. Lo and V. W. W. Yam, *Chem. Sci.*, 2013, **4**, 2453-2462.
134. L. He, Y. Li, C. P. Tan, R. R. Ye, M. H. Chen, J. J. Cao, L. N. Ji and Z. W. Mao, *Chem. Sci.*, 2015, **6**, 5409-5418.
135. K. C. Chang, S. S. Sun, M. O. Odago and A. J. Lees, *Coord. Chem. Rev.*, 2015, **284**, 111-123.

136. D. L. Ma, S. Lin, W. Wang, C. Yang and C. H. Leung, *Chem. Sci.*, 2017, **8**, 878-889.
137. Z. B. Zheng, Z. M. Duan, Y. Y. Ma and K. Z. Wang, *Inorg. Chem.*, 2013, **52**, 2306-2316.
138. W. Xu, S. Liu, Q. Zhao, T. Ma, S. Sun, X. Zhao and W. Huang, *Science China Chemistry*, 2011, **54**, 1750-1758.
139. B. Tong, Q. Mei and M. Lu, *Inorg. Chim. Acta*, 2012, **391**, 15-19.
140. D. Hara, H. Komatsu, A. Son, S. I. Nishimoto and K. Tanabe, *Bioconjugate Chem.*, 2015, **26**, 645-649.
141. S. Medina-Rodriguez, S. A. Denisov, Y. Cudre, L. Male, M. Marin-Suarez, A. Fernandez-Gutierrez, J. F. Fernandez-Sanchez, A. Tron, G. Jonusauskas, N. D. McClenaghan and E. Baranoff, *Analyst*, 2016, **141**, 3090-3097.
142. V. M. Manikandamathavan, N. Duraipandy, M. S. Kiran, V. G. Vaidyanathan and B. U. Nair, *RSC Advances*, 2015, **5**, 24877-24885.
143. G. Y. Wiederschain, *Biochemistry (Moscow)*, 2011, **76**, 1276-1276.
144. X. Fei and Y. Gu, *Prog. Nat. Sci.*, 2009, **19**, 1-7.
145. M. S. T. Gonçalves, *Chem. Rev.*, 2009, **109**, 190-212.
146. H. Tsukube and S. Shinoda, *Chem. Rev.*, 2002, **102**, 2389-2404.
147. Q. Zhao, C. Huang and F. Li, *Chem. Soc. Rev.*, 2011, **40**, 2508-2524.
148. L. Murphy, A. Congreve, L. O. Palsson and J. A. G. Williams, *Chem. Commun.*, 2010, **46**, 8743-8745.
149. K. Suhling, P. M. W. French and D. Phillips, *Photochem. Photobiol. Sci.*, 2005, **4**, 13-22.
150. F. R. Svensson, M. Abrahamsson, N. Strömberg, A. G. Ewing and P. Lincoln, *J. Phys. Chem. Lett.*, 2011, **2**, 397-401.
151. M. Yu, Q. Zhao, L. Shi, F. Li, Z. Zhou, H. Yang, T. Yi and C. Huang, *Chem. Commun.*, 2008, 2115-2117.
152. Y. Chen, L. Qiao, L. Ji and H. Chao, *Biomaterials*, 2014, **35**, 2-13.
153. L. Xiong, Q. Zhao, H. Chen, Y. Wu, Z. Dong, Z. Zhou and F. Li, *Inorg. Chem.*, 2010, **49**, 6402-6408.

Chapter Two

**Synthesis and characterisation of cyclometallated
Ir(III) complexes $[\text{Ir}(\text{C}^{\wedge}\text{N})_2(\text{N}^{\wedge}\text{N})]^{\text{n}+}$ ($\text{N}^{\wedge}\text{N} = 2$
pyrazolylpyridine; $n = 0, 1$) for use as pH sensors**

2.1 Introduction

pH is defined by the expression

$$\text{pH} = -\log [\mathbf{a}_{\text{H}^+}] \quad (1)$$

where \mathbf{a}_{H^+} is the activity of the hydrogen ion. In dilute solutions the activity is essentially equal to the concentration and the pH may be approximately defined as

$$\text{pH} = -\log_{10} [\text{H}^+] \quad (2)$$

In water, pH values of less than 7 are characterized as acidic whereas those with a pH greater than 7 are characterized as alkaline, since pH 7 is the centre of the measurement scale, it is neither acidic nor basic and is where the hydrogen ion concentration exactly equals the hydroxide ion concentration at 25°C.

The value of the acid dissociation constant ($\text{p}K_{\text{a}}$) is an important parameter that indicates the degree of ionization of molecules in solution at different pH values. and can be expressed as

$$\text{pH} = \text{p}K_{\text{a}} + \log_{10} \left(\frac{[\text{A}^-]}{[\text{HA}]}\right) \quad (3)$$

For quantitative pH measurements, it is crucial to match the indicator's $\text{p}K_{\text{a}}$ to the pH of the system of interest, which means $\text{p}K_{\text{a}}$ can be defined as the pH at which a compound is 50% ionised. Reliable and accurate monitoring of pH is crucial to an understanding of the many chemical and biological processes that are impacted by the concentration of H^+ . pH is one of the variables most often controlled in biology because enzymatic activities, and therefore metabolism is very sensitive to its change. Therefore, monitoring pH changes inside living cells is critical for studying cellular functions and understanding better physiological and pathological processes.

There are a number of significant properties to be considered in the design of a pH sensor:

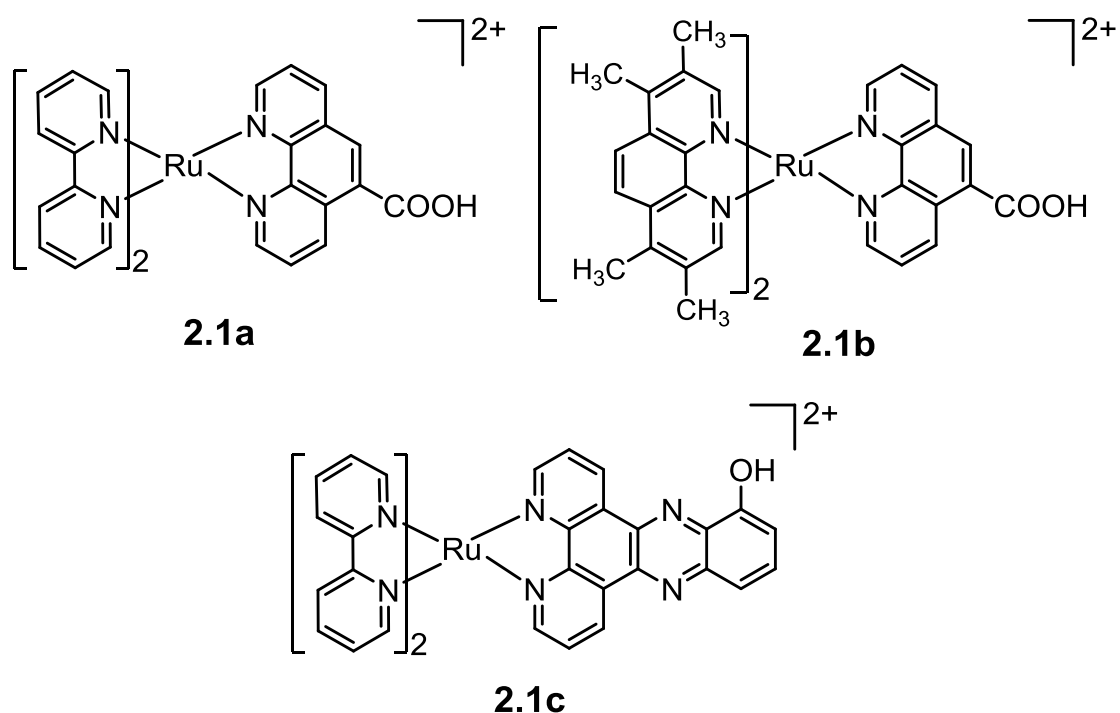
- In biological applications, the range of pH values that are interesting are between pH 6-8,¹ although sensors which are sensitive to more acidic media are also useful in particular for cell's acidic organelles, such as with lysosome whose pH is known to be between 4.5 and 5.5.^{2,3}
- In biological applications, the desired features of luminescent pH sensor include an appropriate $\text{p}K_{\text{a}}$, high extinction coefficient, absorption/excitation and emission bands in the visible region to facilitate the use of low-cost light sources and optical components and, to minimize photobleaching effects, very good

photostability as well as chemical and thermal stability. Fluorescent indicators should also exhibit a large Stokes shift.⁴

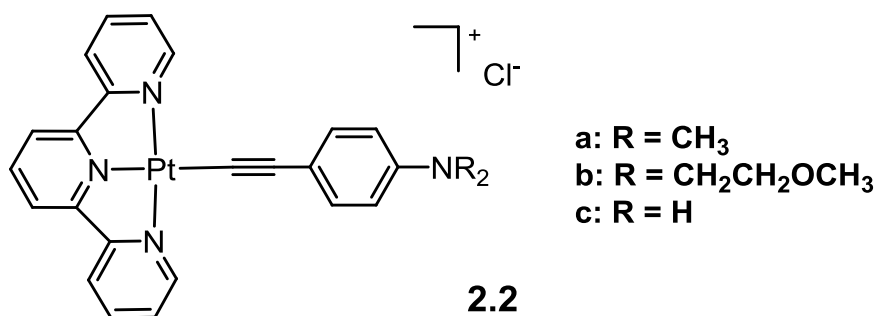
Many methods have been used to monitor pH, particularly in the biological field, including pH-sensitive microelectrodes,⁵ NMR spectroscopy,^{6,7} and optical spectroscopy techniques.⁸⁻¹² Compared to these techniques, luminescent pH sensors have significant advantages due to their excellent sensitivity, minimal damage to living samples, specificity, the availability of a wide range of indicator dyes, high signal-to-noise ratios and the ability to continuously monitor rapid pH changes. Furthermore, fluorescence microscopic imaging allows mapping of the spatial and temporal distribution of H⁺ within living cells.¹³⁻¹⁸

pH sensors have primarily focussed on organic molecules; however, transition metal and rare earth metal complexes have also been recently studied.¹⁹⁻²⁵ In addition to the signal-to-noise advantages inherent to the luminescent measurements mentioned earlier, transition metal complexes (TMCs) have additional merits that make them more attractive as possible pH sensors. These include significant Stokes shifts for easy separation of excitation and emission, emission colour shifts with changing wavelength or intensity, and relatively long emission lifetimes compared to organic molecules^{26,27} (see **Chapter 1** for more details). Currently, the working principle for the design of pH sensors for luminescent metal complexes is to modify a ligand structure to show pH sensitivity. A common approach is to use a ligand, e.g., phen or bpy, containing a pendant functional group such as an amine, or pyridine, which can be protonated, or phenol, pyrazole, imidazole or an acid that can be deprotonated. The reversible acid-base interconversion can lead to significant changes to the optical characteristics of such complexes. Several luminescent complexes of the platinum group metal ions have been used as pH sensors, notably Ru²⁺,²⁸⁻³² Re⁺,³³⁻³⁶ and Pt⁺².^{13, 37, 38}

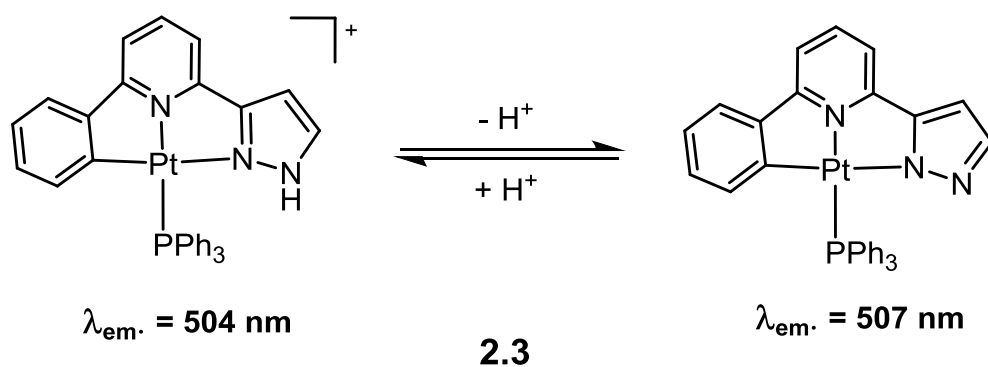
Higgins and DeGraff²⁸ reported that complexes **2.1a-b** work efficiently as pH sensors. Both complexes show good signal-to-noise, even at μM concentrations, and showed changes in both emission intensity and lifetime over the pH range of $2 < \text{pH} < 9$. They have similar $\text{p}K_{\text{a}}$ values of 3 and 4, respectively. The deprotonated forms of the complexes were the stronger emitting and longer-lived species. The authors suggested that the dependence of lifetime on pH could allow for the realization of lifetime-based determination of pH.²⁸



Likewise, the pH effects on the UV-visible and emission spectra of **2.1c** were studied over the pH range 1.0-13.0.³⁹ At pH ~ 6, the UV-visible spectrum of **2.1c** showed four bands at 253, 287, 305 and 443 nm. The lowest-energy absorption MLCT band at 443 nm was almost unchanged over a pH range of 4 to 6; however, between pH 6.0 and 9.0, the intraligand $\pi \rightarrow \pi^*$ (hdppz) transition at 305 nm decreased significantly in intensity and a new band at 330 nm was observed, which was assigned to the $\pi \rightarrow \pi^*$ transition of deprotonated hdppz. The intensities of the $\pi \rightarrow \pi^*$ bands at 253 and 287 nm were moderately reduced, with a blue shift of 5 nm for the band at 287 nm. The ground state pK_a was approximately 7.3. The emission spectrum was strongly sensitive to pH. At pH < 6.0, **2.1c** emitted weakly at 619 nm, which is characteristic of a $^3\text{MLCT}$ ($d\pi(\text{Ru}) \rightarrow d\pi^*(\text{ligand})$) emission state. Upon increasing pH from 6.0 to 11.5, deprotonation of the OH group occurred causing an increase in emission with an on/off ratio of more than 150 with very little change in λ_{max} (ca. 8 nm). The excited-state pK_a^* value is approximately 7.7, about 0.4 units greater than the ground state pK_a , indicating that the excited electron is located on the hdppz rather than the bpy.



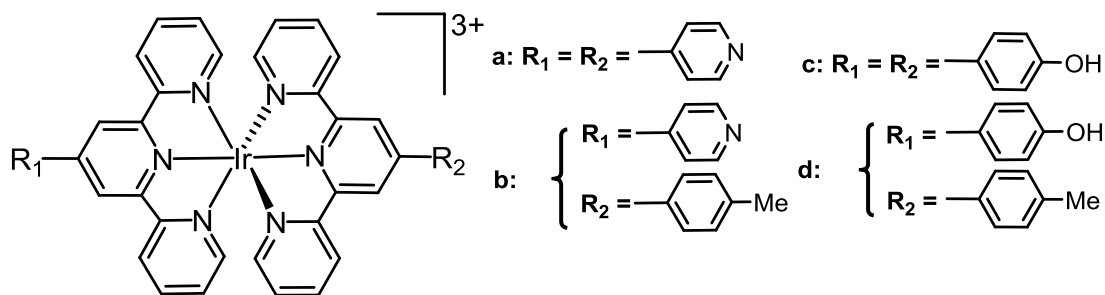
A family of Pt(II) complexes (**2.2a-c**) containing basic amino functionality were employed as colorimetric and luminescent pH sensors.³⁷ Complexes **2.2a-c** exhibit dramatic colour changes upon addition of acid both in organic and in aqueous media, and these are completely reversible upon addition of a base. The electronic absorption spectra of complexes **2.2a-c** in water showed intense absorption bands at 280-290 nm due to the IL transition of the terpyridine ligand, whilst bands at 488-520 nm were assigned to a LLCT transition mixed with MLCT character. The results of pH titrations gave aqueous pK_a values for **2.2a-c** of 3.55, 2.29 and 3.22, respectively. Complexes **2.2a-c** are non-emissive in aqueous solutions in the absence of acid whilst their protonated forms are emissive. These findings demonstrate the capabilities of these complexes to function as colorimetric and luminescence pH sensors.



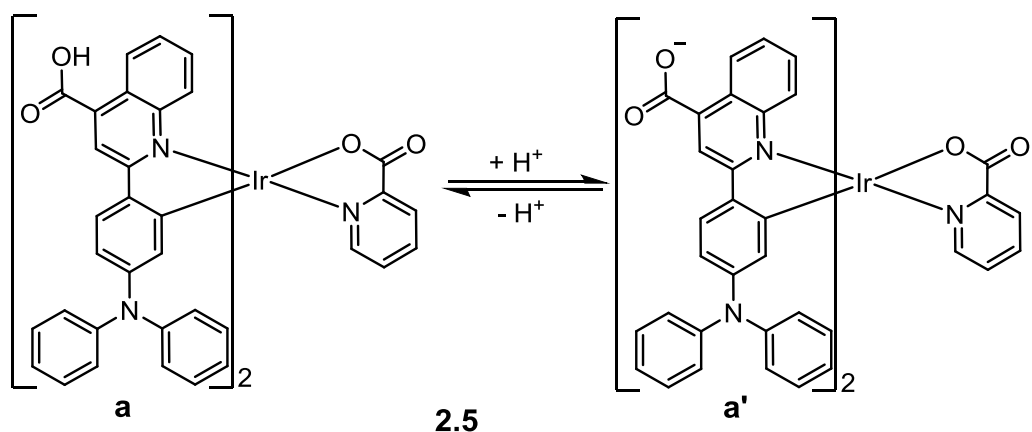
Lam *et al.*⁴⁰ have investigated the potential of complex **2.3** as a pH sensor. They found that increasing the pH from 2.2 to 6.5 caused a continuous red-shift of the absorption bands. The higher energy intraligand absorption band shifts from 313 to 331 nm whilst the lower energy ¹MLCT absorption band shifts from 345 to 355 nm with a well-defined isosbestic point at 322 nm, suggesting a clean conversion between the protonated and deprotonated forms. The complex is relatively weakly luminescent below pH 2.6 with λ_{max} at 504 nm, but on changing to a less acidic environment, i.e., pH > 4.8, led to a small red-shift of the λ_{max} to 507 nm with a three-fold enhancement in emission intensity. The

authors stated that the red-shift in the emission profile is consistent with the reduction of the MLCT energy gap upon the deprotonation of the 1-pyrazolyl-NH. The excited state pK_a was approximately 4.0. Both the pH-induced luminescence and the changes in the absorption spectroscopy of the complex were reversible with alternate addition of base and acid to an acetonitrile solution.

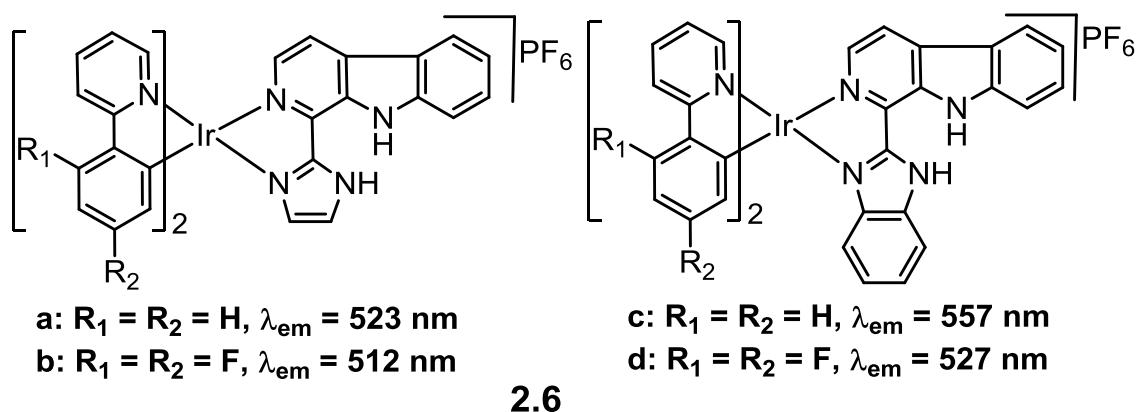
Iridium complexes have also been used for pH sensing. For example, Licini and Williams used Ir bis-terpyridine complexes **2.4a-d** which exhibit changes in lifetime and intensity with changing pH.⁴¹ The absorption spectra of **2.4a-d** in aqueous solution show strong, predominantly ligand-centred transitions in the region 250-400 nm at pH 6. Complexes **2.4a, b** showed no significant change in their absorption spectra upon protonation (pH < 6). In contrast, complexes **2.4c, d** changed from pale yellow at pH 6 to deep orange at pH 10 with the emergence of a new absorption band at 468 nm. The pK_a of **2.4b** is 4.1 (*cf.*, pyridinium has pK_a 5.25) whilst the pK_a of **2.4c** is 8.1 (*cf.*, phenol has pK_a 10.0), in both cases the cationic electron-withdrawing metal terpyridyl unit reduces the basicity of the pendant group, pyridine or phenol, respectively.



Although there are no significant changes in the wavelength of emission of **2.4a-b** upon protonation of the pendent pyridine, the emission intensity at 507 nm of **2.4b** was reduced by *ca.* eight-fold on lowering the pH from 7 to 2. Complex **2.4c** is only weakly emissive and was completely quenched after deprotonation of the OH at pH > 6. Complex **2.4d** is more luminescent and the intensity is only modestly reduced (by a factor of *ca.* 1.6) over the pH range 6-10, where the residual emission at high pH is likely to arise purely from the tolyl-terpyridine ligand. Notably, the lifetime of complex **2.4a** was reduced from 1.1 μ s at pH 7 to 0.34 μ s at pH 2 in air-equilibrated aqueous solution similar effect was seen for **2.4b**. Protonation of the pyridyl nitrogen lowers the energy of the MLCT excited state, which leads to mixing with the emissive LC state, thereby shortening the lifetimes and reducing the intensities.



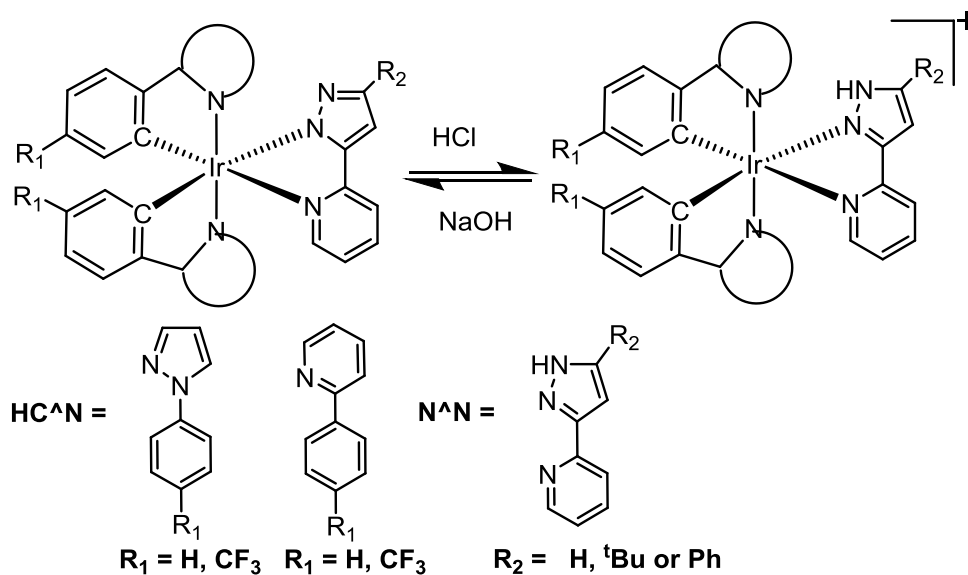
Ir(III) bis-cyclometallated complexes have also been used as pH sensors. For example Huang *et al.*⁴² reported complex **2.5** containing carboxylic acid groups on the cyclometallated ligands. The titration of **2.5a** in an aqueous buffer solution showed that, upon raising the pH from 2 to 4, the absorption spectrum was slightly blue-shifted. (~5 nm) and the absorption intensity of the MLCT band centred at 467 nm declined. Increasing the pH from 4.0 to 8.0 caused the MLCT bands to shift slightly to the blue at 424 nm, and a strong absorption peak at 424 nm was ascribed to the deprotonated form **2.5a'**. Complex **2.5a** was non-emissive at pH 2-5, however upon increasing the pH from 5 to 9, a red emission centred at 625 nm was observed which can be ascribed to the deprotonated form **2.5a'**. The enhancement of the emission at 625 nm based on the pH difference was over 14-fold. The pK_a value was approximately 7.0, suggesting that the probe may be useful for monitoring pH in biological systems.



In 2015, the Mao research group developed four pH-sensitive iridium(III) complexes **2.6a-d** for lysosome targeted photodynamic therapy (PDT).⁴³ Complexes **2.6a-d** showed the phosphorescence with the quantum yield of **2.6a** decreased from 0.077 at pH 3.0 to 0.024 at pH 7.4, with similar results also observed for **2.6b-d**. The excited state pK_a values were between 3.56 and 4.42. Complex **2.6c** was used to monitor lysosomal integrity

during PDT to assess the therapeutic effect. However, the practical application of these photosensitizers in PDT may be limited due to the short excitation wavelength (425 nm). In summary, despite extensive reports on many diverse pH probes, no pH sensors are yet known that perfectly satisfy all the criteria at once, although partial fulfilment may also be useful. The coordination of a functionalised ligand to a metal tends to lead to a reduction in electron density due to electron donation to the metal and hence should lead to a lowering of the pK_a for the ligand in the ground state. However, it should be noted that it is harder to predict the outcome for an excited state. Hence, for pH sensors that are applicable in biological systems it is desirable to choose functional groups that normally have a pK_a which is higher than 8 so that when reduced it may fall within the desired range. Hence, this chapter will focus on ligands with an accessible pyrazole NH; free pyrazole has a pK_a of 19.8,⁴⁴ and the free pyridine pyrazole ligand has a pK_a of 11.6,⁴⁵ however Pt complex **2.3** discussed earlier, featuring a tridentate pyrazole ligand, had an excited state pK_a of 4.0.

This chapter will focus on the synthesis and characterisation of Ir(III) complexes $[\text{Ir}(\text{C}^{\wedge}\text{N})_2(\text{N}^{\wedge}\text{N})]^{n+}$ ($n = 0, 1$) (**Scheme 2.1**). The potential use of these complexes as pH sensors will be investigated, including the effect of changing the heterocycle of the $\text{C}^{\wedge}\text{N}$ and the R groups on subsequent pK_a .

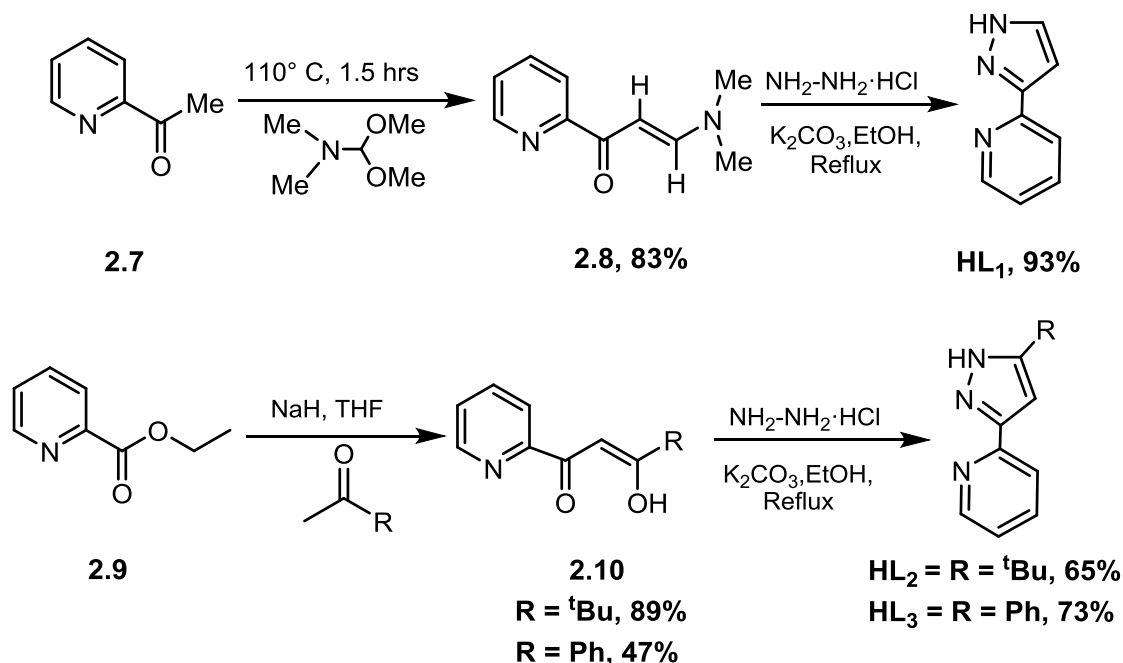


Scheme 2.1

2.2 Results and Discussion

2.2.1 Synthesis of N[^]N Ligands

Ligands **HL**₁₋₃ were synthesized according to literature methods,^{46, 47} as outlined in **Scheme 2.2**. Compound **2.7** was converted to **2.8** under solvent-free conditions and then reacted with hydrazine monohydrochloride to give ligand **HL**₁ in good yield (93%). The ¹H and ¹³C NMR spectra of **HL**₁ are in agreement with the literature.⁴⁸ Ligands **HL**₂ and **HL**₃ were easily obtained by Claisen condensation of **2.9** with the relevant methyl ketone to yield **2.10** (R = ^tBu, 79% and R = Ph 73%), respectively. Subsequently, the compounds **2.10** (R = ^tBu, Ph) were reacted with hydrazine monohydrochloride in the presence of a base to give **HL**₂ and **HL**₃, respectively, in good yields. The ¹H NMR and ¹³C NMR spectra of ligands **HL**₂ and **HL**₃ agree with the literature data.^{47, 49, 50}



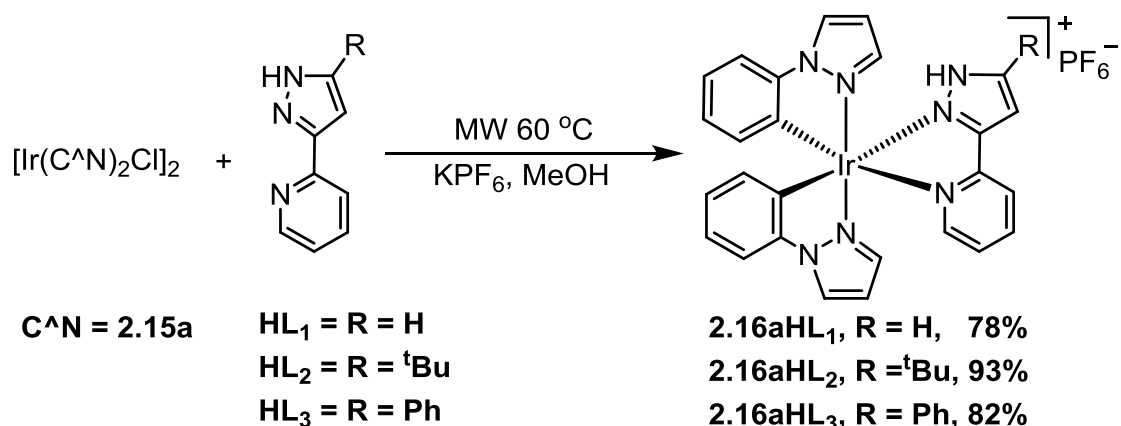
Scheme 2.2: Synthesis of Ligands **HL**₁, **HL**₂ and **HL**₃.

2.2.2 Synthesis of C[^]N Ligands

Ligand **HL**₄ was prepared by a modification of a literature method⁵¹ (**Scheme 2.3**). Compounds **2.11** and **2.12** were heated for 72 hrs. at 110°C in MeCN. After chromatography, **HL**₄ was isolated in good yield (83%) and the ¹H and ¹³C NMR spectra are in agreement with the literature.⁵¹ Ligand **HL**₅ was easily obtained in good yield (73%) by a palladium-catalysed cross-coupling reaction according to the reported method⁵² which is outlined in **Scheme 2.3**. The ¹H and ¹³C NMR spectra of **HL**₅ are also in agreement with the literature.⁵²

2.2.4 Synthesis and Characterisation of Cationic Phenylpyrazole Iridium(III) Complexes

The syntheses of complexes $[\text{Ir}(\text{ppz})_2(\text{N}^{\wedge}\text{NH})]\text{PF}_6$ are outlined in **Scheme 2.5**. The reactions of dimer **2.15a** with ligands (**HL**₁₋₃) and KPF_6 were carried out in methanol at 60°C under microwave irradiation for 20-40 minutes (see experimental section). After work up, complexes **2.16aHL**₁₋₃ were formed in good to excellent yields.



Scheme 2.5: Synthesis of $[\text{Ir}(\text{ppz})_2(\text{N}^{\wedge}\text{NH})]\text{PF}_6$ **2.16aHL**₁₋₃

¹H and ¹³C NMR spectra for all the complexes were assigned using two-dimensional NMR experiments such as TOCSY, COSY, NOESY, and HMQC. The ¹H and ¹³C NMR spectra of **2.16aHL**₁₋₃ are similar to each other for the cyclometallating ligands; therefore, only the assignment of complex **2.16aHL**₁ is discussed in detail.

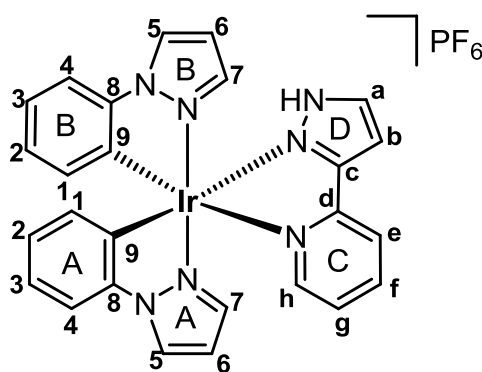


Figure 2.1: Proton numbering for ¹H NMR assignment of complex **2.16aHL**₁

The coordination of the $\text{N}^{\wedge}\text{N}$ ligand removes the C_2 symmetry of the dimers, causing the two $\text{C}^{\wedge}\text{N}$ ligands to become inequivalent and therefore doubling the number of peaks; hence, the ¹H NMR spectrum of complex **2.16aHL**₁ contained twenty-one aromatic environments. Important parts of the TOCSY and NOESY spectra of **2.16HL**₁ are displayed in **Figs. 2.2-3**, respectively.

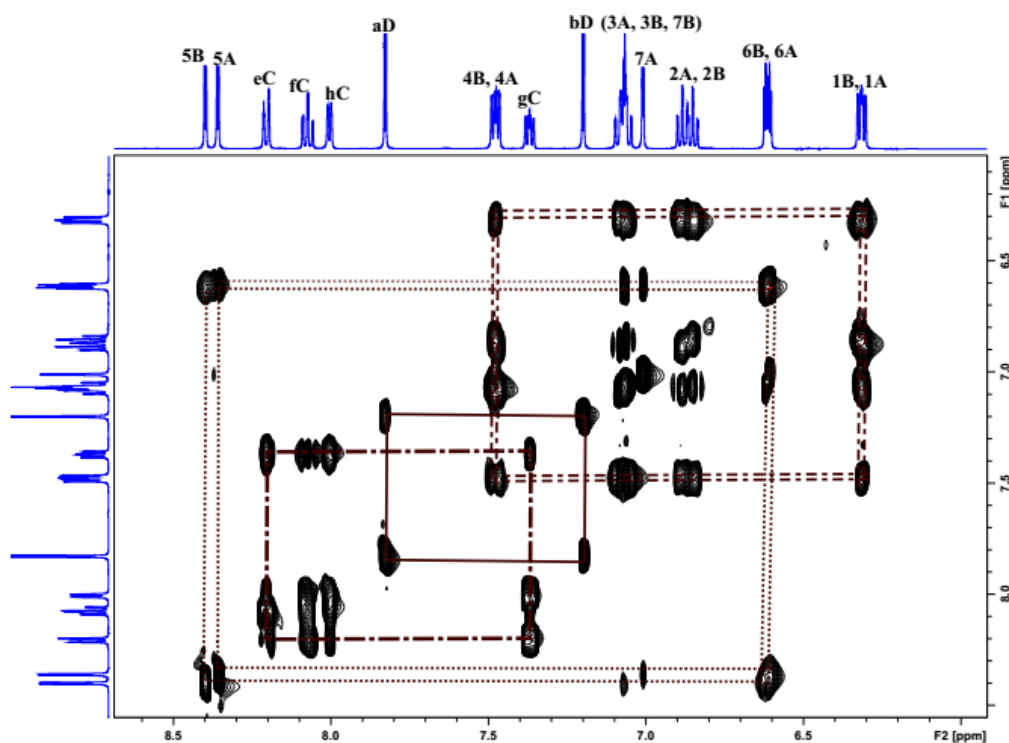


Figure 2.2: Region of the TOCSY spectrum of **2.16aHL₁** showing identification of two cyclometallated phenyls A, B (-----), two pyrazoles A, B (·····), one pyridine C (— · — · — ·) and the other pyrazole D (——) ring, (500 MHz, 298 K in CD₃CN).

The TOCSY spectrum of complex **2.16aHL₁** (**Fig. 2.2**) shows two doublets of doublets at high field (δ 6.30, 6.32), assigned to protons H_{1A} and H_{1B} which are to high field due to ring current effects.⁵⁷ This then allows assignment of the signals for the phenyl (H_{A, B}) and pyrazole (H_{A, B}) rings using the TOCSY and NOESY spectroscopy. Likewise, the protons of pyrazole (D), (H_a and H_b) were easily identified in the TOCSY spectrum as doublets at δ 7.83 and δ 7.20, respectively, which are slightly shifted downfield compared to the free ligand (by *ca.* δ 0.4 and 0.2, respectively) which may be due to the coordination of the (N[^]N) ligand to the metal. H_b shows an NOE to a doublet of triplets at *ca.* δ 8.20 which is therefore assigned as H_e for pyridine (C) (**Fig. 2.3**) and the TOCSY and COSY spectra then allow for assignment of other pyridine proton peaks H_{f-h}. Protons H_{e-g} are shifted slightly downfield compared to the free ligand (*ca.* δ 0.2 to 0.4) as might be expected on coordination to the metal, whilst proton H_h (δ 8.01) is observed about δ 0.7 upfield compared to the free ligand (δ 8.68) due to ring currents from the neighbouring phenyl ring (A), as noted previously, e.g. [Ir(R-ppz)₂(bipy)]PF₆.⁵³ Proton H_h also shows an NOE to a pyrazole proton multiplet at *ca.* δ 7.07 which is therefore assigned as H_{7B}. The other pyrazole protons H_{6B} and H_{5B}, a triplet at δ 6.62 and a doublet at δ 8.40 can

then be assigned via the TOCSY spectrum. H_{5B} is a doublet at δ 8.40 which shows an NOE to a doublet of doublets at δ 7.50 which is therefore assigned as H_{4B}, and the other phenyl protons H_{(1-3)B} can then assigned via the COSY and TOCSY spectra. Proton H_{1B} shows an NOE to the pyrazole proton H_{7A} and the TOCSY spectrum then allows assignment of the other pyrazole protons H_{(5,6)A} at, δ 8.36 and 6.61 respectively.

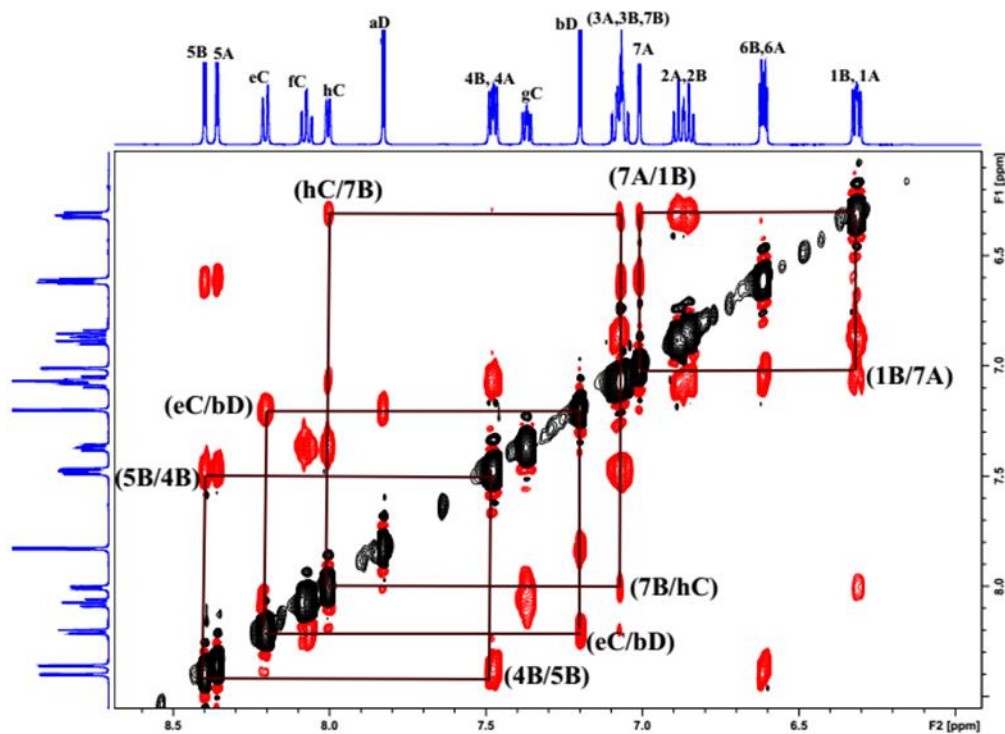


Figure 2.3: NOESY spectrum of **2.16aHL₁** showing some key NOEs (500 MHz, 298 K in CD₃CN).

Proton H_{5A} gives a doublet at *ca.* δ 8.36 and shows an NOE to a doublet of doublets at δ 7.47 which is therefore assigned as phenyl proton H_{4A} and the other phenyl protons H_{(1-3)A} can thus assigned via the COSY and TOCSY spectra. Notably the pyrazole protons H_{5A}, H_{5B} are the most downfield signals. The NH proton was not observed, probably due to exchange with D₂O in the solvent (CD₃CN). Having assigned the proton spectrum, the ¹³C NMR spectrum showed the expected number of signals, with two downfield quaternary resonances corresponding to C_c and C_d at δ 154.0 and δ 153.3, respectively, with the other carbons being assigned using the HSQC spectrum and the quaternary carbons C_{(8-9)A,B} assigned using the HMBC spectrum. The high-resolution mass spectrum (ASAP) shows a molecular ion for the cation at *m/z* 624.1497 (624.1488 calculated for C₂₆H₂₁IrN₇), with characteristic ¹⁹³Ir isotopes pattern

The ^1H NMR spectrum of **2.16aHL**₂ is similar to **2.16aHL**₁ except for the ^tBu group which is observed as a singlet at δ 1.26. As for **2.16aHL**₁, the phenyl protons H_{1A} and H_{1B} are observed as doublet of doublets at high field (δ 6.19 and 6.28, respectively). Proton H_b in pyrazole (D) is easily identified as the only other singlet at δ 6.78. and H_b shows an NOE to a multiplet at *ca.* δ 7.96 which is therefore assigned as H_e of pyridine (C). The other pyridine protons H_{f, g, h} can then be assigned via the COSY and TOCSY spectra and H_h (δ 7.92) is again observed about δ 0.7 upfield compared to the free ligand. The pyridine proton H_h shows an NOE to pyrazole and phenyl protons H_{7B} and H_{1A} which then allows assignment of the other protons of the pyrazole H_{B(5-7)} and phenyl H_{A(1-4)} rings using the COSY and TOCSY spectra. The ^{13}C NMR spectrum shows the expected number of signals. The high-resolution mass spectrum (ASAP) shows an ion at m/z 680.2145 (680.2114 calculated for C₃₀H₂₉IrN₇), with characteristic ^{193}Ir isotopes pattern

The ^1H and ^{13}C NMR spectra of **2.16aHL**₃ are similar to **2.16aHL**₁ and **2.16aHL**₂ except an additional five protons are observed in the aromatic region due to the Ph group on the ring of pyrazole D. A singlet at *ca.* δ 7.51 corresponds to H_b of pyrazole (D) and this shows an NOE to a multiplet at *ca.* δ 7.74 assigned to the *ortho* phenyl protons of the pyrazole substituent and another NOE to a doublet of doublet of doublets at *ca.* δ 8.22 assigned to proton H_e of pyridine C. This leads to assignment of protons H_{f-h}, with H_h (δ 7.99) being about δ 0.6 upfield from the corresponding proton in the free ligand. Once again, protons H_{1B} and H_{1A} were observed as doublets of doublets at high field, δ 6.32 and δ 6.28, respectively, and a downfield singlet at δ 12.01 was assigned to the NH proton. The other signals were assigned in the same way as for the previous two complexes. The ^{13}C NMR spectra showed the expected signals. The high-resolution mass spectrum (ASAP) showed a molecular ion for the cation at m/z 700.1821 (700.1801 calculated for C₃₂H₂₅IrN₇), with characteristic ^{193}Ir isotopes pattern

Crystallisation of **2.16aHL**₁₋₃ from DCM/hexane afforded crystals suitable for X-ray crystallography. The X-ray crystal structures of **2.16aHL**₁₋₃ were determined and are shown with selected bond lengths (\AA) and angles ($^\circ$) in **Fig. 2.4.**, and are reported in **Table 2.1.**

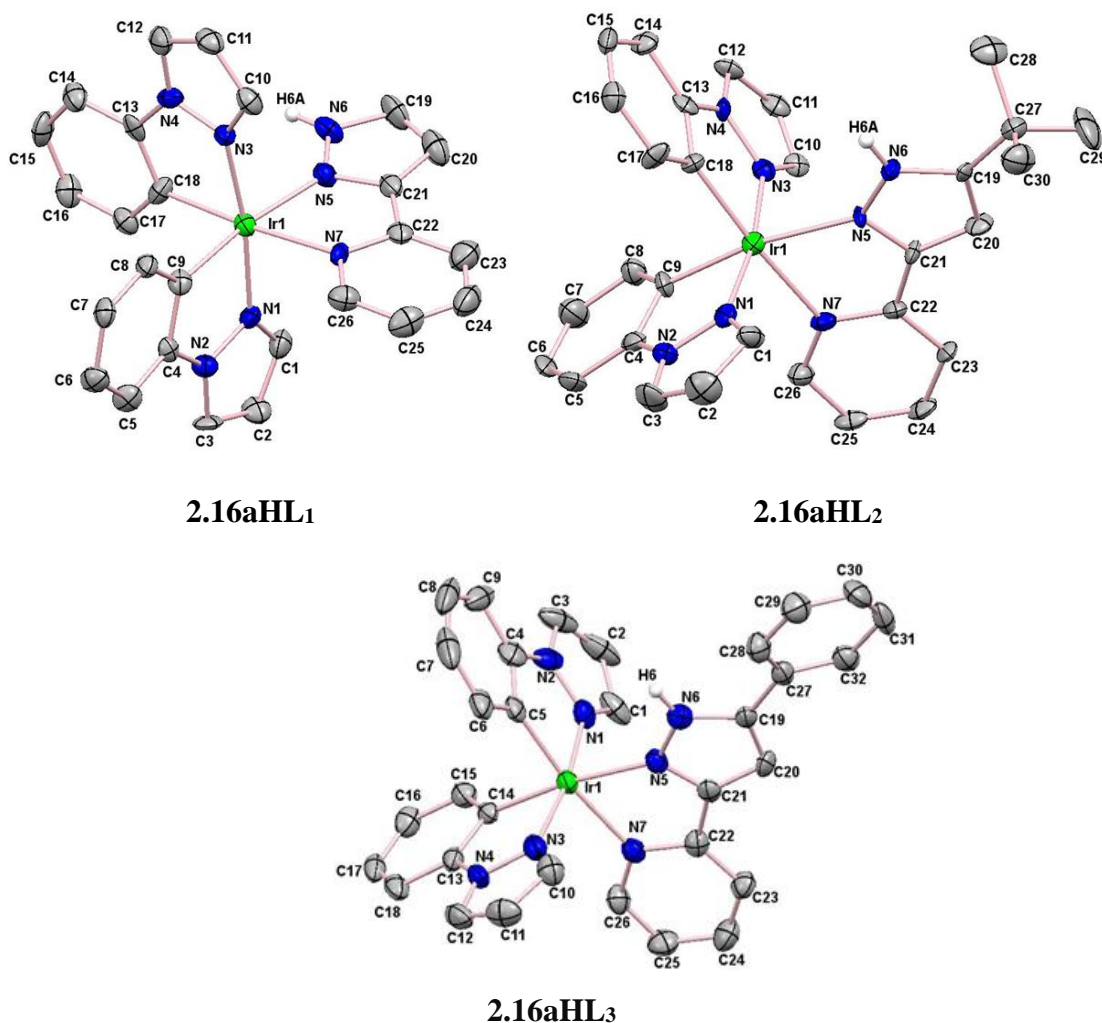


Figure 2.4: X-ray crystal structure of the cations of **2.16aHL₁₋₃** showing 50% ellipsoids, the hydrogens (except NH) have been omitted for clarity.

The crystal structure of **2.16aHL₁₋₃** reveals the expected distorted octahedral coordination geometry with *cis* metallated carbons and *trans* nitrogen atoms (**Fig. 2.4**). The chelate bite angles for the cyclometallated ligands are all about 80°, and about 75° for the N[^]N ligands, considerably less than the ideal 90°. For complex **2.16aHL₁**, the Ir–N bond lengths to the N[^]N ligand [Ir(1)–N(5), 2.116(7) and Ir(1)–N(7), 2.148(6) Å] are longer than those to the cyclometallating ligands [Ir(1)–N(1), 2.036(7), and Ir(1)–N(3), 2.031(6) Å] due to the former being *trans* to the C atoms, as observed previously e.g., [Ir(C[^]N)₂(pta-R)], (pta = pyridinetriazole, R = e.g., CH₃, Ph, Ph-Me Ph-OMe) and [Ir(C[^]N)₂(bipy)]⁺.⁵⁸⁻⁶¹ Similar trends are seen for complexes **2.16aHL₂₋₃**.

Table 2.1: Selected bond lengths (Å) and angles (°) for **2.16aHL₁**, **2.16aHL₂** and **2.16aHL₃**.

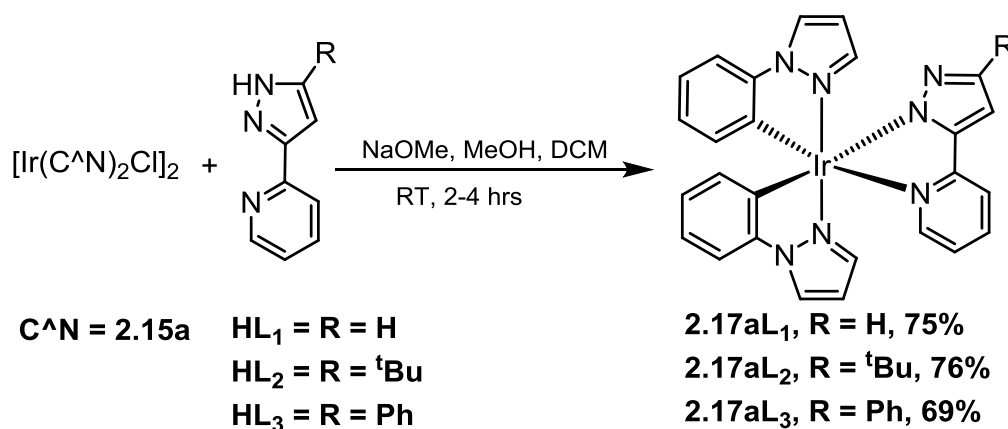
(Å)	2.16aHL₁	2.16aHL₂	2.16aHL₃
Ir(1)—N(1)	2.036(7)	2.033(10)	2.005(6)
Ir(1)—N(3)	2.031(6)	2.033(9)	2.014(5)
Ir(1)—N(5)	2.116(7)	2.175(8)	2.121(5)
Ir(1)—N(7)	2.148(6)	2.160(8)	2.148(5)
Ir(1)—C(9)	2.024(8)	1.989(10)	2.008(7) ^a
Ir(1)—C(18)	2.039(8)	2.005(10)	2.015(6) ^b
(°)			
N(1)—Ir(1)—C(9)	80.2(3)	79.8(4)	80.3(3) ^a
N(3)—Ir(1)—C(18)	80.3(3)	79.6(4)	80.1(2) ^b
N(5)—Ir(1)—N(7)	75.1(3)	75.7(3)	75.7(2)

^a Ir(1)—C(5); N(1)-Ir(1)—C(5) and

^b Ir(1)—C(14); N(3)—Ir(1)—C(14)

2.2.5 Synthesis and Characterisation of Neutral Phenylpyrazole Iridium(III) Complexes

The dimer **2.15a** reacted with ligands **HL₁-HL₃** and NaOMe in a mixture of DCM/methanol (2:1) to form complexes [Ir(ppz)₂(N[^]N)] (**2.17aL₁₋₃**) in good yields (Scheme 2.6).



Scheme 2.6: Synthesis of [Ir(ppz)₂(N[^]N)] **2.17aL₁₋₃**

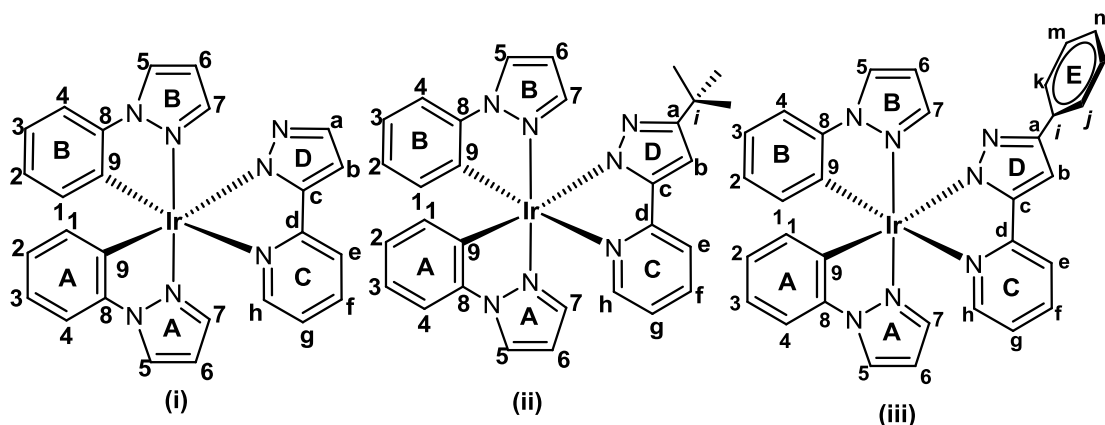


Figure 2.5: Proton numbering for ^1H NMR assignment of (i) **2.17aL₁**, (ii) **2.17aL₂**, and (iii) **2.17aL₃**, respectively.

The ^1H and ^{13}C NMR spectra of **2.17aL₁**, **2.17aL₂** and **2.17aL₃** are similar to those found for **2.16aHL₁**, **2.16aHL₂** and **2.16aHL₃**, respectively, and assignments have been made on this basis. As expected, in the majority of cases the deprotonation of the ancillary ligand causes an upfield shift of the 2-pyrazolylpyridine protons compared to their corresponding cationic complexes. This will be discussed in detail below.

The ^1H NMR spectrum of complex **2.17aL₁** contains twenty aromatic environments. The protons $\text{H}_{1\text{A},1\text{B}}$ are again observed at high field (δ 6.22, 6.34, respectively) due to ring current effects. Protons $\text{H}_{\text{a-b}}$ are observed as mutually coupled doublets at δ 7.47 and 6.82, respectively, upfield compared to the corresponding signals in the cationic complex **2.16aHL₁** (δ 7.83 and 7.20 respectively) consistent with deprotonation of the pyrazole. Proton H_{b} shows an NOE to a multiplet at *ca.* δ 7.89, which is therefore assigned as the pyridine C proton H_{e} , whilst the other pyridine protons $\text{H}_{\text{f-h}}$ are assigned via the COSY and TOCSY spectra. Pyridine protons $\text{H}_{\text{e-g}}$ are slightly (*ca.* δ 0.3) upfield from the corresponding protons in **2.16aHL₁** suggesting some delocalisation of the negative charge onto the pyridine. H_{h} is a multiplet at *ca.* δ 7.87 and shows an NOE to phenyl and pyrazole protons $\text{H}_{1\text{A}}$ and $\text{H}_{7\text{B}}$, respectively, which then allows assignment of all the other protons of the phenyl $\text{H}_{(2-4)\text{A}}$ and pyrazole $\text{H}_{(5-6)\text{B}}$ rings using the TOCSY spectrum. The phenyl protons $\text{H}_{(2-4)\text{A,B}}$ and pyrazole protons $\text{H}_{(5-7)\text{A,B}}$ are shifted slightly upfield compared to the corresponding signals in the cationic complex **2.16aHL₁** (*ca.* δ 0.1 - 0.3), which is expected for the neutral complex **2.17aL₁**. The ^{13}C NMR spectra show the expected signals, and the high-resolution mass spectrum (ASAP) shows an ion due to $[\text{M}+\text{H}]^+$ at m/z 624.1489 (624.1488 calculated for $\text{C}_{26}\text{H}_{21}\text{IrN}_7$), with characteristic ^{193}Ir isotopes pattern

In the ^1H NMR spectrum of **2.17aL₂** the ^tBu group is a singlet at δ 1.29 (*cf.*, δ 1.26 in **2.16aHL₂**). The phenyl protons $\text{H}_{1\text{A},1\text{B}}$ are observed as the two doublets of doublets at high field (δ 6.20 and 6.30 respectively). The only other singlet is assigned to H_b δ 6.49, which is *ca.* 0.3 ppm upfield from the corresponding proton in **2.16aHL₂** (δ 6.78) consistent with deprotonation of pyrazole D. Proton H_b shows an NOE to a broad doublet at δ 7.63 which is therefore assigned as pyridine C proton H_e . Pyridine protons $\text{H}_{\text{h-f}}$ are then assigned via the TOCSY spectrum. The ^{13}C NMR spectra show the expected signals and the high-resolution mass spectrum (ASAP) shows an ion due to $[\text{M}+\text{H}]^+$ at m/z 680.2115 (680.2114 calculated for $\text{C}_{30}\text{H}_{29}\text{IrN}_7$), with characteristic ^{193}Ir isotopes pattern.

The ^1H NMR spectrum of **2.17aL₃** is similar to those recorded for **2.17aL₁** and **2.17aL₂** except for the signals due to the Ph group on the pyrazole ring of the $\text{N}^{\wedge}\text{N}$ ligand. The phenyl protons $\text{H}_{1\text{A}, 1\text{B}}$ are at high field, δ 6.33-6.28, and the only singlet at δ 6.95 is assigned to H_b , which is thus *ca.* δ 0.5 upfield compared to the corresponding proton in **2.16aHL₃** (δ 7.51) due to deprotonation of the pyrazole D. Protons $\text{H}_{\text{e-g}}$ are also shifted (*ca.* δ 0.5 to 0.6) upfield compared to the corresponding signals in cationic complex **2.16aHL₃**, indicating a degree of delocalisation of the negative charge onto the pyridine. All the other protons are within 0.3 ppm of the signals in the corresponding cationic complex **2.16aHL₃**. The ^{13}C NMR spectra show the expected signals and the high-resolution mass spectrum (ASAP) shows an ion due to $[\text{M}+\text{H}]^+$ at m/z 700.1818 (700.1801 calculated for $\text{C}_{32}\text{H}_{25}\text{IrN}_7$), with characteristic ^{193}Ir isotopes pattern.

Crystallisation of **2.17aL₂** from DCM/hexane afforded crystals suitable for X-ray crystallography. The crystal structure of **2.17aL₂** is shown in **Figure 2.6** with selected bond lengths (\AA) and angles ($^\circ$) reported in **Table 2.2**.

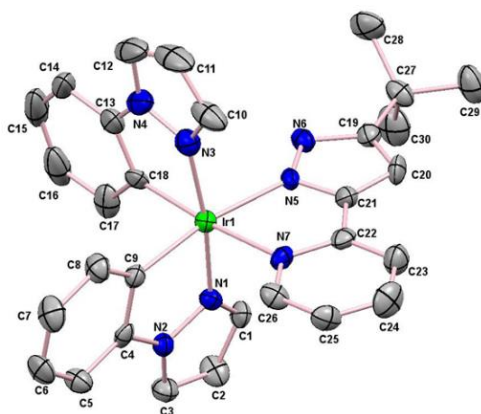
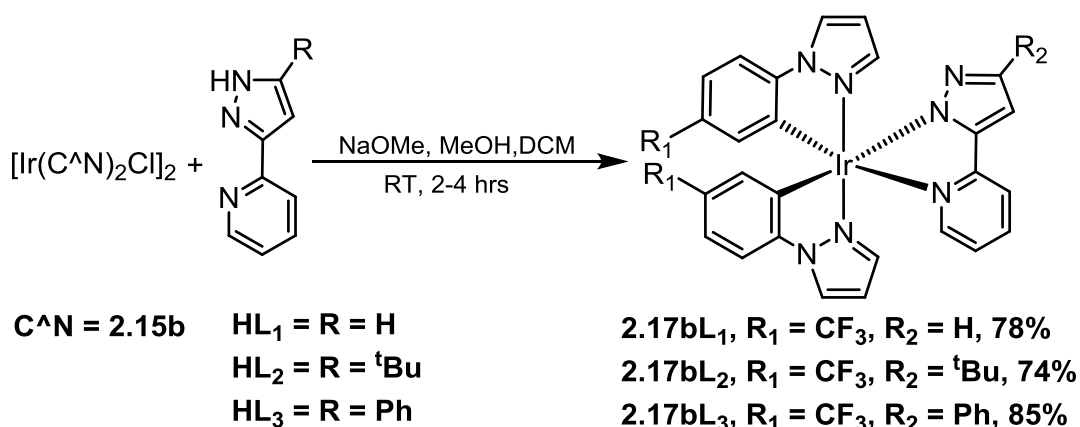


Figure 2.6: X-ray crystal structure for **2.17aL₂** showing 50% ellipsoids. All H atoms are omitted for clarity.

The structure shows a distorted octahedral coordination geometry with *cis* metallated carbons and *trans* pyrazole nitrogen atoms. The chelate bite angles for the cyclometallated ligands are about 80°, and about 76° for the N[^]N ligand, less than the ideal 90°. Table 2.2. shows selected data for neutral and cationic complexes **2.17aL₂** and **2.16aHL₂**. As for **2.16aHL₂**, the Ir—N bond lengths to the N[^]N ligand [Ir(1)—N(5), 2.122(6), and Ir(1)—N(7), 2.148(6) Å] are longer than those to the cyclometallating ligands [Ir(1)—N(1), 2.025(6), and Ir(1)—N(3), 2.015(7) Å] due to the former being *trans* to the C atoms. The Ir(1)—N(5) distance in **2.17aL₂** [2.122(6) Å] with an anionic pyrazolyl pyridine, is shorter than that [2.175(8) Å] in the cationic complex **2.16aHL₂**, though the other Ir—N bonds and Ir—C bonds are statistically almost the same in both complexes. The N[^]N chelate bite angle is very similar in both **2.17aL₂** and **2.16aHL₂**, at 76.8(2) and 75.7(3)°, respectively.

Table 2.2: Selected bond lengths (Å) and angles (°) for **2.17aL₂** and **2.16aHL₂**

(Å)	2.17aL₂	2.16aHL₂
Ir(1)—N(1)	2.025(6)	2.033(10)
Ir(1)—N(3)	2.015(7)	2.033(9)
Ir(1)—N(5)	2.122(6)	2.175(8)
Ir(1)—N(7)	2.148(6)	2.160(8)
Ir(1)—C(9)	2.022(7)	1.989(10)
Ir(1)—C(18)	1.992(8)	2.005(10)
(°)		
N(1)—Ir(1)—C(9)	80.9(3)	79.8(4)
N(3)—Ir(1)—C(18)	80.0(3)	79.6(4)
N(5)—Ir(1)—N(7)	76.8(2)	75.7(3)



Scheme 2.7: Synthesis of $[\text{Ir}(\text{ppz-CF}_3)_2(\text{N}^{\wedge}\text{N})]$ **2.17bL₁₋₃**

Complexes **2.17bL₁₋₃** were synthesised by the same method as for the **2.17aL₁₋₃** (Scheme 2.7) in good yield. In this case only the neutral complexes were made since this was considered sufficient for measuring pH (see section 2.4).

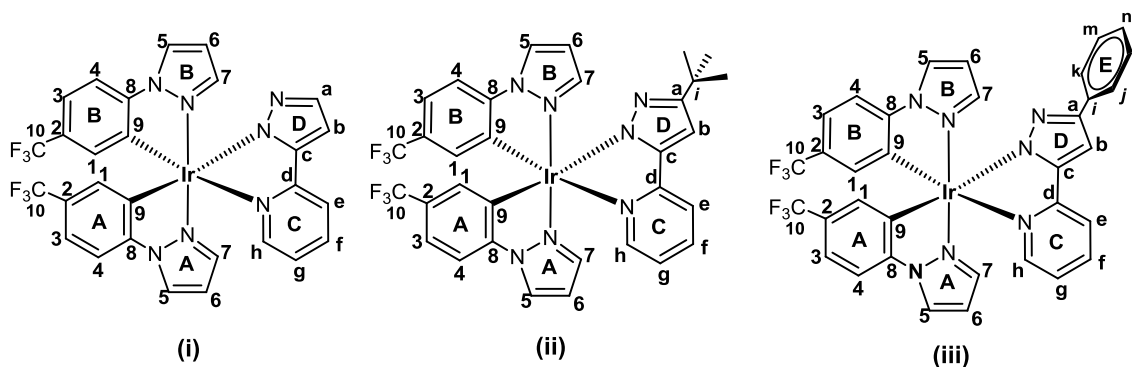


Figure 2.7: Proton numbering for ^1H NMR assignment of (i) **2.17bL₁**, (ii) **2.17bL₂** and (iii) **2.17bL₃**, respectively.

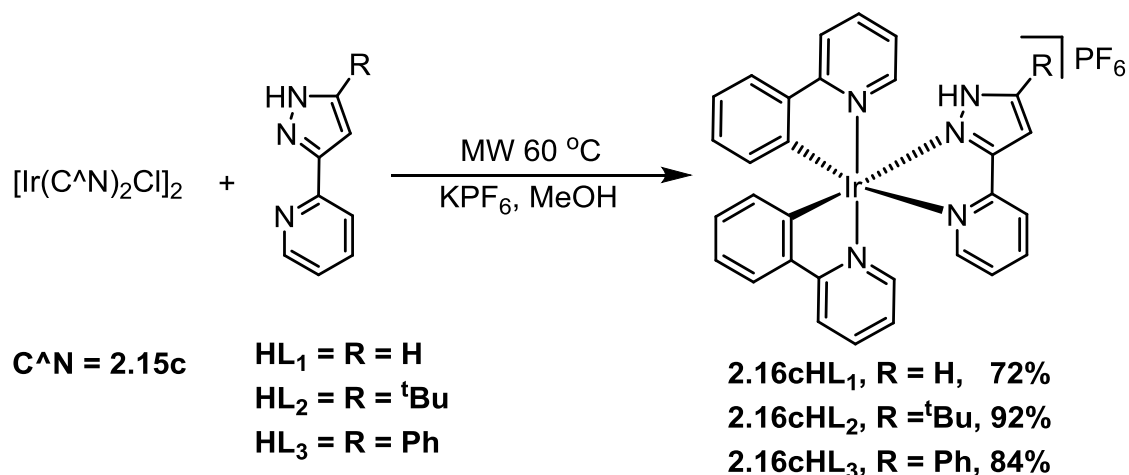
2.17bL₁ is not very soluble in the majority of NMR solvents except DMSO. The ^1H and ^{13}C NMR spectra of **2.17bL₁** are similar to **2.17aL₁**, except there are only three signals for each cyclometallated phenyl, doublets for $\text{H}_{1\text{A},1\text{B}}$, a broad doublet of doublets for $\text{H}_{4\text{A},4\text{B}}$, with proton $\text{H}_{3\text{B}}$ appearing as a doublet of doublets, and $\text{H}_{3\text{A}}$ as a multiplet. Protons $\text{H}_{1\text{A}}, 1\text{B}$ are again at high field (δ 6.51 and 6.35, respectively) and NOEs are observed between $\text{H}_{1\text{A}}$ and H_{h} and between $\text{H}_{1\text{B}}$ and $\text{H}_{7\text{A}}$, with the other NOE between $\text{H}_{1\text{A}}$ and $\text{H}_{7\text{B}}$. The assignments are made on the same basis as for **2.17aL₁**. Proton H_{h} (δ 7.91) is shifted considerably upfield compared to the free ligand (δ 8.68) due to ring currents from the neighbouring phenyl ring A as noted above. In addition to the expected signals, the ^1H NMR showed a broad signal at δ 8.44 that integrated to two protons, and which may be due to a water molecule hydrogen bonded to the pyrazole. The ^{19}F NMR spectrum

exhibited two singlets at $\delta - 61.7$ and $- 61.8$ corresponding to two different CF_3 groups. The ^{13}C NMR spectra show the expected signals and the high-resolution mass spectrum (ESI) shows an ion $[\text{M}+\text{H}]^+$ at m/z 760.1267 (760.1236 calculated for $\text{C}_{28}\text{H}_{19}\text{F}_6\text{IrN}_7$).

The ^1H and ^{13}C NMR spectra of **2.17bL₂** and **2.17bL₃** are similar to **2.17bL₁** except for the pyrazole (D) substituent. All assignments have been on the same basis as **2.17aL₂₋₃**, and indeed the expected NOEs are observed. The only singlet in the aromatic region is therefore assigned to H_b (δ 6.74 and 6.26 for **2.17bL₂** and **2.17bL₃**, respectively). Proton H_h is observed at δ 7.82 and 7.71, for **2.17bL₂** and **2.17bL₃**, respectively, about δ 0.8 upfield from the corresponding proton in the free ligands due to ring currents from the neighbouring phenyl ring (A). The ^{13}C NMR spectra show the expected number of carbon signals for both **2.17bL₂₋₃** and the high-resolution mass spectrum (ESI) spectra shows molecular ions $[\text{M}+\text{H}]^+$ at m/z 816.1871 for **2.17bL₂** (816.1861 calculated for $\text{C}_{32}\text{H}_{27}\text{F}_6\text{IrN}_7$) and 836.1589 for **2.17bL₃** (836.1549 calculated for $\text{C}_{34}\text{H}_{23}\text{F}_6\text{IrN}_7$), with characteristic ^{193}Ir isotopes pattern.

2.2.6 Synthesis and Characterisation of Cationic Phenylpyridine Iridium(III) Complexes

Complexes **2.16cHL₁₋₃** were synthesised using the same method as for **2.16aHL₁₋₃**. The dimer **2.15c** reacts with **HL₁₋₃** and KPF_6 at 60°C under microwave irradiation for 20-40 mins to form compounds **2.16cHL₁₋₃** in good yields (Scheme 2.8).



Scheme 2.8: Synthesis of $[\text{Ir}(\text{ppy})_2(\text{N}^{\text{A}}\text{NH})]\text{PF}_6$ **2.16cHL₁₋₃**

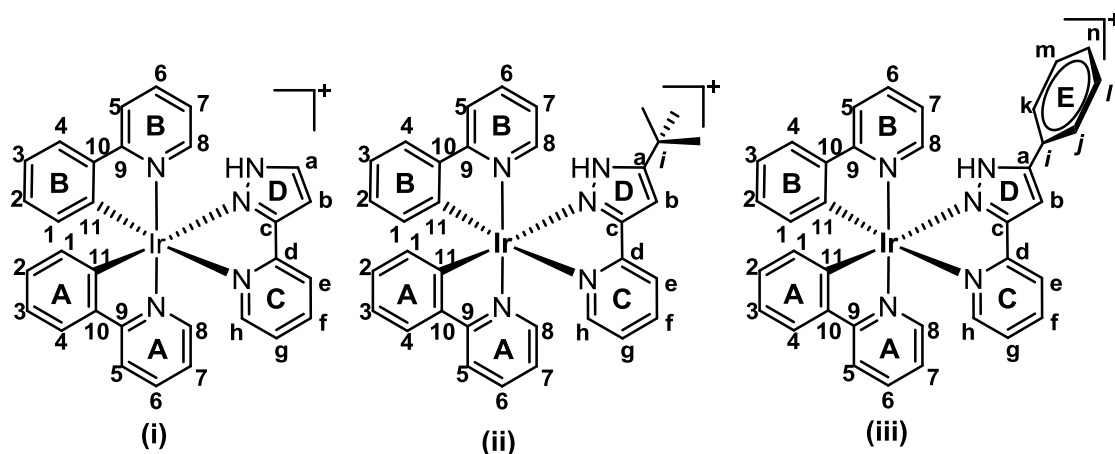


Figure 2.8: Proton numbering for ^1H NMR assignment of (i) **2.16cHL₁**, (ii) **2.16cHL₂** and (iii) **2.16cHL₃**, respectively.

The ^1H NMR spectra of **2.16cHL₁₋₃** are similar to **2.16aHL₁₋₃** except the signals associated with the pyrazole rings of the cyclometallated ligands are replaced by those associated with pyridine. Phenyl protons $\text{H}_{1\text{A}}$, $\text{H}_{1\text{B}}$ are still the most upfield aromatic protons, at between δ 6.23, and 6.35. In all three complexes, proton $\text{H}_{1\text{A}}$ shows NOEs to $\text{H}_{8\text{B}}$ and H_{h} , while proton $\text{H}_{1\text{B}}$ shows an NOE to $\text{H}_{8\text{A}}$ which then allows assignment of all the other protons of the phenyls $\text{H}_{(2-4)\text{A,B}}$ and pyridines $\text{H}_{(5-7)\text{A,B}}$ using the COSY and TOCSY spectra. The pyridine protons next to nitrogen $\text{H}_{8\text{A}}$, $\text{H}_{8\text{B}}$ and H_{h} might be expected to be the most downfield signals; however, all of these are influenced by ring currents from the other ligands and hence are shifted upfield, ultimately being observed between δ 7.9 and 7.5 in all three complexes. Pyridine C proton H_{e} is the most downfield proton in each complex, as found between δ 8.15 and 8.23. The ^{13}C NMR spectra show the expected number of signals for **2.16cHL₁₋₃**. The high-resolution mass spectra (ASAP) each show a molecular ion for the cation (for details, see Chapter 5).

Complexes **2.16cHL₁₋₂** were successfully recrystallized from DCM/hexane and complex **2.16cHL₃** from CHCl_3 /hexane. The X-ray crystal structures of **2.16cHL₁₋₃** were determined as shown in **Fig. 2.9** with selected bond lengths (\AA) and angles ($^\circ$) reported in **Table 2.3**.

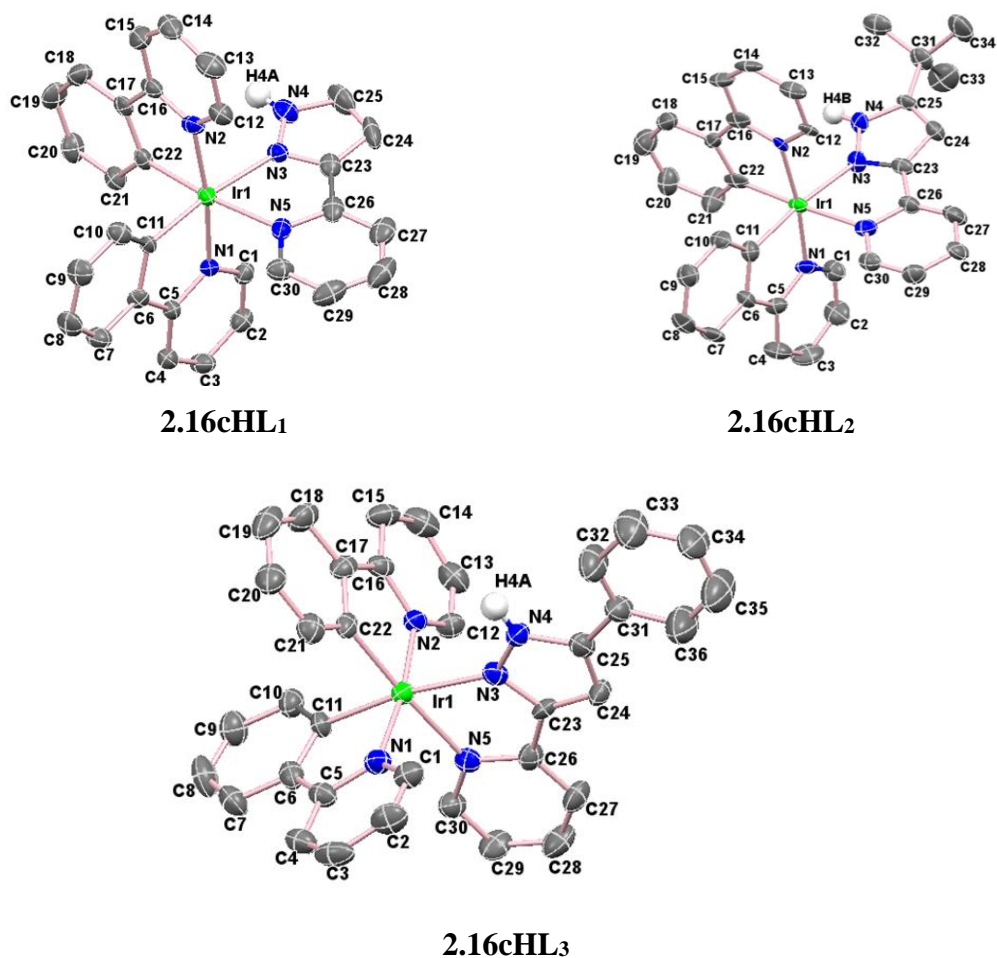


Figure 2.9: X-Ray crystal structures for the cations of **2.16cHL₁₋₃** showing 50% ellipsoids. All hydrogen atoms (except NH) have been omitted for clarity.

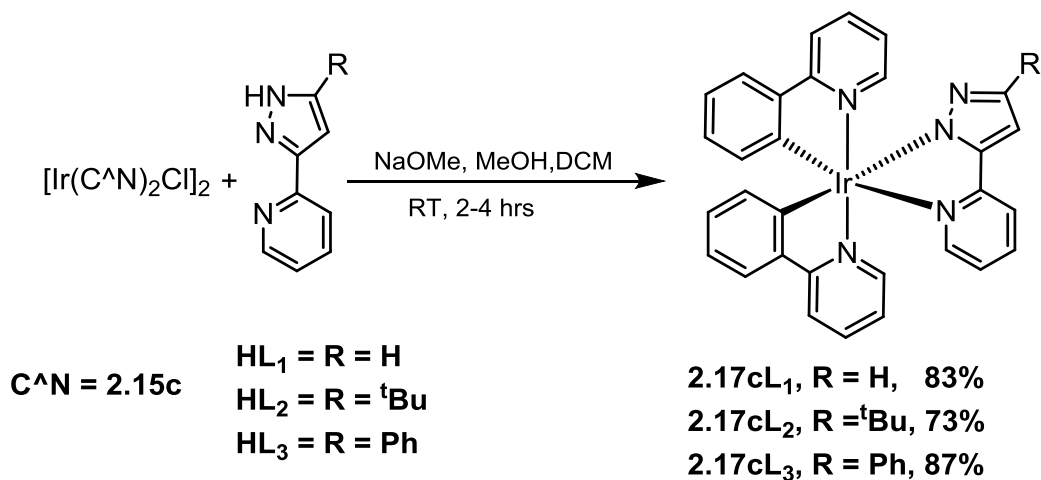
The crystal structures of **2.16cHL₁₋₃** reveal the expected distorted octahedral coordination geometry with *cis* metallated carbons and *trans* nitrogen atoms in each case (**Fig. 2.9**). The chelate bite angles for the cyclometallated ligands are all about 80°, and about 75° for the N^N ligand, both considerably less than the ideal 90°. As found for the phenylpyrazole complexes **2.16aHL₁₋₃**, the Ir—N bond lengths to the N^N ligand in **2.16cHL₁₋₃** (ranging from 2.119(5) to 2.171(7) Å) are longer than those to the cyclometallating ligands (range from 2.027(7) to 2.062(4) Å) due to the former being *trans* to the C atoms, see **Table 2.3**.

Table 2.3: Selected bond lengths (Å) and angles (°) for **2.16cHL₁**, **2.16cHL₂** and **2.16cHL₃**.

(Å)	2.16cHL₁	2.16cHL₂	2.16cHL₃
Ir(1)—N(1)	2.052(5)	2.027(7)	2.056(4)
Ir(1)—N(2)	2.036(5)	2.054(7)	2.062(4)
Ir(1)—N(3)	2.119(5)	2.171(7)	2.149(4)
Ir(1)—N(5)	2.159(6)	2.162(7)	2.170(4)
Ir(1)—C(11)	2.009(6)	2.026(9)	2.014(5)
Ir(1)—C(22)	2.006(7)	2.010(10)	2.010(5)
(°)			
N(1)—Ir(1)—C(11)	80.2(2)	80.8(3)	81.0(2)
N(2)—Ir(1)—C(22)	80.5(3)	79.9(3)	81.2(2)
N(3)—Ir(1)—N(5)	75.1(2)	76.1(3)	74.80(16)

2.2.7 Synthesis and Characterisation of Neutral Phenylpyridine Iridium(III) Complexes

Complexes **2.17cL₁₋₃** were synthesised using the same method as for the **2.17aL₁₋₃**. The dimer **2.15c** reacted with ligands **HL₁₋₃** and NaOMe in a mixture of DCM/methanol (2:1) to form compounds **2.17cL₁₋₃** in good yield (**Scheme 2.9**).



Scheme 2.9. Synthesis of $[\text{Ir}(\text{ppy})_2(\text{N}^{\wedge}\text{N})]$ **2.17cL₁₋₃**

The ^1H and ^{13}C NMR spectra of **2.17cL**₁₋₃ and the associated assignments are made on the same basis as for **2.16cHL**₁₋₃. The ^1H NMR spectra for complexes **2.17cL**₁₋₃ all show protons H_{1A,1B} between δ 6.23 and 6.39 to be essentially unchanged (within 0.1 ppm) of the related cationic complexes. Proton H_b in **2.17cHL**₁₋₃ is observed between δ 6.54 and 7.01, and is shifted to higher field compared to cationic complexes **2.16cHL**₁₋₃ (by *ca.* 0.5 ppm), as expected with deprotonation of the pyrazole. All the other protons are within 0.2-0.3 ppm of the signals in the corresponding cationic complexes **2.16cHL**₁₋₃. The ^{13}C NMR spectra show the expected number of signals for **2.17cL**₁₋₃. The high-resolution mass spectrum (ASAP) shows ions due to protonated complexes $[\text{M}+\text{H}]^+$ (see Chapter 5 for details).

Complex **2.17cL**₃ was successfully recrystallized from DCM/isopropanol; the X-ray crystal structure of **2.17cL**₃ was determined and is shown in **Fig. 2.10** with selected bond lengths (Å) and angles (°) reported in **Table 2.4**.

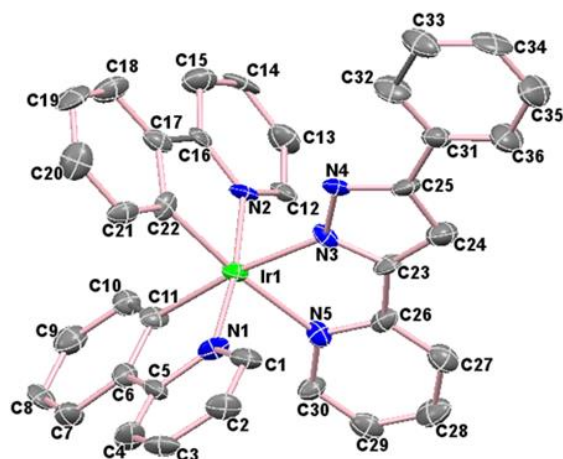


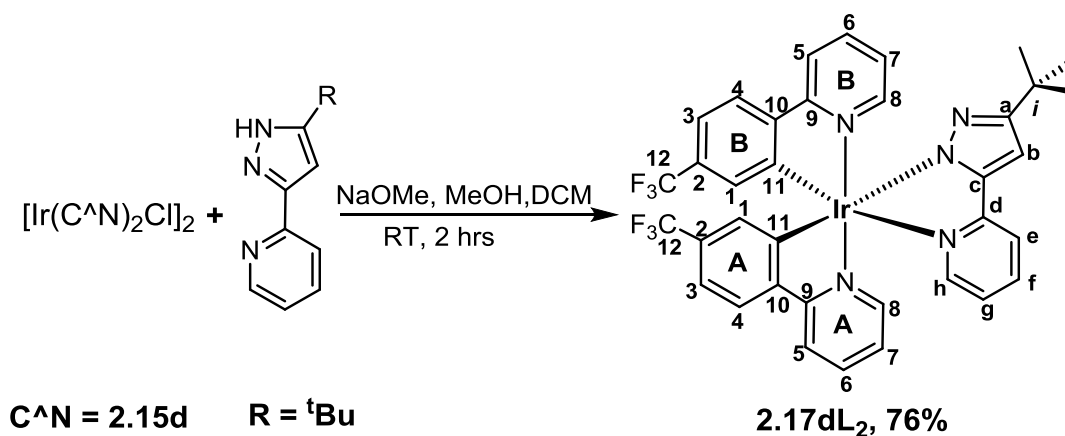
Figure 2.10: X-ray crystal structure for **2.17cL**₃ showing 50% ellipsoids. All H atoms are omitted for clarity.

The Ir(III) centre adopts a distorted octahedral geometry, where the Ir—N (C[^]N) bond distances are shorter than the Ir—N (N[^]N) distances (**Table 2.4**) due to the *trans* influence of the Ir-C bonds. The Ir(1)—N(3) distance (2.088(7) Å) in **2.17cL**₃ with an anionic pyrazole pyridine is shorter than that (2.149(4) Å) in the cationic **2.17cHL**₃ though the other Ir—N bonds and Ir—C bonds are statistically almost the same in both complexes. The pyrazolopyridine chelate bite angle is similar in both complexes (75.6(3) and 74.80(16) ° in **2.17cL**₃ and **2.16cHL**₃, respectively).

Table 2.4: Comparison of selected bond lengths (Å) and angles (°) for **2.17cL₃** and **2.16cHL₃**, respectively.

(Å)	2.17cL₃	2.16cHL₃
Ir(1)—N(1)	2.022(7)	2.056(4)
Ir(1)—N(2)	2.033(7)	2.062(4)
Ir(1)—N(3)	2.088(7)	2.149(4)
Ir(1)—N(5)	2.147(8)	2.170(4)
Ir(1)—C(11)	2.021(10)	2.014(5)
Ir(1)—C(22)	1.999(9)	2.010(5)
(°)		
N(1)—Ir(1)—C(11)	81.5(4)	81.0(2)
N(2)—Ir(1)—C(22)	81.6(4)	81.2(2)
N(3)—Ir(1)—N(5)	75.6(3)	74.80(16)

Complex **2.17dL₂** was synthesised using the same method as for **2.17aL₁₋₃** giving products in good yield (Scheme 2.10). The ¹H and ¹³C NMR spectra of **2.17dL₂** are similar to **2.17cL₂**, except the signals for one proton on each the phenyl rings of the C[^]N ligands have been replaced by a CF₃ group, as subsequently confirmed by ¹⁹F NMR spectroscopy.



Scheme 2.10: Synthesis of [Ir(ppy-CF₃)₂(N[^]N)] **2.17dL₂**

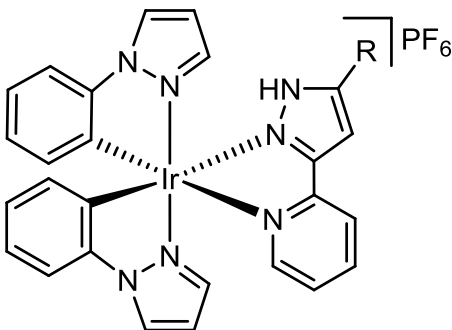
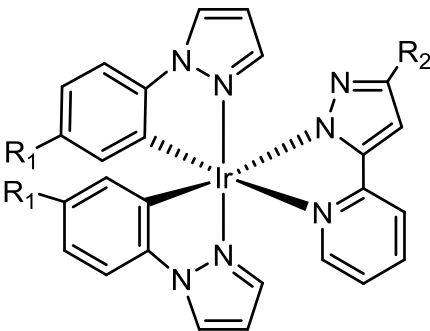
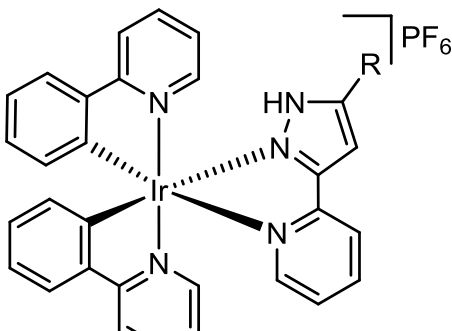
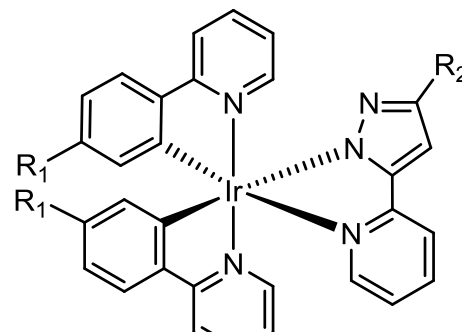
The ^tBu group gives a singlet at δ 1.18. The protons H_{1A}, H_{1B} are overlapping multiplets at δ 6.41-6.42 and show the expected NOEs. Proton H_b is a singlet at δ 6.48 and proton H_h is observed at δ 6.83, to considerably higher field than in the free ligand (δ 8.61), as found in **2.17aL1-3**. The ¹³C NMR spectra show the expected signals and the high-resolution mass spectrum (ESI) shows a protonated molecular ion [M+H]⁺ at *m/z* 838.1959 (838.1956 calculated for C₃₆H₂₉F₆IrN₅), with characteristic ¹⁹³Ir isotopes pattern.

In conclusion, these reactions show that a range of 2-pyrazolylpyridine complexes [Ir(C^N)₂(N^N)]ⁿ⁺ (n = 0, 1) can be synthesised in good yields (> 70%) from [Ir(C^N)₂Cl]₂ using microwave heating for cationic complexes or by reaction with a base for neutral complexes. All the complexes were fully characterised by ¹H and ¹³C NMR spectroscopy, mass spectrometry and in several cases by X-ray crystallography. The use of 2-D NMR techniques allows full assignment of the majority of the protons, where some unusual chemical shifts are due to ring current effects of adjacent ligands. As expected, the deprotonation of the cationic complexes leads to upfield shifts in the ¹H NMR signals for the some of the 2-pyrazolylpyridine protons. The photophysical properties of these complexes are discussed in the following sections.

2.3 Photophysical properties

This section will describe the photophysical properties of the cationic complexes $[\text{Ir}(\text{C}^{\wedge}\text{N})_2(\text{N}^{\wedge}\text{NH})]\text{PF}_6$ (**2.16aHL**₁₋₃, **2.16cHL**₁₋₃) and neutral complexes $[\text{Ir}(\text{C}^{\wedge}\text{N})_2(\text{N}^{\wedge}\text{N})]$ (**2.17aL**₁₋₃, **2.17bL**₁₋₃, **2.17cL**₁₋₃, **2.17dL**₂). The UV-vis and emission spectra were measured in HPLC grade MeCN at 0.2 and 0.02 mM concentrations, respectively, unless otherwise stated. All excitation spectra are in accordance with the absorption spectra (see appendix **Figs. 1** and **2**).

Labelling scheme for the Cationic/Neutral Ir(III) Complexes

Phenylpyrazole Complexes (Cationic)	Phenylpyrazole Complexes (Neutral)
 <p>2.16aHL₁, R = H 2.16aHL₂, R = ^tBu 2.16aHL₃, R = Ph</p>	 <p>2.17aL₁, R₁ = H, R₂ = H 2.17aL₂, R₁ = H, R₂ = ^tBu 2.17aL₃, R₁ = H, R₂ = Ph 2.17bL₁, R₁ = CF₃, R₂ = H 2.17bL₂, R₁ = CF₃, R₂ = ^tBu 2.17bL₃, R₁ = CF₃, R₂ = Ph</p>
Phenylpyridine Complexes (Cationic)	Phenylpyridine Complexes (Neutral)
 <p>2.16cHL₁, R = H 2.16cHL₂, R = ^tBu 2.16cHL₃, R = Ph</p>	 <p>2.17cL₁, R₁ = R₂ = H 2.17cL₂, R₁ = H, R₂ = ^tBu 2.17cL₃, R₁ = H, R₂ = Ph 2.17dL₂, R₁ = CF₃, R₂ = ^tBu</p>

2.3.1 Photophysical properties of Phenylpyrazole Ir(III) Complexes (2.16aHL₁₋₃, 2.17aL₁₋₃ and 2.17bL₁₋₃)

The UV-vis absorption spectra of complexes **2.16aHL**₁₋₃, and **2.17aL**₁₋₃ are shown in **Fig. 2.11**, which illustrate the effect of the pyrazolyl substituent and of deprotonation. The spectra of **2.17bL**₁₋₃ with the CF₃ substituted C^N ligand are compared with their unsubstituted analogues, **2.17aL**₁₋₃ in **Fig 2.12**. The data for all nine complexes are shown in **Table 2.5**. All complexes show strong bands between 225 and 300 nm due to $\pi \rightarrow \pi^*$ transitions. Cyclometallated iridium complexes usually show ¹MLCT, and sometimes ³MLCT, bands around 350-450 nm.⁵⁹ However, there is no clear evidence for separate peaks at longer wavelength in complexes **2.16aHL**₁₋₃, **2.17aL**₁₋₃ and **2.17bL**₁₋₃. **Fig 2.11** shows a number of changes in the intensities of the $\pi \rightarrow \pi^*$ bands when changing the substituents of the N^N ligands. Complexes **2.16aHL**₃ and **2.17aL**₃ show larger extinction coefficients than **2.16aHL**₁₋₂ and **2.17aL**₁₋₂, respectively, which may be due to the extra phenyl group on the N^N ligands. Similar results were also observed with complexes **2.17bL**₁₋₃.

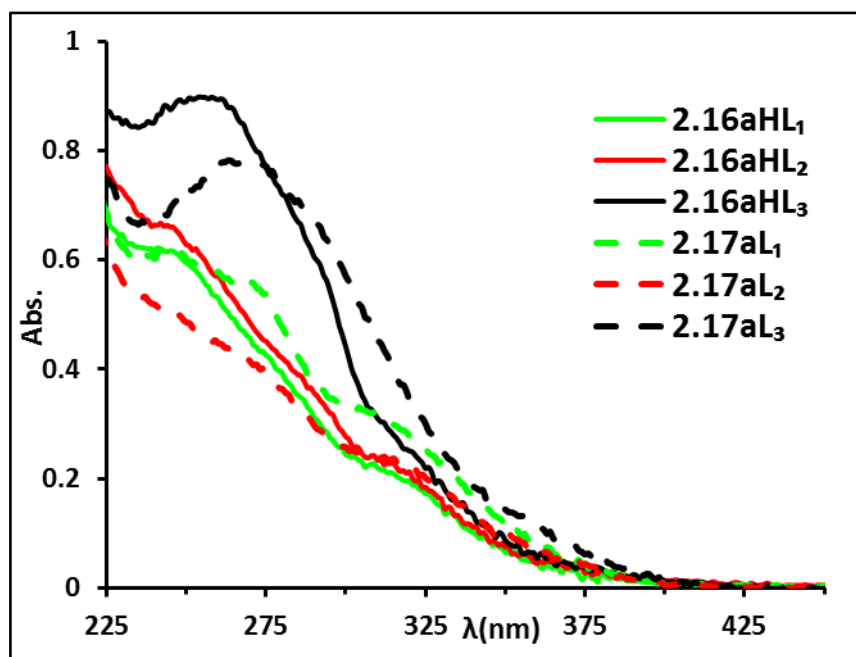


Figure 2.11: Absorption spectra of cationic and neutral complexes **2.16aHL**₁₋₃ (—) and **2.17aL**₁₋₃(---), respectively, in MeCN at 0.02 mM at room temperature.

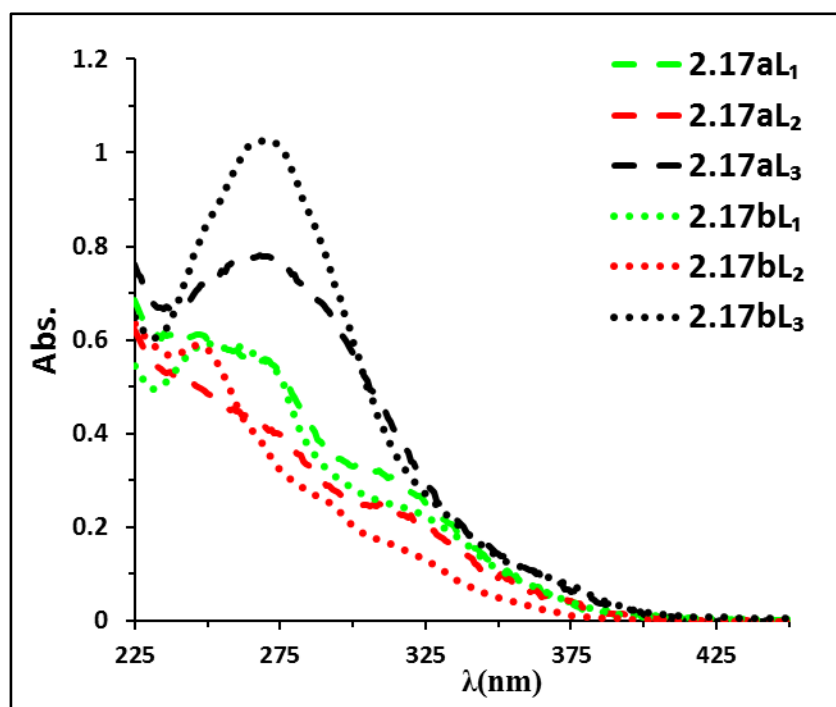


Figure 2.12: Absorption spectra of neutral complexes **2.17aL₁₋₃** (---) and **2.17bL₁₋₃** (...) in MeCN at 0.02 mM at room temperature.

Table 2.5: Electronic absorption spectral data [λ_{abs} (nm), ϵ_{max} ($\text{L mol}^{-1} \text{cm}^{-1}$)] of complexes **2.16aHL₁₋₃**, **2.17aL₁₋₃** and **2.17bL₁₋₃**,

2.16aHL₁	2.16aHL₂	2.16aHL₃
241(31106), 324(8904)	242(33361), 321(9999)	254(44902) 320(12523)
2.17aL₁	2.17aL₂	2.17aL₃
270 sh(27850), 324(13050)	270 sh(27910), 321(10800)	268(39050) 320(17100)
2.17bL₁	2.17bL₂	2.17bL₃
250(29650), 324(11350)	249(29250), 328(6000)	270(51300), 367(4700)

The protonated complexes **2.16aHL₁₋₃** show absorption bands at 240 to 255 nm. On deprotonation (i.e., complexes **2.17aL₁₋₃**) these absorption bands are red-shifted *ca.* 25 to 30 nm, whilst the bands at longer wavelength are very similar in both the protonated and deprotonated complexes. Upon deprotonation there is no significant change (< 20%) in absorbance intensity at any wavelength, and hence these complexes would not be expected to be good pH sensors in their ground states. The effect of adding a CF₃ substituent to the C^N ligand is shown in **Fig 2.12**; as can be seen, there are some minor

changes in the short wavelength region, with the most notable being an increase in intensity at *ca.* 260 nm for **2.17bL₃** compared to **2.17aL₃**. However, above 300 nm, the spectra of **2.17bL₁₋₃** and **2.17aL₁₋₃** are very similar.

The emission spectra were run in MeCN in aerated solutions. Each pair of cationic and neutral complexes (e.g., **2.16aHL₁** and **2.17aL₁**) were illuminated at the same excitation wavelength (see **Figs 1-2** in the appendix for excitation spectra). The emission spectra of complexes **2.16aHL₁₋₃**, **2.17aL₁₋₃** and **2.17bL₁₋₃** are shown in **Fig 2.13** and the associated data are reported in **Table 2.6**.

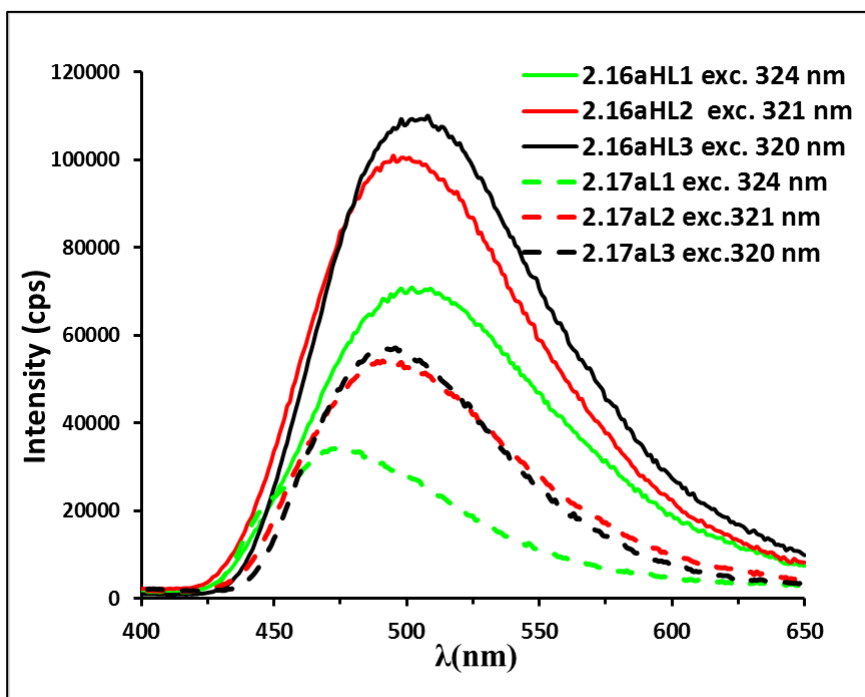


Fig. 2.13: Emission spectra of cationic and neutral complexes **2.16aHL₁₋₃**(—) and **2.17aL₁₋₃**(---), respectively, in MeCN at 0.02 mM at room temperature in air.

All three cationic complexes **2.16aHL₁₋₃** show a broad emission band, each with a similar λ_{max} at 502, 495, and 508 nm, respectively (Table 2.6 entries 1-3 and **Fig. 2.13**). Hence, the substituent on the pyrazole has almost no effect on the emission wavelength. Complexes **2.16aHL_{2,3}** showed slightly higher intensities than **2.16aHL₁**. The corresponding neutral complexes **2.17aL₁₋₃** show similar spectra with a slight blue shift in λ_{max} (27 nm for **2.17aL₁** and *ca.* 10 nm for **2.17aL₂₋₃**) (Table 2.6 entries 4, 5, 6 and **Fig. 2.13**). It is particularly noticeable that the emission intensity for the neutral complexes **2.17aL₁₋₃** are all reduced by about 50% compared with the cationic complexes **2.16aHL₁₋₃**. Hence, these complexes would nominally be expected to be luminescent sensors for pH.

Table 2.6: Emission data of **2.16aHL**₁₋₃, **2.17aL**₁₋₃ and **2.17bL**₁₋₃ complexes.

Entry	Complex	λ_{em} (nm)
1	2.16aHL ₁	502
2	2.16aHL ₂	495
3	2.16aHL ₃	508
4	2.17aL ₁	475
5	2.17aL ₂	493
6	2.17aL ₃	496
7	2.17bL ₁	445sh, 467
8	2.17bL ₂	433sh, 458
9	2.17bL ₃	483

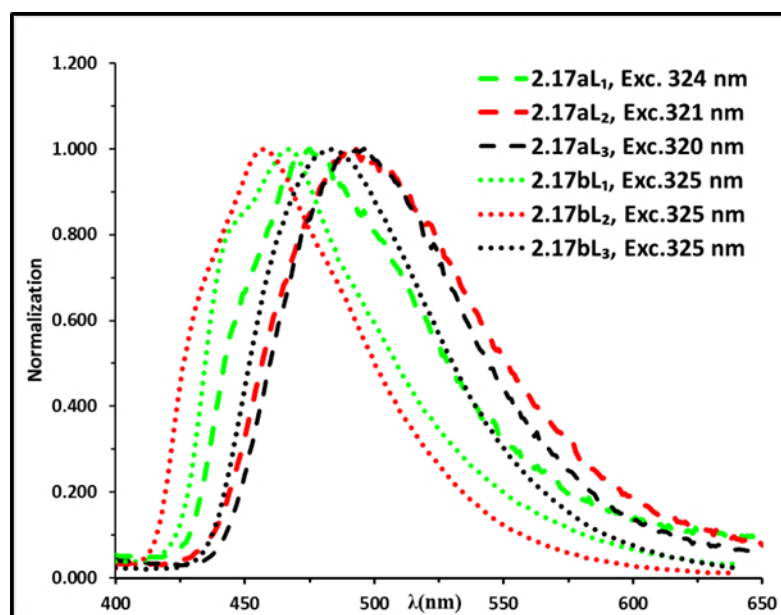


Fig. 2.14: Normalised emission spectra of neutral complexes **2.17aL**₁₋₃ (- - -) and **2.17bL**₁₋₃ (....), respectively, in MeCN at 0.02 mM at room temperature in air.

Neutral complexes **2.17bL**₁₋₃ with an electron-withdrawing substituent (CF₃) on the phenyl ring each show a broad emission band which is blue-shifted compared to the corresponding C^N unsubstituted complexes **2.17aL**_{1,3}, with **2.17bL**₂ showing the largest shift of 35 nm (**Fig. 2.14** and **Table 2.6** entries **4-6** vs. **7-9**), respectively. A blue shift in

emission by addition of electron-withdrawing groups to the C^N cyclometallating ligands is a well-known phenomenon which has been ascribed to the electron-withdrawing group stabilising the HOMO orbital.^{53, 62, 63}

2.3.2 Photophysical properties of Phenylpyridine Ir(III) Complexes (2.16cHL₁₋₃, 2.17cL₁₋₃ and 2.17dL₂).

The UV-vis absorption spectra of complexes **2.16cHL**₁₋₃, **2.17cL**₁₋₃ and **2.17dL**₂ are shown in **Figs 2.15**, **2.16** and their data reported in **Table 2.7**. As for the ppz complexes discussed earlier, all the ppy complexes (cationic and neutral) show strong bands between 225 and 300 nm due to $\pi \rightarrow \pi^*$ transitions. However, for the ppy complexes, weak bands between 380-405 nm (possibly having contributions from ¹MLCT transitions) are also visible. The substituent on the pyrazole has almost no effect on the absorption wavelength, though phenyl-substituted complexes **2.16cHL**₃ and **2.17aL**₃ show higher intensities (**Figs 2.15**). The neutral complexes **2.17cL**₁₋₃ show a small red shift (*ca.* 4-12 nm) in the high energy band compared to their cationic analogues, while the bands to longer wavelength (340 nm) remain essentially unchanged (**Figs 2.15** and **Table 2.7**). The spectrum of the neutral complex **2.17dL**₂, with an electron-withdrawing substituent (CF₃) on the phenyl ring of the C^N ligand, is similar to that of its unsubstituted analogue **2.17cL**₂ (**Fig 2.16** and **Table 2.7**). As for the ppz complexes upon deprotonation, there is no significant change (< 20%) in absorbance intensity at any wavelength, hence these would not be expected to be good pH sensors on the basis of their UV-vis spectra.

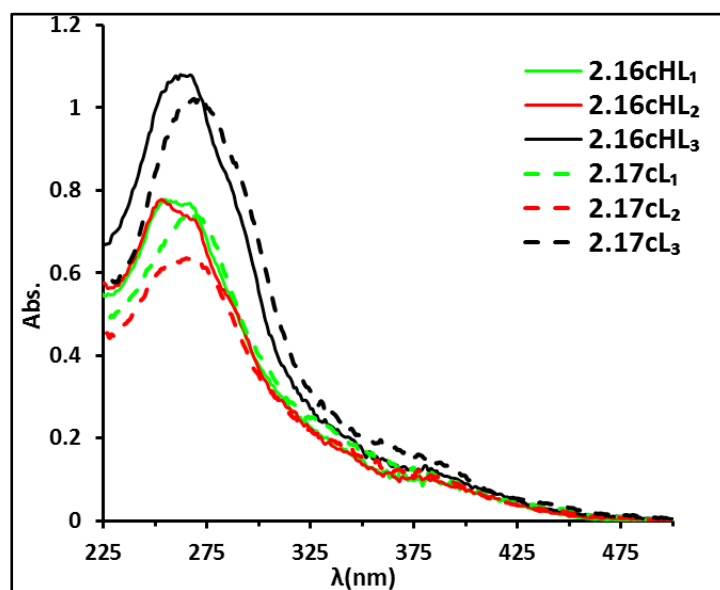


Figure 2.15: Absorption spectra of cationic and neutral complexes **2.16cHL**₁₋₃ (—) and **2.17cL**₁₋₃ (---), respectively, in MeCN at 0.02 mM at room temperature.

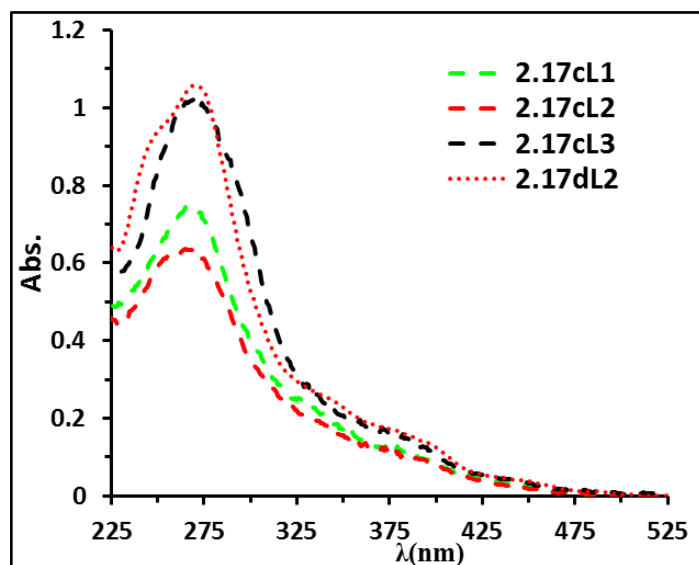


Figure 2.16: Absorption spectra of neutral **2.17cL₁₋₃** (---) and **2.17dL₂** (....), respectively, in MeCN at 0.02 mM at room temperature.

Table 2.7: Electronic absorption spectral data, [λ_{abs} (nm), ϵ_{max} ($\text{L mol}^{-1} \text{cm}^{-1}$)] of complexes **2.16cHL₁₋₃**, **2.17cL₁₋₃** and **2.17dL₂**.

2.16cHL₁	2.16cHL₂	2.16cHL₃
255(38906), 340 sh (8874)	253(38906), 341 sh (8372)	267(53968), 368 sh (6240)
2.17cL₁	2.17cL₂	2.17cL₃
267(36972), 340sh(10111)	265(31775), 341sh (9030)	271(51066), 368 sh (8645)
	2.17dL₂	
	273(52650), 399 sh (6400)	

The emission spectra of **2.16cHL₁₋₃** and **2.17cL₁₋₃** are shown in **Fig 2.17** and their data reported in **Table 2.8**. Complex **2.16cHL₁** shows a broad band (λ_{max} of 505 nm); however, complexes **2.16cHL₂₋₃** both show some structure in the emission band. Thus **2.16cHL₂** shows a λ_{max} at 510 nm with a shoulder at 484 nm, whilst **2.16cHL₃** shows a λ_{max} at 497 nm with a shoulder at 520 nm. As for the ppz complexes, changing the **R₂** group on the N^N ligand has only a small effect on the emission wavelength. The neutral complexes **2.17cL₁₋₃** show very similar spectra to the cationic complexes, with a broad emission band with distinct shoulders observed for some complexes. There is no a significant

change in emission intensity between the cationic and neutral complexes, though the latter, if anything, are slightly more emissive than the former, which is the opposite case to the ppz complexes. Hence, these are not expected to be good pH sensors in their excited states. Alternatively, it is possible that complexes **2.17cL**₁₋₃ were not fully deprotonated (see pH titrations section **2.4**).

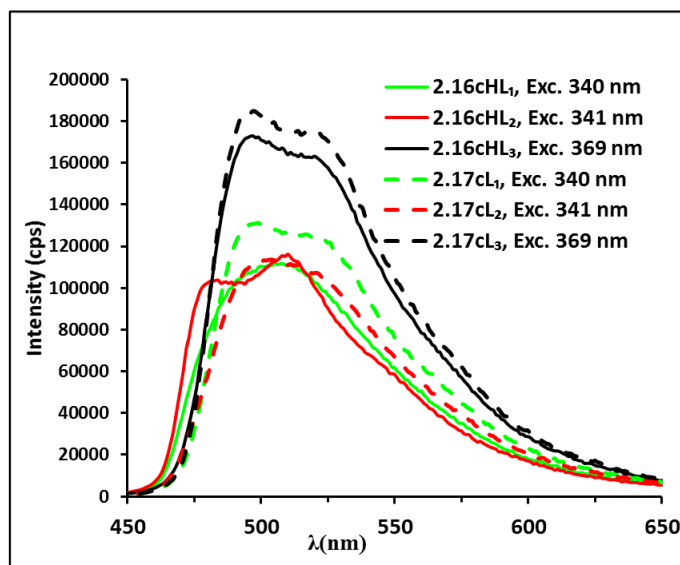


Fig. 2.17: Emission spectra of cationic **2.16cHL**₁₋₃ (—) and neutral **2.17cL**₁₋₃ (---) in MeCN at 0.02 mM at room temperature in air.

Neutral complex **2.17dL**₂ containing a CF₃ group showed a λ_{max} at 502 nm, with a small blue shift *ca.* 4 nm compared to the corresponding unsubstituted complex. **2.17cL**₂ also shows a distinct shoulder at longer wavelength *ca.* 533 nm, and the spectra the of **2.17cL**₂ has some emission to higher wavelength than the **2.17d** complex (**Fig 2.18**).

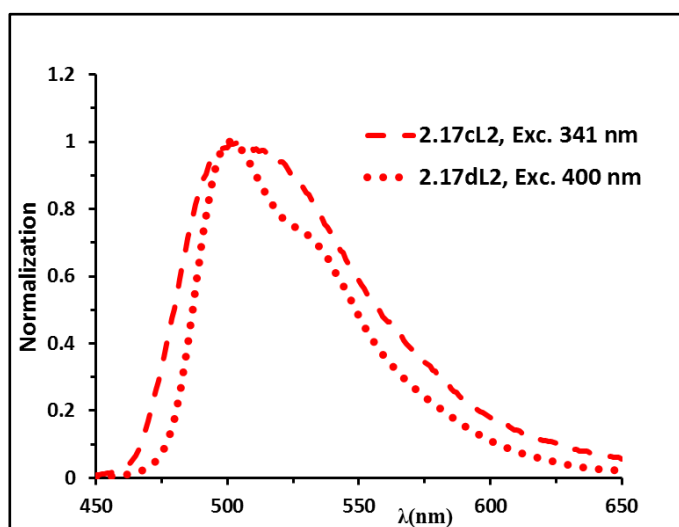


Figure 2.18: Normalised emission spectra of neutral complexes **2.17cL**₂ (---) and **2.17dL**₂ (....), respectively, in MeCN at 0.02 mM at room temperature in air.

Table 2.8: Emission data of **2.16cHL**₁₋₃, **2.17cL**₁₋₃ and **2.17dL**₂ complexes.

Entry	Complex	λ_{em} (nm)
1	2.16cHL ₁	505
2	2.16cHL ₂	484sh, 510
3	2.16cHL ₃	497, 520sh
4	2.17cL ₁	499, 517sh
5	2.17cL ₂	506
6	2.17cL ₃	497, 518sh
7	2.17dL ₂	502, 533sh

In conclusion, the UV-vis absorption spectra of all the complexes show strong bands between 200 and 300 nm due to $\pi \rightarrow \pi^*$ transitions, and the ppy complexes **2.16cHL**₁₋₃, **2.17cL**₁₋₃ and **2.17dL**₂ show weak bands between 380-405 nm (possibly having contributions from ¹MLCT transitions). All the complexes are emissive at room temperature in solution in air. There is no a significant variation in emission wavelength upon changing the substituent on the ancillary N[^]N ligands, whilst for both ppz and ppy complexes there is very little change in λ_{max} on deprotonation, except for complex **2.17aL**₁ which shows a blue shift of approximately 27 nm. However, there are some changes in intensity, particularly for the ppz complexes which may thus be suitable for use as luminescent pH sensors. Substituting H with an electron-withdrawing CF₃ group on the C[^]N ligand causes a blue shift in the emission spectrum, consistent with other bis-cyclometallated Ir complexes, which has been ascribed to the electron-withdrawing group stabilising the HOMO orbital. The effect of changing the cyclometallated ligand from ppz to ppy is not uniform, giving a red shift in some cases and a blue shift in others. For a more detailed understanding of the photochemistry, more data such as quantum yields, lifetimes and DFT calculations are needed.

2.4 pH Titration Studies

To investigate their potential application as pH sensors, pH titrations for all complexes were carried out in MeCN/H₂O (1:9) at a 0.02 mM concentration, altering the pH by addition of 0.1 M HCl or 0.1 M NaOH. The pK_a values for the complexes were determined by the change in emission intensity with pH over the range *ca.* 3 to 12.5. The titrations

with acid and base were carried out for two separate samples. On dissolution, the neutral complexes gave a pH of between 6.9 and 8.2. The first sample was treated with 0.1 M HCl whilst a second was treated separately with 0.1 M NaOH. The results of the titrations are expected to be the same if started with a cationic rather than a neutral complex, which was confirmed using complex **2.16aHL**₁ (the results are shown in **Fig 3** in the appendix).

2.4.1 pH Titrations of Phenylpyrazole Ir(III) Complexes **2.17aL**₁₋₃.

The influence of pH change on the absorption spectrum characteristics of complex **2.17aL**₁ is shown in **Fig. 2.19**. As expected from the studies of the isolated neutral and cationic complexes **2.17aL**₁ and **2.16aHL**₁ described above, there is very little change in the spectrum with changing pH. Complexes **2.17aL**₂₋₃ displayed very similar results, with very little change in the spectrum with changing pH (the results are shown in **Fig 4** in the appendix), hence absorption spectra cannot not be used to determine accurate pK_a values.

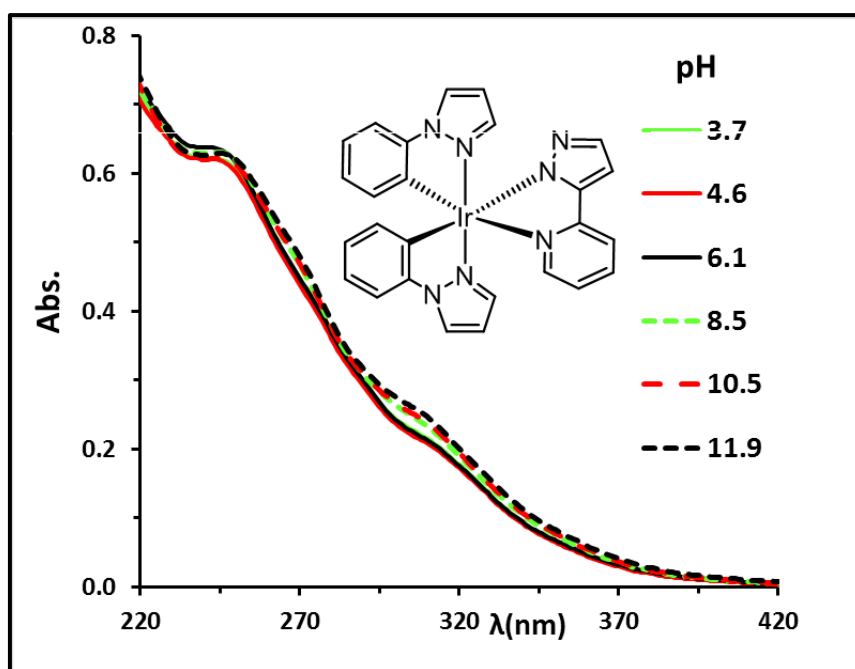
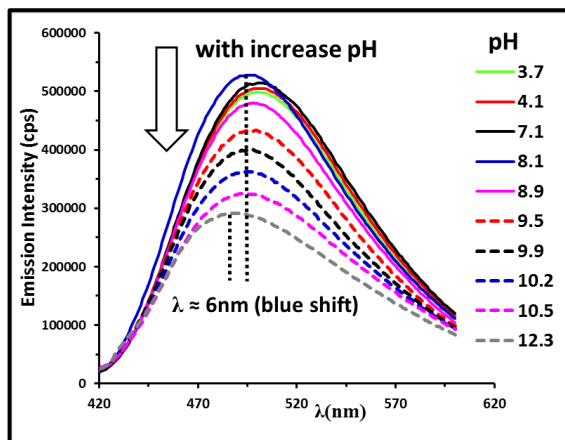


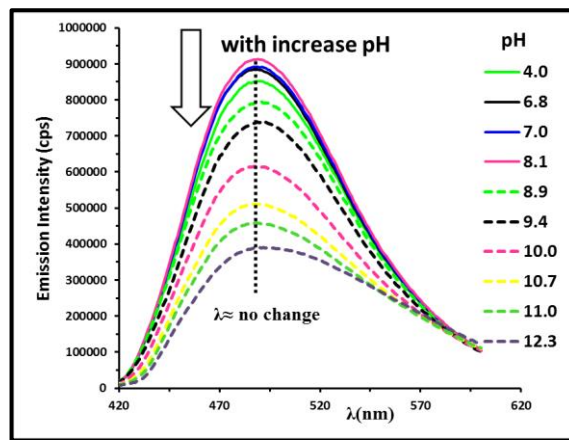
Figure 2.19: Selected absorption spectra of complex **2.17aL**₁ (0.02 mM) at various pH values in MeCN/H₂O (1:9) at RT.

The emission pH titration data and pK_a values of complexes **2.17aL**₁₋₃ are illustrated in (**Fig. 2.20**). As expected from the studies of the cationic and neutral complexes described above, complexes **2.17aL**₁₋₃ show a significant variation in emission intensity at λ_{max} values of 500, 489 and 488 nm, respectively, as a function of pH in aqueous solution. The emission intensity of **2.17aL**₁ at 500 nm was relatively unchanged between pH 7.5 and pH 3.7, but above pH 7.5, there was a gradual decrease in emission intensity by about a

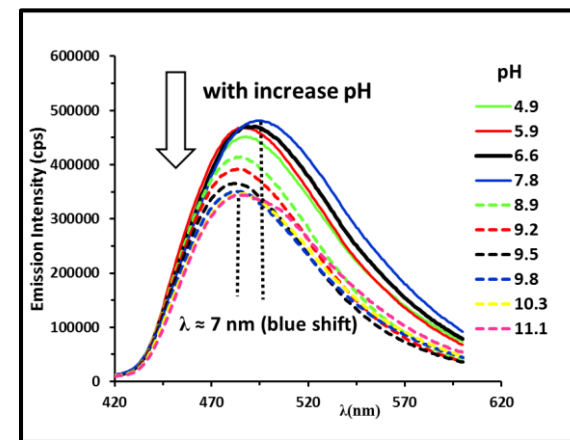
factor of two to around pH 10, above which the intensity remained essentially constant until pH 12.3, as per **Fig. 2.20. A(i)**. Note over the full pH range studied, there is a small blue shift (*ca.* 6 nm) in λ_{max} . The excited state pK_a value was determined to be about 9.9 at the equivalent point, as per **Fig. 2.20 A(ii)**, which is more acidic than the free pyridine pyrazole ligand itself (pK_a 11.6).⁴⁵



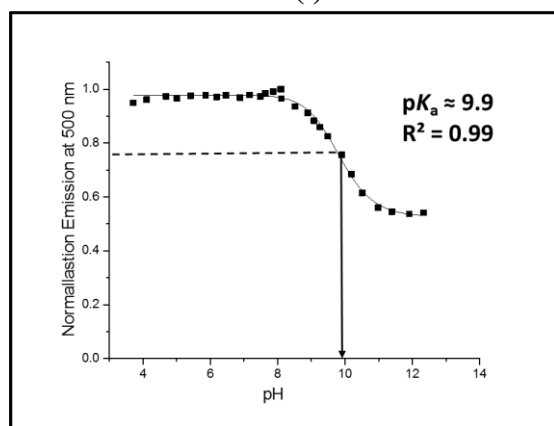
A(i)



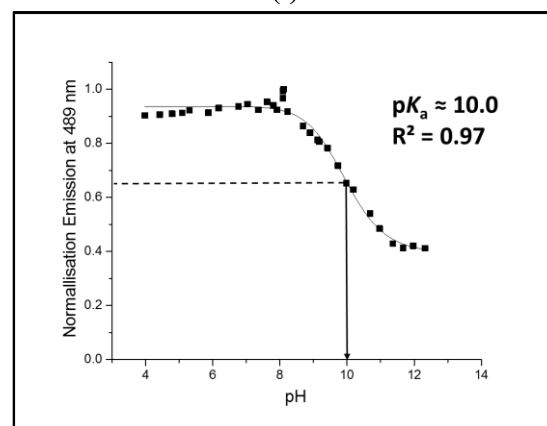
B(i)



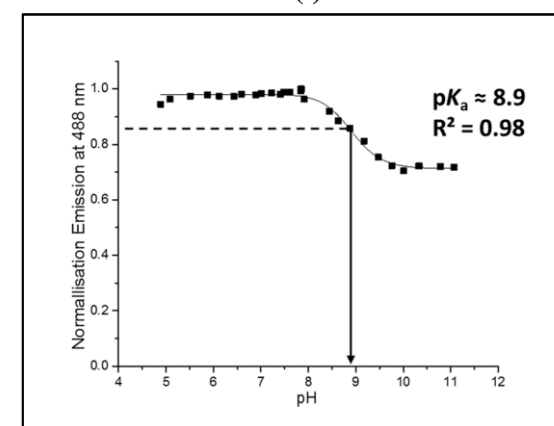
C(i)



A(ii)



B(ii)



C(ii)

Figure 2.20: A-C(i) Selected emission spectra of complexes **2.17aL₁₋₃**, respectively, (0.02mM) at various pH values in MeCN/H₂O (1:9), in air with excitation at 324 nm. A-C(ii) Plot of normalised emission intensity of complexes **2.7aL₁₋₃**, respectively, against pH

The emission pH titration spectra of complexes **2.17aL₂₋₃** **Figs. 2.20. B(i)** and **C(i)** were similar to that of **2.17aL₁**. In both complexes **2.17aL₂₋₃**, the emission intensity is relatively constant over the pH range *ca.* 4.9-7.5. The emission intensity of **2.17aL₂** at *ca.* 488 nm was reduced by *ca.* two-fold at pH 11, whilst the emission intensity of **2.17aL₃** was reduced by only *ca.* 1.3-fold between pH 8 and 10. From these changes, the pK_a values of complexes **2.17aL₂** and **2.17aL₃** were determined to be *ca.* 10.0 and 8.9, respectively (**Figs. 2.20. B-C(ii)**), which are more acidic than the corresponding free ligands at 12.3 and 11.6, respectively.⁴⁵ Hence, all three complexes **2.17aL₁₋₃** can function as pH sensors. However, even though the pK_a of the complexes is between 1.7 and 2.7 units lower than for the free ligands, none of them are low enough to be of use as biological pH sensors. To lower the pK_a further the complexes need to be made more acidic, which can be achieved by adding electron-withdrawing groups to the ligands. Hence, complexes **2.17bL₁₋₃** were examined (see section **2.4.3**).

2.4.2 pH Titrations of Phenylpyridine Ir(III) Complexes **2.17cL₁₋₃**

UV-vis spectrophotometric pH titrations for **2.17cL₁₋₃** were carried out over the pH range 4.1-11.4. The data for **2.17cL₁** are illustrated in **Figs. 2.21** There is almost no change in absorption with pH. Complexes **2.17aL₂₋₃** all displayed very similar results (see **Fig 5** in the appendix). Hence the absorption spectra could not be used to determine accurate pK_a values.

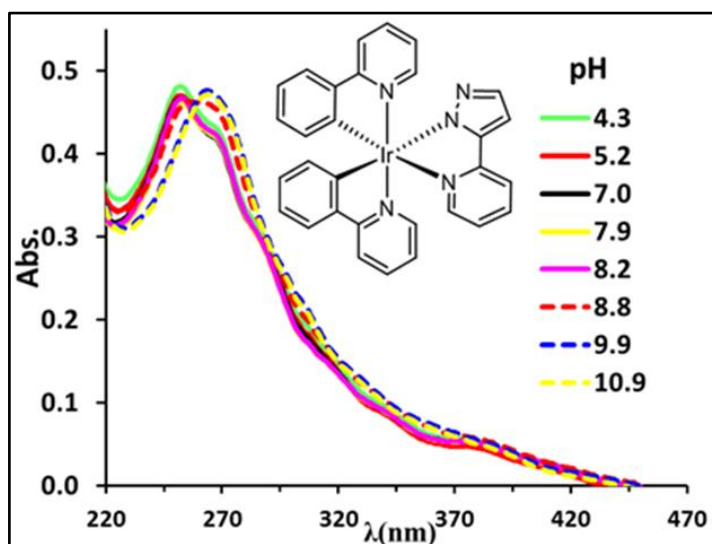


Figure 2.21: Selected absorbance spectra of complex **2.17cL₁** (0.02mM) at various pH values in MeCN/H₂O (1:9) at RT.

The emission pH titration spectra for complexes **2.17cL₁₋₃** are illustrated in **Fig. 2.22**. Complex **2.17cL₁** shows two emission maxima at 479 and 505 nm. The spectra show very

little change in intensity between pH *ca.* 8.0 - 4.3. After increasing the pH above 8.0, these bands start to shift to longer wavelength (492 nm) and increase in intensity up to about pH 10.9, above which the intensity remains essentially constant, as per **Fig. 2.22A(i)**. The overall increase in intensity at 493 nm is by a factor of *ca.* 1.6, whilst the pK_a was determined to be 8.9 (**Fig. 2.22 A(ii)**) which is smaller than that (11.60) of free ligand **HL₁**.⁴⁵ Luminescence spectral changes for **2.17cL₂₋₃** as a function of pH are displayed in **Figs. 2.22 B(i) and C(i)**. At low pH, **2.17cL₂** shows two broad emission peaks at λ_{max} 480 and 509 nm, whilst for **2.17cL₃** the emission is broader, centred at *ca.* 500 nm. The emission intensity and emission wavelength of both complexes were relatively unaffected over the pH range from *ca.* 4 to 7.5. Further increases in pH from *ca.* 7.5 to 10 led to a gradual increase in intensity by a factor of *ca.* 1.8 and 1.7 for **2.17cL₂** and **2.17cL₃**, respectively (see **Figs. 2.22 B(ii), C(ii)**, respectively). The pK_a values of the two complexes **2.17cL₂₋₃** are *ca.* 8.0 and 9.0, respectively. Once again, these are smaller than the ground state pK_a of the free ligands (12.2 for **HL₂** and 11.5 for **HL₃**). Overall, the ppy complexes **2.17cL₁₋₃** show an increase in emission intensity with increasing pH, which is the opposite trend to that observed for the ppz complexes **2.17aL₁₋₃** described above. This suggests that the orbitals involved in the emission are different in the two complexes; indeed the structure emission profile indicates a mixed ³MLCT/³ILCT character to the T₁ stat and a broad emission character for the ppz analogues indicates MLCT/LLCT character your excited electron is in a different position. DFT calculations would be needed to provide further information. It is clear that the pK_a of all the complexes is lower than for the free ligands by between 1.7 and 2.7 units for ppz complexes and between 2.5 and 4.2 units for the ppy complexes; however, they are still a little high to be of use as biological pH sensors. To lower the pK_a further the complexes need to be made more acidic, which can be achieved by adding electron-withdrawing groups to the ligands. Hence, complexes **2.17bL₁₋₃** and **2.17dL₂** were examined (see section **2.4.3**).

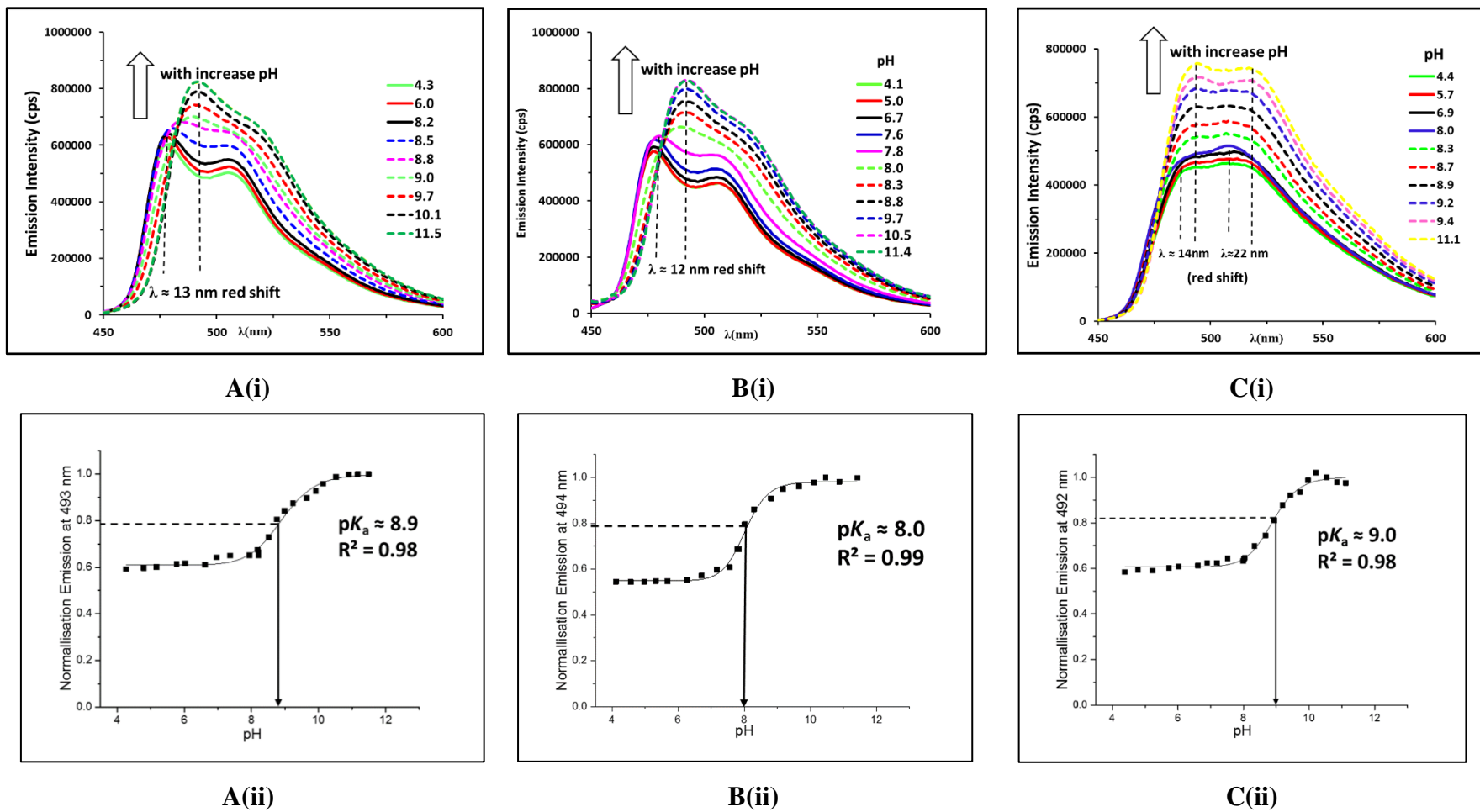


Figure 2.22. A-C(i) Selected emission spectra of complexes **2.17cL1-3** (0.02mM) at various pH values in MeCN/H₂O (1:9), in air, excitation at 400 nm A-C(ii) A plot of normalised emission intensity of complex **2.17cL1-3** against different pH.

2.4.3 pH Titrations of CF₃ Phenylpyrazole Ir(III) Complexes 2.17bL₁₋₃

The influence of pH change on the absorption spectrum characteristics of CF₃-substituted complex 2.17bL₁ is shown in Fig. 2.23. As found for the 2.17aL₁₋₃ complexes, 2.17bL₁ showed no significant spectral variations over a pH range of 2.5-11.1 and only minor changes in intensity with pH at very short wavelength, at *ca.* 265 nm. Attempts to perform the pH titration of complexes 2.17bL₂ and 2.17bL₃ at 0.02 mM did not work particularly well. At this concentration (0.02 mM), the absorbance in MeCN/H₂O (1:9) was substantially reduced as compared with the absorbance in pure MeCN, which may mean that the complex was starting to precipitate even though no solid was observed. Hence, the solutions were diluted to 0.005 mM, and at this concentration the absorbance in MeCN/H₂O (1:9) and in pure MeCN were nearly equal. Therefore, pH titration of these complexes (2.17bL₂ and 2.17bL₃) was performed at 0.005 mM. The pH titrations of complexes 2.17bL₂₋₃ displayed very little change in the absorption spectra with changing pH (the results of which are shown in Fig 6 in the appendix).

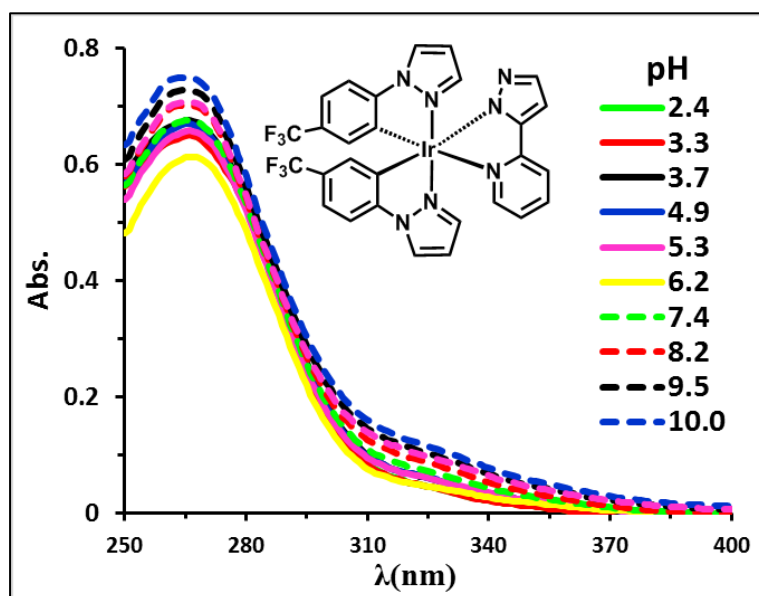


Figure 2.23: Selected absorbance spectra of complex, 2.17bL₁ (0.02mM) at various pH values in MeCN/H₂O (1:9).

The emission pH titration data and pK_a values of complexes 2.17bL₁₋₃ are illustrated in Fig. 2.24. Complexes 2.17bL₁₋₃ show changes in their emission intensity as a function of pH in aqueous solution. Surprisingly, for all three complexes 2.17bL₁₋₃, replacing H with the electron-withdrawing CF₃ group on the C^N ligand led to a complete reversal of the shape of the pH titration curve. Thus, at low pH, the complexes show low emission and at high pH the emission intensity is higher, which is the exact opposite of complexes 2.17aL₁₋₃.

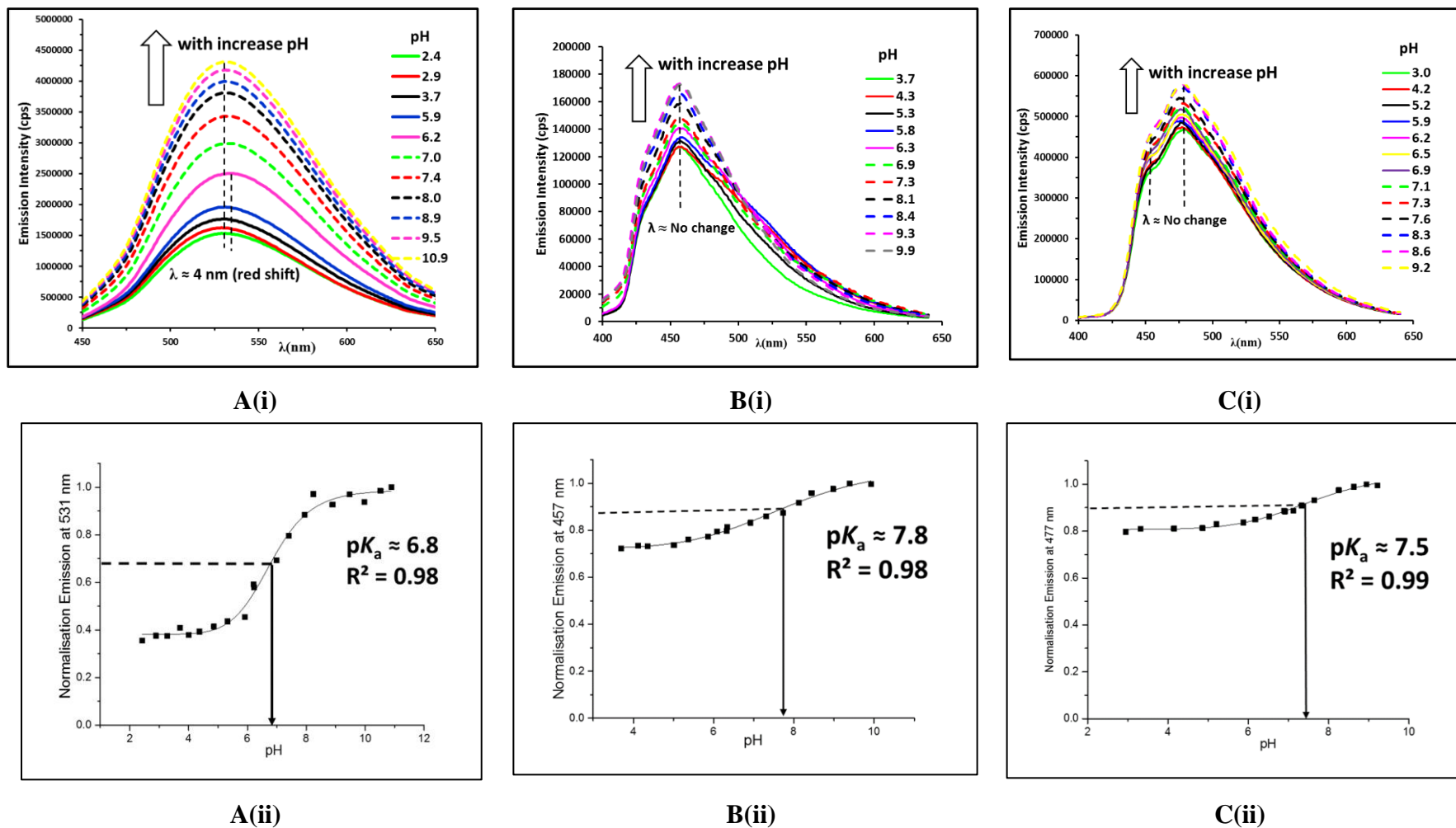


Figure 2.24. A-C(i) Emission titration spectra of complexes **2.17bL1** at 0.02 mM in MeCN/H₂O (1:9), respectively and **2.17bL2-3**, at 0.005 mM in MeCN/H₂O (1:3), respectively, at various pH values in air, excitation at 350, 325 and 325 nm, respectively. A-C(ii) A plot of normalised emission intensity for complexes **2.17bL1-3** against pH.

The emission intensity of **2.17bL₁** was almost unchanged between pH *ca.* 2.5 and 6.0, but increased by a factor of *ca.* 2.5 between pH *ca.* 5.4 to 9.1, and then remained constant from pH from 9.1 to 11.5, as per **Fig. 2.24.A(i)**. From the emission intensity changes, a pK_a value of 6.8 was determined which is much smaller than the pK_a (9.9) for the unsubstituted complex **2.17aL₁**. In addition, as noted above, the emission intensity of complex **2.17bL₁** increased with increasing pH whilst the intensity of the unsubstituted analogue **2.17aL₁** decreased with increasing pH. The reason for this difference is not known and clearly warrants further study.

The emission pH titration spectra of **2.17bL₂** and **2.17bL₃** (**Fig. 2.24. B(i)** and **C(i)**, respectively) were similar to that of complex **2.17bL₁**. The emission intensity of **2.17bL₂** and **2.17bL₃** remained relatively unchanged between pH *ca.* 3.5 - 5.0. Both complexes showed only a small increase (1.2-1.3-fold) in emission intensity with increasing pH over the range *ca.* 5.2 – 8.9. The pK_a values of **2.17bL₂** and **2.17bL₃** were calculated to be 7.8 and 7.5, respectively, both lower than the pK_a of the unsubstituted analogues **2.17aL₂** and **2.17aL₃** of 10.0 and 8.9, respectively. However, even though the pK_a of the complexes are in a range relevant to biological imaging, both complexes showed very low sensitivity and hence will clearly not be particularly good sensors. It is not known why these complexes are less sensitive to change, but one possible explanation is that the emission profiles of these two complexes seem to have underlying structure indicative of a greater extent of stabilisation of both filled and unfilled MOs on the ppz ligand, therefore less influenced by the protonated state of ancillary ligand.

2.4.4 pH Titrations of CF₃ Phenylpyridine Ir(III) Complex 2.17dL₂

As for all the other complexes, **2.17dL₂** showed only minor changes in the UV-vis spectrum with pH, the spectra for which are shown in the appendix (**Fig 7**). The emission pH titration data for **2.17dL₂** complex are shown in **Fig. 2.25 A(i)**. Two emission peaks for λ_{max} at 498 nm and 531 nm were observed over the full pH range studied (3.2 to 10.3). The emission intensity remains almost constant between pH 3.2 and 6.0; however, between pH 6.0 and 9.2, the emission intensity decreased by a factor of *ca.* 1.4 which is the opposite trend to that observed for the unsubstituted complex **2.17cL₂**, which gives an increase in intensity at higher pH. From the intensity changes a pK_a value of 7.8 was determined (**Fig.2.25. A(ii)**), which surprisingly is somewhat similar to that of the unsubstituted complex (pK_a 8.0 for **2.17cL₂**).

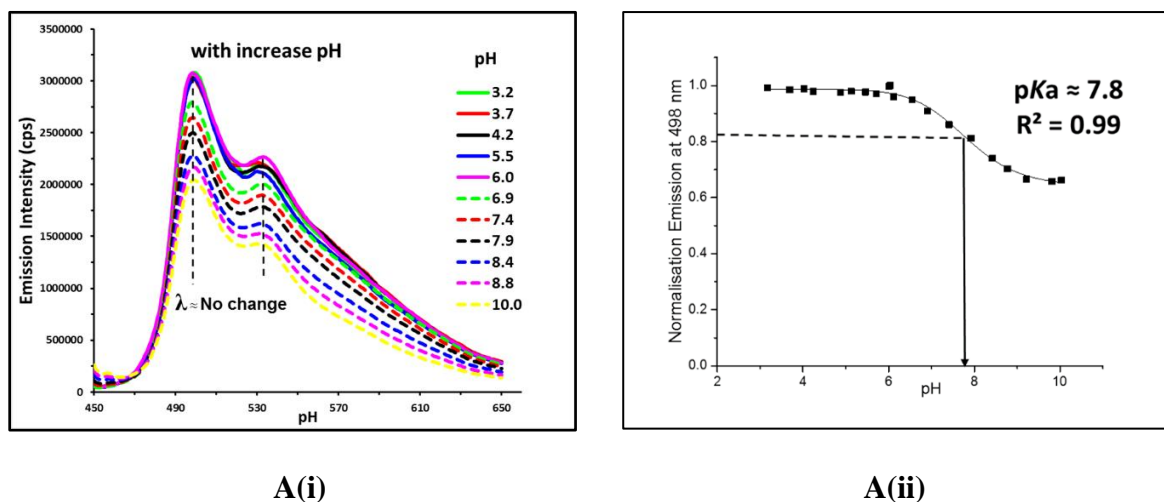


Figure 2.25. **A(i):** Emission titration spectra of complex **2.17dL₂** (0.02mM) at various pH values in MeCN/H₂O (1:9), in air, excitation at 400 nm. **A(ii):** A plot of normalised emission intensity for complex **2.17dL₂** against pH.

2.5 Conclusions and future work

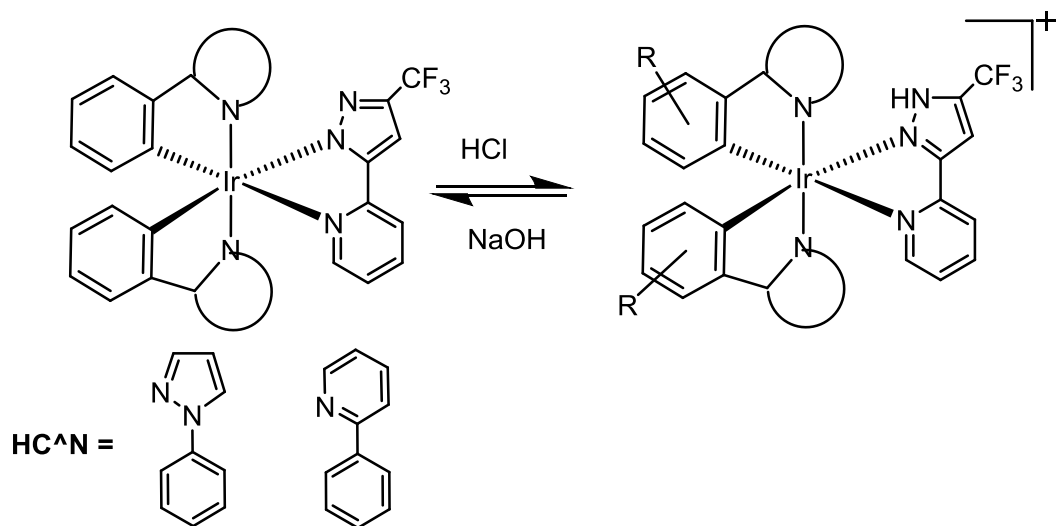
In conclusion, the effect of pH on absorbance in the associated UV-vis spectra was almost negligible over the full pH range studied for these complexes. Hence, these complexes cannot be used as pH sensors using UV-vis spectroscopy and determining the ground state pK_a based on the absorption titration was not feasible. In contrast, the emission intensity of the complexes was significantly modulated (by a factor of 1.2 to 2.9) by altering the pH of the medium, the key data for which are summarised in **Table 2.9**. A key finding is that the complexes can exhibit either a switch on (increase in intensity) or switch off (decrease in intensity) mode, dependent on the cyclometallating ligands. The unsubstituted ppz complexes **2.17aL₁₋₃** showed an intensity decrease with increasing pH; in contrast, the ppy complexes **2.17cL₁₋₃** showed an increase in emission intensity with increasing pH. Changing the R group on the N^N ligand had no significant effect on the subsequent pK_a values. More surprisingly, putting CF₃ groups in the *meta*-position with respect to the coordinating carbon, i.e., complexes **2.17bL₁₋₃** and **2.17dL₁**, resulted in a complete reversal in the direction of the intensity change when compared to their respective unsubstituted congeners. The unsubstituted complexes had pK_a values ranging from 8.0 to 10.0. As anticipated, adding the electron-withdrawing group reduced the pK_a of the complexes (6.8-7.8) compared to the unsubstituted complexes, extending to the pK_a range 8.0 - 10.0. Whilst adding CF₃ substituents had the desired effect on the pK_a , in general it tended to reduce the sensitivity to pH, with these complexes showing a smaller change in intensity. The reason(s) for this difference are not currently known.

Table 2.9: The pK_a values of complexes **2.17aL₁₋₃**, **2.17cL₁₋₃**, **2.17bL₁₋₃** and **2.17dL₁** in a 1:9 MeCN/H₂O medium

Entry	R ₁	R ₂	Complex	pK_a	Sensitivity (Em. intensity)	pH range
1	H	H	2.17aL₁	9.9	decreased by <i>ca.</i> 2-fold	7.5 - 10.0
2		^t Bu	2.17aL₂	10.0	decreased by <i>ca.</i> 2-fold	7.5 - 11.0
3		Ph	2.17aL₃	8.9	decreased by <i>ca.</i> 1.3-fold	8.0 - 10
4	H	H	2.17cL₁	8.9	increased by <i>ca.</i> 1.6-fold	8.0 - 10.9
5		^t Bu	2.17cL₂	8.0	increased by <i>ca.</i> 1.8-fold	7.5 - 10.0
6		Ph	2.17cL₃	9.0	increased by <i>ca.</i> 1.7-fold	7.5 - 10.0
7	CF ₃	H	2.17bL₁	6.8	increased by <i>ca.</i> 2.9-fold	6.0 - 8.0
8		^t Bu	2.17bL₂	7.8	increased by <i>ca.</i> 1.3-fold	5.4 - 9.0
9		Ph	2.17bL₃	7.5	increased by <i>ca.</i> 1.2-fold	5.2 - 9.2
10	CF ₃	^t Bu	2.17dL₂	7.8	decreased by <i>ca.</i> 1.4-fold	<i>ca.</i> 6.0-9.2

In conclusion, this study has shown that pH responsive Ir(III) bis-cyclometallated complexes can be designed to have a pK_a in a range relevant to biological imaging. In particular, complex **2.17bL₁**, with its CF₃ substituted ppz ligand, showed changes in pH over a suitable range with a reasonable sensitivity (the highest of the complexes studied). These results provides a fundamental clue for future work which are outlined as follows:

- 1- Further improvement in the pH sensitivity is needed. This could be achieved by measuring pH titrations for all complexes under degassed conditions.
- 2- For a more detailed understanding of the opposite trend in emission intensity with changing pH, additional data such as lifetimes and DFT calculations are needed.
- 3- In order to improve the pK_a so as to be in a range relevant to biological imaging, this could include the synthesis of $[\text{Ir}(\text{C}^{\wedge}\text{N})_2(\text{N}^{\wedge}\text{N})]^{n+}$ ($n = 0, 1$) complexes bearing the electron-withdrawing CF₃ group on the ancillary ligands, as shown in scheme **2.11**.



Scheme 2.11

Bibliography

1. M. S. Briggs, D. D. Burns, M. E. Cooper and S. J. Gregory, *Chem. Commun.*, 2000, 2323–2324.
2. I. D. Johnson, *The Molecular Probes Handbook: A Guide to Fluorescent Probes and Labeling Technologies*, 11th Edition edn., Life Technologies Corporation, Life Technologies Corporation, Chapter 20, 2010.
3. W. Luo, H. Jiang, X. Tang and W. Liu, *J. Mater. Chem. B*, 2017, **5**, 4768-4773.
4. D. Wencel, T. Abel and C. McDonagh, *Anal. Chem.*, 2014, **86**, 15-29.
5. D. Ellis and R. C. Thomas, *Nature*, 1976, **262**, 224-225.
6. S. J. A. Hesse, G. J. G. Ruijter, C. Dijkema and J. Visser, *J. Biotechnol.*, 2000, **77**, 5-15.
7. T. Li, Y. Liao, X. Jiang, D. Mu, X. Hou, C. Zhang and P. Deng, *Talanta*, 2018, **178**, 538-544.
8. S. G. K. R. G. Zhang, and J. C. LaManna, *J. Appl. Physiol.*, 1990, **68**, 1101-1106.
9. C. Malins, H. G. Glever, T. E. Keyes, J. G. Vos, W. J. Dressick and B. D. MacCraith, *Sens. Actuators, B*, 2000, **67**, 89-95.
10. J. Chao, Y. Liu, J. Sun, L. Fan, Y. Zhang, H. Tong and Z. Li, *Sens. Actuators, B*, 2015, **221**, 427-433.
11. W. Niu, L. Fan, M. Nan, Z. Li, D. Lu, M. S. Wong, S. Shuang and C. Dong, *Anal. Chem.*, 2015, **87**, 2788-2793.
12. J. B. Chao, H. J. Wang, Y. B. Zhang, Z. Q. Li, Y. H. Liu, F. J. Huo, C. X. Yin, Y. W. Shi and J. J. Wang, *Anal. Chim. Acta*, 2017, **975**, 52-60.
13. C. Y. S. Chung, S. P. Y. Li, M. W. Louie, K. K. W. Lo and V. W. W. Yam, *Chem. Sci.*, 2013, **4**, 2453-2462.
14. B. Tang, X. Liu, K. Xu, H. Huang, G. Yang and L. An, *Chem. Commun.*, 2007, 3726–3728.
15. H. R. Kermis, Y. Kostov, P. Harms and G. Rao, *Biotechnol. Prog.*, 2002, **18**, 1047-1053.
16. L. Cao, X. Li, S. Wang, S. Li, Y. Li and G. Yang, *Chem. Commun.*, 2014, **50**, 8787-8790.
17. M. Y. Wu, K. Li, Y. H. Liu, K. K. Yu, Y. M. Xie, X. D. Zhou and X. Q. Yu, *Biomaterials*, 2015, **53**, 669-678.
18. Y. Ge, A. Liu, J. Dong, G. Duan, X. Cao and F. Li, *Sens. Actuators, B*, 2017, **247**, 46-52.

19. K. Qiu, Y. Chen, T. W. Rees, L. Ji and H. Chao, *Coord. Chem. Rev.*, 2017, In Press.
20. S. Das, D. Saha, S. Karmakar and S. Baitalik, *J. Phys. Chem. A*, 2012, **116**, 5216-5226.
21. Q. Zhao, F. Li and C. Huang, *Chem. Soc. Rev.*, 2010, **39**, 3007-3030.
22. B. V. Harbuzaru, A. Corma, F. Rey, J. L. Jordá, D. Ananias, L. D. Carlos and J. Rocha, *Angew. Chem., Int. Ed.*, 2009, **48**, 6476-6479.
23. T.-T. Meng, H. Wang, Z.-B. Zheng and K.-Z. Wang, *Inorg. Chem.*, 2017, **56**, 4775-4779.
24. V. W. W. Yam, V. K. M. Au and S. Y. L. Leung, *Chem. Rev.*, 2015, **115**, 7589-7728.
25. M. Bar, D. Maity, S. Deb, S. Das and S. Baitalik, *Dalton Trans.*, 2017, **46**, 12950-12963.
26. J. N. Demas and B. A. DeGraff, *Anal. Chem.*, 1991, **63**, 829A-837A.
27. J. N. Demas and B. A. DeGraff, *J. Chem. Educ.*, 1997, **74**, 690-695.
28. B. Higgins, B. A. DeGraff and J. N. Demas, *Inorg. Chem.*, 2005, **44**, 6662-6669.
29. J. Kim, Y. Chae Jeong, J. Heo, J. Rhee and K. Hwang, *Bull. Korean Chem. Soc.*, 2009, **30**, 539-540.
30. S. San Tan, S. Yanagisawa, K. Inagaki, Y. Morikawa and M. B. Kassim, *Phys. Chem. Chem. Phys.*, 2017, **19**, 25734-25745.
31. H. j. Yu, Z. f. Hao, H. l. Peng, R. h. Rao, M. Sun, R. Alana W, C. Ran, H. Chao and L. Yu, *Sens. Actuators, B*, 2017, **252**, 313-321.
32. F. Yu, C. Shen, T. Zheng, W. K. Chu, J. Xiang, Y. Luo, C. C. Ko, Z. Q. Guo and T. C. Lau, *Eur. J. Inorg. Chem.*, 2016, **2016**, 3641-3648.
33. T. Mizuno, T. Fukumatsu, M. Takeuchi and S. Shinkai, *J. Chem. Soc., Perkin Trans. 1*, 2000, 407-413.
34. M. H. W. Lam, D. Y. K. Lee, K. W. Man and C. S. W. Lau, *J. Mater. Chem.*, 2000, **10**, 1825-1828.
35. M. Cattaneo, F. Fagalde, C. D. Borsarelli and N. E. Katz, *Inorg. Chem.*, 2009, **48**, 3012-3017.
36. T. W. Tseng, S. Mendiratta, T. T. Luo, T. W. Chen and Y. P. Lee, *Inorg. Chim. Acta*, 2018, **477**, 312-317.
37. K. M. C. Wong, W. S. Tang, X. X. Lu, N. Zhu and V. W. W. Yam, *Inorg. Chem.*, 2005, **44**, 1492-1498.
38. J. L. L. Tsai, T. Zou, J. Liu, T. Chen, A. O. Y. Chan, C. Yang, C. N. Lok and C. M. Che, *Chem. Sci.*, 2015, **6**, 3823-3830.

39. M. J. Han, Y. M. Chen and K. Z. Wang, *New J. Chem.*, 2008, **32**, 970-980.
40. C.-K. Koo, Y.-M. Ho, C.-F. Chow, M. H.-W. Lam, T.-C. Lau and W.-Y. Wong, *Inorg. Chem.*, 2007, **46**, 3603-3612.
41. M. Licini and J. A. Gareth Williams, *Chem. Commun.*, 1999, 1943-1944.
42. J. Weng, Q. Mei, W. Jiang, Q. Fan, B. Tong, Q. Ling and W. Huang, *Analyst*, 2013, **138**, 1689-1699.
43. L. He, Y. Li, C. P. Tan, R. R. Ye, M. H. Chen, J. J. Cao, L. N. Ji and Z. W. Mao, *Chem. Sci.*, 2015, **6**, 5409-5418.
44. F. G. Bordwell, *Acc. Chem. Res.*, 1988, **21**, 456-463.
45. T. Y. Lin, K. C. Tang, S. H. Yang, J. Y. Shen, Y. M. Cheng, H. A. Pan, Y. Chi and P. T. Chou, *J. Phys. Chem. A*, 2012, **116**, 4438-4444.
46. F. Wang and A. W. Schwabacher, *Tetrahedron Lett.*, 1999, **40**, 4779-4782.
47. W. S. Yu, C. C. Cheng, Y. M. Cheng, P. C. Wu, Y. H. Song, Y. Chi and P. T. Chou, *J. Am. Chem. Soc.*, 2003, **125**, 10800-10801.
48. X. Y. Yu, L. Deng, B. Zheng, B. R. Zeng, P. Yi and X. Xu, *Dalton Trans.*, 2014, **43**, 1524-1533.
49. A. Satake and T. Nakata, *J. Am. Chem. Soc.*, 1998, **120**, 10391-10396.
50. S. Kovács and Z. Novák, *Tetrahedron*, 2013, **69**, 8987-8993.
51. H. J. Cristau, Pascal P. Cellier, J. F. Spindler and M. Taillefer, *Eur. J. Org. Chem.*, 2004, **2004**, 695-709.
52. C. Liu, X. Lv, Y. Xing and J. Qiu, *J. Mater. Chem. C*, 2015, **3**, 8010-8017.
53. D. L. Davies, M. P. Lowe, K. S. Ryder, K. Singh and S. Singh, *Dalton Trans.*, 2011, **40**, 1028-1030.
54. A. K. Pal, D. B. Cordes, A. M. Z. Slawin, C. Momblona, E. Ortí, I. D. W. Samuel, H. J. Bolink and E. Zysman-Colman, *Inorg. Chem.*, 2016, **55**, 10361-10376.
55. N. M. Shavaleev, F. Monti, R. Scopelliti, N. Armaroli, M. Grätzel and M. K. Nazeeruddin, *Organometallics*, 2012, **31**, 6288-6296.
56. S. Sprouse, K. A. King, P. J. Spellane and R. J. Watts, *J. Am. Chem. Soc.*, 1984, **106**, 6647-6653.
57. P. J. Spellane, R. J. Watts and C. J. Curtis, *Inorg. Chem.*, 1983, **22**, 4060-4062.
58. F. Neve, M. La Deda, A. Crispini, A. Bellusci, F. Puntoriero and S. Campagna, *Organometallics*, 2004, **23**, 5856-5863.
59. Q. Zhao, S. Liu, M. Shi, C. Wang, M. Yu, L. Li, F. Li, T. Yi and C. Huang, *Inorg. Chem.*, 2006, **45**, 6152-6160.

60. E. Orselli, G. S. Kottas, A. E. Konradsson, P. Coppo, R. Fröhlich, L. De Cola, A. van Dijken, M. Büchel and H. Börner, *Inorg. Chem.*, 2007, **46**, 11082-11093.
61. W. Jiang, Y. Gao, Y. Sun, F. Ding, Y. Xu, Z. Bian, F. Li, J. Bian and C. Huang, *Inorg. Chem.*, 2010, **49**, 3252-3260.
62. M. K. Nazeeruddin, R. T. Wegh, Z. Zhou, C. Klein, Q. Wang, F. De Angelis, S. Fantacci and M. Grätzel, *Inorg. Chem.*, 2006, **45**, 9245-9250.
63. M. S. Lowry, J. I. Goldsmith, J. D. Slinker, R. Rohl, R. A. Pascal, G. G. Malliaras and S. Bernhard, *Chem. Mater.*, 2005, **17**, 5712-5719.

Chapter Three
Synthesis and Characterisation of Ir(III)
pyridylideneamine (PYE) Complexes
[Ir(C^N)₂(PYE)][PF₆]

3.1 Introduction

3.1.1 General Overview

Pyridylideneamines (PYE) have been known for several decades,^{1, 2} and their spectroscopy,^{3, 4} and synthesis,⁵ has been discussed in the literature; however, very little has been written that describes their coordination chemistry,⁶ and indeed their applications.⁷ In general, there are three types of PYE ligands, namely *para*, *ortho* and *meta* substituted, as shown in **Fig. 3.1**. Both *para*- and *ortho*-substituted ligands can have two resonance forms, a neutral one and a zwitterionic one; however, for *meta*-substituted ligands only a zwitterionic resonance structure is feasible, as shown in **Fig. 3.1**. The zwitterionic amide structures seen in *p*-**3.1'**, *o*-**3.1'** and *m*-**3.1'**, have the benefit of aromatic stabilization despite a separation of charge. Note that for simplicity, throughout this chapter reference will be made to the pyridine ring even where it is believed that the resonance structure is the neutral imine and that the heterocycle is not aromatic.

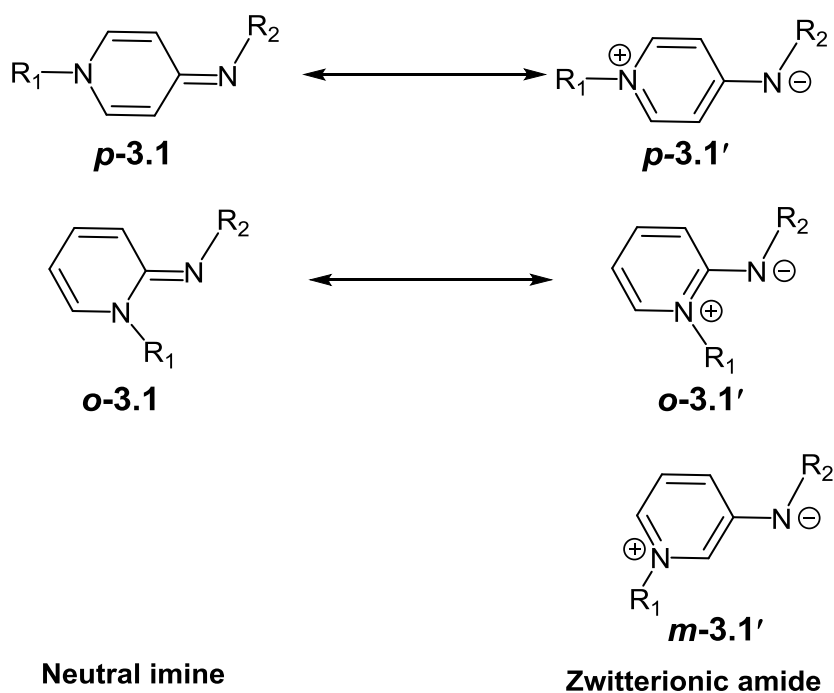


Figure 3.1: Possible resonance structures of PYE ligands

For *para*- and *ortho*-substituted ligands *p*-**3.1**, *o*-**3.1**, if there is a significant proportion of the neutral resonance form then there may be restricted rotation around the C=N imine bond. For *ortho*-PYE ligands *o*-**3.1** such restricted rotation could in principle lead to the possibility of two isomers with the pyridyl *N*-substituent (R₁) *anti* to the imine substituent (R₂) (as shown in Figure 3.1) or with these two substituents *syn*. So far, such isomerisation has not been documented and the *anti*-isomer, which is sterically favoured, is assumed to

be the form present when there is restricted rotation. Hence, an important issue in the study of *para* and *ortho* PYE compounds is the attempt to establish the contribution of the resonance structures, and whether this changes with solvent. Some PYE compounds for which this has been studied are shown in **Fig. 3.2**. The structure of ***p*-3.2** was determined using X-ray crystallography, and selected bond lengths are shown in the diagram. The C(4)—N(1) bond length (1.304(2) Å) displays considerable imine character; typical bond lengths for single and double C—N bonds are 1.47 and 1.28 Å, respectively. Likewise, the C(4)—C(5) and C(4)—C(7) bonds are statistically the same and are considerably longer than a typical aromatic C—C bond (1.34 Å). There is some alternation of bond lengths in the heterocyclic ring with C(5)—C(6) and C(7)—C(8) being noticeably shorter than C(4)—C(5) and C(4)—C(7), whilst the C(6)—N(2) and C(8)—N(2) bonds are between that, and longer than, the expected 1.34 Å for pyridine N—C bonds, respectively. The ¹H NMR spectrum of ***p*-3.2** displays four proton environments for the pyridine ring between δ 7.37 and 8.13, consistent with a considerable double-bond character of the C(4)—N(1) bond. Hence both the X-ray and NMR evidence support a large contribution from the neutral non-aromatic resonance form. Irrespective of this considerable imine character, some of the reactivity of ***p*-3.2** resembles that of an amido salt, as exemplified by its behaviour as a strong base in aqueous solution.⁸

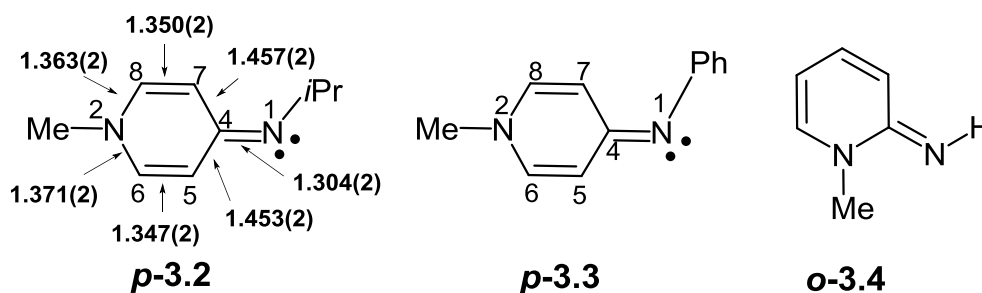


Figure 3.2 Some examples of *para*- and *ortho*-substituted PYE ligands with selected bond lengths in Å

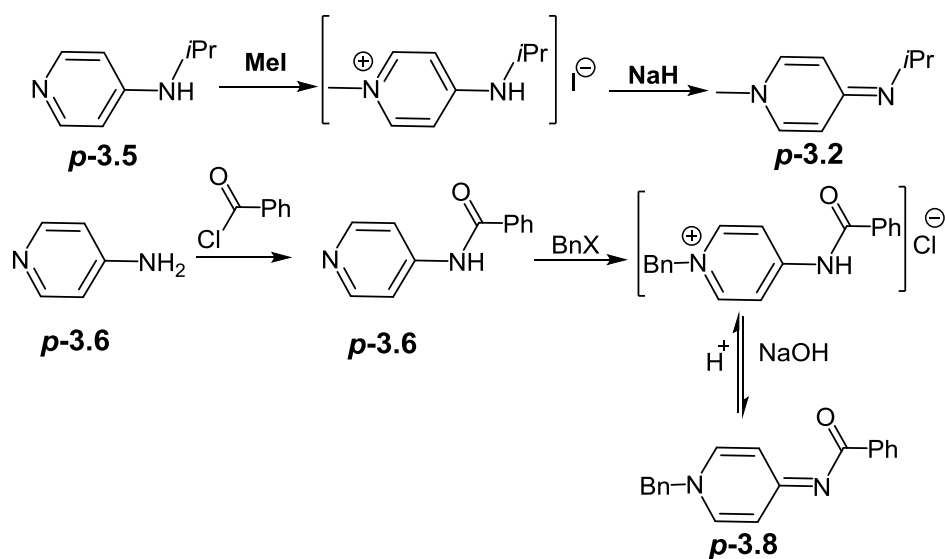
Pagani and co-workers⁹ investigated solvent effects on the resonance structure of ***p*-3.3** using NMR spectroscopy. In the moderate polarity solvent CDCl₃, the ¹H NMR spectrum displays four proton environments for the pyridine ring between δ 6.16 and 6.91, consistent with considerable double-bond character and restricted rotation of the exocyclic C=N bond, owing to a significant contribution by the neutral imine resonance form. The replacement of CDCl₃ with the more polar solvent DMSO at 295 K led to one broad 2H signal (protons 6 and 8) at δ 7.2 and two broad 1H signals at δ 5.95 and 6.05

(protons 5 and 7) for the pyridine ring. The greater difference in chemical shift between protons 6 and 8, and 5 and 7, is indicative of increased contribution from the zwitterionic form, which is consistent with easier rotation about the C=N bond. Recording the spectrum in DMSO at 363 K led to two 2H doublets at δ 7.05 and 6.0 due to protons 6 and 8, and 5 and 7, respectively. This suggests that at 363 K rotation about the exocyclic C—N bond is fast on the NMR timescale, leading to pairwise equivalence of the pyridine protons.

Traore and co-workers⁴ investigated solvatochromism in *o*-**3.4**. The compound is soluble in water and *n*-hexane, and shows two maxima in each solvent. In hexane, the λ_{max} are at 251 nm and 370 nm, whilst in water these shift to 231 nm and 312 nm. The shifts to shorter wavelength in water are consistent with a stronger stabilisation of the ground state compared to the excited state as the solvent polarity increases. However, the authors suggested that the measured spectral changes may be attributed to protonation of the external NH group due to the strong basicity of *o*-**3.4** (pK_a 13.0).

3.1.2 Synthesis of PYE ligands

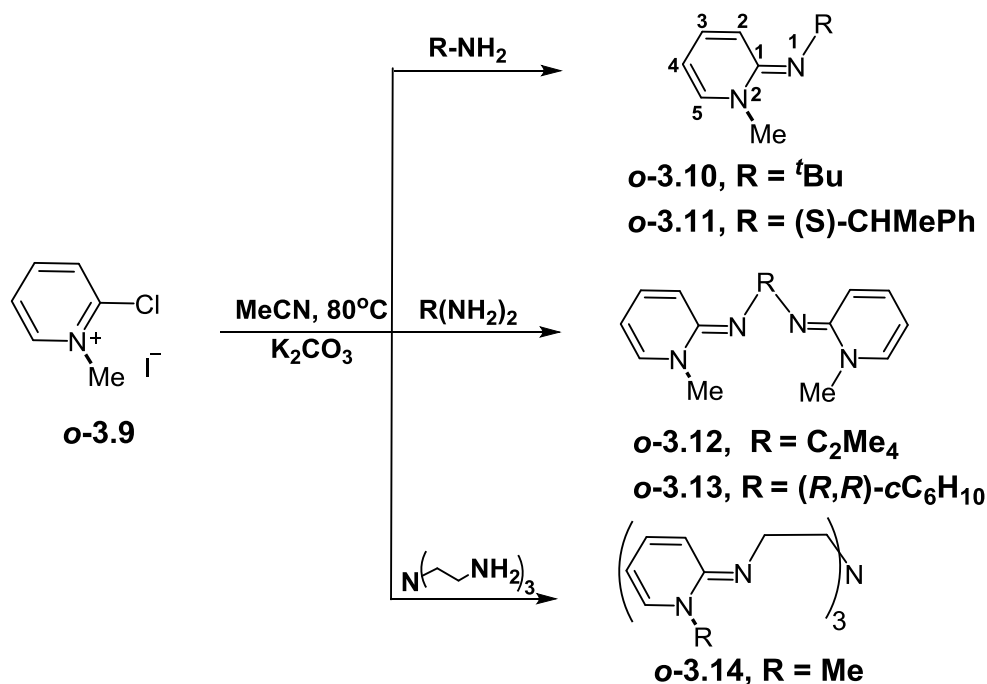
Although PYE ligands have been known for a long time,^{1,2} there are a limited number of procedures for their synthesis. Johnson and co-workers synthesized monodentate PYE ligands as shown in **Scheme 3.1**. Thus, alkylation of 4-(isopropylamino)pyridine *p*-**3.5** with methyl iodide occurs at the pyridine nitrogen atom; deprotonation of the methylpyridinium salt using NaH as base then gives *p*-**3.2** in an 85% yield.⁸



Scheme 3.1: Synthesis of monodentate *para*-PYE ligands.^{7,8}

Wright *et al.* used a similar alkylation of *p*-**3.7** followed by deprotonation to give *p*-**3.8** in an excellent yield of 98% (**Scheme 3.1**).⁷

For *ortho*-substituted PYEs, the alkylation of 2-aminopyridine is usually unselective and condensation reactions between 2-pyridinone and primary amines generally do not take place.⁶ A good method to the production of a variety of *o*-PYE compounds was developed by Douthwaite⁶ involving amination and deprotonation (**Scheme 3.2**). Hence, *o*-**3.9** was converted to monodentate *o*-**3.10** and *o*-**3.11**, bidentate *o*-**3.12** and *o*-**3.13**, and tridentate *o*-**3.14** PYE ligands in good yields. The procedure was also compatible with a range of amine substitution types including chiral derivatives (*o*-**3.11** and *o*-**3.13** in **Scheme 3.2**). It is noteworthy that the exocyclic C=N bond is very resistant to hydrolysis, for example *o*-**3.10** could be heated to reflux in water without undergoing decomposition.⁶ The X-ray structure of *o*-**3.11** was determined and gives good evidence for the imine resonance form being dominant. Thus, there is considerable variation in the C—C bond lengths in the pyridine ring between 1.450(2) and 1.353(2) Å consistent with non-aromaticity in this ring, and the exocyclic C=N bond was found to have a bond length of 1.296(2) Å. In comparison, for 2-aminopyridine the C—C bond lengths are approximately all equal at 1.36 Å and the exocyclic C—NH₂ is significantly longer at 1.384(4) Å, typical of a C(*sp*²)—N single bond.¹⁰



Scheme 3.2: Synthesis of mono-, di- and tridentate *o*-PYE ligands.⁶

Douthwaite *et al.*⁶ also investigated the protonation of a number of PYE ligands. For example, protonation of *o*-**3.10** occurs exclusively at the exocyclic N, where X-ray diffraction showed an increase (0.04 Å) in the exocyclic C(1)—N(1) bond length and a shortening of C(1)—C(2) and C(1)—N(2) bond lengths by a similar amount compared to the neutral precursors. These changes are consistent with a larger contribution of a zwitterionic resonance structure. ¹H NMR spectroscopy of the neutral PYE ligands showed pyridine protons ranging from approximately δ 5.5 to 7.2 with the highest chemical shift being in the proton next to N. By contrast, the protonated PYE ligands showed heterocyclic proton signals shifted significantly downfield (between 1 and 1.5 ppm) from the corresponding neutral precursors; however, the cationic species were still upfield compared to a typical unsubstituted *N*-methylpyridinium salt,¹¹ suggesting incomplete aromatisation of the pyridine.

3.1.3 Synthesis of transition metal complexes with PYE ligands

PYE compounds are potentially strong donor ligands if there is a significant proportion of the anionic amide resonance structure. In addition, the pyridine and imine substituents and the position of the imine can be modified to tune the electronic and steric properties of the ligands. This section will provide an overview of a number of key PYE ligands and complexes whose synthesis has been recently reported. Complex *p*-**3.15** was synthesized by treating *p*-**3.2** with half an equivalent of [RhCl(CO)₂]₂ to generate *p*-**3.15**. The IR spectrum of *p*-**3.15** displays two CO stretching frequencies at 2077 and 1998 cm⁻¹ (av. 2038 cm⁻¹).⁸ By this measure, *p*-**3.2** is a significantly stronger donor than pyridine, the corresponding complex of which displays an average $\nu(\text{CO})$ of 2052 cm⁻¹.¹²

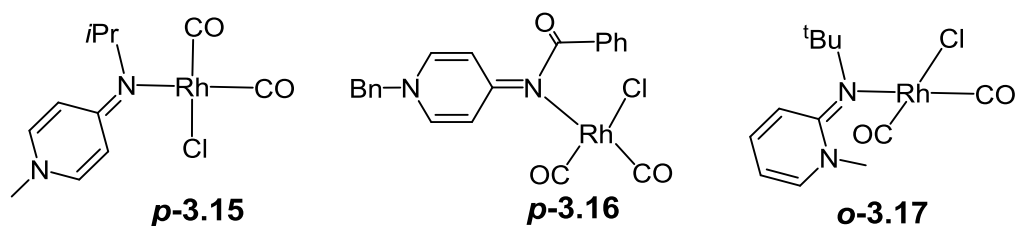
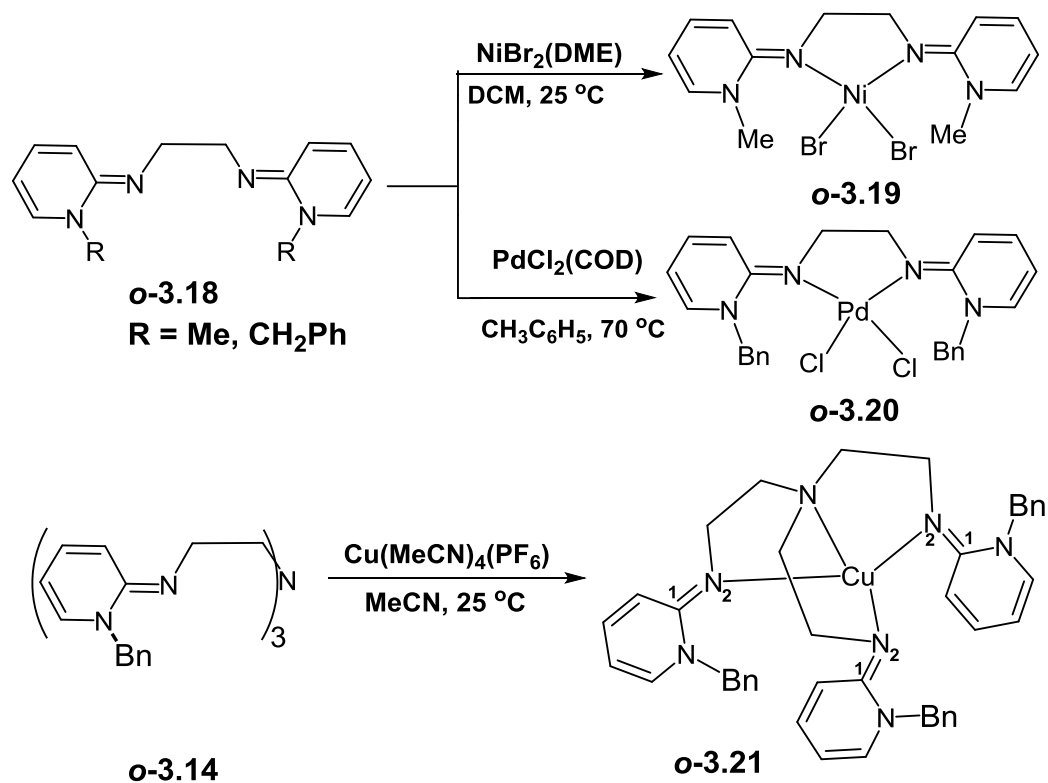


Figure 3.3: PYE-rhodium carbonyl complexes

Similarly complex *p*-**3.16**,⁷ shows two $\nu(\text{CO})$ bands at 2069 and 1987 cm⁻¹ (av. 2028 cm⁻¹) whilst for the ortho-PYE complex *o*-**3.17** the peaks are at 2071 and 1992 cm⁻¹ (av. 2032 cm⁻¹). Hence, for all these PYE complexes the $\nu(\text{CO})$ bands are slightly lower than those reported for *cis*-[RhCl(CO)₂L], where L is a saturated NHC (2081, 1996; av. 2038 cm⁻¹).

¹).¹³ On the basis of these data, the authors suggested that the donor strength of the PYE ligand is at least as great as that of typical NHC ligands.

Douthwaite and co-workers⁶ investigated the coordination of monodentate, bidentate and tridentate *ortho*-PYE ligands with different metals; examples are shown in **Scheme 3.3**.



Scheme 3.3: Synthesis of bidentate and tridentate *ortho*-PYE complexes⁶

The structures of **o-3.19** and **o-3.20** were determined by single-crystal X-ray diffraction. The Ni complex, **o-3.19**, has a tetrahedral geometry at the metal and exhibits pseudo- C_2 symmetry; the nitrogen atoms coordinated to the nickel show a distinct pyramidal geometry (angles around N sum to 342° and 343°). The Pd complex, **o-3.20**, has a distorted square planar geometry with pseudo- C_s symmetry, the conformation of both PYE units is *anti* with the benzyl substituents on the same side as the chlorides. Notably, the ¹H NMR spectrum at room temperature is consistent with C_{2v} symmetry, suggesting the flipping motion of the PYE moieties above and below the Pd square plane is fast on the NMR timescale; this was confirmed by a variable temperature NMR study. Complex **o-3.21** is a diamagnetic yellow solid which has been characterised by NMR spectroscopy and X-ray crystallography, the C(1)—N(2) bond length of *ca.* 1.306(3) Å of which suggests an imine character.⁶

In addition to bis- or tris-PYE ligands, PYE groups have been combined with more conventional donor groups to form heterobidentate ligands. For example, Albrecht *et al.*¹⁴

reported solvatochromic effects on Ru(II)-PYE complex **p-3.22**, the two resonance forms of which are shown in **Fig 3.4**. In this case, the introduction of a carbonyl group adjacent to the imine nitrogen increases the conjugation and enhances the coordinative flexibility of the ligand through the availability of a resonance form **p-3.22''** involving an anionic oxygen. ¹H NMR spectroscopy in different polarity solvents (CD₂Cl₂ and DMSO) showed that the chemical shifts of most of the ligand protons remained unchanged, though the pyridine protons (H_a and H_b) themselves showed more significant changes. In both solvents, protons H_a are equivalent, as are protons H_b, which shows that there is free rotation of the pyridine ring as consistent with a single C—N bond in the zwitterionic resonance form. In CD₂Cl₂, two doublets appear at δ 8.25 for H_a and δ 8.06 for H_b (Δδ = 0.19), whereas in DMSO the difference was larger, with H_a observed at δ 8.35 and H_b at 8.02 (Δδ = 0.33). The increase in Δδ was attributed to an increased contribution of the zwitterionic resonance form, **p-3.22'**.

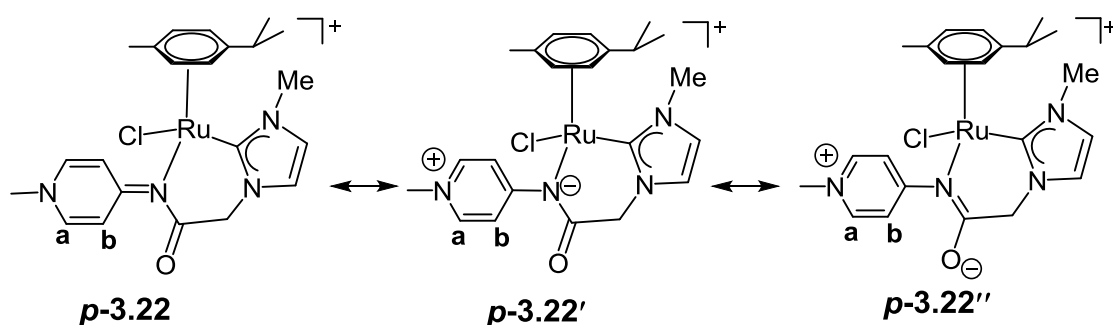
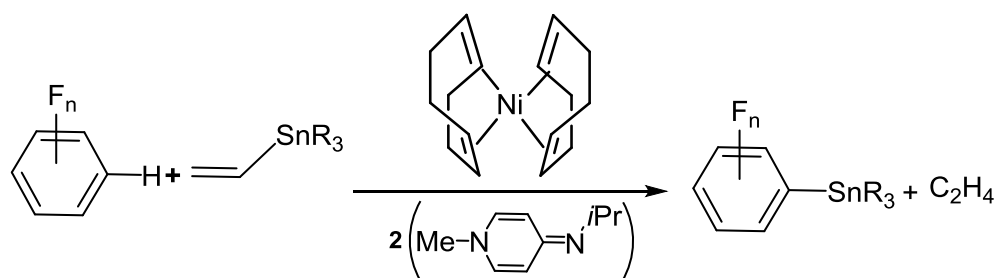


Figure 3.4: Limiting resonance structures of PYE-Ru(II) complex **p-3.22**

3.1.4 Applications of PYE complexes.

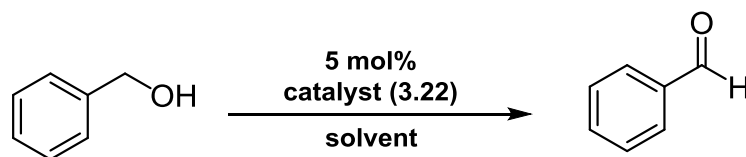
Although there are comparatively few examples of PYE complexes, a number of applications for such complexes have already been determined, particularly in catalysis. They have shown high catalytic activity in different redox transformations including C-F bond activation,⁸ C-H bond stannylation,^{15, 16} transfer hydrogenation,^{14, 17, 18} and water oxidation,¹⁹ all of which warrant the further investigation of PYEs as ancillary ligands in catalysis. Some of these applications are discussed in more detail below.

Johnson and co-workers¹⁵ reported catalytic C-H bond stannylation using a nickel (PYE) complex as a catalyst. Using partially fluorinated arenes, there was no C-F activation; instead, quantitative C-H functionalization was observed, as shown in **Scheme 3.4**.



Scheme 3.4: General reaction for the catalytic stannylation of C-H bonds.

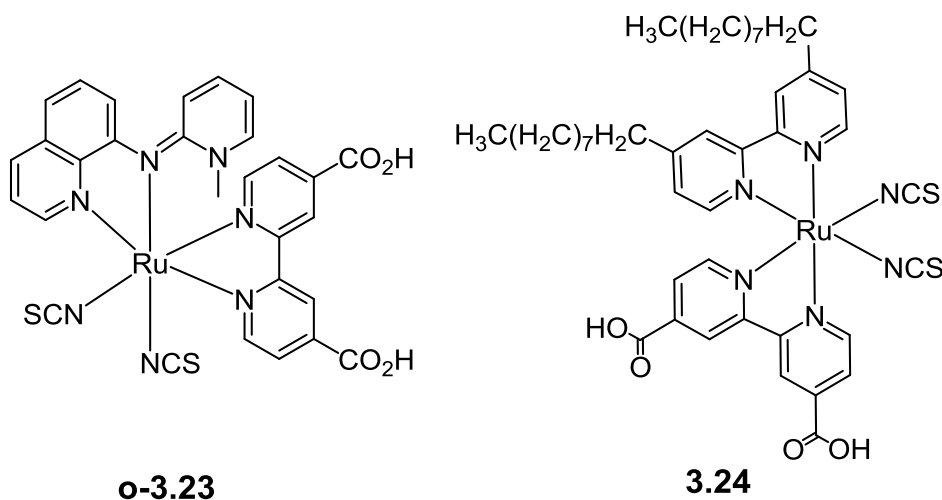
Complex **p-3.22** was tested in the dehydrogenation of benzyl alcohol to benzaldehyde in solvents of varying dielectric constants (**Scheme 3.5**). In 1,4-dioxane or toluene, which have similarly low permittivity ($\epsilon_r = 2.25$ and 2.38 , respectively), no conversion was observed after 2 h. In dichlorobenzene ($\epsilon_r = 9.93$), a very moderate conversion of 6% was obtained, whereas conversion rose to 32% in DMSO ($\epsilon_r = 46.67$). The authors suggested that this higher activity was due to an increased relevance of the zwitterionic resonance structure **p-3.22'** over **p-3.22** with increasing permittivity of the solvent. However, it should be borne in mind that the catalytic cycle involves loss of chloride which may also be favoured in a more polar solvent.



Scheme 3.5: Catalytic dehydrogenation of benzyl alcohol to benzaldehyde using complex **p-3.22** as catalyst

In 2013, the heteroleptic Ru(II) complex **o-3.23** containing a PYE ligand was considered as a dye for a dye-sensitised solar cell.²⁰ The UV-vis spectrum of **o-3.23** in DMF showed bands at 370, 463 and 534 nm that were attributed to MLCT bands, whilst bands in the UV region at 269 and 309 nm correspond to the π - π^* transitions of PYE-8-quinolinamine and 4,4-dicarboxy-2,2-bipyridine, respectively. The lowest energy MLCT band of **o-3.23** was red shifted by 10 nm compared with **3.24** which was attributed to poorer π -acceptor character of PYE-8-quinolinamine relative to bipy, resulting in a slight increase in energy of the metal-based HOMO relative to the bipyridine-based LUMO. Cyclic voltammetry showed the strongly donating PYE led to a cathodic shift of 40 mV for the Ru II/III oxidation for **o-3.23** in comparison with **3.24**. Although **o-3.23** does exhibit some potential advantages, such as absorption at longer wavelengths and a lower oxidation

potential, the photovoltaic performance of **o-3.23** gave an efficiency of 0.42% compared with 4.12% for **3.24**.



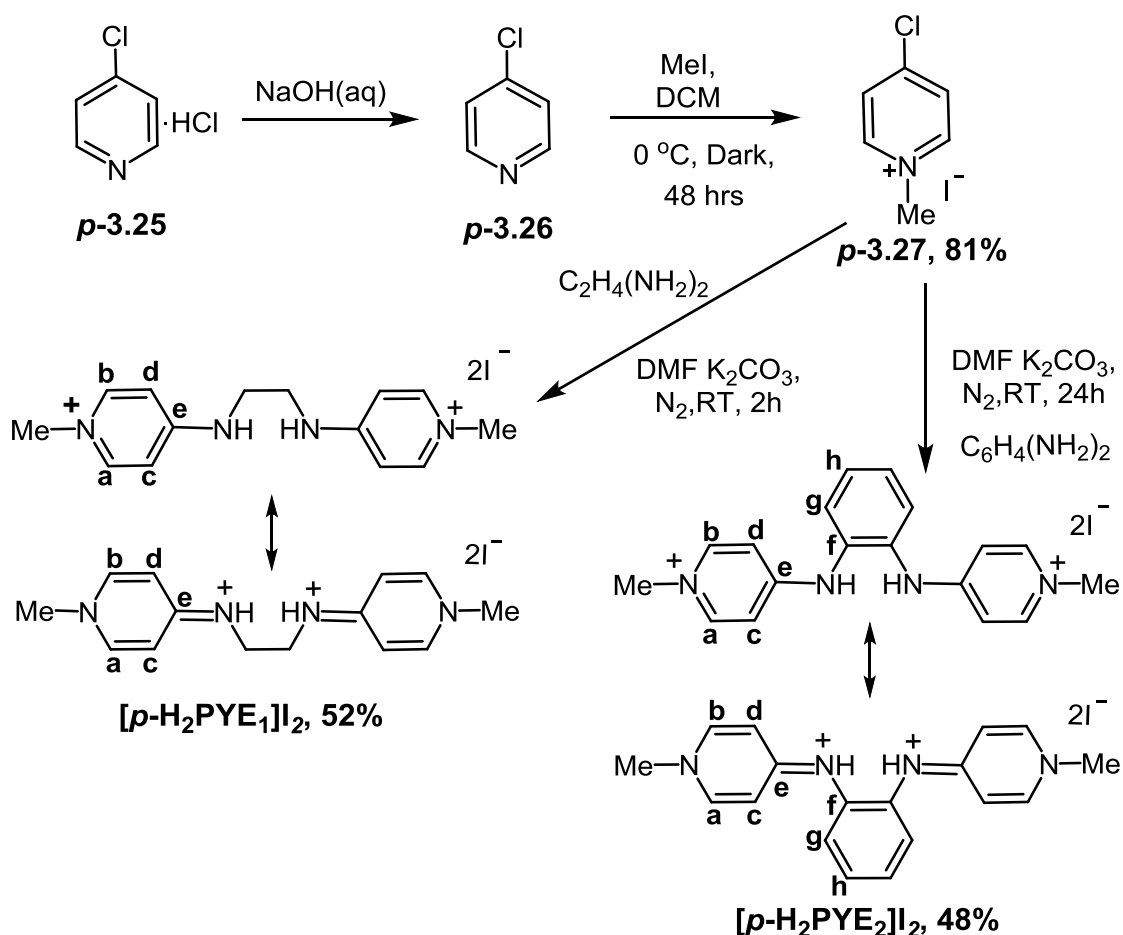
In conclusion, whilst PYE compounds have been known for over a century, it is only recently that their coordination chemistry and potential applications for these complexes have been investigated. PYE ligands can be easily synthesised and modification of the substituents on the pyridinium nitrogen atom and on the amide/imine nitrogen atom can produce a wide variety of substituted derivatives. Structural and NMR studies suggest that in most cases there is a significant contribution from the neutral non-aromatic form, as evidenced by restricted rotation about the C=N bond in *para*-PYE compounds and short C=N bonds in both *para*- and *ortho*-PYE. There is some evidence from NMR spectroscopy that more polar solvents lead to an increase in the zwitterionic resonance structure.⁹ IR studies of metal-PYE complexes indicate that PYEs donate strongly to metal centres,⁶⁻⁸ probably due to the contribution of the zwitterionic amide resonance structure to metal-ligand bonding.

This chapter examines the synthesis and characterisation of cationic Ir(III) complexes [Ir(ppz)₂(N[^]N)][PF₆] (N[^]N = bidentate PYE ligands) and further investigates the donor properties and resonance structures of the ligands and the photophysical properties of the ligands and complexes.

3.2 Results and Discussion

3.2.1 Synthesis of $[p\text{-H}_n\text{PYE}_{1-3}]\text{I}_n$ ($n = 1, 2$)

Compounds $[p\text{-H}_2\text{PYE}_1]\text{I}_2$ and $[p\text{-H}_2\text{PYE}_2]\text{I}_2$ were prepared using literature methods (Scheme 3.6).^{21, 22} An aqueous solution of NaOH was added to $p\text{-3.25}$ until the pH of the mixture reached *ca.* 6-7 to give $p\text{-3.26}$, which was treated immediately with excess MeI in DCM to give $p\text{-3.27}$. Compound $[p\text{-H}_2\text{PYE}_1]\text{I}_2$ was prepared by reaction of $p\text{-3.27}$ with 1,2-diaminoethane in DMF in the presence of K_2CO_3 . $[p\text{-H}_2\text{PYE}_2]\text{I}_2$ was prepared in a similar manner from 1,2-phenylenediamine. The desired ligands were isolated in their protonated form. Attempts to deprotonate the salts by treatment with $\text{NaOH}_{(\text{aq})}$ in a biphasic reaction with DCM and isolate as the neutral $p\text{-PYE}$ ligands were unsuccessful, thus the complexes were prepared from their salts in the presence of a base (see below).



Scheme 3.6: Synthesis of Ligands $[p\text{-H}_2\text{PYE}_1]\text{I}_2$ and $[p\text{-H}_2\text{PYE}_2]\text{I}_2$

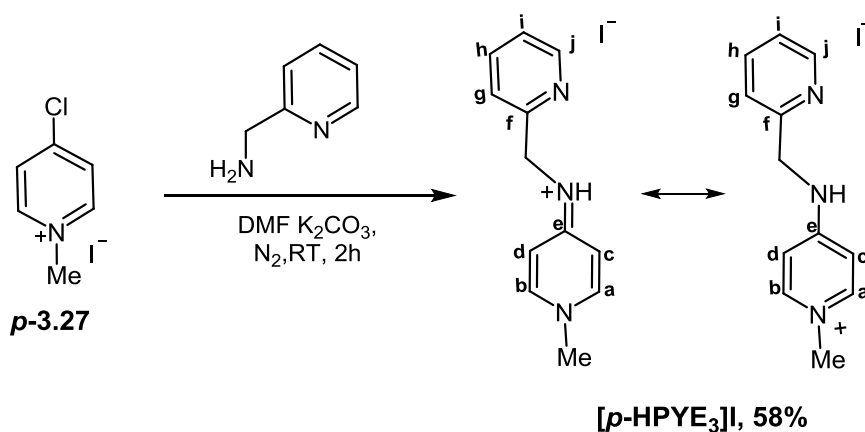
Compound $[p\text{-H}_2\text{PYE}_1]\text{I}_2$ is only soluble in water. The ^1H NMR spectrum (in D_2O) shows two broad doublets, which integrate to two protons each, in the aromatic range at δ 7.88 and δ 6.78, which are assigned to protons $\text{H}_{\text{a, b}}$ and $\text{H}_{\text{c, d}}$, respectively. A 6H singlet at δ 3.84 is assigned to the NMe groups and a 4H singlet at δ 3.62 to the protons of the C_2H_4

bridge. The assignments to H_{a, b} and H_{c, d} are confirmed by NOEs to the NMe and NCH₂ signals, respectively. The NH protons were not observed, probably due to exchange with D₂O. The equivalence of H_{a, b} and of H_{c, d} suggests that there is rotation of the NMe pyridine and hence a preponderance of the pyridinium resonance form, as expected in the very polar solvent. In the ¹³C NMR spectrum, the heterocycle shows a quaternary carbon at δ 157.2 and four different CH carbons at δ 144.2 and 142.2 (for C_{a, b}), and 110.9 and 105.4 (for C_{c, d}), suggesting that rotation around the C—N bond is slow due to the increased frequency separation in the ¹³C NMR spectrum compared to the ¹H NMR spectrum. The carbons of the NMe group and C₂H₄ bridge were observed at δ 44.7 and 41.4, respectively. The high-resolution MS (ASAP) showed an ion at *m/z* 243.1608 (243.1610 calculated for C₁₄H₁₉N₄) due to the loss of a proton from the dication.

The ¹H NMR spectrum (CD₃OD) of [**p-H₂PYE₂**]**I**₂ is similar to [**p-H₂PYE₁**]**I**₂ except the CH₂ bridging group is replaced by a C₆H₄ group. The spectrum shows the pyridine protons as two 4H doublets, one at δ 8.18 and a broad doublet at δ 7.00 with a 4H multiplet at δ 7.58-7.53 assigned to the C₆H₄ group. The NMe group is easily identified as the only singlet at δ 4.01. This signal shows an NOE to the doublet at *ca.* δ 8.18 which is therefore assigned to protons H_{a, b}, whilst the assignment of H_{c, d} was confirmed by NOEs to the H_{g, h} signals. The observation that the H_{c, d} signal is broad might indicate that the rotation about the C=N bond is starting to become restricted. As above, the NH protons were not observed, most likely due to exchange with the solvent. The ¹³C NMR spectrum shows two quaternary carbons at δ 157.4 and 133.7 for carbons C_{e, f} respectively. Carbons C_{a, b} were observed at δ 145.6 whilst carbons C_{c, d} were not observed. However, a weak cross peak in the HSQC spectrum was observed between protons c, d which correlated with a cross peak at 110.7 ppm in the ¹³C spectrum and which was too broad to see in the 1-D spectrum, suggesting a degree of rotation about the C=N bond. The IR spectrum shows a very broad band at *ca.* 3400 cm⁻¹, which was assigned to the N—H bond. The high-resolution MS (ASAP) show an ion at *m/z* 291.1607 (291.1610 calculated for C₁₈H₁₉N₄) due to the loss of a proton from the dication.

Ligand [**p-HPYE₃**]**I** was synthesised using the same method as for [**p-H₂PYE₁₋₂**]**I**₂ (Scheme 3.7). The ¹H NMR spectrum (see Fig. 3.5) of [**p-HPYE₃**]**I** in (CD₃)₂CO displays a 3H singlet at δ 4.12 due to the NMe group and a 2H singlet at δ 4.75 assigned to the NCH₂ signal. The spectrum also shows four inequivalent protons for the NMe pyridine ring, two doublets at δ 8.32 and 8.23 for protons H_b and H_a and two doublets of doublets

at δ 7.42 and δ 7.04 due to H_c and H_d. The assignments to H_{a, b} and H_d were confirmed by NOEs to the NMe and NCH₂ signal, respectively. The observation of four separate resonances for the NMe pyridine suggests there is no free rotation of the NMe pyridine unit, suggesting some double bond character around the exocyclic C=N bond. The assignment of pyridine proton H_g (δ 7.53) was confirmed by an NOE to the NCH₂ signals, whilst the other pyridine protons which are observed between δ 7.32 and 8.55 were assigned using the COSY spectrum. No NH signal was observed, probably due to exchange with D₂O in the solvent (CD₃)₂CO. The ¹³C NMR spectrum shows four different CH carbons for the NMe pyridine ring between δ 145.4 and 107.2, suggesting imine character, whilst the NMe group is observed at δ 45.4. The IR spectrum shows strong bands at *ca.* 1687 and 1646 cm⁻¹ which were assigned to C=N bonds, and the high-resolution MS (ASAP) shows a molecular ion at *m/z* 200.1186 (200.1188 calculated for C₁₂H₁₄N₃).



Scheme 3.7: Synthesis of [p-HPYE₃]I

The replacement of acetone with the more polar solvent D₂O effects the proton shifts of [p-HPYE₃]I, in particular of the NMe-pyridine group. Protons H_{a-b} were observed as a doublet at δ 7.87 whilst protons H_{c-d} appeared as two broad signals at δ 6.91 and δ 6.62, respectively, all of which were *ca.* δ 0.4-0.5 upfield compared to those in (CD₃)₂CO. The fact that H_{a-b} are apparently equivalent and H_{c, d} give broad signals indicates that the speed of rotation of the NMe pyridine increases in the more polar solvent, suggesting increased single bond character of the exocyclic C—N bond in D₂O. However, the observation that all the NMe-pyridine signals are upfield compared to those in (CD₃)₂CO is less consistent with the NMe pyridinium resonance structure, for which H_{a-b} may be expected to show a downfield shift. It should be noted that hydrogen-bonding interactions, e.g., of the second pyridine with the NH of the protonated imine or with water (in D₂O) may also play a role.

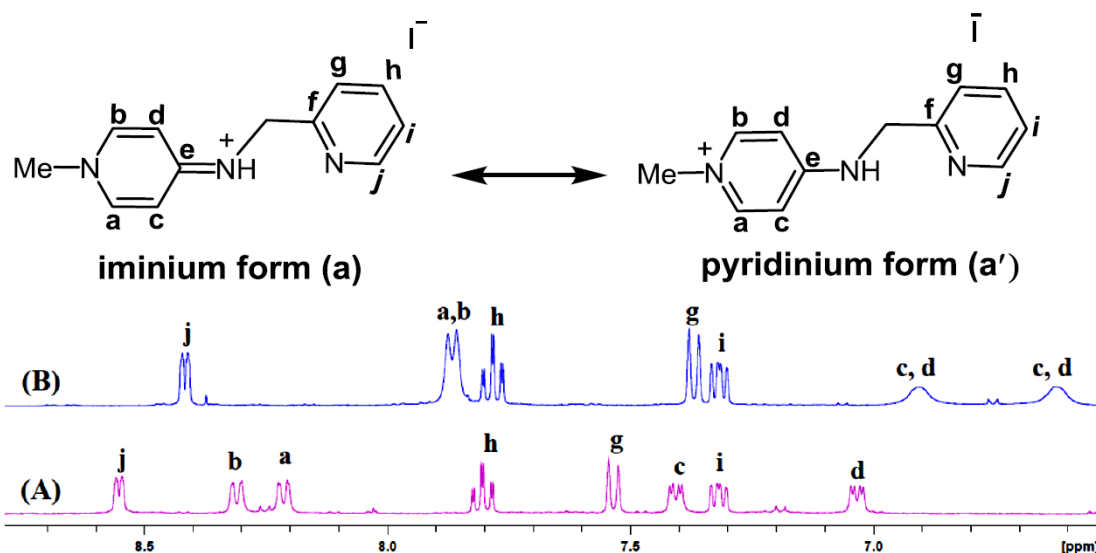


Figure 3.5. Section of the ^1H NMR spectrum of ligand $[\textit{p}\text{-HPYE}_3]\text{I}$; (A) in $(\text{CD}_3)_2\text{CO}$ and (B) in D_2O (500 MHz RT).

A single crystal of $[\textit{p}\text{-H}_2\text{PYE}_1]\text{I}_2$ suitable for X-ray diffraction was grown from D_2O and the molecular structure, is shown in **Fig. 3.6**. The compound shows C_2 symmetry in the solid state. The $\text{N}(2)\text{—C}(3)$ bond length of $1.326(4)$ Å suggests some protonated imine character. In the NMe pyridine, the $\text{C}1\text{—C}2$ and $\text{C}4\text{—C}5$ bond lengths (*ca.* 1.36 Å) are shorter than $\text{C}2\text{—C}3$ and $\text{C}3\text{—C}4$ (*ca.* 1.42 Å) suggesting incomplete aromatisation of the NMe pyridine ring.

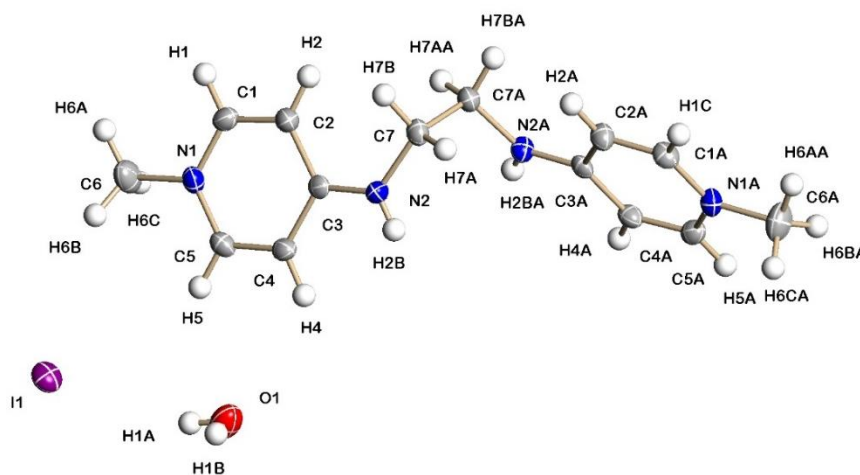
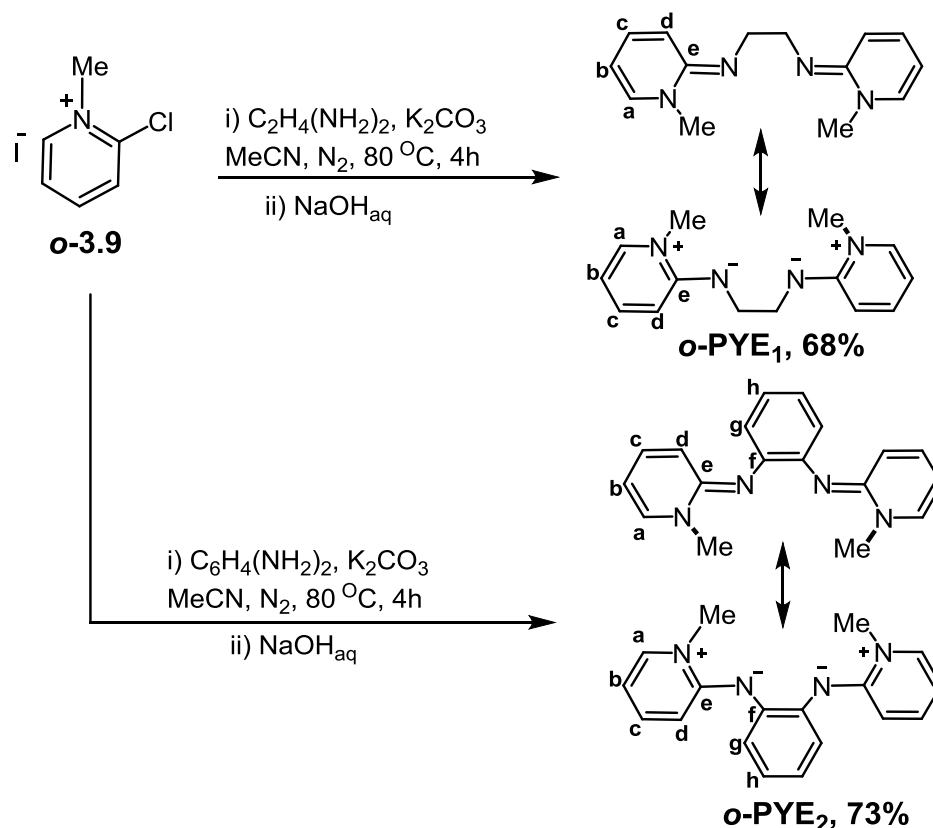


Figure 3.6: X-ray crystal structure for $[\textit{p}\text{-H}_2\text{PYE}_1]\text{I}_2$ with 50% ellipsoids,

3.2.2 Synthesis of *o*-PYE ligands

Ligands *o*-PYE₁₋₂ were synthesized according to literature methods (see **Scheme 3.2** earlier)⁶ which are outlined in **Scheme 3.8**. The reaction between *o*-3.9 and the corresponding amines in the presence of a base occurred at 80°C over 4 hrs. The

protonated PYE compounds were then treated with NaOH_(aq) in biphasic reactions with DCM or toluene solution to form pure neutral *o*-PYE₁₋₂ in good yields.



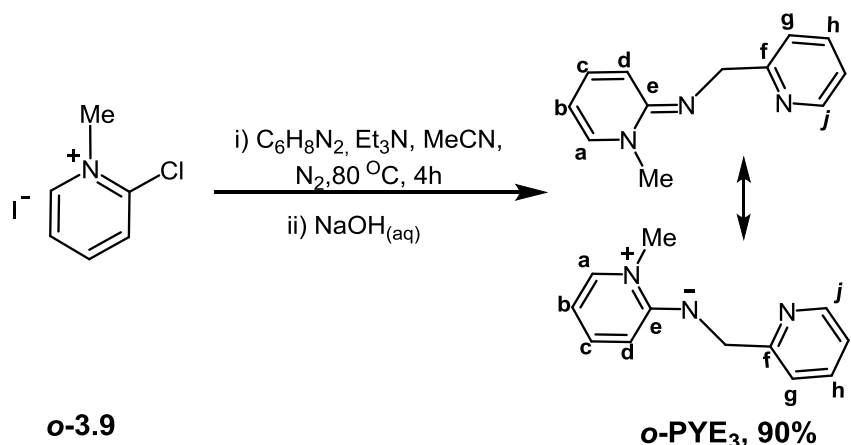
Scheme 3.8: Synthesis of ligands *o*-PYE₁ and *o*-PYE₂

The ¹H NMR spectra of ligands *o*-PYE₁₋₂ are similar to each other as they both show C₂ symmetry. The *o*-PYE₁ is a known ligand and the data so recorded is in agreement with the literature.⁶ The four pyridine protons are inequivalent, ranging from δ 6.95-5.56, all upfield from a typical pyridine group (δ 7.5-8.8), suggesting incomplete aromatisation of the pyridine. This is consistent with some double bond character and the prevalence of the neutral imine resonance form. The ¹³C NMR spectrum shows one quaternary carbon at δ 154.1 and four CH carbons between δ 138.9 and 100.1 for the pyridine. The IR spectrum shows a strong band *ca.* 1636 cm⁻¹ assigned to the C=N stretch, and two strong bands at *ca.* 1559 and 1532 cm⁻¹ which are attributed to C=C bonds in agreement with the literature.⁶ The high-resolution mass spectrum (ASAP), shows an ion due to [M+H]⁺ at *m/z* 243.1605 (243.1610 calculated for C₁₄H₁₉N₄).

The ¹H NMR spectrum of *o*-PYE₂ is very similar to that of *o*-PYE₁ with the pyridine ring protons between *ca.* δ 6.95 and 5.67, an extra signal in the aromatic region (a 4H multiplet at *ca.* δ 6.93) due to the C₆H₄ bridging group, and a singlet at δ 3.29 due to the NMe groups. The assignment to H_a is confirmed by NOEs to the NMe, with the other NMe

pyridine protons H_{b, c, d} then assigned via COSY and NOESY spectra. The pyridine protons are upfield from a typical pyridine ring, suggesting incomplete aromatisation of the N-pyridine and double bond character of the exocyclic C=N bond. The ¹³C NMR spectrum shows two quaternary carbons at δ 151.8 and 142.3 and four CH carbons for the pyridine carbons ranging from approximately δ 137.8 to 102.1. The IR spectrum shows a strong band at 1639 cm⁻¹ which was assigned to the C=N bond and two strong bands at *ca.* 1573 and 1556 cm⁻¹ which were attributed to C=C bonds. All this data is consistent with C=N double bond character and the neutral imine resonance form being predominant. The high-resolution mass spectrum (ASAP), shows an ion due to [M+H]⁺ at *m/z* 291.1607 (291.1610 calculated for C₁₈H₁₉N₄).

The new unsymmetrical ligand ***o*-PYE₃** was synthesised using the same method as for ***o*-PYE₁₋₂** (**Scheme 3.9**). This ligand provides a direct comparison between the NMe pyridine and the substituent pyridine. The ¹H NMR spectrum of ***o*-PYE₃** shows a clear distinction between these two groups where the NMe pyridine protons occur as four protons between δ 5.71 (H_b) and 7.09 (H_a) as for the ligands described above. However, the pyridine substituent shows more conventional aromatic shifts with signals between δ 7.09 (H_i) and 8.53(H_j). This clear difference in shifts shows that the NMe pyridine is not aromatic, consistent with the neutral resonance form. The *N*-methyl resonance was observed as a singlet at δ 3.96, and a singlet at δ 4.57 was assigned to the CH₂ signal. The other assignments are made on the same basis as for previous ligands. The ¹³C NMR spectrum shows the expected number of signals, from δ 139.1(C_a) to 101.3 (C_b) for the NMe pyridine carbons, and from δ 148.8 (C_j) to 121.4 (C_h) for the pyridine substituent. The IR spectrum shows two strong bands at *ca.* 1644 and 1563 cm⁻¹ which were attributed to C=N stretch and C=C, respectively, consistent with the neutral imine resonance structure. The high-resolution mass spectrum (ASAP) showed a molecular ion [M+H]⁺ at *m/z* 200.1178 (200.1188 calculated for C₁₂H₁₄N₃).



Scheme 3.9: Synthesis of ligand *o*-PYE₃

Single crystals of *o*-PYE₂ suitable for X-ray diffraction were grown from CDCl₃. The molecular structure, selected bond lengths and angles are shown in **Fig. 3.7**. The compound exhibits close to *C*₂ symmetry with the bond lengths and angles of both NMe pyridine rings being very similar. See appendix **Table 4** for further data.

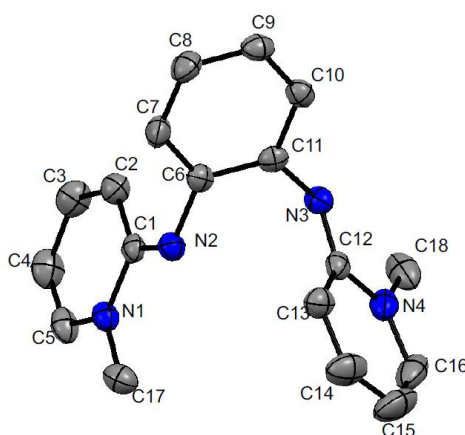


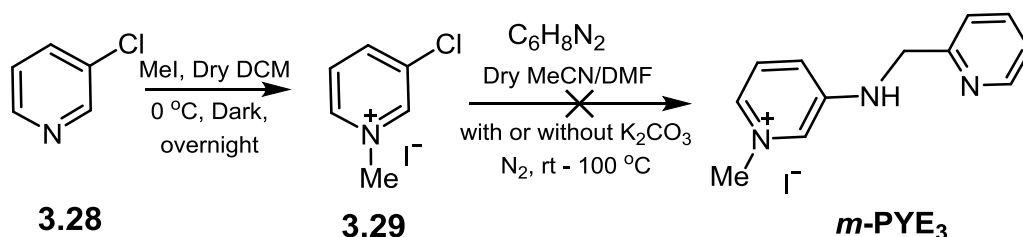
Figure 3.7: X-ray crystal structure for *o*-PYE₂ with 50% ellipsoids; all H atoms are omitted for clarity. Selected bond lengths (Å); N(3)—C(12), 1.294(2); N(3)—C(11), 1.421(2); N(2)—C(1), 1.296(2); N(2)—C(6), 1.416(2); C(6)—C(11), 1.406(2).

The N(2)—C(1) and N(3)—C(12) bond lengths (1.296(2) and 1.294(2) Å, respectively) are shorter than a single bond suggesting that *o*-PYE₂ displays considerable imine character; typical bond lengths for single and double C—N bonds are 1.47 and 1.28 Å, respectively.⁸ The N(2)—C(6) and N(3)—C(11) lengths are also slightly shorter than normal C—N single bonds, suggesting a small amount of delocalisation into the C₆H₄ bridge. There is some evidence for bond length alternation in the NMe-pyridine rings with C—C distances ranging from 1.342(2) to 1.431(2) Å (ring N1) and 1.338 to 1.430(2)

Å (ring N4) with C(4)—C(5) and C(15)—C(16) being the shortest bonds in the two rings, respectively. All this data is consistent with a significant contribution by the neutral resonance structure. The angles C(11)—N(3)—C(12) and C(6)—N(2)—C(1) are both *ca.* 118°, consistent with *sp*² hybridisation for the imine N atoms. The NMe pyridine rings are not coplanar with the C₆H₄ plane with the N(4) ring at an angle of *ca* 67° whilst the N(1) ring is at 83.9°, presumably due to steric interactions.

3.2.3 Attempts to synthesise *m*-PYE ligands

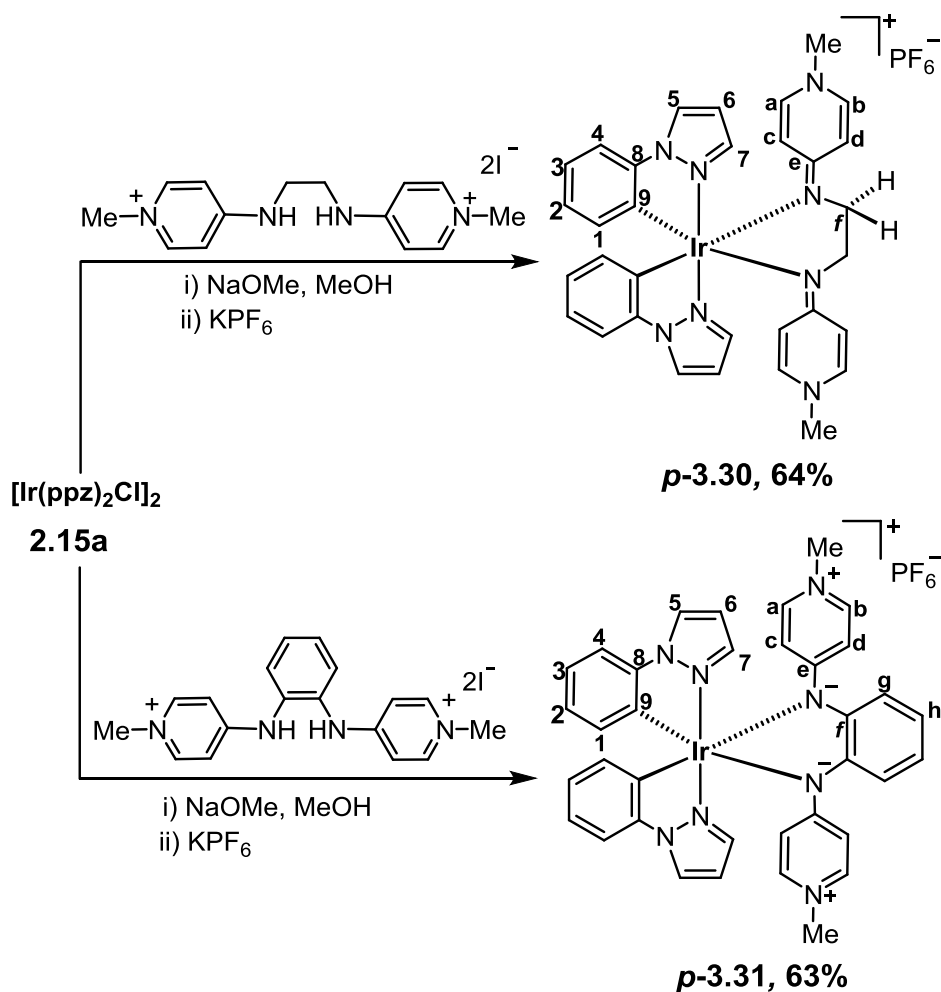
Attempts to make *m*-PYE ligands are shown in **Scheme 3.10**. Methylation of **3.28** gave **3.29** as described in the literature.²² However, treatment of **3.29** with 2-picolyamine, in a range of different solvents or reaction conditions (e.g., MeCN or DMF for 1 h at RT to overnight stirring at RT or overnight heating under reflux) failed to yield any product. The reaction was monitored by ¹H NMR spectroscopy and mass spectrometry, neither of which showed any evidence for the desired product, only showing starting materials as being present throughout.



Scheme 3.10: Attempts to synthesise the *m*-PYE ligand.

3.2.3 Synthesis and characterisation of *para*-PYE Ir(III) complexes

A mixture of [*p*-H₂PYE₁]₂I₂ and NaOCH₃ in methanol (4 ml) were warmed gently at 40°C for 15 mins to deprotonate the ligand, after which a solution of the dimer **2.15a** in methanol was added and the mixture stirred for 4 h at room temperature. The residues were rotary evaporated, dissolved in DCM, and then converted to their PF₆ salts by ion-exchange with aqueous KPF₆ to form complex *p*-**3.30** in good yield (64%) (Scheme 3.11). Complex *p*-**3.31** was synthesised using the same method in a 63% yield (Scheme 3.11).



Scheme 3.11. Synthesis of *para*-PYE Ir(III) complexes *p*-3.30 and *p*-3.31.

The ^1H NMR spectra of *p*-3.30 and *p*-3.31 show a two-fold axis of symmetry in solution, i.e., both cyclometallating ligands were equivalent, as are both halves of the [*p*-PYE₁₋₂] ligands, giving only one set of signals with each signal representing two equivalent protons. The ^1H NMR spectrum of *p*-3.30 showed two doublets at δ 3.57 and 3.18 which were assigned to the C_2H_4 bridge and a 6H singlet at δ 3.84 due to the NMe groups. The two doublets of the C_2H_4 bridge both showed NOEs to a doublet at δ 6.32 which was therefore assigned to the pyridine proton (H_d). Protons H_{a-c} (δ , 6.44, 6.86 and 6.34 respectively) were subsequently assigned via NOESY and COSY spectra. The assignments of $\text{H}_{a,b}$ were confirmed by NOEs to the NMe group. The upfield shifts of protons H_{a-d} compared to free pyridine (*ca.* δ 7.5-8.5) and the fact that they are all inequivalent suggests incomplete aromatisation of the NMe pyridine and restricted rotation about the exocyclic $\text{C}=\text{N}$ bond. The TOCSY spectrum allowed the assignment of the phenyl (H_{1-4}) and pyrazole (H_{5-7}) protons and the expected NOE was observed between the phenyl protons H_4 and pyrazole protons H_5 ; the COSY spectrum then allowed

assignment of the other protons. The pyrazole protons H₅ were the most downfield signal at δ 8.10, whilst the phenyl protons H₁ were the most upfield signal (δ 6.14) due to ring current effects,²³ as discussed in Chapter 2. The ¹³C NMR spectra of **p-3.30** showed four different CH carbons for the NMe-pyridine in the range δ 143.4 to 108.0, respectively, suggesting that there is restricted rotation about the exocyclic C=N bond. The remaining carbon signals were all observed – see chapter 5 for details. The FAB mass spectrum shows a molecular ion at m/z 721.2371 (721.2371 calculated for C₃₂H₃₂IrN₈).

The ¹H NMR spectrum of complex **p-3.30** was carried out in solvents of different polarity, namely CD₂Cl₂, (CD₃)₂CO, and CD₃CN, to determine if this affected the resonance structure of the PYE ligand (see **Fig. 3.8**). In the moderate polarity solvent CD₂Cl₂, the ¹H NMR spectrum displays four proton environments for the NMe pyridine ring between δ 6.16 and 6.91, consistent with considerable double-bond character and restricted rotation of the exocyclic C=N bond owing to a significant contribution from the neutral imine resonance form. In (CD₃)₂CO, or CD₃CN, the NMR spectra still show four proton environments for the NMe pyridine protons. The spectra in (CD₃)₂CO, or CD₃CN, show a greater difference in chemical shift between protons a, b and c, d, suggestive of increased contribution from the zwitterionic form (see introduction to this chapter); however, $\Delta\delta$ is greatest in (CD₃)₂CO, rather than the more polar CD₃CN. It should also be noted that changing the solvent has significant effects on the chemical shifts of pyrazole protons (5 and 7), hence the above changes may not be due to changes in the resonance structure.

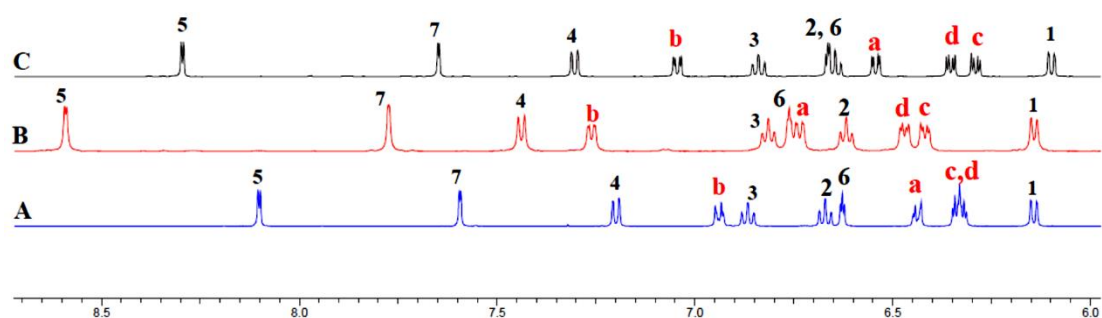


Figure 3.8: Sections of ¹H NMR spectrum (500 MHz, 298 K) of complex **p-3.30**; (A) in CD₂Cl₂, (B) in (CD₃)₂CO and (C) in CD₃CN.

The ¹H NMR spectrum of **p-3.31** is similar to **p-3.30** except the C₂H₄ doublets are replaced with two multiplets for 4H at *ca.* δ 7.16 and 6.89 due to the C₆H₄ bridging group. The NMe group is the only singlet, at δ 3.42, and the phenyl pyrazole protons were assigned in the same manner as for **p-3.30**. The TOCSY spectrum allowed for the

assignment of the phenyl (H₁₋₄) and pyrazole (H₅₋₇) protons and the expected NOE was observed between the phenyl protons H₄ and pyrazole protons H₅; the COSY spectrum then allowed for the assignment of the remaining protons (see Chapter 5 for details). The signals for the NMe pyridine protons H_{a-d} are extremely broad (see **Fig 3.9**), indicating that rotation of the NMe pyridine occurs on a similar timescale to the NMR, suggesting some single bond character and free rotation of the exocyclic C—N bond. The ¹³C NMR spectrum shows four quaternary carbons, the carbon of NMe group, and only ten CH carbons, where the NMe pyridine carbons C_{a-d} were not observed. Presumably the speed of rotation of the NMe pyridine group leads to these carbon signals being very broad. The high-resolution mass spectrum (FAB) shows a molecular ion at *m/z* 769.000 (769.2379 calculated for C₃₆H₃₂IrN₈).

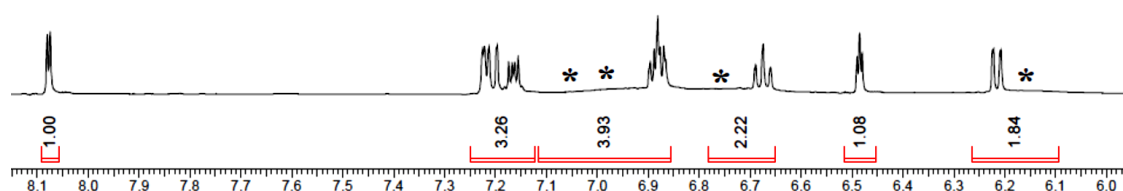


Figure 3.9. Section of the ¹H NMR spectrum (500 MHz, 298 K) of *p*-**3.31** in CD₂Cl₂ at room temperature showing the relevant part of NMe pyridine ring (*) (Integrations apply to one half of the molecule).

Running the ¹H NMR spectrum in a more polar solvent (e.g., (CD₃)₂CO, CD₃CN) led to some sharpening of these signals, however to gain more information a variable temperature NMR study was performed in CD₃CN. Figure **3.10** depicts the temperature-dependent ¹H NMR spectra of *p*-**3.31** between –30 °C and 70 °C in CD₃CN. At low temperatures (–30 °C), the NMe-pyridine signals were observed as four broad signals between *ca.* δ 6.0-7.1 indicating rotation around the exocyclic C—N bond is slow at low temperature. Raising the temperature leads to a pairwise equivalence of the signals; at 70 °C H_{a, b} were observed as a doublet at *ca.* δ 6.9, whilst the signal for H_{c, d} remained still broad at *ca.* δ 6.5. Thus, as expected, the rate of rotation about the C—N bond is faster at higher temperatures.

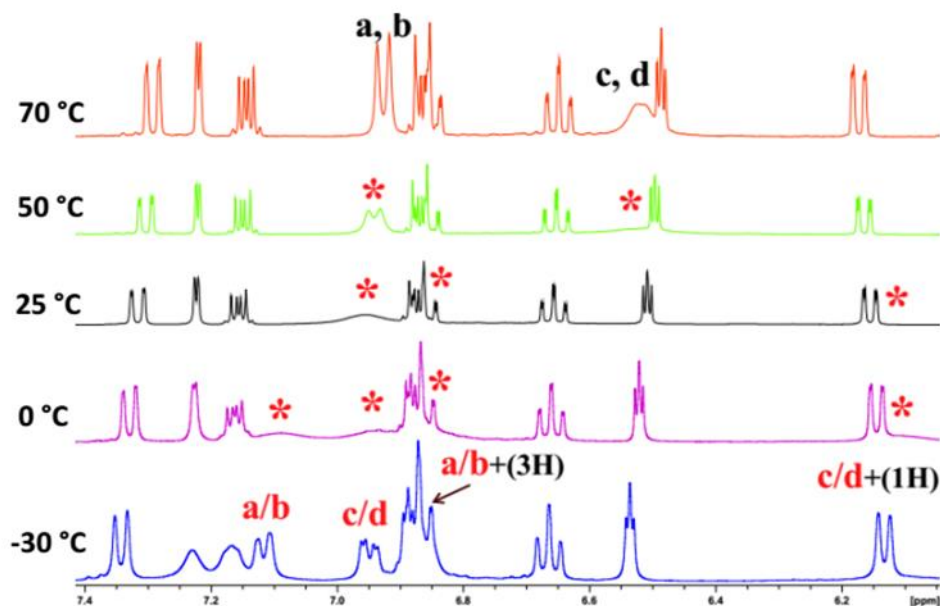
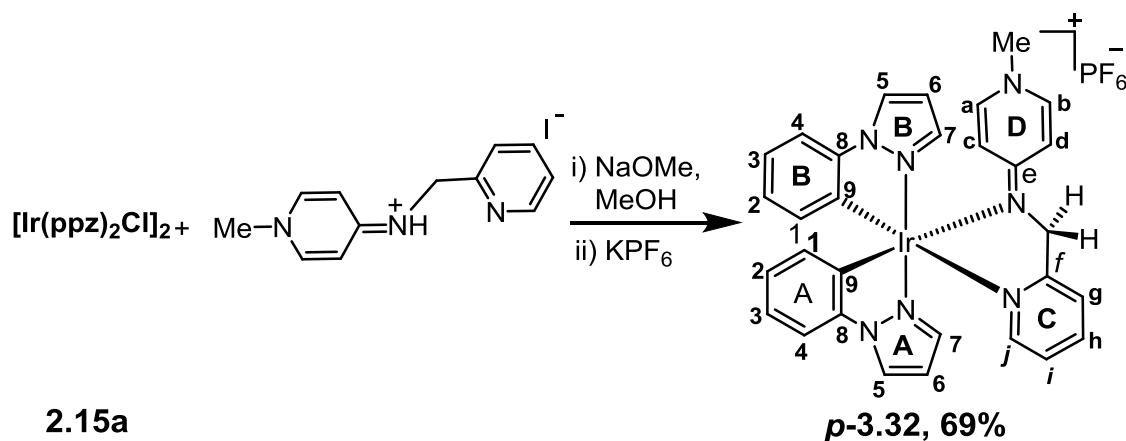


Figure 3.10: Variable-temperature ^1H NMR spectra of complex *p*-3.31 in CD_3CN (the target aromatic region) from -30 - $+70$ $^\circ\text{C}$ showing the relevant part of NMe pyridine ring (*), (400 MHz, 298 K).

Complex *p*-3.32 was synthesised by the same method as for *p*-3.30 and *p*-3.31 to give *p*-3.32 in good yield 69% (Scheme 3.12). The coordination of $[\text{PYE}_3]$ removes the C_2 symmetry, causing the two C^N ligands to become inequivalent and therefore doubling the number of peaks due to the C^N ligands in the ^1H NMR spectrum.



Scheme 3.12 Synthesis of *para*-PYE Ir(III) complex *p*-3.32

The ^1H NMR spectrum of complex *p*-3.32 shows twenty-two aromatic environments. The NMe group was easily identified as the only singlet at δ 3.32 and the NCH_2 group which is a singlet in the free ligand, was observed as two mutually coupled doublets at δ 5.06 and 4.85. The two doublets of the NCH_2 group both showed an NOE to a doublet of doublets at δ 6.46 which was assigned to NMe-pyridine (D) proton H_d . The NOESY and

COSY spectra then allowed assignment of protons H_{a-c} (*ca.* δ 6.65, 7.17, and 6.62, respectively). The assignments of H_{a,b} were also confirmed by NOEs to the NMe group. The observation of four different environments for the NMe-pyridine (D) protons (H_{a-d}) suggests there is restricted rotation about the C=N bond and therefore that the neutral imine resonance form is predominant. The two doublets of NCH₂ also showed an NOE to a doublet at δ 7.67 which was assigned to H_g, and which then allowed assignment of all the other protons of the pyridine (C) (H_{h-j} δ 7.85-7.09) via the COSY spectrum. Protons H_{g-i} were shifted slightly downfield compared to the free ligand (*ca.* δ 0.1 to 0.2), as might be expected on coordination to the metal, whilst proton H_j (δ 7.71) was observed about δ 0.8 upfield compared to the free ligand (δ 8.68) due to ring currents from the neighbouring phenyl ring (A) (similar interactions are discussed in Chapter 2). Proton H_j was a doublet which showed an NOE to the phenyl and pyrazole protons H_{1A} and H_{7B}, respectively, allowing the assignment of all the other protons of the phenyl (A) and pyrazole (B) rings using the COSY spectrum. The remaining signals for phenyl (B) and pyrazole (A) could also then be assigned. The pyrazole protons H_{5A, B} were the most downfield signals at δ 8.19 and 8.12, whilst the phenyl protons H_{1A, B} were the most upfield signals at δ 6.14 and 6.29, respectively. The ¹³C NMR spectrum shows four different CH carbons for the NMe-pyridine carbons at δ 140.0, 137.8, 115.4, and 107.6 for carbons C_{b, a, c, d}, respectively, suggesting that there is restricted rotation about the exocyclic C=N bond. The (FAB) mass spectrum shows a molecular ion at *m/z* 678.1982 (678.1957 calculated for C₃₀H₂₇IrN₇). The NMR analysis of complex **p-3.32** was also carried out in different polarity solvents, CD₂Cl₂, (CD₃)₂CO, and CD₃CN (see **Fig. 8** in the appendix); however, as for **p-3.30**, there was no clear evidence of any change in resonance structure of the PYE ligand.

Complexes **p-3.30** and **p-3.32** were successfully recrystallized from DCM/hexane and chloroform, respectively. The X-ray crystal structures of the complexes were determined and are shown in **Fig. 3.11** with selected bond lengths (Å) and angles (°) reported in **Table 3.3**. The crystal structures of **p-3.30** and **p-3.32** reveal the expected distorted octahedral coordination geometry with *cis* metallated carbons and *trans* nitrogen atoms (**Fig. 3.11**). The chelate bite angles for the cyclometallated ligands are all about 80°, whilst for the N^N ligand is about 79°, considerably less than the ideal 90°. For **p-3.30**, the Ir—N bond lengths to the PYE ligand are 2.185(6) and 2.191(6) Å, whilst in **p-3.32** the Ir—N(2) (PYE) distance, 2.130(8) Å, is statistically the same as the Ir—N(3) bond length of 2.116(7) Å.

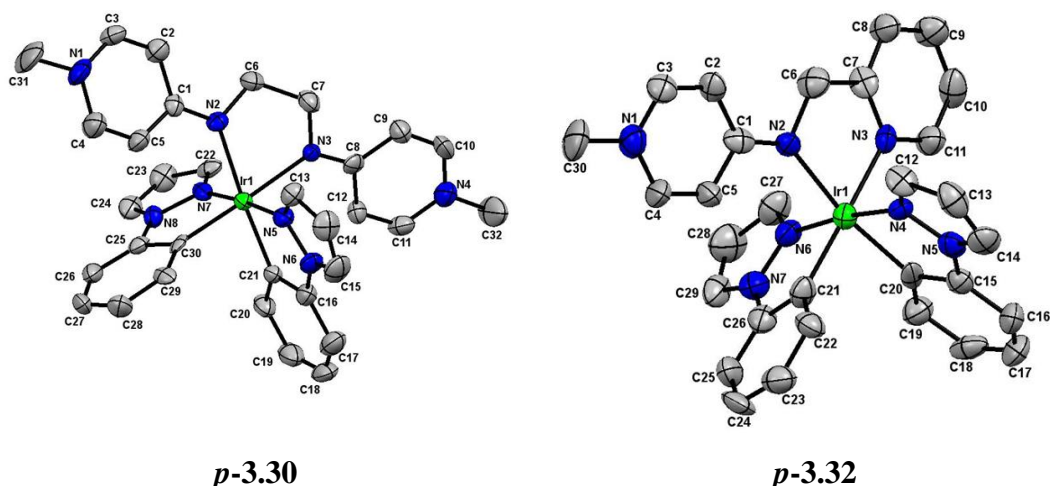


Figure 3.11: X-ray crystal structure of the cations of *p-3.30* and *p-3.32* showing 50% ellipsoids. All H atoms are omitted for clarity.

The N(2)—C(1) and N(3)—C(8) distances (1.333(11) and 1.303(10) Å, respectively) in *p-3.30* and the N(2)—C(1) bond length (1.332(12) Å) in *p-3.32* suggest a certain degree of double bond character. For *p-3.30*, the bond lengths in the NMe-pyridine rings range from 1.33(1) to 1.44(1) Å in the ring containing N(1) and between 1.35(1) to 1.43(1) Å in the ring containing N(4). In both cases, the range is wider than expected for a completely aromatic pyridinium group. Similarly, for *p-3.32* the bond lengths in the NMe-pyridine ring range from 1.32(1) to 1.41(1) Å, whilst those in the pyridine ring have a smaller range, from 1.34(1) to 1.39(1) Å, consistent with a significant contribution from the imine resonance form for the PYE moiety.

Table 3.3: Selected bond lengths (Å) for *p-3.30* and *p-3.32*

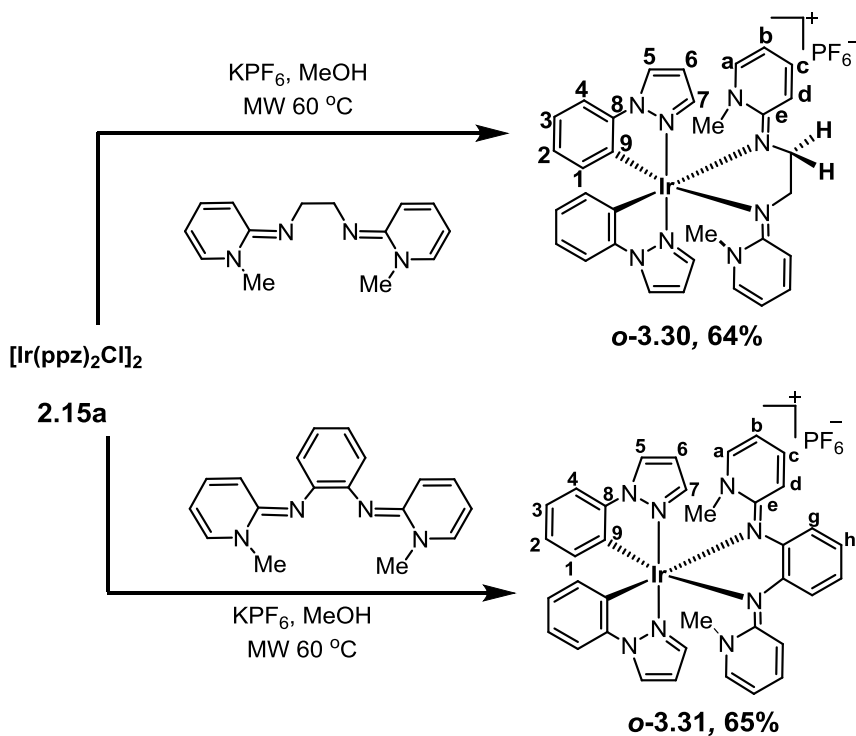
<i>p-3.30</i>		<i>p-3.32</i>	
Ir(1)—N(2)	2.191(6)	Ir(1)—N(2)	2.130(8)
Ir(1)—N(3)	2.185(6)	Ir(1)—N(3)	2.116(7)
Ir(1)—N(5)	2.006(7)	N(1)—C(4)	1.336(12)
Ir(1)—N(7)	2.010(7)	Ir(1)—N(6)	2.037(9)
N(2)—C(1)	1.333(11)	N(2)—C(1)	1.332(12)
N(3)—C(8)	1.303(10)		

For *p-3.30*, the sum of the angles about N(2) is 359.6° whilst that about N(3) is 359.5°. Hence both N(2) and N(3) have almost planar geometries consistent with donation of an sp^2 hybridised lone pair to the Ir. In addition, the NMe pyridine planes are only slightly

out of the N(3)-Ir-N(2) coordination plane, 14.3° for the N(1) ring and 18.8° in the opposite direction for the N(4) ring, respectively. For **p-3.32**, the angles around N(2) add up to 359.7° , consistent with sp^2 hybridisation at N(2). The NMe pyridine is only 10.4° out of the N(3)-Ir-N(2) plane. In conclusion, these structures indicate a considerable contribution from the neutral imine resonance structure in the solid state for both complexes **p-3.30** and **p-3.32**.

3.2.4 Synthesis and characterisation of *ortho*-PYE Ir(III) complexes

The dimer **2.15a** was reacted with ligands *o*-PYE_{1,2} with KPF₆ using microwave irradiation to form compounds **o-3.30** and **o-3.31** in good yields (Scheme 3.13). The ¹H NMR spectra of **o-3.30** and **o-3.31** are similar to **p-3.30** and **p-3.31** in that each show only one set of signals for the cyclometallating ligands and signals for only one half of the PYE ligand, suggesting they adopt C₂ symmetry in solution.

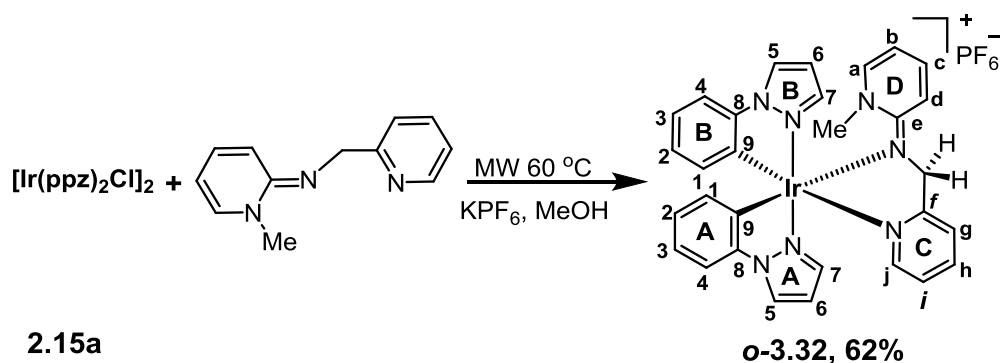


Scheme 3.13. Synthesis of *ortho*-PYE Ir(III) complexes **o-3.30** and **o-3.31**

The ¹H NMR spectrum of **o-3.30** shows two mutually coupled doublets at δ 3.85 and 3.21 which were assigned to the C₂H₄ bridge and a 6H singlet at δ 3.27 for the NMe group. The doublet at δ 3.85 shows an NOE to a doublet at δ 6.50 which was therefore assigned to the pyridine proton (H_d). The NMe group shows an NOE to a doublet at δ 6.65 which was therefore assigned as H_a. The COSY spectrum then allowed for the assignment of H_{b,c} as the multiplet at δ 6.17 and the broad triplet at δ 7.06, respectively. Note, the low

symmetry of the *ortho*-substituted NMe ring means there is no information about rotation around the C=N bond. The TOCSY spectrum allowed assignment of the phenyl (H₁₋₄) and pyrazole (H₅₋₇) protons. The phenyl protons H₁ are the most upfield signals (*ca.* δ 6.14) due to ring current effects. The ¹³C NMR spectrum showed four CH carbons for the NMe pyridine ring between δ 136.3 (C_c) to 108.0 (C_d). The high-resolution mass spectrum (FAB) showed a molecular ion at *m/z* 721.2400 (721.2379 calculated for C₃₂H₃₂IrN₈). Recording the ¹H NMR spectrum in a more polar solvent (e.g., (CD₃)₂CO or CD₃CN), showed only minor changes in chemical shift (See **Fig 9** in the appendix). However, in CD₃CN the spectrum showed the presence of a second species which has not as yet been identified but may be due to the coordination of CD₃CN solvent molecules to the metal.

The ¹H NMR spectrum of *o*-**3.31** was similar to that of *o*-**3.30** except the C₂H₄ doublets were replaced with a 4H multiplet at *ca.* δ 6.71 due to the C₆H₄ bridging group. The NMe group was the only singlet, at δ 3.40, and showed an NOE to the multiplet at *ca.* δ 6.89, and which was assigned as H_a, with NOESY and COSY spectra allowing for the assignment of the other NMe pyridine protons H_{b-d} (δ 6.41, 7.01 and 6.63, respectively). The shifts of H_{a-d} suggest the NMe pyridine ring is not fully aromatic. The assignments of the phenyl and pyrazole protons were made on the same basis as for *o*-**3.30**. The pyrazole protons H₅ were the most downfield signal at δ 7.83, whilst the phenyl protons H₁ were the most upfield at about δ 6.18. There is some evidence for the presence of a second species, which may be an isomer with both NMe groups on the same side giving inequivalent NMe signals. Heating the sample gave no change in the amount of the minor species. The ¹³C NMR spectrum showed the expected number of signals of quaternary and CH carbons, and the high-resolution mass spectrum (ASAP) showed a molecular ion at *m/z* 769.2386 (769.2379 calculated for C₃₂H₃₂IrN₈).



Scheme 3.14. Synthesis of *ortho*-PYE Ir(III) complex *o*-**3.32**

Complex ***o*-3.32** was synthesised using the same method as for the ***o*-3.30** and ***o*-3.31** to give ***o*-3.32** in good yield (Scheme 3.14). The ^1H NMR spectrum showed a singlet at δ 3.32 due to the NMe group whilst the NCH₂ group, which is a singlet in the free ligand, gives diastereotopic protons after complexation, thus giving rise to two mutually coupled doublets at δ 5.17 and δ 4.70. The doublet at δ 5.17 showed an NOE to a doublet of doublets at δ 6.46 which was assigned to NMe pyridine (D) proton H_d. The assignment of H_a as a doublet of doublets at δ 6.77 was confirmed by an NOE to the NMe group, after which NOESY and COSY spectra then allowed for the assignment of protons H_b and H_c at δ 6.23 and 7.19, respectively. Proton H_g is a doublet at δ 7.67 which was confirmed by NOEs to the other CH doublet at δ 4.70 with the COSY spectrum then allowing for the assignment of pyridine (C) protons H_{h-j} between δ 7.87-7.10. The phenyl and pyrazole protons were assigned as for ***p*-3.32**, where once again the pyrazole protons H_{5A, B} were the most downfield signals at δ 8.23 and 7.90 and the phenyl protons H_{1A, B} were the most upfield signals at δ 6.36 and 6.10, respectively. The ^{13}C NMR spectrum showed the expected number of signals. The high-resolution mass spectrum (ASAP) showed a molecular ion at m/z 678.1976 (678.1957 calculated for C₃₀H₂₇IrN₇).

Complex ***o*-3.30** was successfully recrystallized from chloroform, and ***o*-3.31** and ***o*-3.32** from DCM/hexane. The X-ray crystal structures of the complexes were determined and are shown in **Fig. 3.9** with selected bond lengths (Å) and angles (°) reported in **Table 3.4**. The crystal structures of ***o*-3.30**, ***o*-3.31** and ***o*-3.32** reveal the expected distorted octahedral coordination geometries with *cis* metallated carbons and *trans* nitrogen atoms (**Fig. 3.9**). The chelate bite angles for the cyclometallated ligands are all about 80°, whilst for the N[^]N ligands they are all about 77°. Complex ***o*-3.30** and ***o*-3.31** showed approximate C₂ symmetry with the methyl substituents directed above and below the metal–ligand plane defined by N(2)—Ir(1)—N(3) in both complexes. For complex ***o*-3.30**, the Ir—N bond lengths to the N[^]N ligand (Ir(1)—N(2), 2.216(6), and Ir(1)—N(3), 2.239(7) Å) are longer than those to the cyclometallating ligands (Ir(1)—N(7), 2.019(6) and Ir(1)—N(5), 2.027(6) Å) due to the former being *trans* to the C atoms. Similar trends could be seen for complexes ***o*-3.31** and ***o*-3.32**. In addition, the Ir—N bond lengths to the N[^]N ligand are longer than those (2.185(6) and 2.191(6) Å) in the corresponding *para* complex ***p*-3.30** (see above), possibly reflecting the increased steric hindrance imposed by the *ortho* NMe substituents.

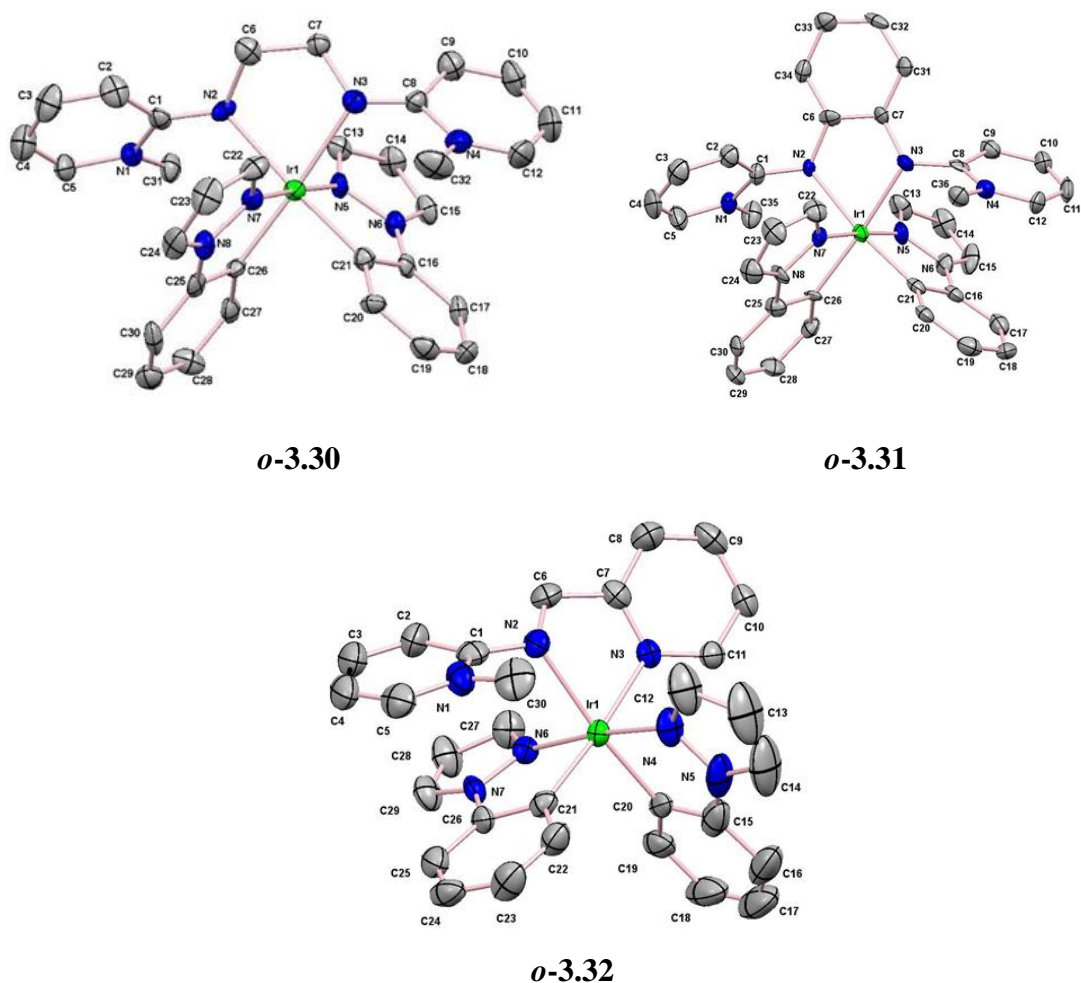


Figure 3.9: X-ray crystal structure of the cations of ***o*-3.30**, ***o*-3.31** and ***o*-3.32**, respectively, showing 50% ellipsoids. All H atoms are omitted for clarity.

In complex ***o*-3.30**, the N(2)—C(1) and N(3)—C(8) bond lengths of 1.321(9) and 1.299(10) Å suggest significant imine character. The bond lengths in the NMe-pyridine rings range from 1.36(1) to 1.41(1) Å in the ring containing N(1) and between 1.34(1) to 1.47(1) Å for the ring containing N(4), the slightly wider range for the latter suggesting slightly less aromaticity in that case. The sum of the angles around the “imine” N(2) is 346.4°, whilst that about N(3) is 339.4° showing these are no longer simply sp^2 hybridised. In addition, the NMe pyridine planes are rotated considerably out of the N(3)—Ir—N(2) plane (57.2° for the N(1) ring and 62.7° for the N(4) ring, respectively). Hence it is clear that the interaction is not well described as being purely that of an sp^2 lone pair interaction with the metal. In addition, the N(7)—Ir—N(5) plane is at an angle of 81.7° from the N(3)—Ir(1)—N(2) plane, showing considerable distortion from an octahedral geometry. It is likely that the steric hindrance from the *ortho* NMe groups is the cause of these significant distortions.

Table 3.4: Selected bond lengths (Å) for *o*-**3.30**, *o*-**3.31** and *o*-**3.32**.

	<i>o</i> - 3.30	<i>o</i> - 3.31		<i>o</i> - 3.32
Ir(1)—N(2)	2.216(6)	2.196(6)	Ir(1)—N(2)	2.235(5)
Ir(1)—N(3)	2.239(7)	2.184(6)	Ir(1)—N(3)	2.120(5)
Ir(1)—N(5)	2.027(6)	2.009(6)	Ir(1)—N(4)	1.998(5)
Ir(1)—N(7)	2.019(6)	2.014(6)	Ir(1)—N(6)	2.027(5)
N(2)—C(1)	1.321(9)	1.367(9)	N(2)—C(1)	1.330(8)
N(3)—C(8)	1.299(10)	1.379(8)		

For complex *o*-**3.31**, the Ir—N bond lengths to the N[^]N ligand (Ir(1)—N(2) 2.196(6) and Ir(1)—N(3) 2.184(6) Å) are significantly shorter than those in *o*-**3.30** (Ir(1)—N(2) 2.216(6) and Ir(1)—N(3) 2.239(7) Å), suggesting the ligand is more strongly bonded in *o*-**3.31**. The N(2)—C(1) and N(3)—C(8) bond lengths of 1.367(9) and 1.379(8) Å, respectively, are still considerably shorter than for an N—C single bond. However, they are substantially longer than the corresponding distances (1.296(2) and 1.294(2) Å) in the free ligand, *o*-**PYE**₂, and indeed are comparable to the N—C bonds in the NMe pyridine rings which range from 1.358(9) to 1.383(9) Å, suggesting a greater contribution from the zwitterionic resonance form in the complex. As in the free ligand *o*-**PYE**₂, the N(2)—C(6) and N(3)—C(11) lengths (1.403(8) and 1.397(9) Å, respectively) are also slightly shorter than normal C—N single bonds, suggesting a small amount of delocalisation into the C₆H₄ bridge. As for *o*-**3.30**, the NMe pyridine planes are rotated considerably out of the N(3)—Ir—N(2) plane (*ca.* 73° in opposing directions for the two rings). The increased contribution of the zwitterionic form is also reflected in the sum of the angles around N(2) (345.9°) and N(3) (348.6°), indicating the N atoms are not *sp*² hybridized.

Unlike in *p*-**3.32** in which the Ir—N(2) and Ir—N(3) distances are statistically the same, in *o*-**3.32** the Ir—N(2) (PYE) distance, 2.235(5) Å, is significantly longer than the Ir—N(3) (pyridine) distance of 2.120(5) Å, possibly due to the steric hindrance of the *ortho* NMe group. The N(2)—C(1) bond length of 1.330(8) Å in *o*-**3.32** (*cf.* 1.332(12) Å in *p*-**3.32**) again suggests some imine character for the PYE moiety. For *o*-**3.32** the bond

lengths in the NMe-pyridine ring range from 1.34(1) to 1.42(1) Å and those for the pyridine ring are very similar, from 1.338(8) to 1.40(1) Å, suggesting reasonably similar aromaticity in the two rings. The sum of the angles around N(2) is 337.3° (*cf.* 359.7° for **p-3.32**) showing considerable distortion from sp^2 hybridisation and thus suggesting a greater contribution from the zwitterionic resonance form for **o-3.32** than for **p-3.32**. Consistent with this, the NMe pyridine ring is at an angle of 63° to the N(3)—Ir—N(2) plane.

In conclusion, a number of *para*- and *ortho*-PYE ligands were synthesised. The *para* ligands were synthesised as salts and deprotonated *in situ* when reacted with $[\text{Ir}(\text{ppz})_2\text{Cl}]_2$. By contrast, the *ortho*-substituted ligands could be isolated as their free bases. The dicationic salts of **p-PYE**_{1,2} only dissolved in polar solvents and showed free rotation in their NMe pyridine groups, suggesting a preponderance of the pyridinium resonance form, though the X-ray structure still suggested some double bond character for the exocyclic C=N bond. The monocationic salt of **p-PYE**₃ showed four distinct proton resonances in $(\text{CD}_3)_2\text{CO}$ for the NMe pyridine group due to restricted rotation and hence a preponderance of the iminium resonance form, whilst in D_2O two of the resonances became equivalent, suggesting increased rotation that was possibly due to an increased proportion of the pyridinium resonance form. The *ortho*-substituted ligands were isolated as free bases and the NMe pyridine protons were all observed to higher field, consistent with a greater contribution of the imine resonance form. New heteroleptic Ir(III) complexes containing *para* or *ortho* (PYE) ligands were successfully synthesized in good yields (> 60 %). All the complexes were fully characterised by ^1H and ^{13}C NMR spectroscopy, mass spectrometry, and in most cases by X-ray crystallography. The ^1H NMR spectra suggest that for the **p-PYE**_{1,3} complexes (**p-3.30** and **p-3.32**) there is a significant contribution from the neutral non-aromatic form, as evidenced by the four separate proton signals for the NMe pyridine that suggested restricted rotation about the C=N bond. However, for complex **p-3.31** with the **p-PYE**₂ ligand, some rotation about the C—N of NMe-pyridine ring clearly occurs even at room temperature, suggesting a greater contribution from the zwitterionic resonance form. It may be that the negative charge on the exocyclic N atom is delocalised onto the C_6H_4 bridge which here stabilises the zwitterionic form. The *ortho* complexes show relatively high field shifts for the NMe ring protons (between 6.2 and 7.2 ppm) suggestive of a degree of double bond character. However, the X-ray structures show that the NMe pyridine rings are significantly out of the $\text{Ir}(\text{N}^{\wedge}\text{N})$ plane and the sum of the angles around the exocyclic N atoms is considerably

less than 360°, both of which suggest significant contributions from the zwitterionic resonance form. The steric crowding of the *ortho* substituent leads to increased distortions in the coordination geometry, as seen previously by Douthwaite *et al.*⁶ There was no clear evidence from NMR spectroscopy that more polar solvents lead to an increased contribution from the zwitterionic resonance structure for the complexed PYE ligands. The photophysical properties of the PYE ligands or their precursors and of their Ir(III) complexes are discussed in next section **3.3**.

3.3 Photophysical properties

This section described the photophysical properties of the PYE ligands or their precursors and of their Ir(III) complexes (*p*-**3.30**, *p*-**3.31**, *p*-**3.32** and *o*-**3.30**, *o*-**3.31** and *o*-**3.32**). As mentioned in the introduction to this chapter, PYE ligands are potentially very strong donors and can sometimes be analogues of *N*-heterocyclic carbenes. Ir complexes with NHCs are known to show a characteristic blue emission due to the strong donor properties of the carbenes.^{24, 25} This study will attempt to evaluate if the strong donor properties of PYE ligands can promote blue emission.

3.3.1 Photophysical properties of [*p*-H₂PYE₁]**I**₂, [*p*-H₂PYE₂]**I**₂ and [*p*-HPYE₃]**I**

The UV-vis absorption spectra for the salts [*p*-H₂PYE₁]**I**₂, [*p*-H₂PYE₂]**I**₂ and [*p*-HPYE₃]**I** are shown in **Fig. 3.10** with corresponding electronic absorption spectra data. Due to the different solubilities of the dicationic and monocationic salts, different solvents were used. All three compounds, [*p*-H₂PYE₁]**I**₂, [*p*-H₂PYE₂]**I**₂ and [*p*-HPYE₃]**I**, exhibit one band, each with a similar λ_{max} , as observed at 286, 280 and 279 nm respectively. Hence the bridge between the two N-pyridine units group has almost no effect on the absorption wavelength.

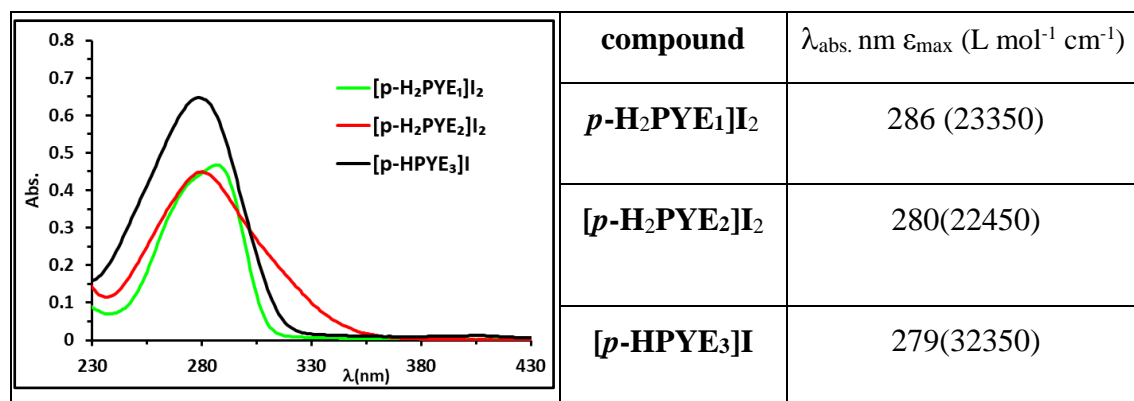


Figure 3.10: Absorption spectra of compounds [*p*-H₂PYE₁]**I**₂, [*p*-H₂PYE₂]**I**₂ in H₂O (0.02 mM) and [*p*-HPYE₃]**I** in DCM at (0.02 mM) at RT, with corresponding electronic absorption data.

The emission spectra of $[p\text{-H}_2\text{PYE}_1]\text{I}_2$, $[p\text{-H}_2\text{PYE}_2]\text{I}_2$ and $[p\text{-HPYE}_3]\text{I}$ are shown in **Fig. 3.11**, and the associated data summarised in **Table 3.6**. As can be seen, all the compounds show some emission which is relatively insensitive to oxygen as would be expected for fluorescence. The emission spectrum of $[p\text{-H}_2\text{PYE}_1]\text{I}_2$ shows a broad emission band at 393 nm, whereas $[p\text{-HPYE}_3]\text{I}$ exhibits an emission band at 423 nm with a shoulder at 394 nm. However, compound $[p\text{-H}_2\text{PYE}_2]\text{I}_2$ showed two emission peaks, one at 386 nm and a more intense one at 538 nm. The reason for this difference is currently not known.

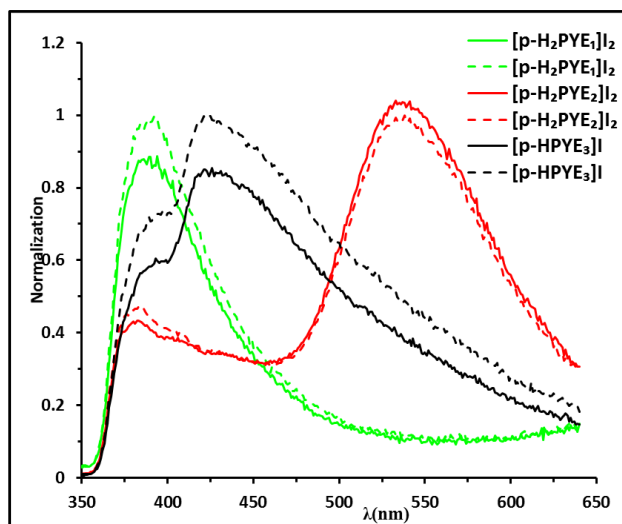


Figure 3.11: Normalised the emission spectra of $[p\text{-H}_2\text{PYE}_1]\text{I}_2$, $[p\text{-H}_2\text{PYE}_2]\text{I}_2$ in H_2O and $[p\text{-HPYE}_3]\text{I}$ in DCM at (0.02 mM), excited 330 nm in air (—) and degassed Ar (- -) at RT.

3.3.2 Photophysical properties of ligands *o*-PYE₁, *o*-PYE₂ and *o*-PYE₃

The UV-vis absorption spectra for *o*-PYE₁, in different solvents are shown in **Fig. 3.12**. It is noticeable that in DCM and DMF two bands are observed at *ca.* 265 nm and 374 nm, whilst in MeOH and H_2O both bands are shifted to shorter wavelength at approximately 240 and 315 nm, respectively. It is possible that these reflect protonation of the basic PYE (none of the solvents were dried before use). Similar effects were noticed in the spectra recorded for *o*-PYE₂ and *o*-PYE₃ (see appendix **Fig 10**) though solubility issues prevented a full comparison.

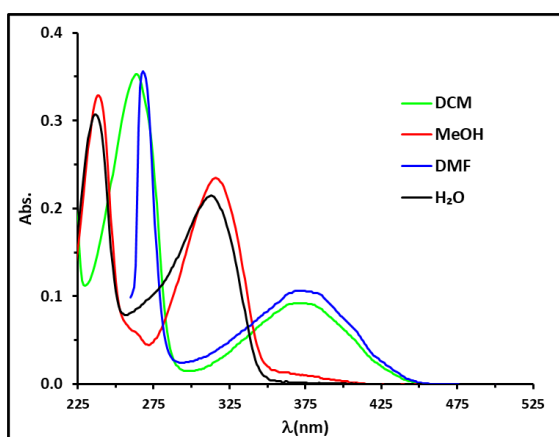


Figure 3.12: Absorption spectra of *o*-PYE₁ at 0.02 mM in different solvents at RT

The UV-vis absorption spectra of *o*-PYE₁, *o*-PYE₂ and *o*-PYE₃ with electronic absorption data in DCM are shown in **Fig.3.13**. All three compounds absorb at similar wavelengths.

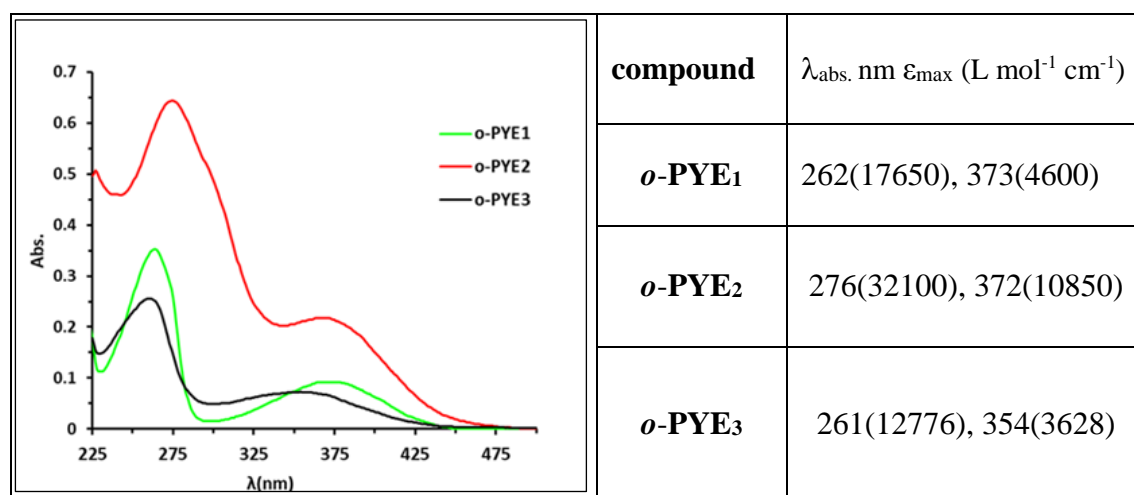


Figure 3.13: Comparison of the UV-vis spectra of *o*-PYE₁, *o*-PYE₂ and *o*-PYE₃ in DCM 0.02 mM at RT with corresponding electronic absorption data.

The emission spectra of *o*-PYE₁, *o*-PYE₂ and *o*-PYE₃ in DCM are shown in **Fig. 3.14** with the data summarised in **Table 3.5**. All compounds show emission which is relatively insensitive to oxygen as would be expected for fluorescence. The ligands *o*-PYE₁, and *o*-PYE₃ show a similar broad emission band, with λ_{max} at 394 and 383 nm, respectively, whilst *o*-PYE₂ showed some structure with peaks at about 387 and 414 nm and a shoulder at 440 nm. Hence, unlike the *para*-substituted ligands, there is very little difference in emission wavelength for all three ligands, see **Fig 3.14** and **Table 3.5**.

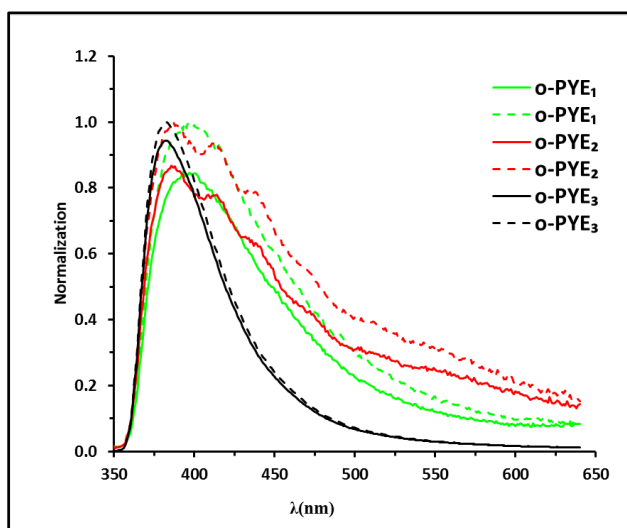


Figure 3.14: Normalised emission spectra for *o*-PYE₁, *o*-PYE₂ and *o*-PYE₃ in DCM in air (—) and degassed, Ar (- - -), at 0.02 mM, excited at 330 nm, at RT.

Table 3.5: Emission data for **PYE**₁, *o*-PYE₂ and *o*-PYE₃ ligands in DCM.

<i>o</i> -PYE ₁	<i>o</i> -PYE ₂	<i>o</i> -PYE ₃
394	387, 414, sh 440	383

3.3.3 Photophysical properties of complexes *p*-3.30, *p*-3.31 and *p*-3.32

The UV-vis absorption spectra and electronic absorption data of complexes *p*-3.30, *p*-3.31 and *p*-3.32 are shown in **Fig. 3.15**. All the complexes show bands at 290 - 320 nm due to $\pi \rightarrow \pi^*$ transitions. Cyclometallated iridium complexes usually show ¹MLCT, and sometimes ³MLCT, bands at around 350-450 nm;²⁶ however, here there was no clear evidence for separate peaks at longer wavelengths in complexes *p*-3.30 and *p*-3.32, whilst complex *p*-3.31 showed a strong band about 400 nm. The absorption spectra of *p*-3.30, *p*-3.31 and *p*-3.32 are almost unchanged above 280 nm in various solvents of different polarities.

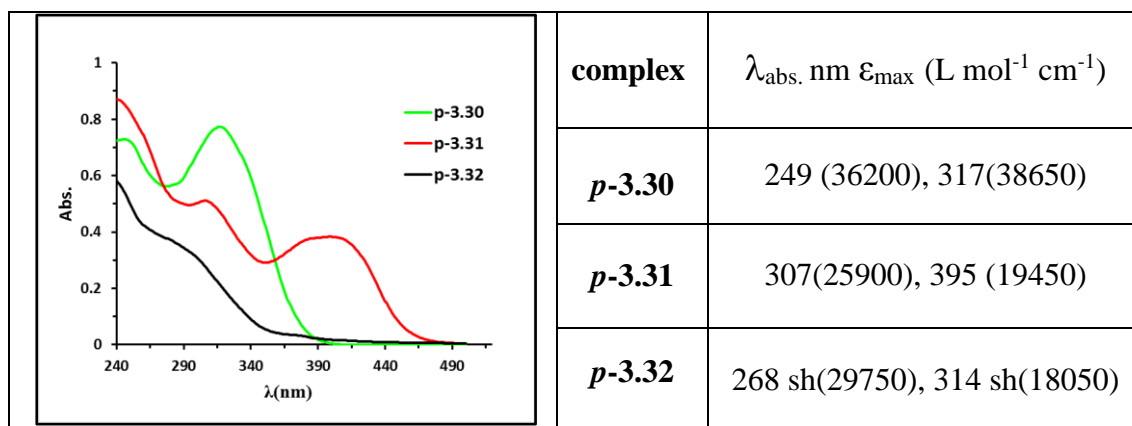


Figure 3.15: Absorption spectra for *p-3.30*, *p-3.31* and *p-3.32* in DCM, at 0.02 mM at RT with corresponding electronic absorption spectra data.

Emission spectra for complexes *p-3.30*, *p-3.31* and *p-3.32* were run in DCM, in aerated solutions. Complexes *p-3.30* and *p-3.31* are almost non-emissive in deaerated DCM solution (see appendix **Fig 11**), which may be to the result of quenching due to rotation around the exocyclic C—N bond of the NMe-pyridine rings. In an attempt to investigate this possibility, the spectra were rerun in a degassed mixture of MeCN/H₂O (1:9) to try to precipitate the complex and hence be able to observe emission from the solid (see Chapter 4 for further discussion of Aggregation Induced Emission). However, this only resulted in small changes in the emission profile. By contrast, complex *p-3.32* is emissive in air with a λ_{max} at 561 nm (**Fig 3.16**). The emission intensity is sensitive to the presence of oxygen; in degassed samples, the emission intensity increased by factor of *ca.* 3.2. This suggests that the excited states for this complex has some triplet character. The fact that the ppz ligand and the coordinated py ring would limit at ³MLCT/³LLCT character given the unstructured emission band stage (further characterisation of the emission would need lifetime measurements and DFT calculations).

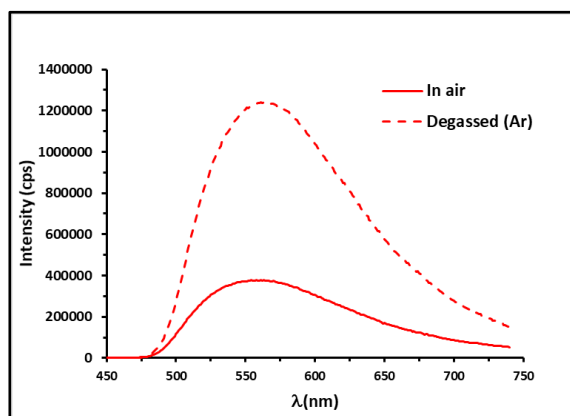


Figure 3.16: Emission spectra of complex *p-3.32* in DCM at 0.02 mM, excited at 380 nm at RT.

3.3.4 Photophysical properties of complexes *o*-3.30, *o*-3.31 and *o*-3.32

As for the *para* complexes discussed earlier, the UV-vis spectra for all the *ortho* complexes (*o*-3.30, *o*-3.31 and *o*-3.32) show strong bands between *ca.* 240-300 nm due to $\pi \rightarrow \pi^*$ transitions (Fig 3.17). Complex *o*-3.30 shows an additional weak band at about 390 nm (possibly having contributions from $^1\text{MLCT}$ transitions) whilst complex *o*-3.31 shows a stronger band about 484 nm.

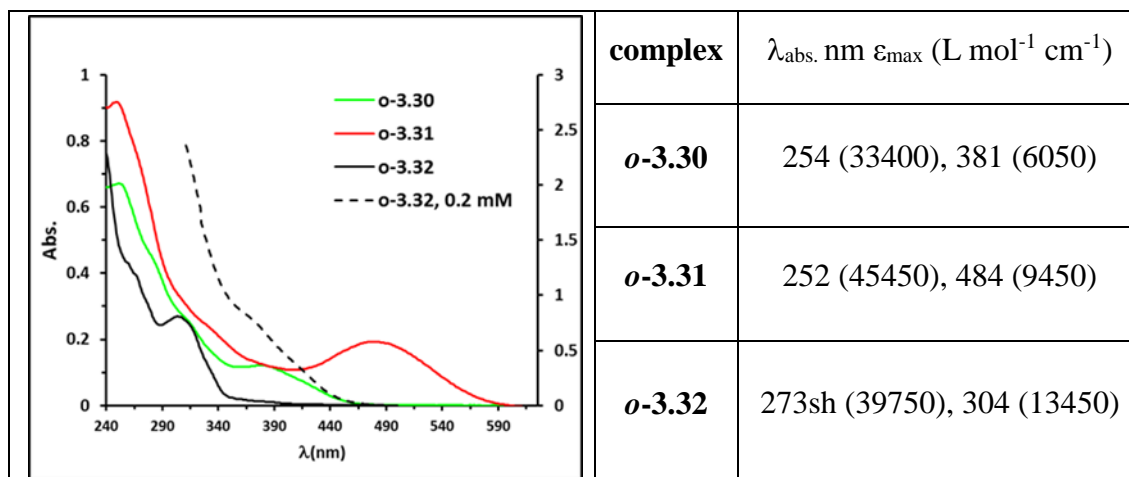


Figure 3.17: Absorption spectra of complexes *o*-3.30, *o*-3.31 and *o*-3.32 in DCM, at 0.02 mM (—) and 0.2 mM (- - -) for complex *o*-3.32 at RT with corresponding electronic absorption data.

The emission spectra for *ortho* complexes *o*-3.30, *o*-3.31 and *o*-3.32 were run in DCM, and MeCN. Complex *o*-3.30 is only weakly emissive in DCM solution and the intensity increases only slightly when degassed. Hence this fluorescence, though further studies would be needed to confirm this. The emission maximum is slightly different to that of the free ligand, as per Fig. 3.18.

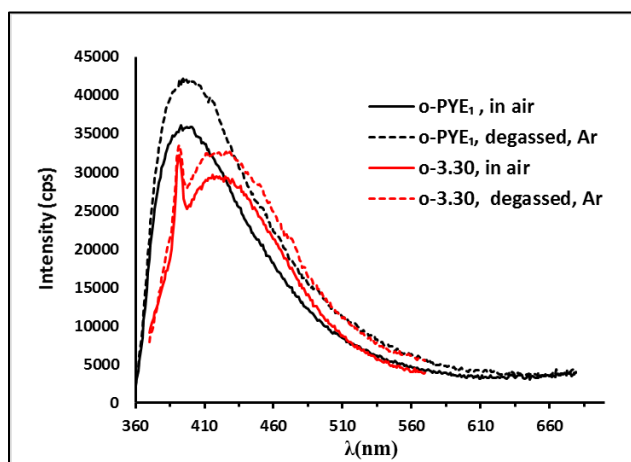


Figure 3.18: Emission spectra of complex *o*-3.30 vs. free ligand *o*-PYE₁ in DCM at 0.02 Mm, excited at 350 nm, at RT.

Complex ***o*-3.31** is non-emissive in either degassed solution or when precipitated in a degassed mixture of MeCN/H₂O (1:9) (see appendix **Fig 12**). As for ***p*-3.32**, complex ***o*-3.32** in DCM shows a broad emission band with a λ_{max} of 552 nm and a shoulder at 519 nm (**Fig 3.19**) which is a blue shifted by *ca.* 9 nm compared to ***p*-3.32**. In degassed samples, the emission intensity of ***o*-3.32** is increased by *ca.* 11.6-fold in DCM, suggesting considerable triplet character in the excited state. The structuring in degassed sample suggest LC (the band shape changes)

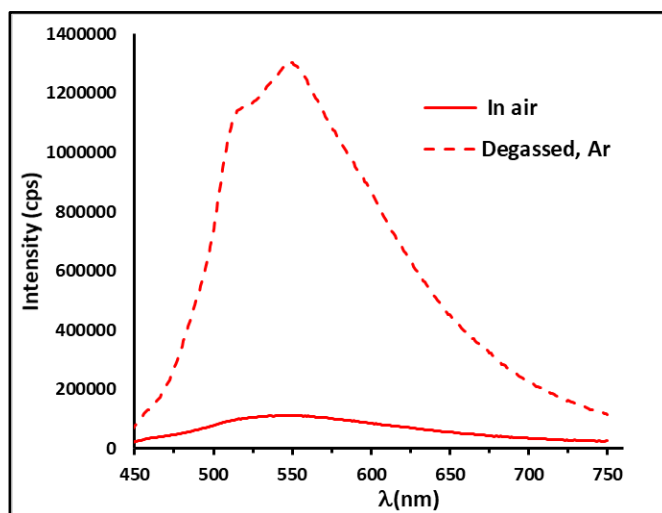


Figure 3.19: Emission spectra of complex ***o*-3.32** in DCM at 0.02 mM, excited at 380 nm at RT.

3.4 Conclusions and future work

In conclusion, the UV-vis absorption spectra of all the ligands or their precursors and all the complexes show strong bands between 240 and 320 nm due to $\pi \rightarrow \pi^*$ transitions. Complex ***o*-3.30** shows a weak band at about 390 nm whilst complexes ***p*-3.31** and ***o*-3.31** show stronger bands at 395 nm and above 485 nm, respectively. In general, there is no clear evidence for any solvatochromic behaviour in the UV-vis absorption spectra of the complexes. Complexes ***p*-3.30**, ***p*-3.31** and ***o*-3.31** are non-emissive in either degassed DCM solution or when precipitated from a mixture of MeCN/H₂O (1:9), whilst complex ***o*-3.30** is only weakly emissive. Complexes ***p*-3.32** and ***o*-3.32** are both emissive in air and show a significant increase in intensity on degassing, consistent with considerable triplet character in their excited states. It is likely that the **PYE**₃ complexes ***p*-3.32** and ***o*-3.32** show MLCT emission with the pyridine as the acceptor ligand. In the other complexes there may be no suitable low-lying LUMO for emission in the visible region. Hence from the emission spectra measured there is no evidence for strong donor

properties of the PYE ligands. Future work could include the synthesis of $[\text{Ir}(\text{ppy})_2(\text{PYE})]$ complexes in an attempt to evaluate the donor properties of the PYE ligands.

Bibliography

1. A. E. Tschitschibabin, R. A. Konowalowa and A. A. Konowalowa, *Berichte der deutschen chemischen Gesellschaft (A and B Series)*, 1921, **54**, 814-822.
2. P. Hong and H. Yamazaki, *Tetrahedron Lett.*, 1977, **18**, 1333-1336.
3. N. Akai, K. Ohno and M. Aida, *J. Photochem. Photobiol., A*, 2007, **187**, 113-118.
4. H. Traore, M. Saunders and S. Blasiman, *Aust. J. Chem.*, 2000, **53**, 951-957.
5. P. Diversi, G. Ingrosso, A. Lucherini and S. Malquori, *J. Mol. Catal.*, 1987, **40**, 267-280.
6. Q. Shi, R. J. Thatcher, J. Slattery, P. S. Sauari, A. C. Whitwood, P. C. McGowan and R. E. Douthwaite, *Chem. Eur. J*, 2009, **15**, 11346-11360.
7. P. D. W. Boyd, L. J. Wright and M. N. Zafar, *Inorg. Chem.*, 2011, **50**, 10522-10524.
8. M. E. Doster and S. A. Johnson, *Angew. Chem., Int. Ed.*, 2009, **48**, 2185-2187.
9. A. Abbotto, S. Bradamante and G. A. Pagani, *J. Org. Chem.*, 2001, **66**, 8883-8892.
10. M. Chao, E. Schemp and R. D. Rosenstein, *Acta Crystallogr., Sect. B: Struct. Sci*, 1975, **31**, 2922-2924.
11. P. Neri, A. Bottino, F. Cunsolo, M. Piattelli and E. Gavuzzo, *Angew. Chem., Int. Ed.*, 1998, **37**, 166-169.
12. B. T. Heaton, C. Jacob and J. T. Sampanthar, *J. Chem. Soc., Dalton Trans.*, 1998, 1403-1410.
13. S.-y. Nakafuji, J. Kobayashi and T. Kawashima, *Angew. Chem., Int. Ed.*, 2008, **47**, 1141-1144.
14. V. Leigh, D. J. Carleton, J. Olguin, H. Mueller-Bunz, L. J. Wright and M. Albrecht, *Inorg. Chem.*, 2014, **53**, 8054-8060.
15. M. E. Doster, J. A. Hatnean, T. Jestic, S. Modi and S. A. Johnson, *J. Am. Chem. Soc.*, 2010, **132**, 11923-11925.
16. M. E. Doster and S. A. Johnson, *Organometallics*, 2013, **32**, 4174-4184.
17. K. F. Donnelly, C. Segarra, L. X. Shao, R. Suen, H. Müller Bunz and M. Albrecht, *Organometallics*, 2015, **34**, 4076-4084.
18. M. Navarro, C. A. Smith and M. Albrecht, *Inorg. Chem.*, 2017, **56**, 11688-11701.

19. M. Navarro, M. Li, H. Müller-Bunz, S. Bernhard and M. Albrecht, *Chem. Eur. J.*, 2016, **22**, 6740-6745.
20. C. Sahin, C. Varlikli, C. Zafer, Q. Shi and R. E. Douthwaite, *J. Coord. Chem.*, 2013, **66**, 1384-1395.
21. J. Y. Li, C. Lee, C. Y. Chen, W. L. Lee, R. Ma and C. G. Wu, *Inorg. Chem.*, 2015, **54**, 10483-10489.
22. E. Cristina Souza Brenelli and P. Moran, *The reactivity of some primary amines in SN2Ar reactions with 2- and 4-chloro-1-methylpyridinium ions*, 1989.
23. P. J. Spellane, R. J. Watts and C. J. Curtis, *Inorg. Chem.*, 1983, **22**, 4060-4062.
24. C.-H. Yang, J. Beltran, V. Lemaire, J. Cornil, D. Hartmann, W. Sarfert, R. Fröhlich, C. Bizzarri and L. De Cola, *Inorg. Chem.*, 2010, **49**, 9891-9901.
25. B. D. Stringer, L. M. Quan, P. J. Barnard, D. J. D. Wilson and C. F. Hogan, *Organometallics*, 2014, **33**, 4860-4872.
26. Q. Zhao, S. Liu, M. Shi, C. Wang, M. Yu, L. Li, F. Li, T. Yi and C. Huang, *Inorg. Chem.*, 2006, **45**, 6152-6160.

Chapter Four

Enhanced Phosphorescent Emission in the Solid State (EPESS) of Cyclometallated Pt(II) Complexes

4.1 Introduction

4.1.1 Aggregation-induced Emission

Concentration quenching or aggregation-caused quenching (ACQ) is usually suggested to be the cause of reduced emission intensity of compounds at high concentration or in the solid state.¹ For example, for perylene (**4.1**) (**Fig. 4.1**), π - π stacking is known to quench emission as the concentration increases.² In contrast Tang *et al.* found that hexaphenylsilole (**4.2**), which is non-planar and hence does not undergo π - π stacking, is not emissive in solution but is highly emissive in the solid state. This phenomenon is called aggregation-induced emission (AIE).^{3, 4} In a dilute solution, the six phenyl rotors of **4.2** (**Fig. 4.1**) undergo rotations which non-radiatively quench the excited state and renders the molecule to be non-, or at best weakly, luminescent.⁴ In the solid state, intramolecular rotations of the aryl rotors of **4.2** are greatly restricted, blocking the non-radiative pathway, thus radiative decay becomes possible and **4.2** is thus strongly emissive in the solid state. This discovery represented a major breakthrough, and the AIE effect in organic molecules was instigated.



Figure 4.1: Some AIE active molecules

Although the restriction of intermolecular rotation (RIR) is an established cause of AIE, Tang and co-workers showed that molecules lacking any rotors could still show AIE. For example, in **4.3** (**Fig. 4.1**), no rotation is possible but AIE is nevertheless observed.⁵ In this case, a restricted intermolecular vibration (RIV) mechanism was proposed where the in-plane/out-of-plane vibrational (twisting) motions would dissipate the excited state energy causing non-radiative pathways to diminish the emission in solution. Restriction of these vibrational motions in the solid state resulted in emission in solid **4.3** being turned on.

A quick way to ascertain if molecules are AIE active is to precipitate them from solution and see if the emission intensity increases significantly. This can be done by dissolving the molecule in a 'good' solvent and measuring the emission, which should be weakly or

non-emissive. When a ‘poor’ solvent is added, aggregates are formed that restrict internal motions and induce AIE, leading to a large increase in the intensity of emission.

4.1.2 Aggregation-induced Emission in Transition Metal Complexes

This next section will describe the AIE effect in transition metal complexes and the proposed origin(s) for this effect. For metal complexes a wide range of metal-ligand combinations is possible, therefore predicting the origin of AIE is more difficult than for purely organic molecules; indeed, additional mechanisms may be possible for metal complexes. Heavy transition metal complexes can undergo ISC due to high-spin-orbit coupling which allows the emission to be of a triplet nature, i.e., phosphorescence. Hence, another term that has been used in conjunction with AIE in heavy transition metal complexes is EPESS (Enhanced Phosphorescent Emission in the Solid State). Similar to organic molecules, the metal complex is non- or weakly emissive in solution but emission is enhanced when aggregates are formed.^{2, 6, 7} For example, the cyclometallated Ir(III) complexes shown in **Fig. 4.2** have been reported as being AIE (or EPESS) active.⁸⁻¹⁰ The cause of EPESS in the complexes [Ir(ppy)₂(N[^]O)] has been disputed in the literature; two different mechanisms were originally proposed, those of (i) restricted intermolecular rotations of substituents on the bidentate ancillary ligand N[^]O⁹ (**4.4a-d**) and (ii) π -stacking of cyclometallating 2-phenylpyridine ligands (**4.5a-d**). The two mechanisms are discussed in more detail below.

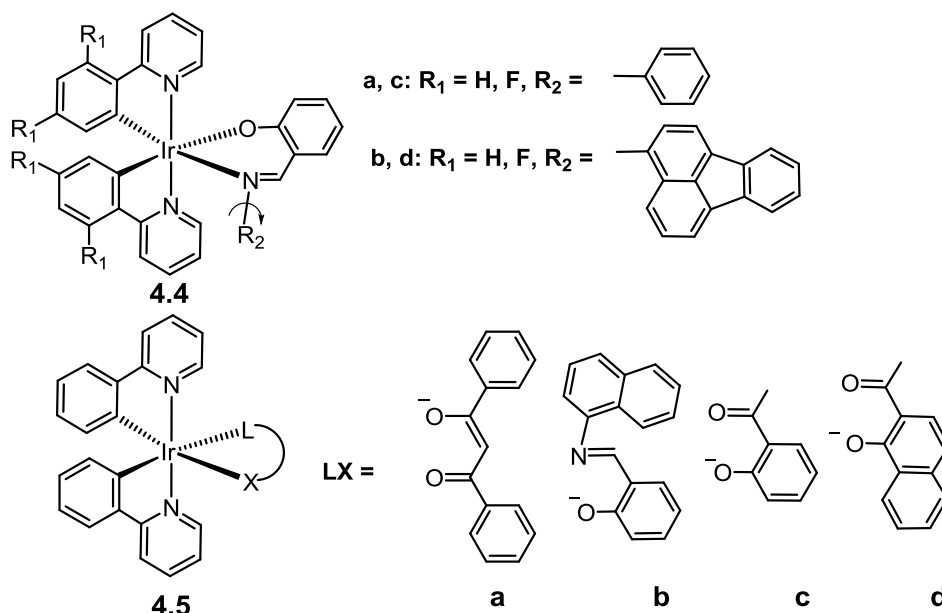


Figure 4.2: Some Ir(III) complexes that show EPESS

Park *et. al.*⁹ showed that complexes **4.4a-d** are non-emissive in the solution (DCM) but in neat films, or in various polymer films, strong emission is observed. Using a

combination of low temperature emission and TD-DFT studies, they concluded that the rotation around the *N*-aryl bond in the solution gives rise to a non-radiative decay pathway causing these complexes to be non-emissive in solution.⁹ In the solid state, the rotation is restricted giving rise to the observed strong emission. On the other hand, Li and co-workers found that **4.5a** and **4.5b** are non-emissive in solution but are EPESS active.¹⁰ They proposed that in solution a non-emissive triplet ligand (³L) state is of lower energy than the emissive ³MLLCT state. However, in the solid state, π -stacking of the ppy ligand lowers the emissive ³MLLCT state below the low-lying, non-emissive triplet ligand (³L) state thus **4.5a** and **4.5b** show intense emission in the solid state in comparison to solution.¹⁰ In addition, the same research group later showed⁸ that complexes **4.5c** and **4.5d**, with no rotatable substituents, are also EPESS active, suggesting the Park mechanism involving restricted intramolecular rotation may be incorrect for these molecules. X-Ray crystallography was used to show that complexes **4.5c** and **4.5d** also have π - π intermolecular interactions in the solid state, consistent with Li's theory of π -stacking.⁸ However, as mentioned above, complexes **4.4a-d** showed strong emission in polymer films;⁹ π -stacking interactions are less likely to occur in such instances due to low loading in the polymer. This is inconsistent with the interpretation^{8, 10} put forward by Li that π - π stacking is the cause of EPESS.

In 2014, Davies and co-workers¹¹ reported a new mechanism for EPESS in cyclometallated Ir complexes **4.6a-b** and **4.7a-b** (**Fig. 4.3**). These show either very weak or no phosphorescence at room temperature in a solution of DCM while all of the complexes display EPESS in the solid state in both powder and crystalline forms, although it should be noted that the solid-state quantum yields are not particularly high. Photophysical and computational studies showed that neither π -stacking nor restricted rotation caused the observed EPESS in these complexes, and rather that ligand distortions in the triplet excited state were responsible.

Liao and co-workers reported the first EPESS-active cationic Ir(III) complex, **4.8** (**Fig. 4.3**).¹² In MeCN solution, emission is not observed, whilst in a mixture of MeCN/H₂O the emission is observed. The authors suggested that restricted intramolecular rotation is responsible for the emission in the solid state of **4.8**.

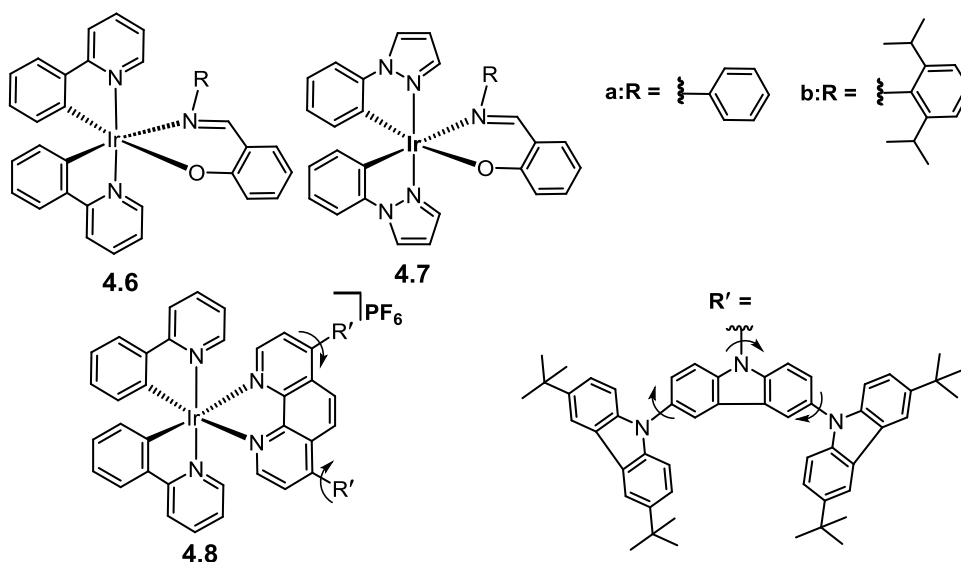


Figure 4.3: Complexes **4.6a-b**, **4.7a-b** and **4.8** show EPSS

Huang *et al.*¹³ prepared a series of Pt(II) complexes with different N[^]O ligands **4.9a-b**. They found that all the complexes are non-emissive in different solvents (DMF, MeCN, CH₂Cl₂, and toluene). However, they exhibit aggregation-induced phosphorescent emission (AIPE) with an absolute quantum efficiency of up to 38% in the crystal state. Furthermore, their AIPE properties can be tuned significantly by changing the chemical structures of the N[^]O ligands. In this case, based on experimental and theoretical investigations, the mechanism of AIPE was ascribed to “restricted distortion of excited-state structure (RDES)” similar to that proposed by Davies for the Ir complexes described above.

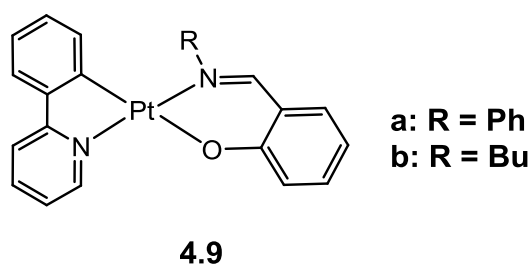


Figure 4.4: Complexes **4.9a-b** show AIPE

Yam and co-workers showed that in THF solution, complexes **4.10a-b** (Fig 4.5), have a weak emission, which is enhanced in a THF/H₂O mixture.¹⁴ Similarly, complex **4.11** is non-emissive in MeCN, but increasing the volume percentage of PBS (phosphate buffer saline) in a mixture with MeCN results in enhancement in the emission intensity.¹⁵ In both cases, details of the cause of the AIE effect were not given; however, Tang suggested that it was due to RIR of the phenyl and triazole moieties in **4.10** and of the phenyl and carbazole groups in **4.11**.¹⁶

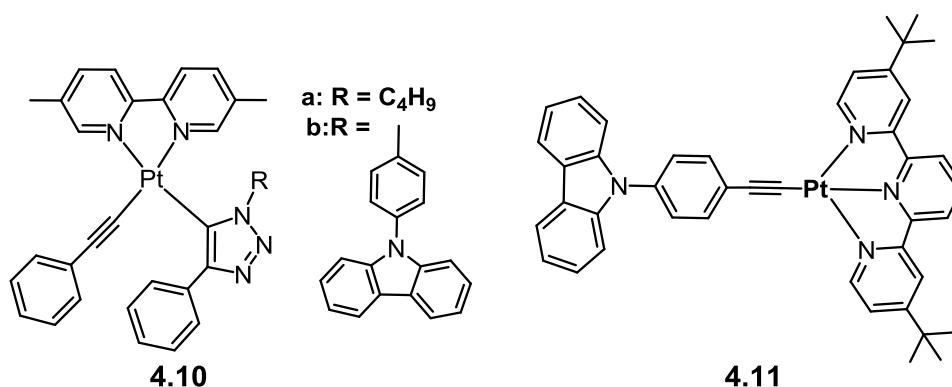


Figure 4.5: Complexes **4.10a-b** and **4.11** show AIE

As mentioned above, it is well known that rotation of substituents can lead to non-radiative decay and hence a reduction in emission intensity. This phenomenon has been used to provide an emission sensor for viscosity.¹⁷⁻²⁰ Thus complex **4.12** Fig 4.6 has different constraints on rotation hence, as the viscosity increases, the rotation slows and the emission intensity increases.²⁰ In addition, the viscosity has an effect on the lifetime of the emission, so in principle lifetime imaging may be used to map viscosity. To date, such an approach has only been used with fluorescent compounds. The much longer lifetimes of phosphorescent metal complexes may provide greater range or sensitivity in viscosity measurements.

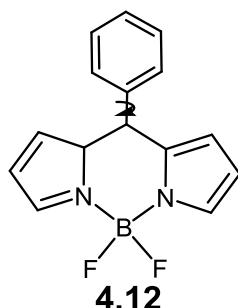


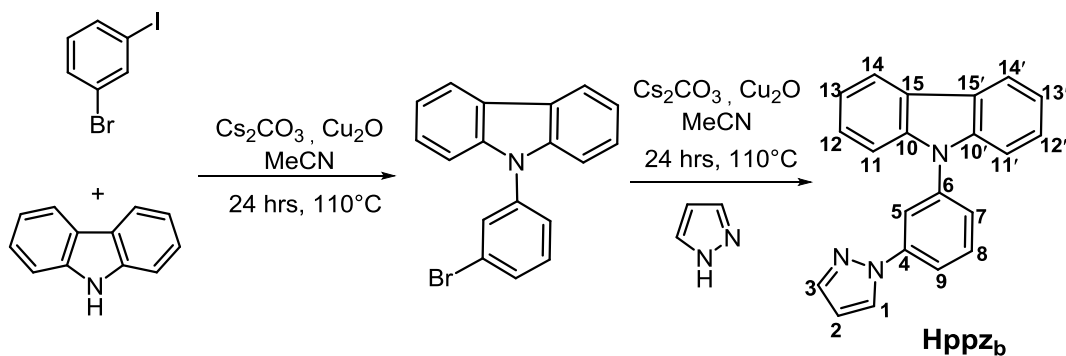
Figure 4.6: The structure of *p*-substituted BODIPY dye with various degrees of constraint on the rotation of the meso-phenyl group.²⁰

The purpose of this study was to evaluate whether Pt metal complexes can be designed to show EPESS and hence whether they have any potential in application as viscosity sensors. As mentioned in Chapter 1, Pt cyclometallated complexes of the form [Pt(C[^]N)(X[^]Y)]ⁿ⁺ (n = 0, 1) are often highly emissive. Hence the design strategy was to synthesise complexes [Pt(C[^]N)(X[^]Y)]ⁿ⁺ with additional substituents that are free to rotate in solution such that they are only weakly emissive in solution but are strongly emissive in the solid state.

4.2 Results and Discussion

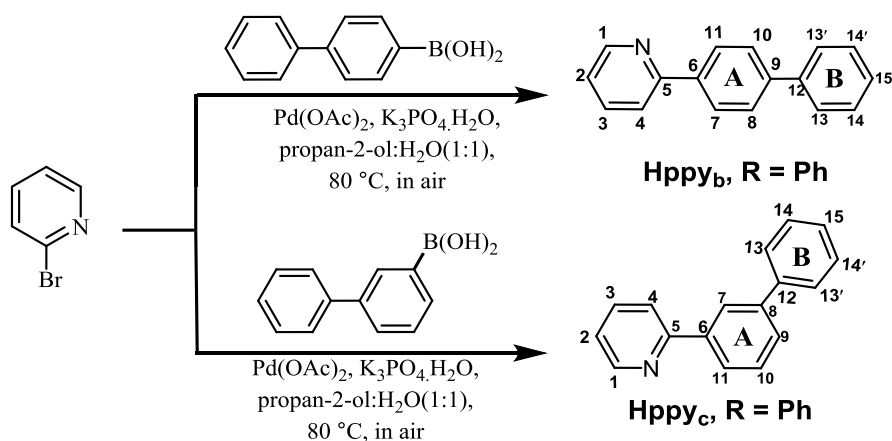
4.2.1 Synthesis of C^N ligands

Hppz_a (1-Phenylpyrazole) and **Hppy_a** (2-Phenylpyridine) are commercially available and were used as received. Ligand **Hppz_b** was prepared as shown in Scheme 4.1. Arylation of carbazole occurred in a 92% yield via Cu-catalysed CN-coupling;²¹ the reaction with pyrazole under the same conditions gave **Hppz_b** in a good yield (66%) (Scheme 4.1). The ¹H NMR spectrum of **Hppz_b** shows a total of fifteen protons. The carbazole protons were observed as four 2H doublets consistent with the free rotation of the carbazole group. The pyrazole and phenyl protons were easily assigned via TOCSY and COSY spectra. The ASAP mass spectrum shows a molecular ion [M+H]⁺ at *m/z* 310.1347 (310.1344 calculated for C₂₁H₁₆N₃).



Scheme 4.1: Synthesis of Ligand **Hppz_b**

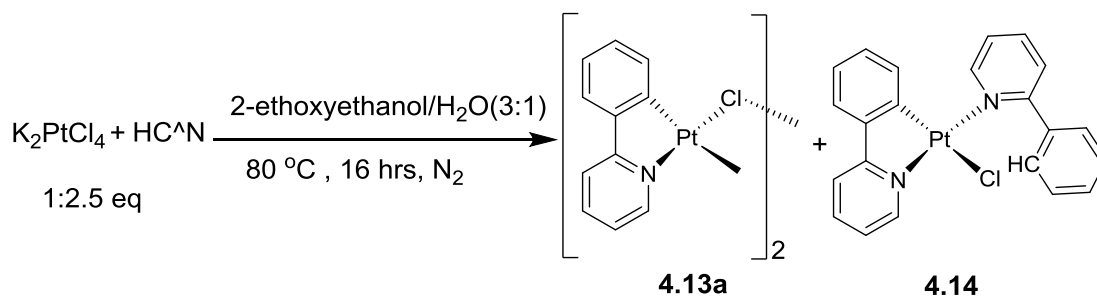
Phenyl pyridine derivatives **Hppy_b** and **Hppy_c** were synthesized in good yields, 73% and 61%, respectively, by a Suzuki reaction from 2-bromopyridine according to a literature method²² (Scheme 4.2). The ¹H NMR and ¹³C NMR spectra of ligands agree with the literature data.²² The ¹H NMR spectrum of **Hppy_b** showed that protons H_{7,11}, H_{8,10}, H_{13,13'}, and H_{14,14'} are pairwise equivalents, demonstrating free rotation of the biphenyl group. For **Hppy_c** H_{13,13'} and also H_{14,14'} are pairwise equivalents, suggesting there is free rotation of the phenyl (B) group. However, the lack of symmetry in ring A means no conclusion can be drawn regarding rotation of this group but there is no obvious reason why it should not be free to rotate.



Scheme 4.2: Synthesis of ligands **Hppy_b** and **Hppy_c**

4.2.2 Synthesis of Pt(II)- μ -dichloro-bridged Dimers

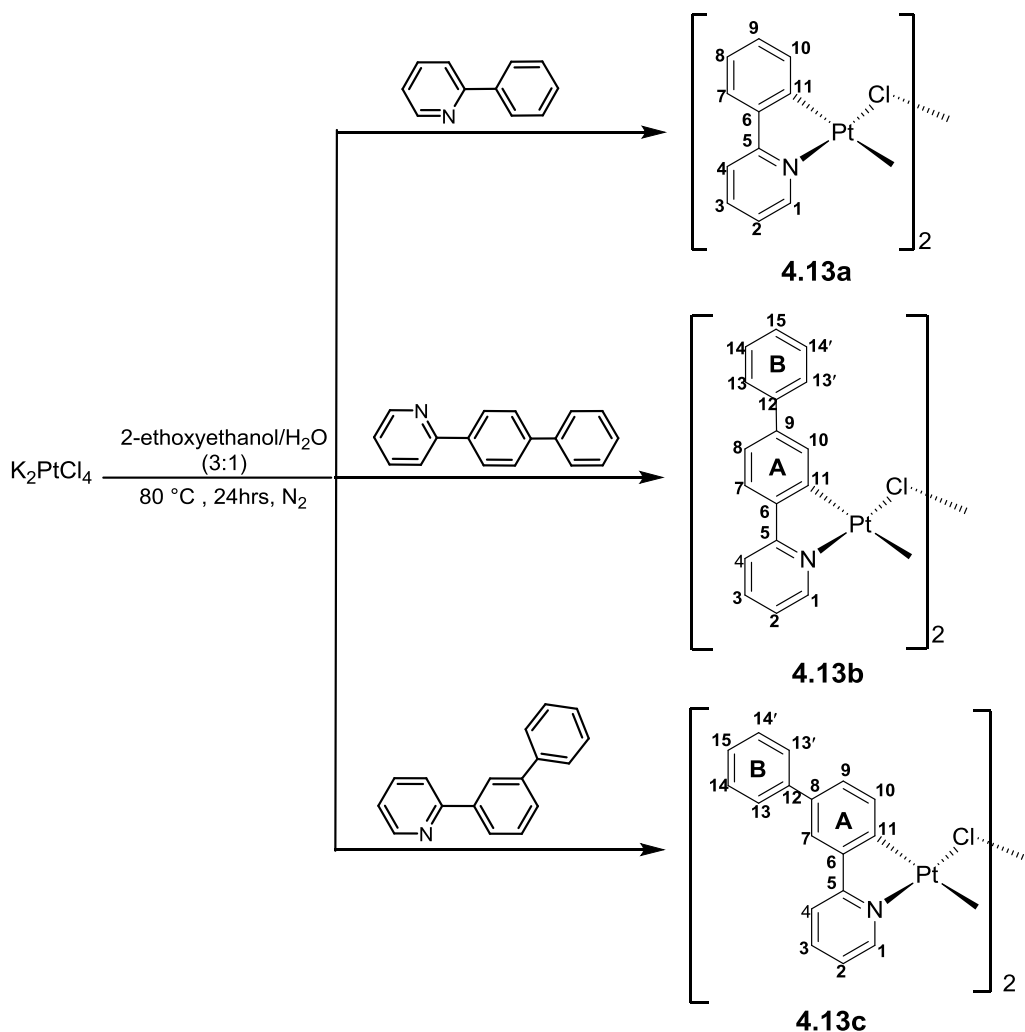
The synthesis of cyclometallated dimers is usually undertaken by reacting $K_2[PtCl_4]$ with excess phenyl pyridine (Scheme 4.3);²³ however, this can lead to a mixture of the dimer $[Pt(C^{\wedge}N)_2Cl]_2$ (**4.13a**) and the monomer $[Pt(C^{\wedge}N)(HC^{\wedge}N)Cl]$ (**4.14**). Esmailbeig *et al.*²⁴ reported that the use of a 1:1 ratio of $HC^{\wedge}N$ to Pt salt avoids the formation of by-product **4.14**.



Scheme 4.3: Synthesis of $[Pt(ppy)Cl]_2$ **4.13a**

Dimers **4.13a-c** were synthesised in a 57-67% yield using the same method but with only one equivalent of the cyclometallating ligand (Scheme 4.4). The dimer **4.13a** is known and the NMR data are consistent with that in the literature.²⁵ The 1H and ^{13}C NMR spectra of **4.13b-c** each showed 12 protons, one fewer than each of the free ligands, **Hppy_b** and **Hppy_c**. The TOCSY spectra of **4.13b** and **4.13c** allowed identification of the signals for the pyridine and the two phenyl rings. For **4.13b**, assignment of H_4 (δ 8.15) was confirmed by an NOE to the doublet at δ 7.86 which was therefore assigned as H_7 on phenyl (A). The other pyridine protons and phenyl A were then assigned via COSY and NOESY spectra. Protons $H_{8,10}$ show an NOE to a broad doublet at δ 7.68, which was assigned to the phenyl (B) ring $H_{13,13'}$. The COSY spectrum then allowed for the assignment of

protons H_{14, 14'} as multiplets at *ca.* δ 7.49. The fact that protons H_{13, 13'} and H_{14,14'} are pairwise equivalents suggests that the phenyl B ring is rotating. The ¹³C NMR spectrum shows the expected signals. The ESI mass spectrum shows ions at *m/z* 926 due to [Pt₂(C[^]N)₂Cl(MeCN)]⁺.

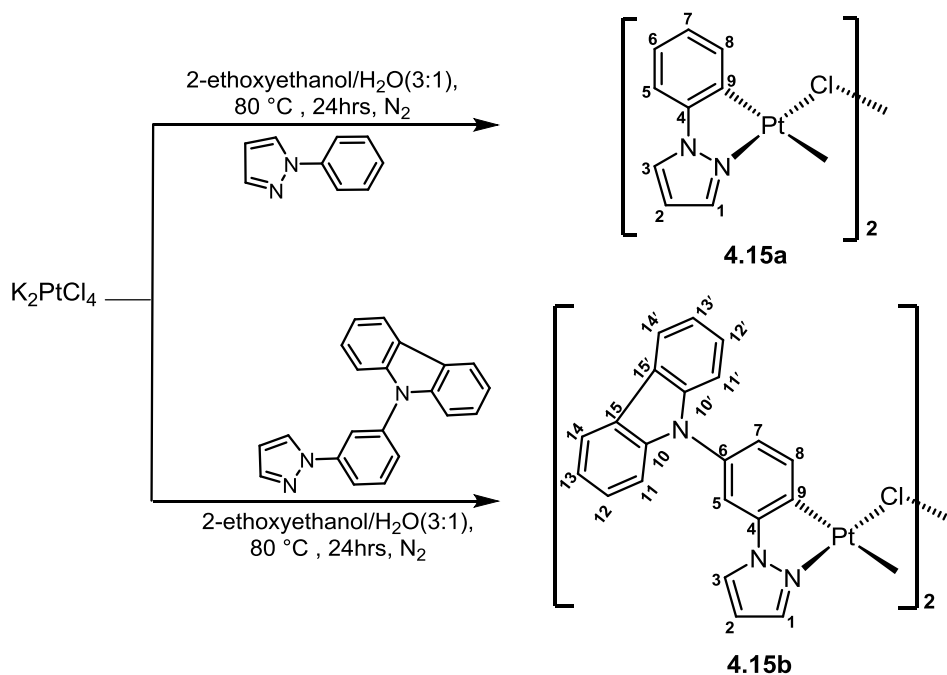


Scheme 4.4: Synthesis of [Pt(R-ppy)Cl]₂ dimers **4.13a-c**

The ¹H and ¹³C NMR spectra of **4.13c** are similar to those of **4.13b** and were assigned in the same manner. The only singlet in the aromatic region is assigned to H₇ (δ 8.09). Proton H₇ shows NOE to doublet at δ 8.41 which was assigned to H₄ and an NOE to a broad 2H doublet at δ 7.79, which was assigned to H_{13,13'}. Protons H_{14,14'} were observed as a multiplet at *ca.* δ 7.48, suggesting free rotation of phenyl (B). The ¹³C NMR spectrum showed the expected signals with one signal for C_{13, 13'} and one for C_{14, 14'}. The ES mass spectrum shows ions at *m/z* 885 due to [Pt₂(C[^]N)₂Cl(MeCN)]⁺.

The dimers **4.15a-b** were prepared by the same method²⁴ (Scheme 4.5) via the reaction of K₂PtCl₄ and the corresponding ligands **Hppz**_(a-b). After work-up, dimers **4.15a-b** were

formed in yields between 51-67% (see experimental section). The dimers were insoluble in most solvents apart from DMSO, so consequently the NMR spectra were only recorded in DMSO. It should be further noted that the complexes actually react with DMSO so the NMR spectra are really those of $[\text{Pt}(\text{C}^{\wedge}\text{N})(\text{DMSO-d}_6)\text{Cl}]$.



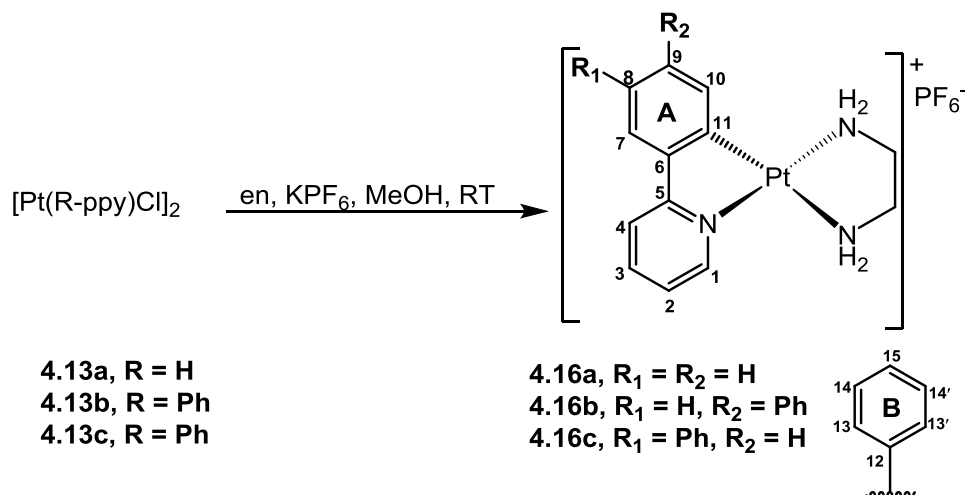
Scheme 4.5: Synthesis of $[\text{Pt}(\text{R-ppz})\text{Cl}]_2$ dimers **4.15a-b**

The dimer **4.15a** is known and has been reported in the literature,²⁶ and the ^1H NMR spectrum is consistent with that published. Proton H_3 is the most downfield signal, a doublet at δ 8.87, and shows an NOE to the doublet at δ 7.65 which is therefore assigned as H_5 . The pyrazole protons H_{1-2} (δ 8.16 and 6.82), and phenyl protons H_{6-8} (ca. δ 7.21, 7.02 and 8.13 respectively) were assigned by using the TOCSY and COSY spectra. The high-resolution mass spectroscopy (ASAP) showed molecular ions at m/z 711.0203 assigned to $[\text{Pt}_2(\text{ppz})_2\text{Cl}]^+$ (711.0203 calculated for $\text{C}_{18}\text{H}_{14}\text{ClN}_4\text{Pt}_2$).

Dimer **4.15b** was hard to purify due to its low, or indeed complete lack of solubility in most organic solvents, and it was therefore used without further purification. Analysis of the ^1H NMR spectrum of the crude product showed the majority of peaks corresponded to the desired dimer. The ES mass spectrum in MeCN shows ions at 1083 assigned to $[\text{Pt}_2(\text{C}^{\wedge}\text{N})_2(\text{MeCN})\text{Cl}]^+$, confirming the ease at which the dimer could be split in the presence of a coordinating solvent; however, the presence of ions at m/z 853 suggest the presence of one cyclometallated ($\text{C}^{\wedge}\text{N}$) ligand and one monodentate on one Pt $[\text{Pt}(\text{C}^{\wedge}\text{N})(\text{HC}^{\wedge}\text{N})(\text{MeCN})]$.

4.2.3 Synthesis and Characterisation of [Pt(C^N)(en)]PF₆ **4.16a-c**

The synthesis of complexes **4.16a-c** via the reaction of dimers **4.13a-c** with ethylenediamine (en) and KPF₆ were carried out as shown in **Scheme 4.6** to form compounds **4.16a-c** in 60-76 % yields. Complex **4.16a** is known and has been reported in the literature and is included here for comparison. Its NMR data are consistent with those published.²⁷



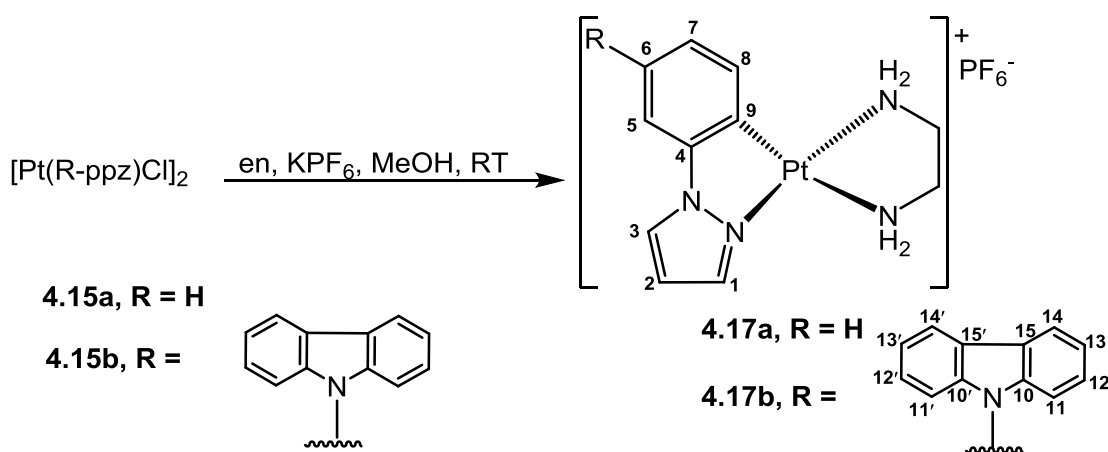
Scheme 4.6. Synthesis of [Pt(R-ppy)(en)]PF₆ **4.16a-c**

The ¹H NMR spectrum of **4.16b** is similar to that of the dimer **4.13b** but an extra two broad singlets of 2H each were observed at δ 6.16 and 5.30 which are assigned to the NH₂ groups and one a broad singlet which integrates to 4H at δ 2.71 due to the CH₂-CH₂ protons. A TOCSY spectrum allowed identification of the signals for the pyridine and phenyl rings (A-B). Proton H₄ was observed as a doublet at δ 8.12 and shows an NOE to a doublet at δ 7.79 which is therefore assigned to H₇. Assignment of the pyridine protons (H₁₋₃) and phenyl A(H_{8,10}) protons follows from the COSY and NOESY spectra. A broad 2H doublet at δ 7.75 shows NOEs to H₈ and H₁₀ and was therefore assigned to the phenyl B protons H_{13, 13'}. The COSY spectrum then allowed for the assignment of other phenyl protons. H_{14, 14'}, which were observed as a broad triplet at δ 7.49 and H₁₅ which gives a multiplet at *ca.* δ 7.38. The fact that H_{13, 13'} and H_{14, 14'} are pairwise equivalents indicates that phenyl B is rotating. The ¹³C NMR spectra showed the expected signals with the two carbons of CH₂-CH₂ of the en ligand being observed at δ 47.3 and 43.6. High-resolution mass spectroscopy (ESI) showed a molecular ion [M]⁺ at *m/z* 485.1303 (485.1305 calculated for C₁₉H₂₀N₃Pt).

The ¹H NMR spectrum of **4.16c** is similar to that of **4.16b** except for the phenyl B ring being at the *para* position with respect to the metal, and assignments were made on the

same basis as for **4.16b**. The broad singlets of 2H each were observed at δ 6.11 and 5.30, which were assigned to NH_2 and a broad singlet which integrated to 4H at δ 2.70 due to the $\text{CH}_2\text{-CH}_2$ protons. Protons $\text{H}_{13, 13'}$ are equivalent giving a broad doublet at δ 7.78, and similarly $\text{H}_{14, 14'}$ gave rise to a multiplet at *ca.* δ 7.47, hence the phenyl ring is rotating. The ^{13}C NMR spectrum showed the expected signals and four CH carbons of double intensity which were assigned to the phenyl B carbons at δ 126.2 for $\text{C}_{13, 13'}$ and at δ 127.7 for $\text{C}_{14, 14'}$, suggesting the phenyl B may be rotating. The two carbons in the $\text{CH}_2\text{-CH}_2$ bridge of the en ligand were observed at δ 47.9 and 43.5. High-resolution mass spectroscopy (ESI) showed a molecular ion $[\text{M}]^+$ for details, see Chapter 5.

The syntheses of related phenylpyrazole complexes **4.17a-b** is outlined in **Scheme 4.7**. After work-up, complexes **4.17a-b** were formed in 45-60% yields. Complex **4.17a** is a known complex, this is included here for comparative purposes; its NMR data are consistent with those in the literature.²⁸



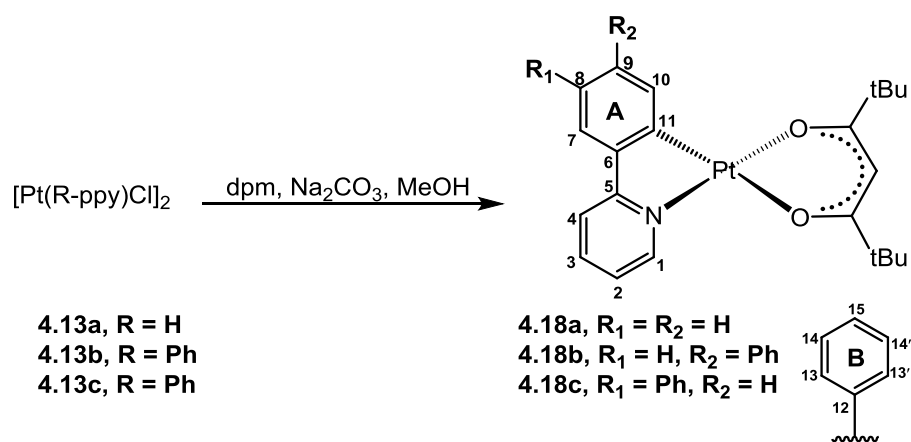
Scheme 4.7. Synthesis of $[\text{Pt}(\text{R-ppz})(\text{en})]\text{PF}_6$ **4.17a-b**

The ^1H NMR spectrum of **4.17b** is similar to that of the starting dimer **4.15b** except an additional two broad singlets were observed at δ 5.03 and 4.29 as assigned to the two NH_2 groups, and a broad 4H singlet at δ 2.85 due to the $\text{CH}_2\text{-CH}_2$ protons. The TOCSY spectrum allowed identification of the signals due to the pyrazole (H_{1-3}), phenyl ($\text{H}_{5, 7-8}$) and carbazole rings; however, there is some considerable overlap of these signals. Proton H_3 is a multiplet at *ca.* δ 8.17 and shows an NOE to a doublet at δ 7.56 which is therefore assigned as H_5 , after which the COSY spectrum then allows assignment of the other pyrazole protons H_{1-2} (δ 7.80, and 6.60, respectively) and phenyl protons H_{7-8} (δ 7.27 and *ca.* 8.16, respectively). Proton H_5 shows an NOE to a 5H multiplet at δ 7.44-7.37 that arose due to the carbazole protons. The remaining carbazole protons were observed as a 1H multiplet at *ca.* δ 8.15, a 1H doublet of doublet of doublets at δ 7.27 and another 1H

doublet of doublets at δ 7.20, suggesting the carbazole protons are not pairwise equivalent, suggesting rotation may be slow on the NMR timescale. The ^{13}C NMR spectrum of **4.17b** showed six aromatic CH carbons and four CH carbons of double intensity which were assigned to the carbazole and the two $\text{CH}_2\text{-CH}_2$ carbons of the ethylenediamine ligand were observed at δ 47.3 and 44.0. The high-resolution mass spectrum (ESI) showed a signal at m/z 563.1534 (563.1523 calculated for $\text{C}_{23}\text{H}_{22}\text{N}_5\text{Pt}$).

4.2.4 Synthesis and Characterisation of $[\text{Pt}(\text{C}^{\wedge}\text{N})(\text{dpm})]$ **4.18a-c**

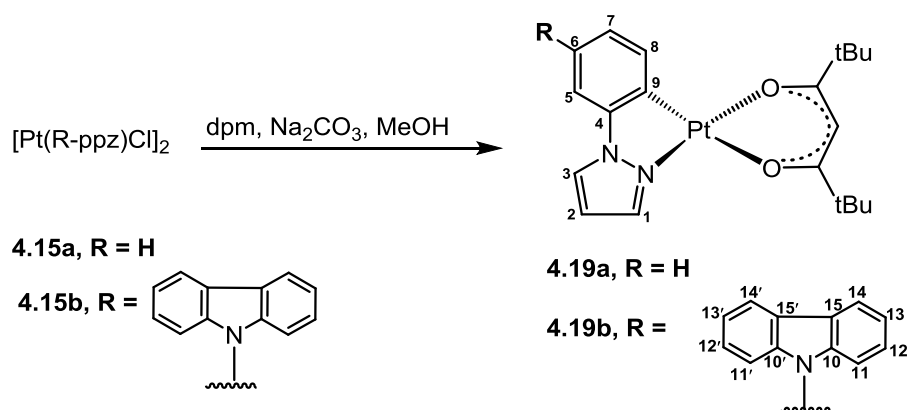
Complexes **4.18a-c** were synthesised in good yields (66-73%) according to a literature procedure,²³ as shown in **Scheme 4.8**. Complex **4.18a** is known and the NMR data are consistent with those reported in the literature.²⁹



Scheme 4.8. Synthesis of $[\text{Pt}(\text{R-ppy})(\text{dpm})]$ **2.18a-c**

The ^1H NMR spectra of **4.18b-c** are similar to **4.16b-c** except the signals for the ethylenediamine group are replaced by those associated with dipivaloylmethane (dpm). The two ^tBu groups are inequivalent, giving two different singlets at δ 1.31 and 1.30 for **4.18b** and at δ 1.23 and 1.21 for **4.18c**, whilst the CH group was observed as a singlet at δ 5.82 and δ 5.76 for **4.18b** and **4.18c**, respectively. All assignments were made on the same basis as those for **4.16b, c** and similarly the expected NOEs were observed. The ^1H NMR spectrum of **4.18b** showed that protons $\text{H}_{13, 13'}$ and $\text{H}_{14, 14'}$ are pairwise equivalent, demonstrating the free rotation of the phenyl substituent. This also applies to complex **4.18c**. The ^{13}C NMR spectra show the expected signals in both complexes. The high-resolution mass spectrum (ASAP) shows molecular ions $[\text{M}+\text{H}]^+$ at m/z 609.2084 for **4.18b** (609.2081 calculated for $\text{C}_{28}\text{H}_{32}\text{NO}_2\text{Pt}$) and 609.2091 for **4.18c** (609.609.81 calculated for $\text{C}_{28}\text{H}_{32}\text{NO}_2\text{Pt}$).

Complexes **4.19a-b** were synthesized in the same manner, giving 50 and 61% yields as per **Scheme 4.9**. Complex **4.19a** is a known complex, and the NMR data are consistent with those reported in the literature.³⁰



Scheme 4.9. Synthesis of $[\text{Pt}(\text{R-ppz})(\text{dpm})]$ **4.19a-b**

The ^1H NMR spectrum of **4.19b** is similar to that of **4.17b** except the signals for the ethylene diamine group are replaced by those associated with dipivaloylmethane (dpm). The ^tBu groups were singlets at δ 1.28 and 1.27, while the CH group was observed as a singlet at δ 5.95. All assignments were made on the same basis as **4.17b**. The carbazole protons were observed as a broad 2H doublet at δ 8.20, a 4H multiplet at δ 7.45-7.43 and a 2H multiplet at δ 7.31-7.28, suggesting the carbazole ring could freely rotate. Full assignments are given in Chapter 5. The ^{13}C NMR spectrum shows two double intensity quaternary carbons assigned to four C—C carbons and were assigned to carbazole, whilst four CH carbons of double intensity were assigned to the carbazole CH carbons, again suggesting the carbazole ring was rotating. The high-resolution mass spectroscopy (ASAP) showed a molecular ion $[\text{M}+\text{H}]^+$ at m/z 687.2318 (687.2299 calculated for $\text{C}_{32}\text{H}_{34}\text{N}_3\text{O}_2\text{Pt}$).

In conclusion, these reactions show that a range of cationic or neutral cyclometallated Pt(II) complexes can be synthesised in reasonable yields. All the complexes were characterised by ^1H and ^{13}C NMR spectroscopy and high-resolution mass spectrometry. The use of 2-D NMR techniques allowed for the assignment of the majority of the protons. The NMR spectroscopy indicated that the substituents on the cyclometallated ligands are freely rotating in solution. The photophysical properties of these complexes are discussed in the following sections.

4.3 Photophysical properties

4.3.1 Photophysical Properties of $[\text{Pt}(\text{C}^{\wedge}\text{N})(\text{en})]\text{PF}_6$ (**4.16a-c** and **4.17a-b**).

The UV-vis absorption spectra of complexes **4.16a-c** and **4.17a-b** are shown in **Fig. 4.7** and the data for all five complexes are reported in **Table 4.1**. The absorption spectra of complexes **4.16a-c** in MeCN show strong bands between 225 and 300 nm due to $\pi \rightarrow \pi^*$ transitions, whilst there are weaker bands around 350-400 nm; however, there was no clear evidence for separate peaks above 400 nm. Putting a phenyl group in the *meta* or *para* position with respect to the coordinating carbon, i.e., complexes **4.16b-c**, respectively, resulted in a red shift to shorter wavelengths by *ca.* 52 and 29 nm, respectively, compared to unsubstituted complex **4.16a** (241 nm). The greater shift for the *meta*-substituted complex suggests there may be better delocalisation of the phenyl substituent in this position. The absorbance of **4.16a-c** and **4.17a-b** in MeCN/Et₂O (1:9) (ppt) was reduced as compared with the absorbance in pure MeCN, which may mean that the complex was starting to precipitate even though no solid was observed. the spectra for which are shown in the appendix (**Figs 13**).

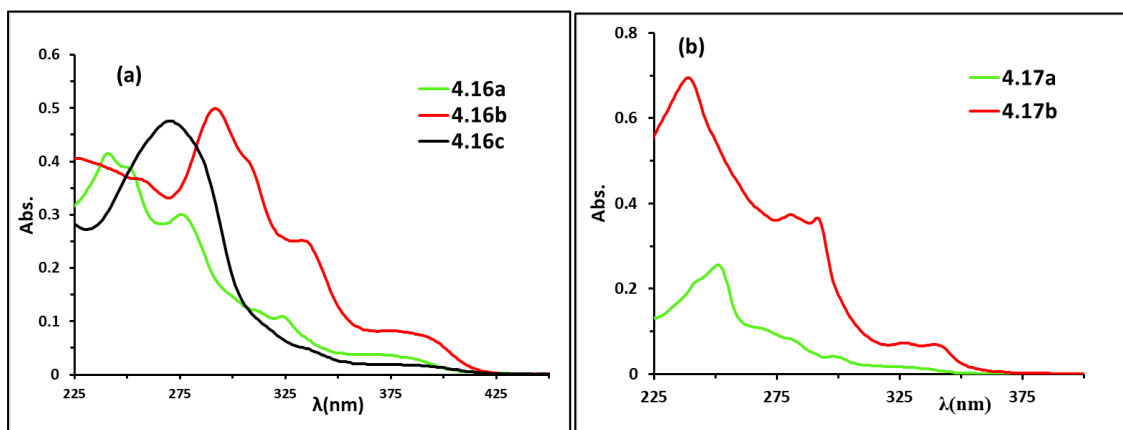


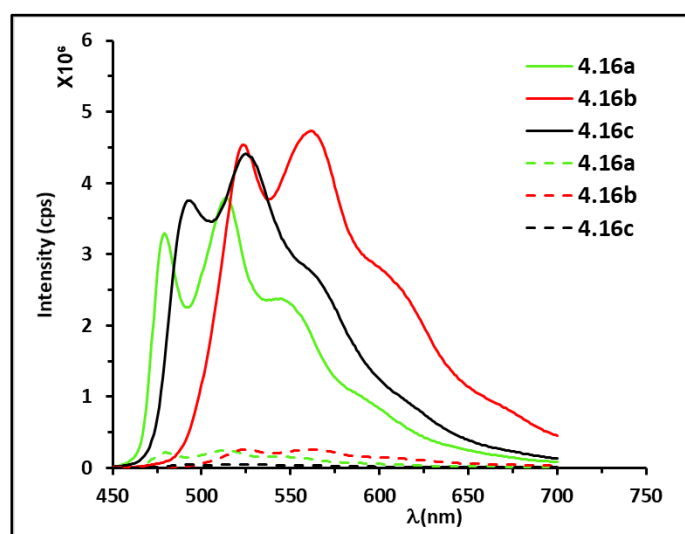
Figure 4.7: Absorption spectra of $[\text{Pt}(\text{C}^{\wedge}\text{N})(\text{en})]\text{PF}_6$ (a): **4.16a-c** and (b) **4.17a-b** in MeCN, 0.02 mM, at room temperature.

The absorption spectra of **4.17a-b** in MeCN show strong bands between 240 and 290 nm due to $\pi \rightarrow \pi^*$ transitions, but there is no clear evidence for separate peaks at longer wavelengths for complex **4.17a**, whilst complex **4.17b** showed some weak bands at longer wavelength between *ca.* 354-360 nm. For complex **4.17b**, the band at 240 nm was blue-shifted by *ca.* 12 nm as compared with the unsubstituted complex **4.17a**.

Table 4.1: Electronic absorption data for complexes **4.16a-c** and **4.17a-b** in MeCN

Complex	λ (nm), ϵ (L mol ⁻¹ cm ⁻¹)
4.16a	241 (20450), 251 sh (19350), 278(14800), 325 (5400), 381 sh (1650)
4.16b	293 (24850), 334 sh (12550), 384 sh (3900)
4.16c	270 (23800), 380 sh (12100)
4.17a	252 (12700), 300 (2400)
4.17b	240 (34600), 292 (18300), 341 sh (3400)

The emission spectra of complexes **4.16a-c** are shown in **Fig. 4.8** and the associated data are reported in **Table 4.2**. In air, all three complexes (**4.16a-c**) show weak emission intensities, but when degassed these intensities increased by *ca.* 15, 18 and 87-fold, respectively, hence **4.16c** shows the greatest sensitivity to oxygen. Complex **4.16a** showed emission peaks at 479 and 514 nm with a weak shoulder at 544 nm, which is very similar to the literature data (481 and 510 nm with a weak shoulder at 550 nm)²⁷ for the same complex with a chloride counter ion [Pt(ppy)(en)]Cl. The emission has been assigned as a mixture of ILCT and MLCT,²⁷ as found previously for related Pt cyclometallated complexes²³ (see Chapter 1). Complexes **4.16b** and **4.16c** show very similar emission spectra but in each case with a red shift of *ca.* 45 to 50 nm for **4.16b** and 10-15 nm for **4.16c** compared to **4.16a** (**Fig. 4.8**). The red shift is similar to the effect of an OMe substituent at the same position in the [Pt(OMe-ppy)(dpm)] complexes.²³

**Figure 4.8:** Emission spectra of [Pt(C^N)(en)]PF₆ (**4.16a-c**) in MeCN under Ar (—) and in MeCN in air (---) at 0.02 mM, λ_{ex} 376 nm at RT.

To test for EPSS, an anti-solvent is added to precipitate the complex and determine the effects this has on the emission. Hence the spectra were run in a 1:9 mixture of MeCN/Et₂O and are shown in **Fig 4.9**. The spectra in the mixed solvent are very similar in appearance to those recorded in pure MeCN and with almost unchanged emission wavelengths, but under argon emission intensities for all three complexes **4.16a-c** were enhanced by *ca.* 1.6-, 2.2- and 1.6-fold, respectively, compared with their emission in pure MeCN solutions (see **Table 4.2** and **Fig. 4.9a**). In air a similar situation is observed with the precipitates showing higher emission intensity, the increase is much higher for **4.16c** than for **4.16a,b**. It is possible that for **4.16c** which is most sensitive to air in solution, the precipitate partially protects the complex from air leading to a bigger enhancement in this case.

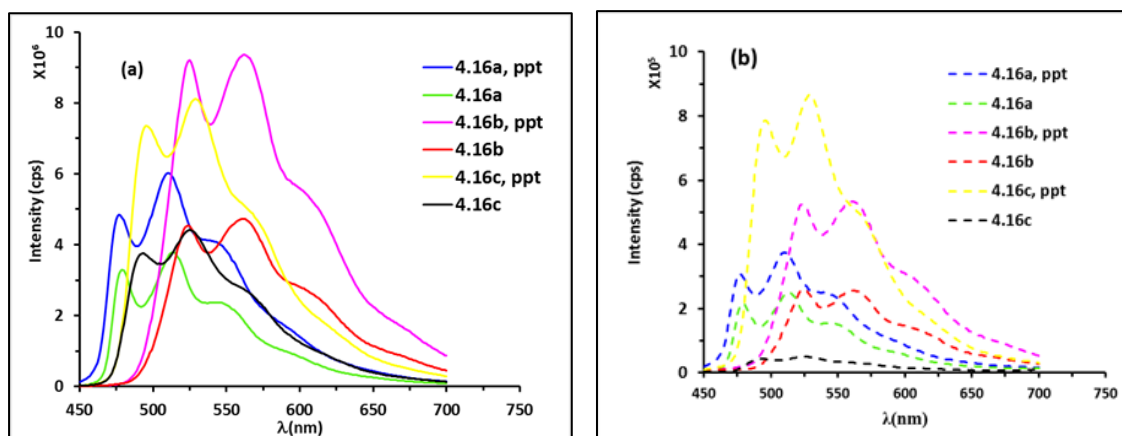


Figure 4.9: Emission spectra of [Pt(C^N)(en)]PF₆ (**4.16a-c**) in MeCN/Et₂O (ppt) and in solution at 0.02 mM MeCN (a): under Ar and (b): in air, (λ_{ex} 376 nm) at RT.

Table 4.2: Electronic emission spectral data for **4.16a-c**

Entry	Complex	% Et ₂ O in MeCN under Ar	λ_{max} (nm)	Increase in emission intensity (from solution)
1	4.16a	0	479, 514, 544 sh	<i>ca.</i> 1.6
		90	477, 511, 546 sh	
2	4.16b	0	524, 561, 611 sh	<i>ca.</i> 2.2
		90	525, 562, 609 sh	
3	4.16c	0	493, 525, 567 sh	<i>ca.</i> 1.6
		90	496, 531, 568 sh	

It should be noted that the emission of Pt cyclometallated complexes is often different in the solid state than in solution.³¹ For example the emission of [Pt(ppy)(en)]Cl in the solid state is quite different to that in solution (λ_{max} 510 nm in H₂O and 553 nm in the solid state). Hence it is possible that the similarity between spectra here mean that the emission

being seen is still from residual monomeric complex in solution. The modest increase in intensity may be due to dilution and hence a reduction in self-quenching as has been observed previously. Further studies of effect of dilution on emission intensity would be needed to clarify this. Overall these complexes do not show a significant EPSS effect except possibly **4.16c** in air.

Complex **4.17a** is known not to be emissive at room temperature, and rather is only emissive at low temperature, i.e., 77 K.^{28,30} Complex **4.17b** is also not emissive in MeCN at room temperature. Running the emission spectra of **4.17a-b** in a MeCN/Et₂O (1:9) mixture at ambient temperature also gave no emission (see **Fig 14** in the appendix).

4.3.2 Photophysical properties of [Pt(C[^]N)(dpm)] (**4.18a-c** and **4.19a-b**).

The UV-vis absorption spectra of complexes **4.18a-c**, and **4.19a-b** are shown in **Figs. 4.10a-b** and their data reported in **Table 4.3** and their absorption spectra in a mixed solvent of MeCN/H₂O(1/9) (ppt) are shown in **Fig. 1.15** in an appendix. Complex **4.18a** has been previously identified, and its absorption data are in agreement with that reported in the literature.^{23,29} Complex **4.18a** showed high intensity bands at about 256 nm which were assigned to π - π^* transitions; however, there is no clear evidence for separate peaks at longer wavelength (above 350 nm). Complexes **4.18a-c** show highly intense absorption bands below *ca.* 300 nm which were assigned to π - π^* ligand-centred (LC) transitions and low-energy transitions in the range 350-400 nm were assigned as MLCT transitions based on the spectra reported for related complexes.^{23,29} The highest energy transitions for **4.18b-c** were red-shifted by *ca.* 36 and 23 nm, respectively, and both complexes show larger extinction coefficients than **4.18a** (**Table 4.3**, entries **1-3**)

Complex **4.19a** is also known and its absorption data are in good agreement with the literature.³⁰ Intense, high-energy absorption bands at *ca.* 239 nm were assigned to allowed π - π^* ligand-centred (LC) transitions, whereas the low-energy, less intense transitions in the range 350-375 nm were assigned to MLCT transitions. As for **4.19a**, complex **4.19b** showed strong bands below 300 nm due to $\pi \rightarrow \pi^*$ transitions, with less intense transitions around 350 nm. However, there is no clear evidence for separate peaks at longer wavelength above 350 nm in complexes **4.19a-b**. Complex **4.19b** shows larger extinction coefficients than **4.19a** which may be attributed to the carbazole substituent on the C[^]N ligand (entries **4** and **5** in **Table 4.3** and **Fig. 4.10b**).

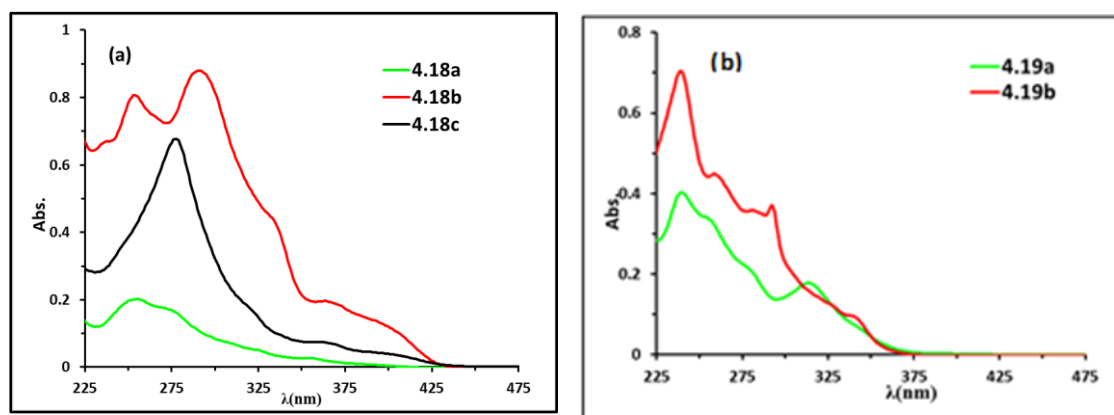


Figure 4.10: Absorption spectra of $[\text{Pt}(\text{C}^{\wedge}\text{N})(\text{dpm})]$ (a). **4.18a-c** and (b). **4.19a-b** in MeCN, 0.02 mM at RT.

Table 4.3: Electronic absorption data for **4.18a-c** and **4.19a-b** in MeCN

Entry	Complex	λ (nm), (ϵ ($\text{L mol}^{-1} \text{cm}^{-1}$))
1	4.18a	256 (10100), 277 sh (8200), 327 sh (2400), 357 sh (1300)
2	4.18b	254 (40300), 290 (44000), 332 sh (22400), 374 sh (8900),
3	4.18c	279 (33600), 370 sh (3300),
4	4.19a	239 (20100), 256 sh (16800), 315 (8800)
5	4.19b	240 (35100), 261 sh (22150), 293 (18400), 340 sh (4750)

The emission spectra of complexes **4.18a-c** were recorded in MeCN and in an MeCN/H₂O (1:9) mixture at ambient temperature; their emission spectra are shown in **Fig. 4.11** and their data are reported in **Table 4.4**. Complex **4.18a** showed emission bands at 481 and 515 nm with a shoulder at longer wavelength *ca.* 548 nm, which was very similar to the literature data (477, 512, 541 sh nm).²⁹ Complexes **4.18b-c** were red-shifted by *ca.* 40 to 45 nm for **4.18b** and by *ca.* 15 nm for **4.18c** compared to the unsubstituted complex **4.18a**. The emission for complexes **4.18a-c** were found to be sensitive to oxygen, showing weak emission in air; however, in degassed MeCN the emission intensities of the complexes were increased by *ca.* 20-, 30- and 50-fold, respectively, suggesting considerable triplet character in the excited state. Surprisingly, the intensity for **4.18a** was considerably less than for the two substituted complexes (**4.18b-c**), despite the presence of the rotatable phenyl substituents in the latter two (**Fig. 4.11**). The reason for this increase is not known and requires further study.

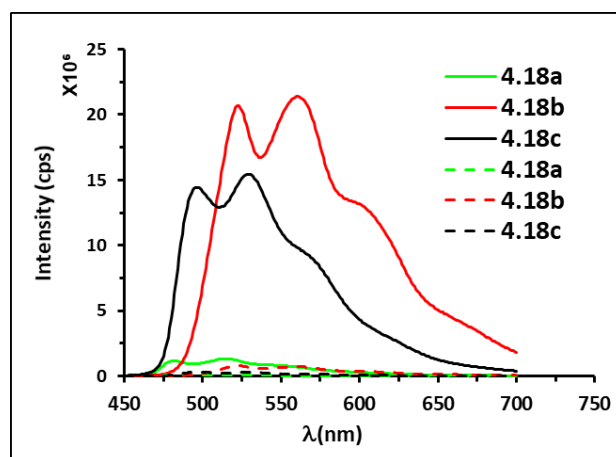


Figure 4.11: Emission spectra of $[\text{Pt}(\text{C}^{\wedge}\text{N})(\text{dpm})]$ (**4.18a-c**) in MeCN under Ar (—) in air (---) at 0.02 mM, λ_{ex} 400 nm at RT.

To test for EPSS, an anti-solvent is added to precipitate the complex in order to examine the associated effect on the emission. In contrast to $[\text{Pt}(\text{ppy})(\text{en})]^+$ (**4.16a**) complex **4.18a** showed lower intensity emission after precipitation compared to in solution though the spectrum of the precipitate is very similar to that in solution (**Fig 4.12**). Under argon complexes **4.18b** and **4.18c** were found to be much less emissive when precipitated, compared to in solution. However under air for complexes **4.18b, c** the emission of the solution and the precipitate are much more comparable and it is also notable that, the precipitates show an extra broad emission band with emission maxima red-shifted by *ca.* 107-133 nm to longer wavelength compared to in solution. The reason for this difference is not known however solid state effects in emission of Pt cyclometallated complexes have been observed previously³¹ a full understanding of these results requires further study.

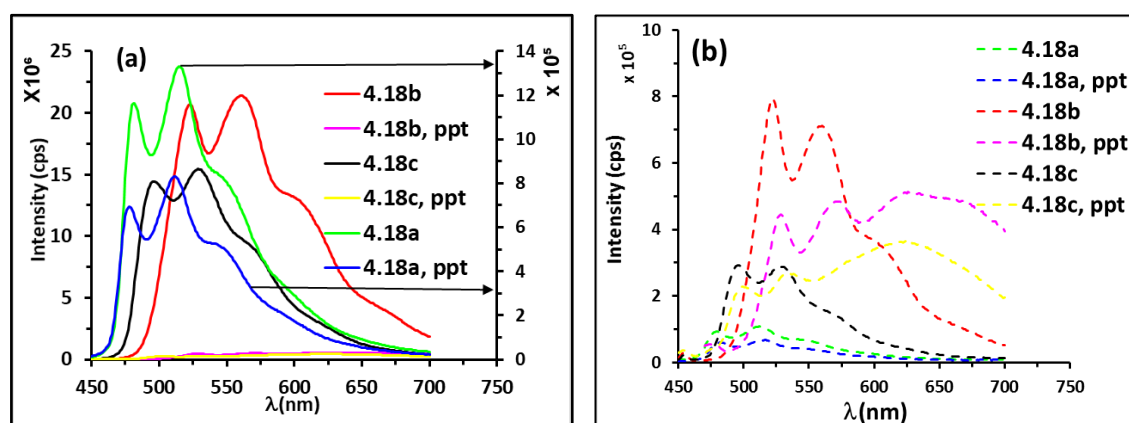


Figure 4.12: Emission spectra of $[\text{Pt}(\text{C}^{\wedge}\text{N})(\text{dpm})]$ (**4.18a-c**) in MeCN/ H_2O (ppt) and in solution at 0.02 mM MeCN (**a**) under Ar and (**b**) in air, (λ_{ex} 400 nm) at RT.

As reported in the literature, complex **4.19a** is not emissive in MeCN at RT.³⁰ Running the spectrum in a MeCN/ H_2O (1:9) mixture at ambient temperature also gave no emission.

Complex **4.19b** was found to show very weak emission in air; however, after degassing the emission intensity increased by a factor of *ca.* 15-fold, with a λ_{max} at 472 nm and a weak shoulder at 522 nm (**Fig 4.13**). This was consistent with phosphorescent emission.

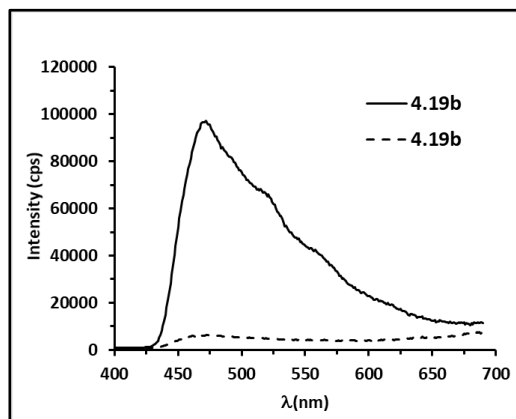


Figure 4.13: Emission spectra of $[\text{Pt}(\text{C}^{\wedge}\text{N})(\text{dpm})]$ **4.19b** in MeCN, under Ar (—) and in air (---) at 0.02 mM, λ_{ex} 350 nm at RT.

To test for EPSS, the spectra were run in a mixture of MeCN/H₂O (1:9), with the resultant spectra shown in **Fig 4.14**. Under argon complex **4.19b** shows an enhancement in the emission intensity by *ca.* 1.8-fold, with a more broad emission and a red-shift in the emission maximum to 524 nm with a shoulder at *ca.* 551 nm. In air the precipitate again shows an intensity enhancement by *ca.* 13.5 times) and red-shift in emission. The increased enhancement in air may be due to a combination of restricted rotation as well as less sensitivity to oxygen because of it being a precipitate. The red shift in the emission is a well-known phenomenon in Pt(II) complexes due to the interaction between the monomers in the excited and ground states that may lead to excimer formation with Pt which shows a red shift in the emission; this can be affected by the structure or the dispersion state.³²⁻³⁴

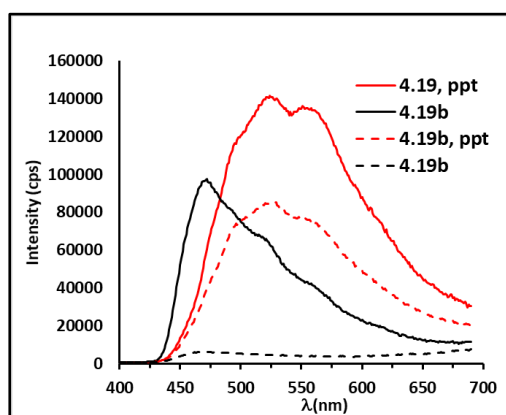


Figure 4.14: Emission spectra of $[\text{Pt}(\text{C}^{\wedge}\text{N})(\text{dpm})]$ (**4.19b**) in MeCN/H₂O (ppt) and in solution in at 0.02 mM MeCN in air (---) and under Ar (—), λ_{ex} 350 nm at RT.)

Table 4.4: Electronic emission data for complexes 4.18a-c and 4.19b			
Entry	Complex	% H₂O in MeCN under Ar	λ_{max} (nm)
1	4.18a	0	481, 515, 548 sh
		90	478, 511, 550 sh
2	4.18b	0	523, 561, 602 sh
3	4.18c	0	497, 529, sh 569
4	4.19b	0	472, 522 sh
		90	524, 551 sh

4.4 Conclusions and future work

In conclusion, the UV-vis absorption spectra of all the complexes show strong bands between 200 and 300 nm due to $\pi \rightarrow \pi^*$ transitions, and the complexes **4.16a-c**, **4.17b**, **4.18a-c** and **4.19a-b** show weak bands around 340-380 nm (possibly having contributions from ¹MLCT transitions). The phenylpyridine derivatives **4.16a-c** are emissive in MeCN but under argon the intensity increases by a rather modest *ca.* 1.6-2.2-fold upon aggregation in MeCN:Et₂O (1:9). In air the intensity increase is larger (1.4, 2.1 and 17.1 times) particularly for **4.16c**. Under argon complexes **4.18a-c** are highly emissive in MeCN solution while becoming weakly emissive in MeCN/H₂O. The spectra in air show evidence for different emissive processes from the precipitates for **4.18b, c**.

Complexes **4.16b** and **4.18b**, which have a Ph substituent at the *meta* position, show a red-shift in emission wavelength by *ca.* 45 to 50 nm relative to the unsubstituted complexes **4.16a** and **4.18a**, and by *ca.* 25-30 nm compared to the *para* complexes **4.16c** and **4.18c**. The phenylpyrazole complexes **4.17a-b** and **4.19a** were not emissive in either MeCN or the MeCN/Et₂O (1:9) mixture at ambient temperature. However, **4.19b** showed weak emission in MeCN, the intensity of which increased by *ca.* 1.8-fold upon aggregation in MeCN/H₂O (1:9) with a red shift in the emission maximum by *ca.* 52 nm. The study indicated that for all of the complexes, **4.16a-c**, **4.18a-c** and **4.19b** the emission is sensitive to the presence of oxygen as found for related Pt cyclometallated complexes consistent with considerable triplet character in the excited state. Overall only minor increases in intensity were found on precipitation and these were most noticeable in air. Hence these complexes are rather poor EPSS materials. Future work could include the synthesis of [Pt(CⁿN)(XⁿY)]ⁿ⁺ (n = 0, 1) (**Fig. 4.15**) with additional substituents that are free to rotate in solution so as to evaluate whether these complexes can be designed to

show EPES and hence whether they have any potential in application as viscosity sensors.

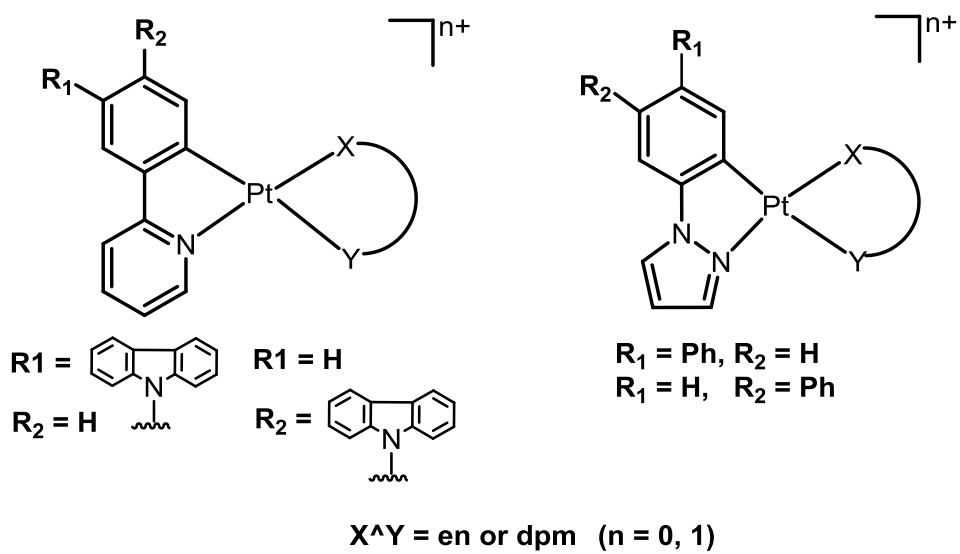


Figure 4.15: cyclometallated **Pt(II)** complexes can be designed to show EPES

Bibliography

1. J. B. Birks, *Photophysics of Aromatic Molecules*. Wiley, London, 1970.
2. J. Mei, Y. Hong, J. W. Y. Lam, A. Qin, Y. Tang and B. Z. Tang, *Adv. Mater.*, 2014, **26**, 5429-5479.
3. J. Luo, Z. Xie, J. W. Y. Lam, L. Cheng, H. Chen, C. Qiu, H. S. Kwok, X. Zhan, Y. Liu, D. Zhu and B. Z. Tang, *Chem. Commun.*, 2001, 1740-1741.
4. B. Z. Tang, X. Zhan, G. Yu, P. P. Sze Lee, Y. Liu and D. Zhu, *J. Mater. Chem.*, 2001, **11**, 2974-2978.
5. N. L. C. Leung, N. Xie, W. Yuan, Y. Liu, Q. Wu, Q. Peng, Q. Miao, J. W. Y. Lam and B. Z. Tang, *Chem. Eur. J.*, 2014, **20**, 15349-15353.
6. Y. Hong, J. W. Y. Lam and B. Z. Tang, *Chem. Commun.*, 2009, 4332-4353.
7. Y. Hong, J. W. Y. Lam and B. Z. Tang, *Chem. Soc. Rev.*, 2011, **40**, 5361-5388.
8. K. Huang, H. Wu, M. Shi, F. Li, T. Yi and C. Huang, *Chem. Commun.*, 2009, 1243-1245.
9. Y. You, H. S. Huh, K. S. Kim, S. W. Lee, D. Kim and S. Y. Park, *Chem. Commun.*, 2008, 3998-4000.
10. Q. Zhao, L. Li, F. Li, M. Yu, Z. Liu, T. Yi and C. Huang, *Chem. Commun.*, 2008, 685-687.
11. A. J. Howarth, R. Patia, D. L. Davies, F. Lelj, M. O. Wolf and K. Singh, *Eur. J. Inorg. Chem.*, 2014, **2014**, 3657-3664.
12. G. G. Shan, D. X. Zhu, H. B. Li, P. Li, Z. M. Su and Y. Liao, *Dalton Trans.*, 2011, **40**, 2947-2953.
13. S. Liu, H. Sun, Y. Ma, S. Ye, X. Liu, X. Zhou, X. Mou, L. Wang, Q. Zhao and W. Huang, *J. Mater. Chem.*, 2012, **22**, 22167-22173.
14. Y. Li, D. P. K. Tsang, C. K. M. Chan, K. M. C. Wong, M. Y. Chan and V. W. W. Yam, *Chem. Eur. J.*, 2014, **20**, 13710-13715.
15. Z. Chen, K. M. C. Wong, E. C. H. Kwok, N. Zhu, Y. Zu and V. W. W. Yam, *Inorg. Chem.*, 2011, **50**, 2125-2132.
16. J. Mei, N. L. C. Leung, R. T. K. Kwok, J. W. Y. Lam and B. Z. Tang, *Chem. Rev.*, 2015, **115**, 11718-11940.
17. M. A. Haidekker and E. A. Theodorakis, *Org. Biomol. Chem.*, 2007, **5**, 1669-1678.
18. M. K. Kuimova, *Phys. Chem. Chem. Phys.*, 2012, **14**, 12671-12686.

19. C. Sijie, H. Yuning, Z. Yan, S. Qiqi, L. Yang, Z. Engui, B. Gongxun, Q. Jianan, H. Jianhua and T. B. Zhong, *Chem. Eur. J.*, 2015, **21**, 4315-4320.
20. M. K. Kuimova, G. Yahiolglu, J. A. Levitt and K. Suhling, *J. Am. Chem. Soc.*, 2008, **130**, 6672-6673.
21. F. Chen, N. Liu, E. Ji and B. Dai, *RSC Advances*, 2015, **5**, 51512-51523.
22. S. K. Gurung, S. Thapa, B. Shrestha and R. Giri, *Org. Chem. Front*, 2015, **2**, 649-653.
23. J. Brooks, Y. Babayan, S. Lamansky, P. I. Djurovich, I. Tsyba, R. Bau and M. E. Thompson, *Inorg. Chem.*, 2002, **41**, 3055-3066.
24. A. Esmailbeig, H. Samouei, S. Abedanzadeh and Z. Amirghofran, *J. Organomet. Chem.*, 2011, **696**, 3135-3142.
25. T. Pawlak, D. Niedzielska, J. Vícha, R. Marek and L. Pazderski, *J. Organomet. Chem.*, 2014, **759**, 58-66.
26. W. Wu, H. Guo, W. Wu, S. Ji and J. Zhao, *Inorg. Chem.*, 2011, **50**, 11446-11460.
27. S. S. Pasha, P. Das, N. P. Rath, D. Bandyopadhyay, N. R. Jana and I. R. Laskar, *Inorg. Chem. Commun.*, 2016, **67**, 107-111.
28. E. A. Katlenok, E. V. Ivanova, M. V. Puzyk and K. P. Balashev, *Optics and Spectroscopy*, 2012, **113**, 279-283.
29. A. F. Henwood, J. Webster, D. Cordes, A. Z. Slawin, D. Jacquemin and E. Zysman-Colman, *RSC Advances*, 2017, **7**, 25566-25574.
30. B. K. T. Batagoda, P. I. Djurovich, S. Bräse and M. E. Thompson, *Polyhedron*, 2016, **116**, 182-188.
31. G. Y. Zheng and D. P. Rillema, *Inorg. Chem.*, 1998, **37**, 1392-1397.
32. B. D'Andrade and S. R. Forrest, *Chem. Phys.*, 2003, **286**, 321-335.
33. J. Kalinowski, M. Cocchi, L. Murphy, J. A. G. Williams and V. Fattori, *Chem. Phys.*, 2010, **378**, 47-57.
34. Y. J. Cho, S. Y. Kim, H. J. Son, D. W. Cho and S. O. Kang, *Phys. Chem. Chem. Phys.*, 2017, **19**, 5486-5494.

Chapter Five:

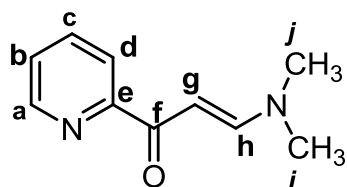
Experimental

5.1 General Experimental Procedures

All reactions were carried out under an inert atmosphere of nitrogen unless otherwise mentioned though all work-up was carried out in air. Liquid reagents were distilled under nitrogen; 1,2-diaminoethane, 1, 3-diaminopropane and triethylamine were distilled over CaO, BaO and KOH respectively and stored over molecular sieves 4Å. Microwave reactions were carried out in a CEM Explorer hybrid 12 microwave synthesiser, solutions were degassed by bubbling nitrogen through the solution for 3 minutes before sealing the tube with a plastic cap. NMR spectra were recorded on a Bruker DRX400 spectrometer operating at 400.13 (^1H), 376.50 (^{19}F), 100.61 MHz (^{13}C) and or a Bruker DRX500 spectrometer at 500 (^1H) and 125 MHz (^{13}C) respectively at ambient temperature; chemical shifts (ppm) are referred to the residual protic solvent peaks and coupling constants are expressed in Hertz (Hz). Assignments of ^1H and ^{13}C NMR signals were made where possible, using COSY, NOESY, TOCSY, HMQC, HMBC, DEPT and APT experiments. Electrospray (ES) mass spectra and ASAP were obtained using a micromass Quattro LC spectrometer in HPLC grade MeCN. The FAB samples were run on a Kratos Analytical Concept H series Mass Spectrometer, using Xenon gas at an ionising voltage of 8kV, and the data was processed using Mach 3 software. The UV/Vis spectra measurements were carried out on a Shimadzu UV-1600 series spectrometer in 1 cm quartz cuvette at room temperature. Luminescence studies were performed on a Jobin Yvon Horiba Fluoromax-P spectrofluorimeter, in either reagent grade DCM, or MeOH, HPLC grade MeCN or spectroscopy grade DMF (N,N-Dimethylformamide). Complexes were excited at a wavelength between 320-405 nm using a filter of 370, 399 and 450 nm. The pH values were determined using a Jenway 3510 pH meter, calibrated prior to use with standard buffer solutions of pH 4, 6 and 10 at room temperature. The pKa values for all complexes were determined by the change of emission intensity upon the pH changing from about ca. 2.5 to 12.5. Data analysis was performed using Microsoft Excel and Origin program 2015. Effect of solvent polarity on absorption and emission were measured in reagent grade DCM, HPLC grade MeOH and spectroscopy grade DMF at 0.02 mM.

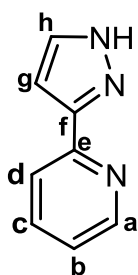
5.2 Data for compounds in Chapter Two

Synthesis of **2.8**



Compound **2.8** was prepared by a literature method,¹ 2-acetylpyridine (5 ml, 42.01 mmol) and N, N-dimethyl formamide dimethyl acetal (2.5 ml, 20.7 mmol) were heated at 110 °C for 90 mins in an oil bath. The sample was left overnight in the refrigerator, producing an orange powder which was filtered and washed with petroleum ether. Compound **2.8** was isolated as an orange solid (3.04 g, 83.7%). ¹H NMR (400 MHz, CDCl₃, 300 K): δ 8.63 (1H, ddd, *J* = 4.7, 1.7, 0.8 Hz, H_a), 8.15 (1H, dt, *J* = 7.8, 0.9 Hz, H_d), 7.91 (1H, d, *J* = 12.7 Hz, H_g), 7.80 (1H, td, *J* = 7.8, 1.7 Hz, H_b), 7.36 (1H, ddd, *J* = 7.5, 4.7, 1.3 Hz, H_c), 6.45 (1H, d, *J* = 12.5 Hz, H_h), 3.17 (3H, s, H_{i/j}), 3.00 (3H, s, H_{i/j}). ¹³C NMR (100 MHz, CDCl₃, 300 K): δ 187.0 (C_f), 156.3 (C_e), 154.8 (C_g), 148.3(C_a), 136.7(C_b), 125.4 (C_c), 122.0 (C_d), 91.2 (C_h), 45.2 (C_{i/j}), 37.5 (C_{i/j}). HRMS(ASAP): *m/z*: 176.0949 [176.0950 calculated for C₁₀H₁₂N₂O]. MP: 131-133.6 °C.

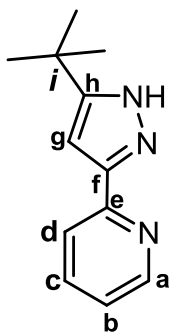
Synthesis of **HL1**



Compound **2.8** (1.000 g, 5.68 mmol), hydrazine monohydrochloride (2.720 g, 39.70 mmol), K₂CO₃ and EtOH (15 ml) were placed into a 100 ml RBF containing a stirrer bar. The mixture was heated at 60° C for one hour. After cooling the solvent was removed in vacuum leaving behind a solid which was dissolved in DCM (15 ml) and passed through celite. The filtrate was extracted with water (3×20 ml), the organic layer was collected and the solvent was removed on the rotary evaporator. The filtrate was reduced in volume and hexane was added slowly to induce precipitation. The product, **HL1**, was isolated as a white solid. (773 mg, 93%), ¹H NMR (500 MHz, CDCl₃, 298 K): δ 12.19 (1H, br. s, NH), 8.69 (1H, d, *J* = 5.3 Hz, H_a), 7.76(1H, d, *J* = 1.1 Hz, H_d), 7.75-7.73(1H, m, H_c), 7.67 (1H, d, *J* = 2.1 Hz, H_h), 7.18 (1H, t, *J* = 4.0 Hz, H_b), 6.81 (1H, d, *J* = 1.9 Hz, H_g). ¹³C NMR (100 MHz, CDCl₃, 298 K): 149.5(C_a), 137.1(C_{e/f}), 136.4(C_h), 122.8 (C_b), 120.3 (C_{e/f}), 120.3 (2C_{c, d}), 103.5(C_g). HRMS (ESI): [M+H]⁺ *m/z* 146.718 [146.071 calculated for C₈H₈N₃]. MP: 127-129 °C. The characterization matches that previously reported.²

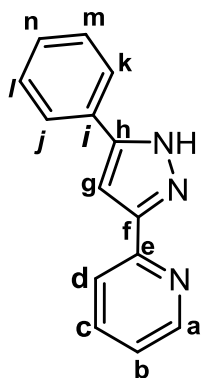
Synthesis of **HL2**

Ligand **HL2** was synthesized according to the reported method.³ To a suspension of NaH (0.895 mg g, 37.3 mmol) in dry THF (18 ml) at 0°C, pinacolone (2.24 g, 22.4 mmol) and ethyl-2-picolinate (2.2 ml, 15.68 mmol) were added slowly. The mixture was stirred for



30 minutes without heating and then heated to 70°C for 20 minutes. After cooling to room temperature dilute HCl was added until a pH of 8~9 was achieved. The aqueous solution was then extracted with diethyl ether (3 × 10 ml). The combined organic phase was washed with brine and dried over MgSO₄. The solvent was removed via rotary evaporation to produce crude 1, 3-dione. This was dissolved in ethanol (20 ml) and treated with an excess of hydrazine monohydrochloride (0.060 mol) and potassium carbonate (0.064 mol). The mixture was then left to reflux for 2 hrs. The solvent was removed via rotary evaporation and the residue dissolved in CH₂Cl₂ (20 ml), and this was washed with water to remove any unreacted hydrazine and dried over MgSO₄. The solution was then filtered and dried via rotary evaporation to leave a solid which was dried under high vacuum to give the HL₂ as brown solid (930 mg, 79%). ¹H NMR (500 MHz, CDCl₃, 298 K): δ 8.61(1H, br. d, *J* = 4.6 Hz, H_a), 7.80(1H, br d, *J* = 7.8 Hz, H_d), 7.71(1H, td, *J* = 7.7, 1.7 Hz, H_c), 7.20(1H, ddd, *J* = 7.4, 4.9, 1.1 Hz, H_b), 6.67(1H, s, H_g), 1.39(9H, s, H^t_{Bu}). ¹³C NMR (126 MHz, CDCl₃, 298 K): δ 159.1 (C_{f/h}), 150.0(C_e) 149.3(C_a), 145.0(C_{f/h}), 136.7(C_c), 122.5 (C_b), 119.9 (C_d), 99.8(C_g), 31.6(C_i), 30.4 (C^t_{Bu}). HRMS (ASAP): [M+H]⁺ at *m/z*: 202.1340 [201.1344 calculated for C₁₂H₁₆N₃]. MP: 104-107 °C.

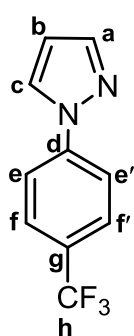
Synthesis of HL₃



Acetophenone (2.8 ml, 23.3 mmol) was added dropwise to a stirred suspension of sodium ethoxide (44.2 g, 1.841 mmol) in dry THF solution approximately (80 ml) at RT using schlenk round bottom flask under an inert nitrogen atmosphere, and the mixture left to mix for 30 minutes. After that, ethyl-2-picolinate (2.4 ml, 17.9 mmol) was added slowly, and the mixture reaction was reflux for 4.5 hrs. Next, the reaction was neutralized with conc. acetic acid 1M, water and then extracted with diethyl ether (3 × 15 ml). The organic phases were then dried over MgSO₄, filtered and the solvent was evaporated, leaving behind a white flaky solid (1.78 g, 47.3%). The resulting solid material (crude dione) was then (0.891 g, 3.96 mmol) was then dissolved in ethanol (20 ml) and treated with an excess of hydrazine monohydrochloride (0.310 g, 4.526 mmol) and K₂CO₃ (1.314 g, 9.504 mmol), and brought to reflux for 12 hours. The ethanol solvent was removed in rotary evaporator, the residue dissolved in DCM (40 ml), and the organic phase was washed with water to remove unreacted and then the organic phase was dried with MgSO₄ and filtered. The

solvent was then removed via rotary evaporation and and left to dry on the high vacuum to afford the the desired product as a white solid (0.64 g, 73%). ^1H NMR (500 MHz, CD_3CN , 298.0 K): δ 11.82(1H, br. s, H_{NH}), 8.65(1H, dt, $J = 1.3, 4.8$ Hz, H_a), 7.90-7.88(2H, m, $\text{H}_{j, k}$), 7.88-7.85(2H, m, H_c , d), 7.49(2H, br. t, $J = 7.2$ Hz, H_l , m), 7.39(1H, t, $J = 7.4$ Hz, H_n), 7.34(1H, dd, $J = 8.62, 4.8$ Hz, H_b), 7.24(1H, s, H_g). ^{13}C NMR (101 MHz, CD_3CN , 298.0 K): δ 153.1(C_{quat}), 149.2(C_a), 144.0(C_{quat}), 136.78(C_{quat}), 134.9(C_{ph}), 130.0(C_{quat}), 128.52(C_{ph}), 127.69 (C_{ph}), 126.2(C_{ph}), 125.1(C_{ph}), 122.7(C_b), 119.5(C_{py}), 117.0(C_{py}), 100.2(C_g). HRMS (ASAP): $[\text{M}+\text{H}]^+$ at m/z : 222.1031[221.1031 calculated for $\text{C}_{14}\text{H}_{12}\text{N}_3$]. MP: 184-186 °C. Data consistent with literature.³

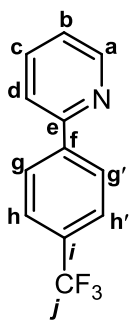
Synthesis of HL4



The compound was synthesized using a procedure similar to that employed in literature.⁴ A mixture of 1-bromo-4(trifluoromethyl)benzene (1125 mg, 4.99 mmol), carbazoles (510.4 mg, 7.56 mmol), Cu_2O (71.50 mg, 0.49 mmol), and Cs_2CO_3 (1627 mg, 4.98 mmol) were added to schlenk tube that was evacuated, back-filled with nitrogen, followed by dry acetonitrile(10 ml). The mixture was allowed to stir under nitrogen atmosphere at 110° C for 72 hrs. After cooling to room temperature, the solvent was removed *in vacuo* leaving behind a solid which was dissolved in DCM (30 ml) and filtered through a plug of celite. The filtrate was added to brine (10 ml) and extracted three times with dichloromethane (3×10 ml), and dried over MgSO_4 . The solvent was evaporated and the crude brown oil was purified by flash chromatography on silica gel (eluent: ethyl acetate/petroleum ether 10:90), respectively to provide (880 mg, 83 % yield) of the desired product as white solid. ^1H NMR (500 MHz, CDCl_3 , 298 K): δ 7.92(1H, d, $J = 1.8$ Hz, H_a), 7.76(2H, d, $J = 8.3$ Hz, H_e, e'), 7.69(1H, s, H_b), 7.64(2H, d, $J = 8.3$ Hz, H_f, f'), 6.44(H, br. s, H_c). ^{13}C NMR (126 MHz, CDCl_3 , 298 K): δ 142.8(C_{CH}), 142.5(C_{quat}), 142.0(C_{CH}), 128.5 (q, $J_{\text{CF}_3} = 33.0$ Hz), 126.9(C_{CH}), 126.8(C_{CH}), 126.7(C_{quat}), 122.9(C_{CH}), 118.8(C_{CH}), 108.5(C_{CH}). ^{19}F NMR (376 MHz, CDCl_3 , 298 K): δ -62.28 (F, s). HRMS (ASAP): $[\text{M}+\text{H}]^+$, m/z : 213.0638 [212.0640 calculated for $\text{C}_{10}\text{H}_8\text{F}_3\text{N}_2$]. MP: 72-75 °C.

Synthesis of HL5

Ligand **HL5** was conveniently synthesized according to the reported method.⁵ A mixture of 2 pyridyl bromide, (350 mg, 2.21 mmol), 4 (Trifluoromethyl) phenylboronic acid (631 mg, 3.32 mmol), $\text{Pd}(\text{OAc})_2$ (99 mg, 0.44 mmol 20%), K_2CO_3 (613 mg, 4.43 mmol) and the mixture was stirred in ethanol/water (3:1 v/v) at 80 °C in air for 3hrs. After cooling to room temperature, the solvent was removed *in vacuo* leaving behind a solid which was

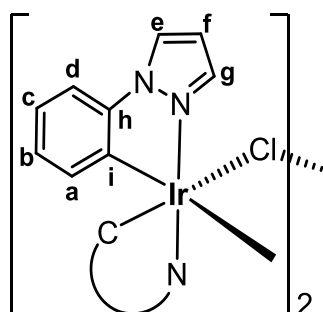


dissolved in DCM (30 ml) and filtered through a plug of celite. The filtrate was added to brine (10 ml) and extracted three times with dichloromethane (3×10 ml), and dried over MgSO₄. The solvent was evaporated and the crude was purified by flash chromatography on silica gel, eluting with 100% petroleum ether and increasing the polarity to 20% ethyl acetate in petroleum ether, to provide (361 mg, 73 %) of the desired product as white solid. ¹H NMR (400 MHz, CDCl₃, 298 K): δ 8.72(1H, d, *J* = 4.57 Hz, H_a), 8.10(2H, d, *J* = 8.19 Hz, H_{h, h'}), 7.74-7.80(2H, m, H_{g, g'}), 7.72(2H, d, *J* = 8.33 Hz, H_{b, c}), 7.26-7.30(1H, m, H_d). ¹³C NMR (126 MHz, CDCl₃, 298 K): δ 155.86(C_{quat.}), 149.9(C_{CH}), 142.7(C_{quat.}), 137.0(C_{CH}), 130.8(q, *J*_{C-CF₃} = 32.4 Hz), 127.2(C_{CH}), 125.7(C_{CH}), 125.6(C_{CH}), 124.2(q, *J*_{C-F} = 273.3 Hz), 123.0(C_{CH}), 120.8(C_{CH}). One CH, one C-F, and one quaternary carbons peaks were not observed. This could be overlapping with others peaks. ¹⁹F NMR (376 MHz, CDCl₃, 298 K): δ -62.55(F, s). HRMS (ASAP): [M+H]⁺, *m/z*: 224.0687[223.0609 calculated for C₁₂H₉F₃N]. MP: 74-77 °C.

General Procedure for the Synthesis of Cyclometallated Ir(III) Dichloro-Bridged Dimers [Ir₂(C^N)₄(μ-Cl)₂]

IrCl₃(H₂O)₃ and the suitable cyclometallating ligands (2.2 equiv.) were placed in a microwave vial along with a mixture of PrOH/H₂O (3:1) (4 ml). The vial was heated under microwave irradiation at 110°C for 90 minutes, at a maximum pressure of 247 psi. After this period, the solvent was removed by rotary evaporation to give a solid which was dissolved in DCM (30-40 ml) and passed through Celite. The filtrate was reduced in volume and hexane was added slowly to induce precipitation. The precipitate was isolated, washed with hexane and dried under high vacuum⁶

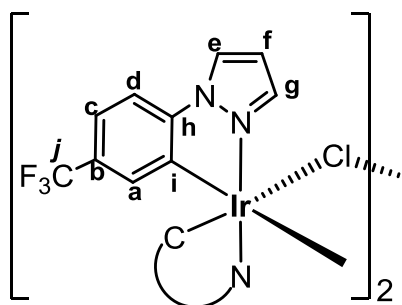
Synthesis of [Ir₂(ppz)₂(μ-Cl)₂] (2.15a)



2.15a was prepared from IrCl₃(H₂O)₃ (500 mg, 1.41 mmol), and 1-phenylpyrazole (449 mg, 3.12 mmol) using the general procedure. After work up, a grey solid was obtained (650 mg, 89%). ¹H NMR (400 MHz, CD₂Cl₂, 298 K): δ 8.19 (4H, dd, *J* = 3.2, 0.8, H_e), 7.82 (4H, dd, *J* = 2.4, 0.8, H_g), 7.19 (4H, dd, *J* = 7.9, 1.1, H_d), 6.84 (4H, td, *J* = 7.4, 1.6, H_c), 6.69 (4H, t, *J* = 5.1, H_f), 6.57 (4H, td, *J* = 7.5, 1.3, H_b), 5.95 (4H, dd, *J* = 7.7, 1.2, H_a). ¹³C NMR (100 MHz, CD₂Cl₂, 298 K): δ 141.7 (C_i), 139.0 (C_g), 130.9 (C_a), 125.9 (C_h), 124.94 (C_e), 123.7 (C_b), 120.4 (C_c), 109.1

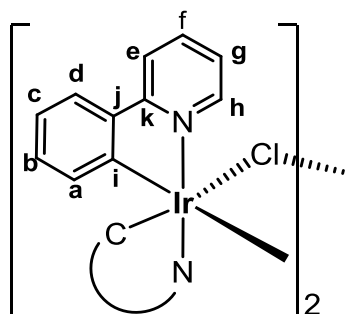
(C_d), 105.2 (C_f). HRMS (FAB) *m/z*: 1028 [M]⁺, 991 [M-Cl]⁺. MS (ES): (*m/z*): 561 [Ir(ppz)₂(MeCN)₂]⁺. The data was in agreed with the literature.⁶

Synthesis of [Ir₂(ppz-CF₃)₂(μ-Cl)]₂ (2.15b)



Dimer **2.15b** was prepared from IrCl₃(H₂O)₃ (300 mg, 0.85 mmol), and 1-(4(trifluoromethyl)phenyl)-1H-pyrazole (397.1 mg, 1.87 mmol) using the general procedure. After work up, a grey solid was obtained (506 mg, 91%). ¹H NMR (400 MHz, CDCl₃, 298 K): δ 8.22(4H, d, *J* = 2.8 Hz, H_e), 7.88(1H, d, *J* = 2.1 Hz, H_g), 7.21(4H, d, *J* = 8.3 Hz, H_d), 7.10(4H, dd, *J* = 0.9, 8.2 Hz, H_c), 6.77(4H, t, *J* = 2.6 Hz, H_f), 6.20(4H, d, *J* = 1.2 Hz, H_a). ¹³C NMR (126 MHz, CDCl₃, 298 K): δ 145.4(C_{quat.}), 142.0(C_{CH}), 141.3(C_{CH}), 128.8(C_{CH}), 127.3(C_{CH}), 127.0(C_{quat.}), 126.9(C_{quat.}), 123.7(q, *J*_{C-F} = 273.4 Hz), 120.0(C_{CH}), 119.9(C_{CH}), 110.6(C_{CH}), 107.6(C_{CH}). Two C-F carbons peaks were not observed. This could be overlapping with others peaks. ¹⁹F NMR (376 MHz, CDCl₃, 298° K): δ -62.27 (F, s). HRMS (FAB): *m/z* 1301 [M]⁺, 1323 [MNa]⁺. MS (ES): *m/z* 697 [Ir(CF₃-ppz)₂(MeCN)₂]

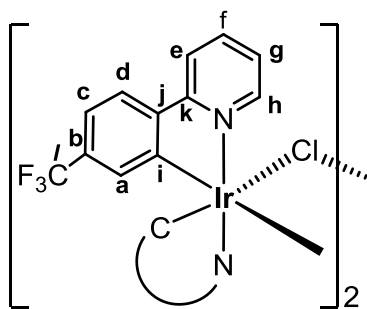
Synthesis of [Ir₂(ppy)₂(μ-Cl)]₂ (2.15c)



Dimer **2.15c** was prepared from IrCl₃(H₂O)₃ (400 mg, 1.13 mmol) and 2-phenylpyridine (386 mg, 2.49 mmol). After passing through celite, the solution was washed with dilute 2M HCl (3×30 ml) and dried over MgSO₄. and the residue was recrystallised from DCM/hexane to give **2.15c** as a yellow solid (442 mg, 77%). ¹H NMR (400 MHz, CD₂Cl₂, 298 K): δ 9.25 (4H, bd, *J* = 5.5, H_h), 7.92 (4H, bd, *J* = 7.8, H_e), 7.77 (4H, td, *J* = 7.8, 1.6, H_f), 7.55 (4H, bd, *J* = 7.4, H_d), 6.82 – 6.79 (8H, m, H_{c,g}), 6.59 (4H, td, *J* = 7.8, 1.2, H_b), 5.87 (4H, bd, *J* = 7.4, H_a). ¹³C NMR: (100 MHz, CD₂Cl₂, 298 K): δ 168.5 (C_k), 151.9 (C_h), 145.3 (C_j), 144.4 (C_i), 137.1 (C_f), 130.8 (C_a), 129.50 (C_b), 124.1 (C_d), 123.0 (C_c), 121.8 (C_g), 119.1 (C_e). HRMS (FAB), *m/z*: 1072 [M]⁺, 1035 [M-Cl]⁺. The data was in agreed with the literature.⁶

Synthesis of [Ir₂(ppy-CF₃)₂(μ-Cl)]₂ (2.15d)

2.15d was prepared from IrCl₃(H₂O)₃ (252 mg, 0.713 mmol), and 2-(4 (Trifluoromethyl) phenyl)-pyridine (351 mg, 1.569 mmol) using the general procedure. After work up, yellow solid was obtained (372 mg, 78%). ¹H NMR (500 MHz, CDCl₃, 298 K): δ 9.22(4H, d, *J* = 5.4 Hz, H_h), 7.99(4H, d, *J* = 7.9 Hz, H_e), 7.88(4H, t, *J* = 7.9 Hz, H_f),



7.60(4H, d, $J = 7.9$ Hz, H_d), 7.04(4H, d, $J = 8.0$ Hz, H_c), 6.93(4H, t, $J = 6.3$ Hz, H_g), 6.09(4H, s, H_a). ^{13}C NMR (126 MHz, CDCl_3 , 298 K): δ 167.1(C_{quat}), 151.6(C_h), 147.2(C_{quat}), 144.0(C_{quat}), 137.3(C_f), 130.1(q, $J_{\text{C-CF}_3} = 30.12$ Hz), 126.4(C_a), 124.7(C_i), 123.6(q, $J_{\text{C-F}} = 272.6$ Hz), 123.7(C_d), 123.5(C_g), 119.7(C_e), 118.9(C_c). one quaternary carbons peaks were not observed. This could

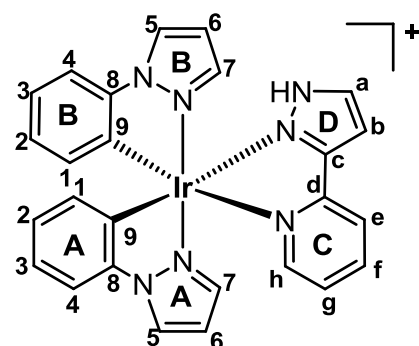
be overlapping with others peaks. ^{19}F NMR (376 MHz, CDCl_3 , 298° K): δ -63.20(F, s). HRMS (ASAP): m/z 637 $[\text{M-Cl}]^+$, MS (ES): m/z 719 $[\text{Ir}(\text{CF}_3\text{-ppy})_2(\text{MeCN})_2]$. Data consistent with literature.⁷

General procedure for the synthesis of $[\text{Ir}(\text{C}^{\wedge}\text{N})_2(\text{N}^{\wedge}\text{N})]\text{PF}_6$

The dimer **2.5a-c**, ligand (**HL**₁/**HL**₂/**HL**₃) (2.2-2.4 equiv) and KPF_6 (2.4 equiv) were placed in a microwave vial and methanol (3 ml) was added. After degassing with nitrogen the tube was heated under microwave irradiation at 60°C for 20-40 mins at a maximum pressure of 250 psi. After this time, the solvent was removed in vacuo leaving behind a solid which was dissolved in DCM (15 ml) and passed through celite. The filtrate was reduced in volume and hexane was added slowly to induce precipitation. The precipitate was isolated, washed with hexane and dried in vacuo.

Synthesis of **2.16aHL**₁

Using the general procedure, **2.16aHL**₁ was prepared from **2.15a** (50 mg, 0.049 mmol), **HL**₁ (16 mg, 0.10 mmol) and KPF_6 (22 mg, 0.12 mmol). After work up, the compound was isolated as a grey yellow solid (58 mg, 78%), See appendix **Table 1** for X-Ray crystal data. ^1H NMR (500 MHz, CD_3CN , 300K): δ 8.40 (1H, d, $J = 2.9$ Hz, H_{5B}), 8.36 (1H, d, $J = 2.9$ Hz, H_{5A}), 8.20 (1H, dt, $J = 7.9, 0.9$ Hz, H_e), 8.10 (1H, td, $J = 7.9, 1.7$ Hz, H_f), 8.01

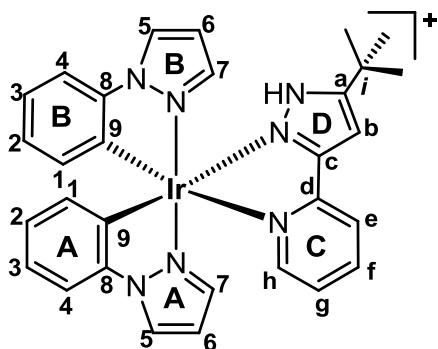


(1H, ddd, $J = 5.5, 1.7, 0.8$ Hz, H_h), 7.83 (1H, d, $J = 2.9$ Hz, H_a), 7.50 (1H, dd, $J = 4.7, 1.0$ Hz, H_{4B}), 7.47 (1H, dd, $J = 4.7, 1.0$ Hz, H_{4A}), 7.37 (1H, ddd, $J = 7.7, 5.5, 1.3$ Hz, H_g), 7.20 (1H, d, $J = 2.9$ Hz, H_b), 7.11-7.03 (3H, m, $H_{3A, 3B, 7B}$), 7.01 (1H, d, $J = 2.2$ Hz, H_{7A}), 6.90(1H, td, $J = 7.5, 1.2$ Hz, H_{2B}), 6.85 (1H, td, $J = 7.5, 1.2$ Hz, H_{2A}), 6.62 (1H, t overlapping, $J = 2.7$ Hz, H_{6B}),

6.61(1H, t overlapping, $J = 2.7$ Hz, H_{6A}), 6.32 (1H, dd, $J = 5.0, 1.3$ Hz, H_{1B}), 6.30 (1H, dd, $J = 5.1, 1.3$ Hz, H_{1A}). ^{13}C NMR (125 MHz, CD_3CN , 300 K): δ 154.0 (C_c), 153.3 (C_d), 151.8 (C_h), 144.8 ($\text{C}_{9A/9B}$), 144.6 ($\text{C}_{9A/9B}$), 140.6 (C_f), 140.1 (C_{7A}), 139.7 ($\text{C}_{3A/3B, 7B}$), 135.0

(C_a), 134.4 (C_{1A/1B}), 134.1(C_{1A/1B}), 132.4 (C_{8A/8B}), 128.8 (C_{5B}), 128.7 (C_{5A}), 128.6 (C_{8A/8B}), 127.5 (C_{2A/2B}), 127.1 (C_{2A/2B}), 127.0 (C_g), 124.3 (C_{3A/3B,7B}), 124.2 (C_{3A/3B, 7B}), 123.9 (C_e), 113.0 (C_{4B}), 112.7 (C_{4A}), 109.3 (C_{6A/6B}), 109.1 (C_{6A/6B}), 106.3 (C_b). HRMS (ASAP): *m/z* 624.1497 [624.1488 calculated for C₂₆H₂₁¹⁹³IrN₇].

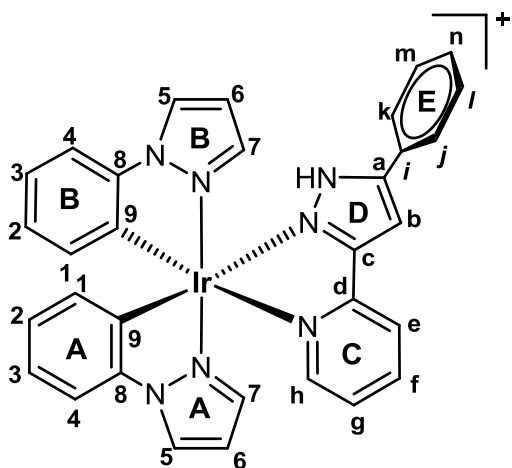
Synthesis of 2.16aHL₂



Complex **2.16aHL₂** was prepared from **2.15a** (71 mg, 0.07 mmol) and **HL₂** (31 mg, 0.154 mmol) and KPF₆ (31 mg, 0.168 mmol). After work up, the compound was isolated as a yellow solid (107 mg, 93%). See appendix **Table 1** for X-Ray crystal data. ¹H NMR (500 MHz, CD₂Cl₂, 300 K): δ 8.11 (1H, d, *J* = 2.5 Hz, H_{5B}), 8.17 (1H, d, *J* = 2.5 Hz, H_{5A}), 7.97-7.95(1H, m, H_e), 7.94-7.93(1H, m, H_f), 7.92(1H, br. d, *J* = 2.0 Hz, H_h), 7.29 (1H,dd, *J* = 8.0, 0.9 Hz, H_{4B}), 7.23(1H, dd, *J* = 5.5, 1.4 Hz, H_{4A}), 7.21-7.20 (1H, m, H_g), 7.12 (2H, tdd, *J* = 7.6, 6, 1.3 Hz, H_{3A,3B}), 6.84(1H, br. d, *J* = 1.8 Hz, H_{7B}), 6.80 (1H, br. t, *J* = 1.4 Hz, H_{2B}), 6.79 (1H, br. t, *J* = 1.3 Hz, H_{2A}), 6.78(1H, s, H_b), 6.76 (1H, br. d, *J* = 1.8 Hz, H_{7A}), 6.52 (1H, t, *J* = 2.6 Hz, H_{6B}), 6.49(1H, t, *J* = 2.6 Hz, H_{6A}), 6.28 (1H, dd, *J* = 7.6, 1.2 Hz, H_{1B}), 6.19 (1H, dd, *J* = 7.6, 1.0 Hz, H_{1A}), 1.26 (9H, s, H^t_{Bu}). ¹³C NMR (125 MHz, CD₂Cl₂, 300 K): δ 159.2 (C_a), 153.4 (C_{quat.}), 152.9(C_{quat.}), 151.0(C_h), 144.0(C_{quat.}), 143.8 (C_{quat.}), 139.9(C_f), 139.1(C_{7A}), 138.7(C_{7B}), 127.2(C_{5B}), 126.7(C_{5A}), 134.3 (C_{1B}), 133.5 (C_{1A}), 130.8(C_{9A/9B}), 128.6 (C_{9A/9B}), 127.5 (C_{2A/2B}), 127.4 (C_{2A/2B}), 126.2 (C_g), 123.9 (C_{3A/3B}), 123.8 (C_{3A/3B}), 123.0 (C_e), 112.2 (C_{4A}), 112.1(C_{4B}), 108.7 (C_{6A}), 108.5 (C_{6B}), 102.2(C_b), 32.1 (C_i), 30.0 (C^t_{Bu}). HRMS (ASAP):

m/z 680.2145 [680.2114 calculated for C₃₀H₂₉¹⁹³IrN₇]

Synthesis of 2.16aHL₃



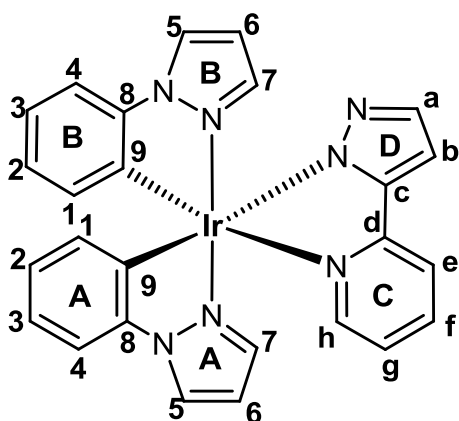
Complex **2.6aHL₃** was prepared from **2.15a** (50 mg, 0.046 mmol) and **HL₃** (23 mg, 0.11 mmol) and KPF₆ (21 mg, 0.12 mmol). After work up, the crude material was purified by column chromatography on silica gel DCM/ ethyl acetate (2:1) to give a grey yellowish solid (68 mg, 82%). See appendix **Table 1** for X-Ray crystal data ¹H NMR (500 MHz, CD₃CN, 298 K): δ 8.41 (1H, d, *J* = 2.7 Hz,

H_{5B}), 8.36 (1H, d, $J = 2.7$ Hz, H_{5A}), 8.22 (1H, br.d, $J = 7.8$ Hz, H_e), 8.10 (1H, td, $J = 7.8$, 1.1 Hz, H_f), 7.99 (1H, br. d, $J = 5.3$ Hz, H_h), 7.74 (2H, br. d, $J = 6.9$ Hz, H_{j, k}), 7.55-7.50 (4H, m, H_{b, l, m, n}), 7.49-7.46(2H, m, H H_{4A, 4B}), 7.38 (1H, br. t, $J = 6.2$ Hz, H_g), 7.21 (1H, d, $J = 2.1$ Hz, H_{7A}), 7.10-7.04 (3H, m, H_{3A, 3B, 7B}), 6.87 (2H, br. dt $J = 14.6$, 7.3 Hz, H_{2A, 2B}), 6.63 (1H, t, $J = 2.5$ Hz, H_{6A}), 6.61 (1H, t, $J = 2.5$ Hz, H_{6B}), 6.32 (1H, d, $J = 7.3$ Hz, H_{1B}), 6.28 (1H, d, $J = 7.3$ Hz, H_{1A}). ¹³C NMR: (125 MHz, CD₃CN, 298 K): δ 155.0(C_{quat.}), 153.2 (C_{quat.}), 151.6 (C_h), 149.0(C_{quat.}), 145.0(C_{quat.}), 144.6(C_{quat.}), 140.7 (C_f), 140.3(C_{7A}), 139.7 (C_{3A/3B/7B}), 135.3 (C_{1A/1B}), 134.0 (C_{1A/1B}), 132.2 (C_{quat.}), 131.0 (C_{4A/4B// m/n}), 130.2 (2C_{4A/4B, // m/n}), 129.0(C_{quat.}), 128.8(C_{5A}), 128.7(C_{5B}), 128.4(C_{quat.}), 127.7(2C_{j, k}), 127.5 (C_{2A/2B}), 127.2(C_{2A/2B}), 127.0 (C_g), 124.4 (C_{3A/3B/7B}), 124.1(C_{3A/3B/7B}), 124.0(C_e), 113.0(C_{4A/4B//m/n}), 112.6 (C_{4A/4B/ // m/n}), 109.3(C_{6B}), 109.1(C_{6A}), 104.0(C_b). HRMS (ASAP): m/z 700.1821 [700.1801 calculated for C₃₂H₂₅¹⁹³IrN₇].

General procedure for the synthesis of [Ir(C^AN)₂(N^AN)]

A mixture of the ligand (**HL**₁/ **HL**₂/**HL**₃) (2.2-2.4 equiv) and an equimolar amount of NaOMe in MeOH (3 ml) was warmed gently at 40 °C for 15 mins. A solution of the appropriate dimer **2.15a-d** (1 equiv) in DCM (6 ml) was added and the mixture was stirred for 2-4 hrs at room temperature. After this time, the solvent was removed in vacuo and the residue was dissolved in DCM (15 ml) and passed through celite. The filtrate was reduced in volume and hexane was added slowly to induce precipitation. The precipitate was isolated, washed with hexane and dried in vacuo.

Synthesis of **2.17aL**₁

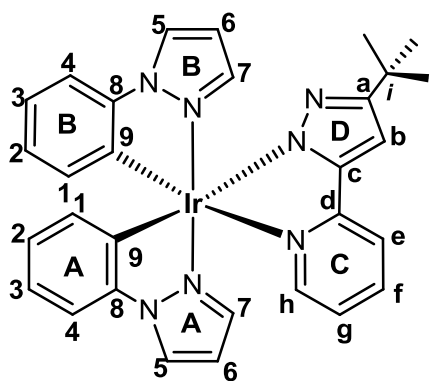


Complex **2.17aL**₁ was prepared from the **2.15a** (50 mg, 0.08 mmol), **HL**₁ (16 mg, 0.11 mmol) and NaOMe (5mg, 0.11 mmol). After work up, the crude product was purified by column chromatography (aluminium oxide); the product was eluted with CH₂Cl₂/MeOH (30:1), respectively. **2.17aL**₁ was isolated as a grey yellow solid (45 mg, 75.6%). ¹H NMR: (500

MHz, CD₃CN, 298K): δ 8.29 (1H, d, $J = 2.7$ Hz, H_{5B}), 8.26 (1H, d, $J = 2.7$ Hz, H_{5A}), 7.90-7.86 (2H, m Hz, H_{h, e}), 7.83 (1H, td, $J = 7.7$, 1.5 Hz, H_f), 7.47 (1H, d, $J = 2.1$ Hz, H_a), 7.39 (1H, d, $J = 7.6$ Hz, H_{4A}), 7.35 (1H, d, $J = 7.8$ Hz, H_{4B}), 7.06 (1H, ddd, $J = 7.6$, 5.6, 1.2 Hz, H_g), 7.07-7.01 (1H, m, H_{7B}), 6.98-6.96 (1H, m, H_{3A}), 6.91(1H, td, $J = 7.7$, 1.1 Hz, H_{3B}), 6.82 (1H, d, $J = 2.1$ Hz, H_b), 6.81 (1H, m, H_{2A}), 6.72-6.69(2H, m, H_{2B, 7A}),

6.53 (1H, t, $J = 2.5$ Hz, H_{6B}), 6.50 (1H, t, $J = 2.5$ Hz, H_{6A}), 6.34 (1H, dd, $J = 7.3, 1.0$ Hz, H_{1A}), 6.22 (1H, dd, $J = 7.4, 1.0$ Hz, H_{1B}). ¹³C NMR (125 MHz, MeOD, 298 K): δ 154.2 (C_c), 154 (C_d), 151.7 (C_h), 145.1 (C_{8A/8B}), 145.0 (C_{8A/8B}), 140.8 (C_f), 139.9 (C_{3A/3B/7A/7B}), 139.4 (C_{3A/3B/7A/7B}), 135.1 (C_{1B}), 134.7 (C_a), 134.2 (C_{1A}), 132.6 (C_{9A/9B}), 129.1 (C_{9A/9B}), 128.8 (C_{5A}), 128.6 (C_{5B}), 127.6 (C_{2A/2B}), 127.1 (C_{2A/2B}), 127.0 (C_g), 124.4 (C_{3A/3B/7A/7B}), 124.1 (C_{3A/3B/7A/7B}), 123.8 (C_e), 113.0 (C_{4B}), 112.6 (C_{4A}), 109.4 (C_{6A/6B}), 109.2 (C_{6A/6B}), 106.3 (C_b). HRMS (ASAP): [M+H]⁺, m/z 624.1489 [624.1488 calculated for C₂₆H₂₁¹⁹³IrN₇].

Synthesis of 2.17aL₂

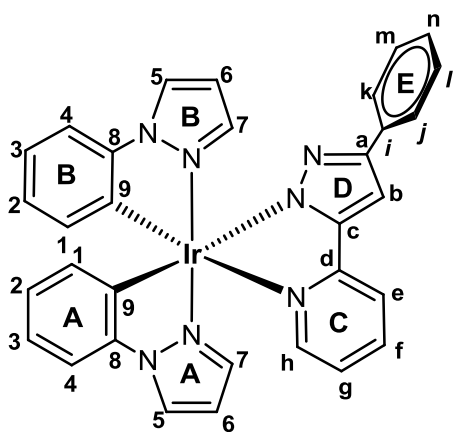


Complex **2.17aL₂** was prepared from the **2.15a** (71mg, 0.069 mmol), **HL₂** (31 mg, 0.15 mmol) and NaOMe (30 mg, 0.15 mmol) in MeOH (3ml) and DCM (6ml), and was allowed to stir for 2.5 h. After work up, **2.17aL₂** was isolated as grey yellow solid (73 mg, 76%). See appendix **Table 1** for X-Ray crystal data. ¹H NMR (500MHz, CDCl₃, 300K): δ

7.93 (1H, d, $J = 2.9$ Hz, H_{5B}), 7.84(2H, br. d, $J = 3.5$ Hz, H_{5A,f}), 7.63(1H, br. d, $J = 7.4$ Hz, H_e), 7.60(1H, td, $J = 7.7, 1.3$ Hz, H_h), 7.15 (1H, d, $J = 7.7$ Hz, H_{4B}), 7.11 (1H, d, $J = 7.6$ Hz, H_{4A}), 6.91 (1H, td, $J = 7.6, 1.1$ Hz, H_{3B}), 6.86 (1H, td, $J = 7.6, 0.8$ Hz, H_{3A}), 6.82-6.76 (4H, m, H_{2A,2B,7B,g}), 6.74(1H, d, $J = 2.1$ Hz, H_{7A}), 6.49 (1H, s, H_b), 6.37 (1H, t, $J = 2.4$ Hz, H_{6B}), 6.33 (1H, dd, $J = 7.6, 1.1$ Hz, H_{1B}), 6.30 (1H, dd, $J = 7.5, 1.1$ Hz, H_{1A}), 6.20 (1H, t, $J = 2.4$ Hz, H_{1A}), 2.98(2H, br. s, Hydrogen bond H₂O), 1.29 (9H, s, H^t_{Bu}). ¹³C NMR: (125 MHz, CDCl₃, 300K): δ 163.9 (C_{quat.}), 157.2 (C_{quat.}), 149.5 (C_{quat.}), 149.4 (C_{5A/f}), 144.1 (C_{quat.}), 143.3 (C_{quat.}), 138.7 (C_{2A/2B/7B/g}), 137.3 (C_h), 137.1 (C_{quat.}), 136.8 (C_{2A/2B/7B/g}), 134.0 (C_{1A/1B}), 133.7 (C_{1A/1B}), 133.0 (C_{quat.}), 126.3 (C_{5A/f}), 126.0 (C_{7A}), 125.6 (C_{2A/2B/7B/g}), 125.4(C_{5B}),122.0 (C_{3B}), 121.5 (C_{3A}), 120.7 (C_{2A/2B/7B/g}), 119.0 (C_e),111.1 (C_{4B}), 110.8 (C_{4A}), 107.3 (C_{6B}), 107.0 (C_{6A}), 98.8 (C_b), 32.2 (C_i), 31.2 (C^t_{Bu}). HRMS (ASAP): [M+H]⁺, m/z 680.2115 [680.2114 calculated for C₃₀H₂₉¹⁹³IrN₇]

Synthesis of 2.17aL₃

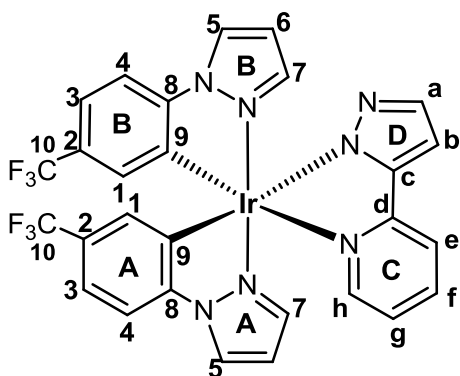
Complex **2.17aL₃** was prepared from the **2.5a** (50 mg, 0.048 mmol), **HL₃** (23.7 mg, 0.11 mmol) and NaOMe (6 mg, 0.11 mmol) in MeOH (3ml) and DCM (6ml). After work up, the compound was isolated as a pale yellow solid (47 mg, 69%). See appendix **Table 1** for X-Ray crystal data. ¹H NMR (500 MHz, CD₂Cl₂, 298 K): δ 8.01 (1H, dd, $J = 3.0, 0.4$



Hz, H_{5A}), 7.94 (1H, dd, $J = 2.9, 0.4$ Hz, H_{5B}), 7.82 (1H, ddd, $J = 5.5, 1.4, 0.8$ Hz, H_h), 7.70-7.67 (3H, m, H_{e, j, k}), 7.63 (1H, td, $J = 7.7, 1.2$ Hz, H_f), 7.23-7.16 (4H, m, H_{4A, 4B, l, m}), 7.09-7.05 (1H, m, H_n), 6.95 (1H, s, H_b), 6.91 (2H, qd, $J = 7.7, 1.3$ Hz, H_{3A, 3B}), 6.85 (1H, d, $J = 1.6$ Hz, H_{7A}), 6.84-6.80 (2H, m, H_{7B, g}), 6.76 (1H, td, $J = 7.4, 1.2$ Hz, H_{2A}), 6.73 (1H, td, $J = 7.4, 1.2$ Hz, H_{2B}), 6.40 (1H, t, $J = 2.5$ Hz, H_{6B}), 6.35 (1H, t, $J = 2.5$ Hz, H_{6A}), 6.33 (1H, dd, $J = 7.4, 1.2$ Hz, H_{1A}), 6.28 (1H, dd, $J = 7.5, 1.1$ Hz, H_{1B}). ¹³C NMR (125 MHz, CD₂Cl₂, 298 K): δ 157.1 (C_{quat.}), 153.6 (C_{quat.}), 152.0 (C_{quat.}), 150.1 (C_h), 144.5 (C_{quat.}), 143.6 (C_{quat.}), 139.1 (C_{7B}), 138.2 (C_f), 137.6 (C_{quat.}), 137.5 (C_{7A/g}), 136.1 (C_{quat.}), 134.3 (C_{1A}), 134.1 (C_{1B}), 133.7 (C_{quat.}), 128.7 (2C_{4A/4B, l/m}), 126.6 (C_{C-H}), 126.4 (2C_{C-H}), 126.2 (C_{C-H}), 126.0 (C_{C-H}), 125.4 (2C_{C-H}), 122.5 (C_{2A/2B}), 121.8 (C_{2A/2B}), 121.7 (C_{7A/g}), 119.7 (C_{C-H}), 111.4 (C_{4A/4B, l/m}), 111.3 (C_{4A/4B, l/m}), 107.8 (C_{6A}), 107.5 (C_{6B}), 100.7 (C_b). HRMS (ASAP): [M+H]⁺, m/z 700.1818 [700.1801 calculated for C₃₂H₂₅¹⁹³IrN₇].

Synthesis of 2.17bL1

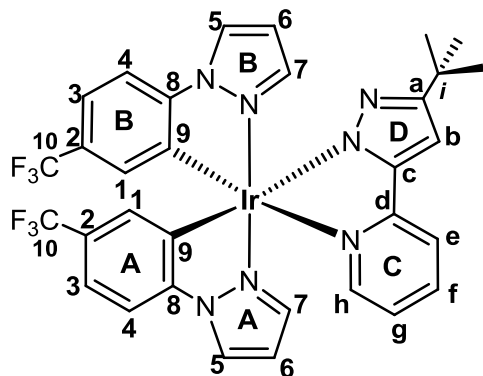
Complex **2.17bL1** was prepared from the dimer **2.15b** (60 mg, 0.046 mmol), **HL1** (14.7 mg, 0.101 mmol) and NaOMe (12 mg, 0.22 mmol). After work up gave **2.17bL1** a grey yellow solid (65 mg, 92%). ¹H NMR (500 MHz, DMSO, 298 K): δ 8.95 (2H, br. dd,



$J = 6.4, 2.9$ Hz, H_{5A, 5B}), 8.44 (2H, br. s, H_{2O}), 7.94-7.93 (1H, m, H_e), 7.91 (1H, t.d, $J = 7.6, 1.4$ Hz, H_h), 7.85 (1H, br. d, $J = 8.2$ Hz, H_{4A}), 7.80 (1H, br. d, $J = 8.3$ Hz, H_{4B}), 7.70 (1H, br. d, $J = 5.4$ Hz, H_g), 7.37-7.35 (1H, m, H_{3A}), 7.34 (1H, d, $J = 1.6$ Hz, H_a), 7.27 (1H, dd, $J = 1.4, 8.4$ Hz, H_{3B}), 7.21 (1H, d, $J = 2.2$ Hz, H_{7B}), 7.15 (1H, br. t, $J = 5.8$ Hz, H_f), 6.81 (1H, d, $J = 1.9$ Hz, H_b), 6.76 (1H, br. t, $J = 4.0$ Hz, H_{6A}), 6.73 (1H, br. t, $J = 2.0$ Hz, H_{6B}), 6.68 (1H, d, $J = 2.0$ Hz, H_{7A}), 6.51 (1H, d, $J = 1.8$ Hz, H_{1A}), 6.35 (1H, d, $J = 1.6$ Hz, H_{1B}). ¹³C NMR (126 MHz, DMSO, 298 K): δ 166.61 (C_{CH}), 155.8 (C_{quat.}), 149.0 (C_{quat.}), 148.9 (C_{CH}), 147.1 (C_{quat.}), 146.2 (C_{quat.}), 139.7 (C_{CH}), 139.1 (C_{CH}), 138.9 (C_{CH}), 138.3 (C_{quat.}), 133.9 (C_{quat.}), 129.4 (C_{CH}), 128.9 (C_{CH}), 128.5 (C_{CH}), 126 (q, C_{CF3}, $J = 31.1$ Hz), 122.2 (C_{CH}), 1120.0 (C_{CH}), 119.5 (C_{CH}), 119.0 (C_{CH}), 118.9 (C_{CH}), 111.9 (C_{CH}), 111.3 (C_{CH}), 108.9 (C_{CH}), 108.7 (C_{CH}), 103.6 (C_{CH}). The C-F and one of C-CF₃ carbons peaks

were not observed, may be owing to the solubility problem. ^{19}F NMR (376 MHz, DMSO, 298 K): δ -61.73 (F, s), -61.86(F, s). HRMS (ESI): $[\text{M}+\text{H}]^+$, m/z 760.1267 [760.1236 calculated for $\text{C}_{28}\text{H}_{19}\text{F}_6^{193}\text{IrN}_7$].

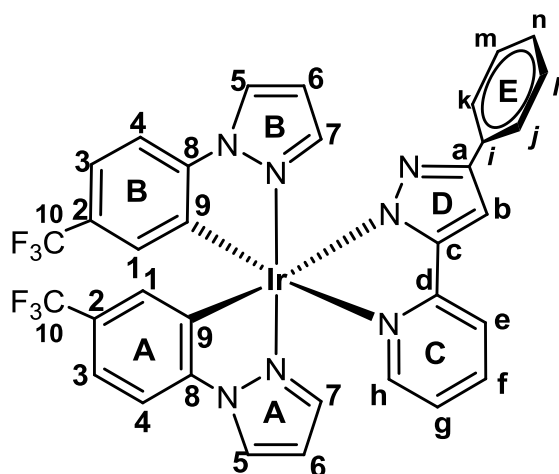
Synthesis of 2.17bL₂



This was prepared from dimer **2.15b** (70 mg, 0.054 mmol), **HL₂** (24.0 mg, 0.118 mmol), NaOMe (13 mg, 0.236 mmol). After work up gave **2.17bL₂** as a pale yellow solid (61 mg, 74%). ^1H NMR (500 MHz, CDCl_3 , 298 K): δ 8.40(1H, d, $J = 2.2$ Hz, $\text{H}_{5\text{B}}$), 8.33(1H, d, $J = 2.9$ Hz, $\text{H}_{5\text{A}}$), 8.02(1H, br. d $J = 7.7$ Hz, H_e), 7.97(1H, br. t, $J = 7.6$ Hz, H_f), 7.82(1H, br.

d, $J = 5.2$ Hz, H_h), 7.51(1H, d, $J = 7.9$ Hz, $\text{H}_{4\text{B}}$), 7.46(1H, d, $J = 8.3$ Hz, $\text{H}_{4\text{A}}$), 7.25(1H, dr. d, $J = 8.5$ Hz, $\text{H}_{3\text{A}}$) 7.23-7.21(1H, m, H_g), 7.17(1H, br. d, $J = 7.7$ Hz, $\text{H}_{3\text{B}}$), 7.02(1H, d, $J = 2.1$ Hz, $\text{H}_{7\text{A}}$), 6.82(1H, d, $J = 2.2$ Hz, $\text{H}_{7\text{B}}$), 6.74(1H, s, H_b), 6.57(1H, t, $J = 2.6$ Hz, $\text{H}_{6\text{A}}$), 6.47(1H, t, $J = 2.3$ Hz, $\text{H}_{6\text{B}}$), 6.43(1H, br. d, $J = 1.2$ Hz, $\text{H}_{1\text{A}}$), 6.40(1H, br. d, $J = 0.6$ Hz, $\text{H}_{1\text{B}}$), 1.36(9H, s, H^{tBu}). ^{13}C NMR (125 MHz, CDCl_3 , 298 K): δ 160.1($\text{C}_{a/c}$), 153.4(C_d), 151.3($\text{C}_{a/c}$), 150.0(C_h), 145.8($\text{C}_{2\text{A}/2\text{B}}$), 140.2($\text{C}_{7\text{A}}$), 139.3(C_f), 138.3($\text{C}_{7\text{B}}$), 132.0($\text{C}_{8\text{A}/8\text{B}}$), 130.1($\text{C}_{1\text{B}}$), 129.4($\text{C}_{1\text{B}}$), 129.0($\text{C}_{5\text{B}}$), 128.3 ($\text{C}_{8\text{A}/8\text{B}}$), 128.1($\text{C}_{5\text{A}}$), 127.5($\text{C}_{9\text{A}/9\text{B}}$), 127.3(q, $J_{\text{C-F}} = 33.5$ Hz), 125.0($\text{C}_{10\text{B}}$), 122.9($\text{C}_{2\text{A}/2\text{B}}$), 122.7 ($\text{C}_{9\text{A}/9\text{B}}$), 122.1(C_e), 121.1($\text{C}_{3\text{A}}$), 120.9($\text{C}_{3\text{B}}$), 112.4($\text{C}_{4\text{B}}$), 111.7($\text{C}_{4\text{A}}$), 109.1($\text{C}_{6\text{A}}$), 108.4 ($\text{C}_{6\text{B}}$), 101.2(C_b), 32.0(C_i), 30.2 (C^{tBu}). The remaining of C-F carbon were not observed. This could be overlapping with others peaks. ^{19}F NMR (376 MHz, CDCl_3 , 298 K): δ -61.73(F, s), -62.00(F, s). HRMS (ESI): $[\text{M}+\text{H}]^+$ m/z 816.1871 [816.1861 calculated for $\text{C}_{32}\text{H}_{27}\text{F}_6^{193}\text{IrN}_7$]

Synthesis of 2.17bL₃



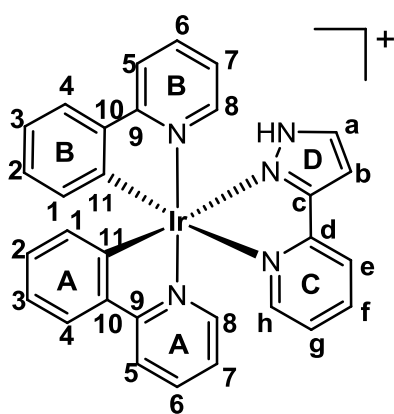
This was prepared from dimer **2.15b** (70 mg, 0.053 mmol), **HL₃** (26.2 mg, 0.12 mmol) and NaOMe (12.7 mg, 0.23 mmol). After work up gave **2.17bL₃** as a pale yellow solid (77 mg, 85%). ^1H NMR (500 MHz, DMSO, 298 K): δ 8.98(1H, d, $J = 2.5$ Hz, $\text{H}_{5\text{B}}$), 8.95(1H, d, $J = 2.5$ Hz, $\text{H}_{5\text{A}}$), 8.47(1H, s, H_{NH}), 7.99(1H, br. d, $J = 8.0$ Hz, H_e), 7.93(1H,

br. t, $J = 7.2$ Hz, H_f), 7.85(1H, br. d, $J = 8.2$ Hz, H_{4A}), 7.82(1H, br. d, $J = 8.2$ Hz, H_{4B}), 7.71(1H, d, $J = 5.0$ Hz, H_h), 7.64(2H, br.d, $J = 7.3$ Hz, H_{j, k}), 7.35(1H, br. d, $J = 8.0$ Hz, H_{3A}), 7.31-7.25(5H, m, H_{3B, 7B, b, l, m}), 7.18(1H, t, $J = 6.1$ Hz, H_g), 7.13(1H, t, $J = 7.3$ Hz, H_n), 6.84(1H, d, $J = 1.4$ Hz, H_{7A}), 6.77(1H, t, $J = 2.5$ Hz, H_{6B}), 6.71(1H, t, $J = 2.5$ Hz, H_{6A}), 6.47(1H, br. d, $J = 1.7$ Hz, H_{1A}), 6.40(1H, br. d, $J = 1.6$ Hz, H_{1B}). ¹³C NMR (126 MHz, DMSO, 298 K): δ 155.5(C_{quat.}), 152.0(C_{quat.}), 151.0(C_{quat.}), 149.0(C_h), 147.0(C_{quat.}), 146.2(C_{quat.}), 139.4 (C_{7A}), 139.0(C_f), 138.2(C_{quat.}), 135.3(C_{quat.}), 129.4 (C_{5A}), 129.0(C_{5B}), 128.8 (C_{3B/7B/l/m}), 128.6(C_{1A}), 128.4(C_{3B/7B/l/m}), 128.2(C_{1B}), 126.2(C_{quat.}), 126.0(C_{quat.}), 125.7(C_n), 125.3 (C_{quat.}), 25.0(C_{j/k}), 124.4(C_{j/k}), 122.4 (C_g), 119.9(C_{3B/7B/l/m}), 120.2 (C_{3A}), 119.6(C_{3B/7B/l/m}), 119.0(C_e), 111.9(C_{4A}), 111.4(C_{4B}), 109.0(C_{6B}), 108.8(C_{6A}), 100.8(C_b). Fluorinated carbons were difficult to find in ¹³C spectra with low signal-to-noise ratios, which could be buried in the noise. ¹⁹F NMR (376 MHz, DMSO, 298 K): δ - 60.24(F, s), - 60.37(F, s). HRMS (ESI): [M+H]⁺, m/z 836.1589 [836.1549 calculated for C₃₄H₂₃F₆¹⁹³IrN₇].

Synthesis of 2.16cHL₁

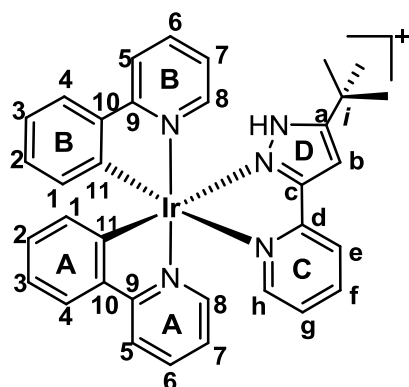
Complex **2.16cHL₁** was prepared from **2.15c** (50 mg, 0.048 mmol), **HL₁** (16 mg, 0.10) and KPF₆ (21.5 mg, 0.12 mmol) in MeOH (3ml) were heated in a microwave irradiation for 40 mins. After work up, the product was isolated as a yellow solid (53 mg, 72%). See appendix **Table 2** for X-Ray crystal data. ¹H NMR (500 MHz, CD₃CN, 298K): δ 8.20

(1H, dt, $J = 7.8, 1.1$ Hz, H_e), 8.08 (1H, d, $J = 8.09$ Hz, H_{5B}), 8.05 (2H, td, $J = 7.9, 1.5$ Hz, H_{5A, f}), 7.90-7.86 (2H, m, H_{6A, 6B}), 7.84 (1H, ddd, $J = 6.0, 1.5, 0.9$ Hz, H_h), 7.81 (1H, d, $J = 1.1$ Hz, H_{4A}), 7.79-7.78 (2H, m, H_{4B, a}), 7.66 (1H, ddd, $J = 5.9, 1.5, 0.7$ Hz, H_{8B}), 7.61 (1H, ddd, $J = 5.8, 1.4, 0.7$ Hz, H_{8A}), 7.35 (1H, ddd, $J = 7.6, 5.5, 1.4$ Hz, H_g), 7.18 (1H, d, $J = 2.7$ Hz, H_b), 7.11-7.01 (4H, m, H_{3A, 3B, 7A, 7B}), 6.92 (1H, td, $J = 7.5, 1.4$ Hz, H_{2A}), 6.88 (1H, td, $J = 7.4, 1.3$ Hz, H_{2B}), 6.32 (1H, dd, $J = 7.6, 0.6$ Hz, H_{1B}), 6.29 (1H, dd, $J = 7.6, 0.7$ Hz, H_{1A}). ¹³C NMR (125 MHz, CD₃CN, 298 K): δ 168.8 (C_{quat.}), 168.4 (C_{quat.}), 153.2 (C_{quat.}), 153.0 (C_{quat.}), 151.3 (C_h), 150.8 (C_{quat.}), 150.7 (C_{8A}), 150.4 (C_{8B}), 147.1 (C_{quat.}), 145.7 (C_{quat.}), 145.5 (C_{quat.}), 140.5 (C_{5A/f}), 139.5 (C_{6A/6B}), 139.4 (C_{6A/6B}), 135.0 (C_{4B/a}), 133.3 (C_{1A}), 132.5 (C_{1B}), 131.3 (C_{2B}), 130.8 (C_{2A}), 127.4 (C_g), 125.8 (C_{4A}), 125.6 (C_{4B/a}), 124.6 (C_e), 124.3 (C_{3A/3B/7A/7B}), 124.0 (C_{3A/3B/7A/7B}), 123.6 (C_{3A/3B/7A/7B}), 123.4



(C_{3A/3B/7A/7B}), 120.7 (C_{5A/f}), 120.5 (C_{5B}), 106.4 (C_b). HRMS (ASAP): *m/z* 646.1584 [646.1583 calculated for [C₃₀H₂₃¹⁹³IrN₅]

Synthesis of 2.16cHL₂

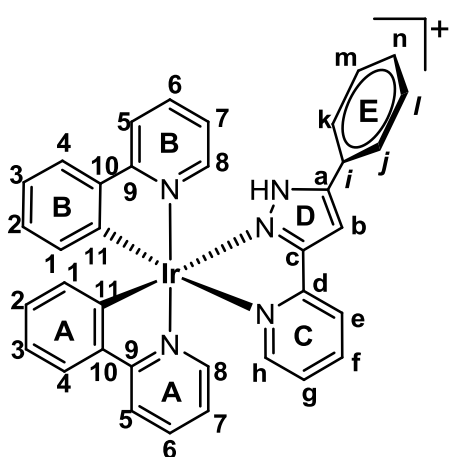


Complex **2.16cHL₂** was prepared from **2.15c** (50 mg, 0.046 mmol), **HL₂** (21 mg, 0.10) and KPF₆ (21 mg, 0.11 mmol) in MeOH (3 ml). After work up, the compound was isolated as a yellow solid (73 mg, 92%). See appendix **Table 2** for X-Ray crystal data.

¹H NMR (500 MHz, CD₃CN, 300 K): δ 8.15 (1H, dt, *J* = 7.9, 0.8 Hz, H_e), 8.09 (1H, tt, *J* = 7.9, 0.8 Hz, H_{5B}), 8.06-8.01 (2H, m, H_{5A, f}), 7.91 7.84 (2H, m, H_{6A,6B}),

7.81-7.76 (2H, m, H_{h,4B}), 7.77 (1H, d, *J* = 7.6 Hz, H_{4A}), 7.65 (1H, br. d, *J* = 5.8, Hz, H_{8B}), 7.58 (1H, br.d, *J* = 5.8 Hz, H_{8A}), 7.33 (1H, br. t, *J* = 6.6 Hz, H_g), 7.13-7.11 (1H, m, H_{7A}), 7.09-6.99 (4H, m, H_{3A, 3B, 7B, b}), 6.91 (1H, td, *J* = 7.4, 1.2 Hz, H_{2A}), 6.87 (1H, td, *J* = 7.4, 1.1 Hz, H_{2B}), 6.30 (1H, dd, *J* = 7.6, 0.8 Hz, H_{1B}), 6.23 (1H, dd, *J* = 7.5, 0.8 Hz, H_{1A}), 1.34 (9H, s, H^t_{Bu}). ¹³C NMR: (125 MHz, CD₃CN, 298 K) : δ 169.3 (C_{quat.}), 168.6 (C_{quat.}), 160.4 (C_{quat.}), 153.6 (C_{quat.}), 153.4 (C_{quat.}), 151.4 (C_{4A/4B, h}), 151.0 (C_{8A}), 150.7 (C_{8B}), 150.0 (C_{quat.}), 148.0 (C_{quat.}), 146.1 (C_{quat.}), 146.0 (C_{quat.}), 141.0 (C_{5A/f}), 139.8 (C_{6A/6B}), 139.7 (C_{6A/6B}), 134.0 (C_{1B}), 132.6 (C_{1A}), 131.7 (C_{2A}), 131.1 (C_{2B}), 127.8 (C_g), 126.1 (C_{4A/4B, 9}), 126.0 (C_{4A/4B, 9}), 125.0 (C_{7A}), 124.6 (C_{3A,3B, 7B, b}), 124.2 (C_e), 124.0 (C_{3A,3B, 7B, b}), 123.7 (C_{3A,3B, 7B, b}), 121.1 (C_{5A/f}), 120.8 (C_{5B}), 103.5 (C_{3A,3B, 7B, b}), 32.9 (C_i), 30.7 (C^t_{Bu}). HRMS (ASAP): *m/z* 702.2244 [702.2209 calculated for C₃₄H₃₁¹⁹³IrN₅]

Synthesis of 2.16cHL₃

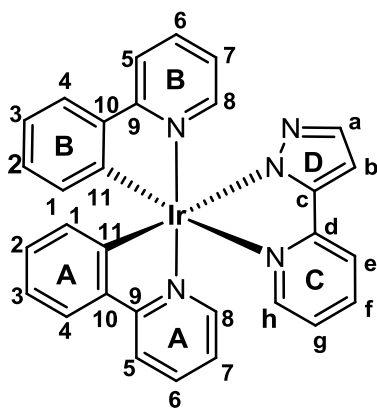


Complex **2.16cHL₃** was prepared from **2.15c** (50 mg, 0.046 mmol), **HL₃** (23.5 mg, 0.10) and KPF₆ (20.4 mg, 0.11 mmol) in MeOH (3ml). After work up, the compound was isolated as a yellow solid (68 mg, 84%). See appendix **Table 2** for X-Ray crystal data. ¹H NMR (500 MHz, CD₃CN, 298 K): δ 8.23 (1H, dt, *J* = 7.8, 1.1 Hz, H_e), 8.11-8.09 (1H, m, H_{5B}), 8.08-8.06 (1H, m, H_f), 8.05 (1H, dd, *J* = 1.2 Hz, H_{5A}), 7.89-7.85

(3H, m, H_{6A, 6B, 8A}), 7.83 (1H, ddd, *J* = 5, 1.6, 0.8 Hz, H_h), 7.82-7.78 (2H, m, H_{4A,4B}), 7.72-7.71 (2H, m, H_{j/k}), 7.68 (1H, ddd, *J* = 5.9, 1.4, 0.63 Hz, H_{8B}), 7.52 (1H, s, H_b), 7.52-7.46

(3H, m, H_l, m, n), 7.36(1H, ddd, $J = 7.6, 5.5, 1.4$ Hz, H_g), 7.13-7.01 (4H, m, H_{3A,3B, 7A, 7B}), 6.91 (2H, dtd, $J = 8.1, 3.8, 1.3$ Hz, H_{2A, 2B}), 6.35 (1H, dd, $J = 7.6, 0.9$ Hz, H_{1A}), 6.27 (1H, dd $J = 7.6, 0.8$ Hz, H_{1B}). ¹³C NMR (125 MHz, CD₃CN, 298 K): δ 169.0 (C_{quat.}), 168.2 (C_{quat.}), 154.3 (C_{quat.}), 152.8 (C_{quat.}), 151.2 (C_{4A/4B/6A/6B/8A/h}), 151.1 (C_{4A/4B/6A/6B/8A/h}), 150.4 (C_{8B}), 150.3 (C_{quat.}), 149.3 (C_{quat.}), 147.5 (C_{quat.}), 146.0 (C_{quat.}), 145.5 (C_{quat.}), 140.6 (C_{5B}), 140.4(C_{5A}), 139.5 (C_{4A/4B/6A/6B/8A/h}), 139.4 (C_{4A/4B/6A/6B/8A/h}), 133.5 (C_{1B}), 132.4 (C_{1A}), 131.3 (C_{2A/2B}), 131.5(C_{2A/2B}), 131.9 (C_{l/m/n}), 130.7 (C_{l/m/n}), 130.2 (C_{j/k}), 128.6 (C_{quat.}), 127.6 (C_{l/m/n}), 127.5 (C_g), 125.8 (C_{4A/4B/6A/6B/8A/h}), 125.6 (C_{4A/4B/6A/6B/8A/h}), 124.6 (C_{j/k}), 124.3(C_f), 124.0 (C_e), 123.6 (C_{3A/3B/7A/7B}), 123.4 (C_{3A/3B/7A/7B}), 120.7 (C_{3A/3B/7A/7B}), 120.5 (C_{3A/3B/7A/7B}), 104.2 (C_b). HRMS (ASAP): m/z 722.11901 [722.1896 calculated for C₃₆H₂₇¹⁹³IrN₅]

Synthesis of 2.17cL₁

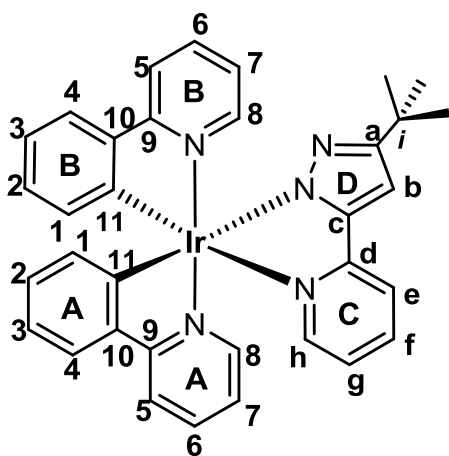


Complex **2.17cL₁** was prepared from the **2.15c** (50 mg, 0.046 mmol), **HL₁** (15 mg, 0.10 mmol) and NaOMe (6 mg, 0.10 mmol) in MeOH (3mL) and DCM (6ml). After work up, the compound was isolated as grey yellow solid (50 mg, 83%). ¹H NMR (500 MHz, CD₂Cl₂, 298 K): δ 7.80 (1H, bd, $J = 8.0$ Hz, H_{5B}), 7.76 (1H, bd, $J = 8.0$ Hz, H_{5A}), 7.73 (1H, dt, $J = 7.9, 1.1$ Hz, H_c), 7.66(1H, dd, $J = 7.5, 1.6$ Hz, H_f), 7.64 (1H, m, H_h),

7.60-7.56 (4H, m, H_{4A, 4B, 6A, 6B}), 7.52 (1H, dd, $J = 5.8, 0.7$ Hz, H_{8B}), 7.47(1H, m, H_{8A}), 7.46(1H, d, $J = 1.9$ Hz, H_a), 6.92-6.90(1H, m, H_g), 6.89-6.87(1H, m, H_{3B}), 6.86-6.78 (4H, m, H_{2B, 3A, 7A, 7B}), 6.70-6.69 (1H,m, H_{2A}), 6.68(1H, d, $J = 2.2$ Hz, H_b), 6.27 (1H, dd, $J = 7.5, 0.8$ Hz, H_{1B}), 6.23 (1H, dd, $J = 7.5, 0.8$ Hz, H_{1A}). ¹³C NMR (125 MHz, CD₂Cl₂, 298 K): δ 168.8 (C_{quat.}), 168.4 (C_{quat.}), 165.0 (C_{quat.}), 156.0 (C_{quat.}), 155.0 (C_{quat.}), 150.5 (C_{quat.}), 150.1 (C_h), 150.4 (C_{8B}), 149.0 (C_{8A}), 145.1 (C_{quat.}), 144.2 (C_{quat.}), 139.3 (C_a), 138.4 (C_f), 137.5 (C_{4A,4B, 6A, 6B}), 137.2 (C_{4A,4B, 6A, 6B}), 132.4 (C_{1B}), 132.3 (C_{1A}), 130.5 (C_{2B, 3A, 7A, 7B}), 130.0 (C_{2A}), 125.0 (C_{4A,4B, 6A, 6B}), 124.6 (C_{4A,4B, 6A, 6B}), 123.3 (C_{3B}), 123.2 (C_{2B, 3A, 7A, 7B}), 122.6 (C_g), 122.3 (C_{2B, 3A, 7A, 7B}), 121.7 (C_{2B, 3A, 7A, 7B}), 120.7 (C_e), 119.5 (C_{5B}), 119.3 (C_{5A}), 104.2(C_b). HRMS (ASAP): [M+H]⁺ m/z 646.1578 [656.1583 calculated for C₃₀H₂₃¹⁹³IrN₅].

Synthesis of 2.17cL₂

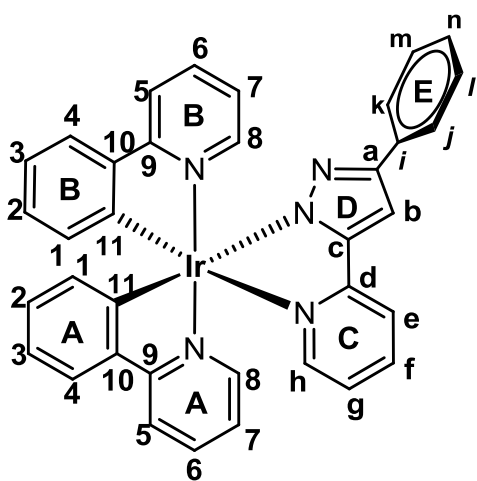
Complex **2.17cL₂** was prepared from the **2.15c** (75 mg,0.070 mmol), **HL₂** (31 mg, 0.15 mmol) and NaOMe (30 mg, 0.154 mmol) in MeOH/DCM (3:6 ml). After work up, the



compound was isolated as yellow solid (72 mg, 73%). See appendix **Table 2** for X-Ray crystal data. ^1H NMR (500 MHz, CDCl_3 , 300 K): δ 7.76(1H, d, $J = 4.8$ Hz, $\text{H}_{\text{pyA/B}}$), 7.74(1H, $J = 4.4$ Hz, $\text{H}_{\text{pyA/B}}$), 7.72 (1H, bd, $J = 7.9$ Hz, H_e), 7.67 (1H, td, $J = 7.7, 1.3$ Hz, H_f), 7.66-7.62(3H, m, $\text{H}_{4\text{A},4\text{B}, 8\text{A}}$), 7.61-7.55(2H, m, $\text{H}_h, \text{pyA/B}$), 7.49-7.44(2H, m, $\text{H}_{8\text{B}, \text{pyA/B}}$), 6.91-6.86 (4H, m, $\text{H}_{3\text{A}, 3\text{B}, 7\text{A}, \text{g}}$), 6.80-6.76 (3H, m, $\text{H}_{2\text{A},2\text{B}, 7\text{B}}$), 6.54 (1H, s,

H_b), 6.28 (1H, dd, $J = 7.5, 0.5$ Hz, $\text{H}_{1\text{B}}$), 6.20 (1H, dd, $J = 7.5, 0.8$ Hz, $\text{H}_{1\text{A}}$), 1.22 (9H, s, H_{tBu}). ^{13}C NMR (100 MHz, CDCl_3 , 300 K): δ 167.4 (C_{quat}), 167.2 (C_{quat}), 166.8 (C_{quat}), 161.5 ($\text{C}_{\text{C-H}}$), 154.0 ($\text{C}_{\text{C-H}}$), 151.9 ($\text{C}_{\text{C-H}}$), 149.4 ($\text{C}_{8\text{B}/\text{pyA}}$), 148.7 ($\text{C}_{8\text{B}/\text{pyA}}$), 148.5 (C_{quat}), 147.3 (C_{quat}), 143.4 ($\text{C}_{\text{C-H}}$), 143.0 (C_{quat}), 137.3 (C_f), 137.0 (C_{quat}), 136.0 ($\text{C}_{\text{C-H}}$), 135.7 (C_{quat}), 131.3 ($\text{C}_{\text{C-H}}$), 130.9 ($\text{C}_{\text{C-H}}$), 129.2 (C_{quat}), 128.8 ($\text{C}_{\text{C-H}}$), 123.3 ($\text{C}_{\text{C-H}}$), 122.0 ($\text{C}_{\text{C-H}}$), 121.9 ($\text{C}_{\text{C-H}}$), 121.2 ($\text{C}_{\text{C-H}}$), 120.8 ($\text{C}_{\text{C-H}}$), 120.6 ($\text{C}_{\text{C-H}}$), 119.5 ($\text{C}_{\text{C-H}}$), 118.3 ($\text{C}_{\text{C-H}}$), 117.7 (C_e), 99.3 (C_b), 31.1 (C_{quat}), 29.7 (C_{tBu}). HRMS (ASAP): $[\text{M}+\text{H}]^+$, m/z 702.2236 [702.2209 calculated for $\text{C}_{34}\text{H}_{31}^{193}\text{IrN}_5$]

Synthesis of 2.17cL3

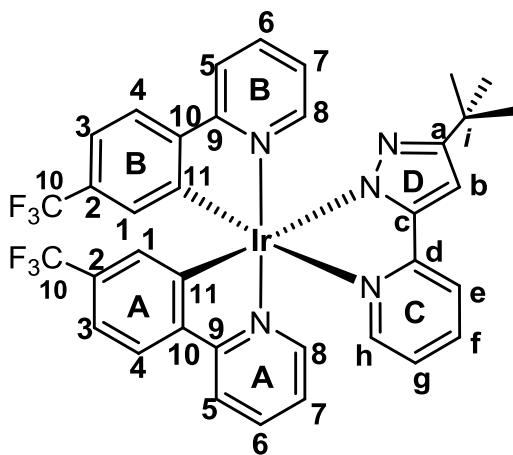


This complex was prepared from the **2.15c** (50 mg, 0.046 mmol), **HL3** (23 mg, 0.10 mmol) and NaOMe (6 mg, 0.10 mmol) in MeOH/DCM (3:6 ml). After work up, the product was isolated as yellow solid (50 mg, 87%). ^1H NMR (500 MHz, CDCl_3 , 298 K): δ 7.83 (1H, bd, $J = 5.55$ Hz, $\text{H}_{8\text{A}}$), 7.78(2H, br. d, $J = 7.3$ Hz, $\text{H}_{e, f}$), 7.74 (2H, br. t, $J = 7.4$ Hz, $\text{H}_{j, k}$), 7.71(1H, br. d, $J = 8.4$ Hz, $\text{H}_{5\text{B}}$), 7.66-7.62 (2H m, $\text{H}_{l, m}$), 7.61-7.59(1H, m, $\text{H}_{5\text{A}}$), 7.58-7.53 (4H m,

$\text{H}_{4\text{A},4\text{B}, 6\text{A}, 8\text{B}}$), 7.45 (1H, td, $J = 7.2, 1.1$ Hz, $\text{H}_{6\text{B}}$), 7.24(2H, t, $J = 7.6$ Hz, $\text{H}_{g, n}$), 7.11(1H, br. t, $J = 7.4$ Hz, H_h), 7.01 (1H, s, H_b), 6.92(1H, td, $J = 7.4, 0.8$ Hz, $\text{H}_{3\text{B}}$), 6.90-6.88(1H, m, $\text{H}_{3\text{A}}$), 6.87-6.83 (2H, m, $\text{H}_{2\text{B}, 7\text{A}}$), 6.81(1H, br. dd, $J = 7.3, 0.8$ Hz, $\text{H}_{2\text{A}}$), 6.75 (1H, td, $J = 6.1, 0.9$ Hz, $\text{H}_{7\text{B}}$), 6.39 (1H, bd, $J = 7.3$ Hz, $\text{H}_{1\text{B}}$), 6.33 (1H, bd, $J = 7.2$ Hz, $\text{H}_{1\text{A}}$). ^{13}C NMR (125 MHz, CDCl_3 , 298 K): δ 168.7 (C_{quat}), 168.14 (C_{quat}), 155.8 (C_{quat}), 155.2 (C_{quat}), 153.5 (C_{quat}), 151.1 (C_{quat}), 150.7 (C_{quat}), 150.4 ($\text{C}_{\text{C-H}}$), 149.4 ($\text{C}_{\text{C-H}}$), 148.2 ($\text{C}_{\text{C-H}}$), 144.7 (C_{quat}), 143.8 (C_{quat}), 137.6 ($\text{C}_{\text{C-H}}$), 136.7 ($\text{C}_{\text{C-H}}$), 136.3 ($\text{C}_{\text{C-H}}$), 134.7 (C_{quat}),

132.2 (C_{C-H}), 132.1 (C_{C-H}), 130.1 (C_{C-H}), 129.6 (C_{C-H}), 128.3 (C_{2C-H}), 126.3 (C_{C-H}), 125.5 (C_{C-H}), 124.2 (C_{C-H}), 124.1 (C_{C-H}), 122.7 (C_{C-H}), 122.0 (C_{C-H}), 121.9 (C_{C-H}), 121.5 (C_{C-H}), 121.0 (C_{C-H}), 119.7 (C_{C-H}), 119.0 (C_{C-H}), 118.5 (C_{C-H}), 101.0(C_{C-H}). HRMS (ASAP): [M+H]⁺, *m/z* 722.1862 [722.1896 calculated for C₃₆H₂₇¹⁹³IrN₅]

Synthesis of 2.17dL₂

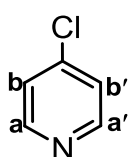


This complex was prepared from the dimer **2.15d** (70 mg, 0.053 mmol), **HL₂** (23.0 mg, 0.114 mmol) and NaOMe (13.6 mg, 0.252 mmol). After work up gave **2.17dL₂** as a yellow solid (66 mg, 76%). ¹H NMR(500 MHz, CD₂Cl₂, 298 K): δ 7.90(1H, br. d, *J* = 7.9 Hz, H_{5A/5B}), 7.82(1H, br. d, *J* = 8.1 Hz, H_{5A/5B}), 7.70-7.64(5H, m, H_{4A}, 4B, 6A, 6B, 8B), 7.60(1H, d, *J* = 1.1 Hz, H_c), 7.59(1H, dd, *J*

= 2.7, 1.2 Hz, H_f), 7.45(1H, br.d, *J* = 5.6 Hz, H_h), 7.41(1H, br. d, *J* = 5.4 Hz, H_{8A}), 7.14(1H, dd, *J* = 1.2, 8.2 Hz, H_{3A}), 7.10(1H, dd, *J* = 1.2, 8.1 Hz, H_{3B}), 6.99-6.95(2H, m, H_{7A}, 7B), 6.78(1H, td, *J* = 5.7, 2.9 Hz, H_g), 6.48(1H, s, H_b), 6.41-6.42(2H, overlapping, m, H_{1A}, 1B), 1.18(9H, s, H^t_{Bu}). ¹³C NMR (126 MHz, CD₂Cl₂, 298 K): δ 167.3(C_{quat.}), 167.0(C_{quat.}), 165.4(C_{quat.}), 156.8(C_{quat.}), 155.9(C_{quat.}), 152.2(C_{quat.}), 150.9(C_{8A}), 149.7(C_{quat.}), 149.5(C_h), 149.4 (C_{4A/4B/6A/6B/8B}), 149.1(C_{quat.}), 148.0(C_{quat.}), 138.34(C_{f/e}), 137.8(C_{4A/4B/6A/6B/8B}), 137.4 (C_{4A/4B/6A/6B/8B}), 130.9(C_{quat.}), 130.3(C_{quat.}), 129.1(q, *J*_{C-F} = 273 Hz), 128.1(C_{1A/1B}), 127.9 (C_{1A/1B}), 124.6(C_{4A/4B/6A/6B/8B}), 124.3 (C_{4A/4B/6A/6B/8B}), 124.2(C_{7A/7B}), 123.9(C_{7A/7B}), 121.9(C_g), 120.5(C_{5A/5B}), 120.1(C_{5A/5B}), 119.7(C_{f/e}), 119.1(C_{3A}), 118.2(C_{3B}), 100.4(C_b), 32.5(C_j), 31.2(C^t_{Bu}). The fluorinated carbons were difficult to find it, this could be buried in the noise or they may be they overlapping with others peaks. ¹⁹F NMR (376 MHz, CD₂Cl₂, 298 K): δ -62.86 (F, s), -62.91(F, s). HRMS (ESI): [M+H]⁺ *m/z* 838.1959 [838.1956 calculated for C₃₆H₂₉F₆¹⁹³IrN₅].

5.3 Data for compounds in Chapter Three

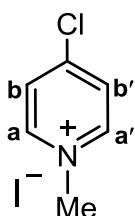
Synthesis of 4-chloropyridine (*p*-3.26)



Compound *p*-3.26 was prepared by a literature method.⁸ 4-Chloropyridine hydrochloride (1.5 g, 10.1mmol) was dissolved in 40 ml NaOH(aq) (0.2M, 0.2 mmol), and the resulting solution was stirred for 13 min, until the pH value of the mixture reaches *ca.* 6-7. Fresh DCM (30 ml × 4) was used to extract the product and the organic layer was washed with distilled water

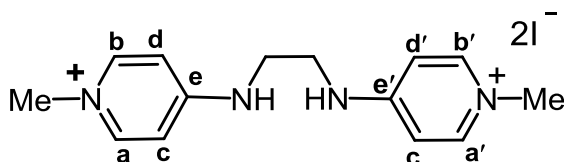
(40 ml × 2). The organic layer was collected and dried over MgSO₄, filtered, evaporated to dryness to give **p-3.26** as pale yellow liquid, 0.78 g, 70%. ¹H NMR (400 MHz, CDCl₃, 300 K): δ 8.52(2H, d, *J* = 1.60 Hz, H_{a, a'}), 7.30(2H, d, *J* = 1.56 Hz, H_{b, b'}). ¹³C NMR (100 MHz, CDCl₃): δ 150.7 (C_{a, a'}), 144.0(C^{quat.}), 124.1(C_{b, b'}). GC/MS, *m/z* 113.2330 [113.0032 calculated for C₅H₄ClN].

Synthesis of 4-Chlorolpyridinium iodide (**p-3.27**)



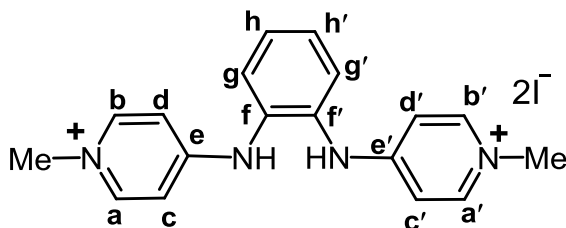
Compound **p-3.26** (0.799g, 7.04 mmol) was dissolved in 3 ml DCM, followed by the addition of iodomethane (28.1 mmol). The resulting mixture was stand together in the dark at zero °C for two days. After this time, forming yellow precipitate was collected by rotary evaporation. Removal of the volatiles led to changing precipitate to be dark brown colour, that was washed with petroleum ether several time, to give 4-Chlorol-methylpyridinium iodide **p-3.27** of sufficient purity as dark brown solid, 1.18 g, 66 %. ¹H NMR (500MHz, D₂O, 298 K): δ 8.70(2H, d, *J* = 6.9 Hz, H_{a, a'}), 8.05(2H, , br d, *J* = 6.6 Hz, H_{b, b'}), 4.30 (3H, s, H_{NMe}). ¹³C NMR (126 MHz, D₂O, 298 K): δ 153.79(C_{quat.}), 146.0(C_{a, a'}), 140.34, 128.5(C_{b, b'}), 48.0(C_{NMe}). HRMS (ASAP): *m/z*, 128.0255 [128.0267 calculated for C₆H₇NI]. MP: 148-153 °C. The characterization matches that previously reported.⁹

Synthesis of [**p-H₂PYE₁**]₂



In dry condition, **p-3.27** (100 mg, 0.391 m.mol) and potassium carbonate(162.3 mg, 1.174 m.mol) were mixed with dry DMF (10 ml) and ethylene diamine (13 μl, 0.186 mmol) was quickly added to reaction mixture. The reaction mixture was stirred at RT under N₂ for 2 hrs. After this time, the solvent was evaporated, leaving behind light brown solid, washed with DCM and MeOH several time, dried in high vacuo. to give [**p-H₂PYE₁**]₂ as pale yellow, 205 mg, 52 %. See appendix **Table 3** for X-Ray crystal data. ¹H NMR (500 MHz, D₂O, 298 K): δ 7.88(4H, br d, *J* = 1.00 Hz, H_{a, a'/b, b'}), 6.78(4H, br d, *J* = 1.00 Hz, H_{c, c'/d, d'}), 3.84(6H, s, H_{NMe}), 3.62 (4H, s, H_{CH2}). ¹³C NMR (125.7 MHz, D₂O, 298 K): δ 157.2(C_{e, e'}), 144.2(C_{a, a'/b, b'}), 142.2(C_{a, a'/b, b'}), 110.9(c, c'/d, d'), 105.4(C_{c, c'/d, d'}), 44.7(C_{2NMe}), 41.4(C_{2CH2}). HRMS (ASAP): *m/z* 243.1608 [244.1677 calculated for C₁₄H₂₀N₄]. MP: 217.1-219.7 °C

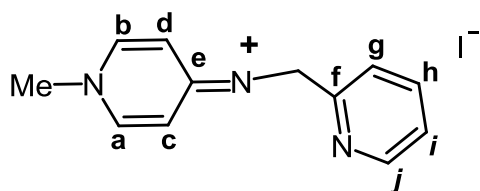
Synthesis of [*p*-H₂PYE₂]**I**₂



Compound **p-3.27** (200 mg, 0.782 m.mol) and 1,2-phenyl diamine (40.3 mg, 0.372 m.mol) were dissolved in DMF (9 ml), with stirring forming a dark brown solution. The reaction mixture was

heated at 100 °C under N₂ for overnight. After this time, the reaction mixture was cooled to room temperature and the solvent was removed by rotary evaporation, leaving behind a dark brown solid. The precipitate was isolated, washed with methanol and diethyl ether (1:9%), respectively and dried under high vacuum to give [**p**-H₂PYE₂]**I**₂ as a dark brown solid, 98 mg, 48 %. ¹H NMR (500 MHz, MeOD, 298 K): δ 8.18(4H, d, *J* = 7.6 Hz, H_{a, a'}, H_{b, b'}), 7.58-7.53(4H, m, H_{g, g'}, H_{h, h'}), 7.00(4H, br d, *J* = 6.4 Hz, H_{c, c'}, H_{d, d'}), 4.01(6H, s, H_{NMe}). ¹³C NMR (126 MHz, MeOD, 298 K): δ 157.4(C_{e, e'}), 145.6(C_{a, a'}, H_{b, b'}), 133.7(C_{f, f'}), 130.3(C_{g, g'/h, h'}), 128.2(C_{g, g'/h, h'}), 110.7(C_{c, c'}, H_{d, d'}), 45.9(C_{NMe}). HRMS (ASAP): *m/z* 291.1340 [292.1677 calculated for C₁₈H₂₀N₄]. MP: 220-222 °C.

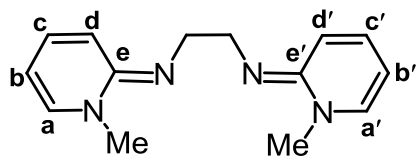
Synthesis of [*p*-HPYE]**I**



In dry conditions, **p-3.27** (200 mg, 0.782 m.mol) and potassium carbonate (108.2 mg, 0.782 mmol) were mixed with dry DMF (8 ml) and 2-picolylamine (82 μl, 0.782 mmol) was quickly

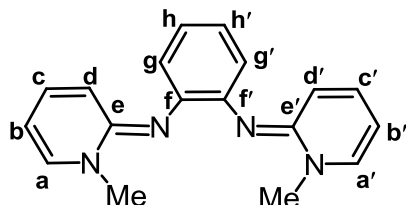
added to the reaction mixture. The reaction mixture was stirred at RT under N₂ for 3 hours. After this time the solvent was evaporated with toluene 15 ml and methanol 10 ml respectively, leaving behind a dark brown solid which was dissolved in MeOH (30 ml) and passed through celite. The filtrate was reduced in volume and diethyl ether was added slowly and left it in the fridge for overnight to induce precipitation. The precipitate was isolated, washed with diethyl ether and DCM several times, dried in vacuum to give [**p**-HPYE]**I** as a dark brown solid, 191 mg, 58 %. ¹H NMR (500 MHz, CD₃COCD₃, 298 K): δ 8.55(1H, br d, *J* = 4.8 Hz, H_j), 8.32(1H, br d, *J* = 7.4 Hz, H_b), 8.23(1H, br d, *J* = 7.4 Hz, H_a), 7.80(dt, *J* = 7.7, 1.7 Hz, H_h), 7.53(1H, d, *J* = 7.9 Hz, H_g), 7.42(1H, dd, *J* = 7.2, 2.8 Hz, H_c), 7.32(1H, dd, *J* = 7.4, 5.0 Hz, H_i), 7.04(1H, dd, *J* = 7.4, 2.6 Hz, H_d), 4.75(2H, s, H_{CH2}), 4.12(3H, s, H_{NMe}). ¹³C NMR (125 MHz, CD₃COCD₃, 298 K): δ 150.2(C_j), 145.4(C_{a/b}), 143.3(C_{a/b}), 142.5(C_{quat.}), 138.0(C_h), 123.7(C_i), 123.0(C_g), 112.0(C_{c/d}), 107.2(C_{c/d}), 48.4(C_{CH2}), 45.4(C_{NMe}). One quaternary carbon peak was not observed. HRMS (ASAP): *m/z* 200.1186 [200.1188 calculated for C₁₂H₁₄N₃]. MP: 203.2-205.7 °C

Synthesis of *o*-PYE₁



o-PYE₁ was prepared by a literature method.¹⁰ 2-Chloro-1-methyl pyridinium iodide (*o*-**3.9**) (0.247g, 0.0041 mol), anhydrous potassium carbonate (3.408 g, 0.020 mol) and dry MeCN 15 ml, ethylene diamine (0.39 ml, 8.33 mmol) was quickly added with stirring under nitrogen. The resulting mixture was heated at reflux at 80 °C for 2 hr. After this time the solvent was evaporated and then the solid was dissolved in DCM (40 ml) and passed through celite. Filtrate was removed under reduced pressure and toluene (90 ml) and NaOH_(aq) (90 mL, 0.475 mol) were added. After extraction three times the organic phase was dried over MgSO₄, filtered and evaporated to dryness to give *o*-PYE₁ as yellow solid, 0.68 g, 68%. ¹H NMR (400 MHz, CDCl₃, 300 K): δ 6.95(2H, dd, *J* = 6.9, 1.4 Hz, H_a), 6.83(2H, ddd, *J* = 9.6, 6.26, 2.0 Hz, H_c), 6.56(2H, d, *J* = 9.4 Hz, H_d), 5.56(2H, dt, *J* = 6.5, 1.3, Hz, H_b), 3.45(4H s, H_{CH2}), 3.33(6H, s, H_{NMe}). ¹³C NMR (100 MHz, CDCl₃, 300 K): δ 154.1(C_e), 138.9(C_a) 134.1(C_c), 112.3(C_b), 100.1(C_d), 50.1(C_{CH2}), 39.4(C_{NMe}). HRMS (ASAP): *m/z* 243.1605 [242.1531 calculated for C₁₄H₁₈N₄]. MP: 143-145.6 °C. The characterization matches that previously reported.¹⁰

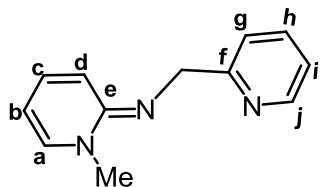
Synthesis of *o*-PYE₂



o-PYE₂ was prepared by a literature method¹⁰, compound *o*-**3.9** (2.37 g, 0.00929mol), anhydrous potassium carbonate (2.49 g, 0.0180 mol), 1,2-phenyl diamine (0.5g, 0.00462 mol) was dissolved in dry MeCN 15 ml. The work up was the same as for ligand *o*-PYE₁. The product *o*-PYE₂, was isolated as brown solid, 980 mg, 73%. See appendix **Table 4** for X-Ray crystal data. ¹H NMR (500 MHz, CDCl₃, 300 K): δ 6.96-6.94 (2H m, H_a, a'), -6.93-6.90 (4H m, H_g, g', h, h'), 6.75(2H, ddd, *J* = 9.4, 6.4, 1.86 Hz, H_c, c'), 6.21(2H, br d, *J* = 9.2 Hz, H_d, d'), 5.67(2H, dt, *J* = 6.6, 1.3 Hz, H_b, b'), 3.29(6H, s, H_{NMe}), ¹³C NMR (100 MHz, CDCl₃, 300 K): δ 151.8(C_{quat.}), 142.3(C_{quat.}), 137.8(C_a, a'), 133.6(C_d, d'), 123.6(C_g, g'/h, h), 122.4(C_g, g'/h, h), 116.5(C_c, c'), 102.1(C_b, b'), 39.4(C_{NMe}). HRMS (ASAP): *m/z* 291.1607 [290.1531 calculated for C₁₈H₁₈N₄]. MP: 134-136 °C.

Synthesis of *o*-PYE₃

2-Picolylamine (0.2, 0.0019mol) was added to compound *o*-**3.9** 0.5 g, 0.0019mol, dry triethylamine (3.90 mL, 27.8 mmol) in dry acetonitrile (15 ml) and the mixture was stirred



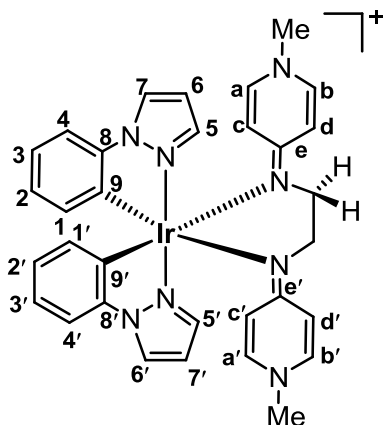
for 4 hr at 80 °C. After this time, The solvent was removed under reduced pressure and was then dissolved in DCM, passed through the celite and the filtrate was evaporated. The crude was extracted with DCM (50 ml) and NaOH aq (5 M, 50 ml).

The organic phase was separated and the aqueous phase was washed with DCM (3×50 ml). DCM extracts were collected and the solvent was removed under reduced pressure to give ***o*-PYE₃** as a dark brown oil, 0.351 g, 90%. ¹H NMR (400 MHz, CDCl₃, 300 K): δ 8.53(1H, br ddd, *J* = 4.86, 1.8, 1.0 Hz, H_j), 7.62-7.66(1H m, H_h), 7.57-7.60 (1H, m, H_g), 7.06-7.13(2H, m, H_{a,i}), 6.95(1H, ddd, *J* = 9.4, 6.4, 2.0 Hz, H_c), 6.45(1H, br d, *J* = 1.0 Hz, H_d), 5.71(1H, dt, *J* = 1.3, 6.6 Hz, H_b), 4.57(2H, s, H_{CH₂}), 3.51(3H, s, H_{NMe}). ¹³C NMR (101 MHz, CDCl₃, 300K): δ 162.4(C_f), 154.8(C_e), 148.8(C_j), 139.1(C_{a/i}), 136.4(C_{g/h}), 135.4(C_c), 121.4(C_{g/h}), 121.2(C_{a/i}), 112.5(C_d), 101.3(C_b), 54.0(C^{CH₂}), 39.6(C_{NMe}). HRMS (ASAP): *m/z* 200.1178 [199.1109 calculated for C₁₂H₁₃N₃].

General procedure for the synthesis of *para*-PYE-Ir(III) complexes

Complexes ***p*-3.30**, ***p*-3.31** and ***p*-3.32** were performed using standard Schlenk techniques and utilized nitrogen. A mixture of the [*p*-H₂PYE₁]₂ or [*p*-H₂PYE₂]₂ or [*p*-HPYE₃]₂ and NaOCH₃ (2.5-3 equiv.) in methanol (4 ml) were warmed gently at 40 °C for 30 mins. A solution of the dimer [Ir(ppz)₂Cl]₂ (1 equiv.) in methanol (3 ml) was added to the reaction mixture and the mixture was stirred at room temperature for 2-4 hrs. After this time the solvent was removed in rotary evaporator and the residue was dissolved in DCM (15 ml) and passed through celite, filtrate subject to ion-exchange with aqueous KPF₆ (4 equiv). The DCM phase was separated and dried over MgSO₄, The filtrate was reduced in volume and hexane was added slowly to induce precipitation. The precipitate was isolated, washed with hexane and diethyl ether (5 ml each) respectively, and dried in high vacuo that led to give the desired complexes.

Synthesis of *p*-3.30

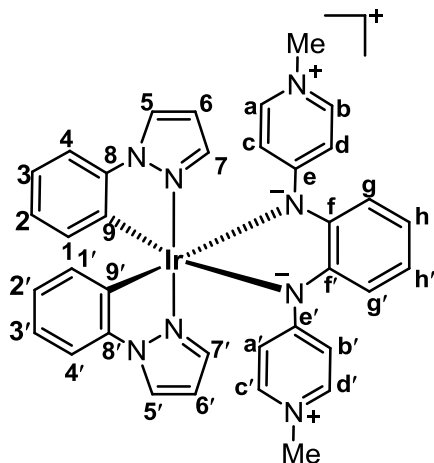


Complex ***p*-3.30** was prepared from dimer **2.15a** (70 mg, 0.0680 mmol), [*p*-H₂PYE₁]₂ (71.2 mg 0.142 mmol) and NaOMe (23.0 mg, 0.427 m. mol). After work up, gave ***p*-3.30** as a pale yellow solid (76 mg, 64%), See appendix **Table 5** for X-Ray crystal data. ¹H NMR (500MHz, CD₂Cl₂, 298 K): δ 8.10(2H, d, *J* = 2.8 Hz, H_{5,5'}), 7.59(2H, d, *J* = 2.2 Hz, H_{7,7'}), 7.20(2H, br. d, *J* = 7.9 Hz, H_{4,4'}), 6.87-6.85(2H, m, H_{b,b'}),

6.87(1H, td, $J = 7.6, 1.9$ Hz, H_{3,3'}), 6.67(2H, td, $J = 7.4, 0.9$ Hz, H_{2,2'}), 6.63(2H, t, $J = 2.6$ Hz, H_{6,6'}), 6.44(2H, dd, $J = 7.8, 2.1$ Hz, H_{a,a'}), 6.34(2H, dd, $J = 5.1, 2.5$ Hz, H_{c,c'}), 6.32(2H, dd, $J = 5.0, 2.6$ Hz, H_{d,d'}), 6.14(2H, dd, $J = 1.0, 7.6$ Hz, H_{1,1'}), 3.57(2H, d, $J = 8.3$ Hz, H_{CH2}), 3.36(6H, s, H_{NMe}), 3.18(2H, d, $J = 8.3$ Hz, H_{CH2}). ¹³C NMR (126MHz, CD₂Cl₂, 298 K): δ 161.5(C_{e,e'}), 143.4(C_{9,9'}), 139.9(C_{7,7'}), 139.1(C_{a,a'}), 137.0(C_{b,b'}), 135.6(C_{8,8'}), 134.8(C_{1,1'}), 126.4(C_{5,5'}), 126.2(C_{2,2'}), 121.8(C_{3,3'}), 114.9(C_{c,c'}), 111.6(C_{4,4'}), 108.0(C_{d,d'}), 107.7(C_{6,6'}), 54.8(C_{CH2}), 42.9(C_{NMe}). HRMS (FAB): m/z 721.2371 [721.2379 calculated for C₃₂H₃₂¹⁹³IrN₈].

Synthesis of *p*-3.31

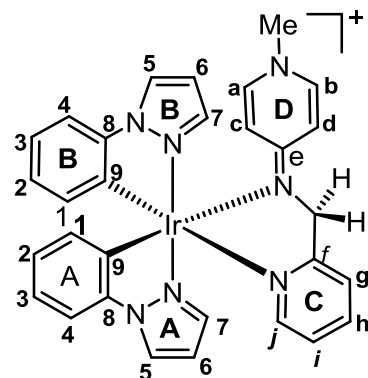
Complex *p*-3.31 was prepared from dimer **2.15a** (65 mg, 0.0632 mmol), [*p*-H₂PYE₂]**I**₂ (40.3, 0.139 mmol), and NaOMe (8 mg, 0.139 mmol). After work up gave *p*-3.31 as a yellow solid (73 mg, 63 %). ¹H NMR (500 MHz, CD₂Cl₂, 298K): δ 8.08(2H, d, $J = 2.8$ Hz, H_{5,5'}), 7.22(2H, d, $J = 2.0$ Hz, H_{7,7'}), 7.20(2H, d, $J = 7.9$ Hz, H_{4,4'}), 7.18-7.14(2H, m,



H_{g,g'/h,h'}), 7.08-6.71(8H, m, H_{3,3'a,a',b,b'g,g'/h,h'}), 6.67(2H dt, $J = 7.5, 1.0$ Hz, H_{2,2'}), 6.48(2H, t, $J = 2.6$ Hz, H_{6,6'}), 6.22 (2H, dd, $J = 1.1, 7.5$ Hz, H_{1,1'}), 3.42 (6H, s, H_{NMe}). Two protons more likely to be H_{c,d} were missing, this may be due to the rotation about C—N bond. ¹³C NMR (126 MHz, CD₂Cl₂, 298 K): δ 162.0(C_{e,e'}), 150.0(C_{f,f'}), 143.7(C_{8,8'}), 139.7(C_{4,4'/7,7'}) 139.3(C^{CH}), 134.4(C_{1A,B}), 133.4 (C_{9,9'}), 126.7(C_{5,5'}), 126.0(C_{2,2'}), 124.0(C_{CH}),

122.5(C_{g,g'/h,h'}), 122.3 (C_{g,g'/h,h'}), 111.4(C_{4,4'/7,7'}), 107.7(C_{6,6'}), 43.4(C_{NMe}), the remaining C-H carbons were not observed, this is likely due to rotation around C—N bond. HRMS (FAB): m/z 769.000 [769.2379 calculated for C₃₆H₃₂¹⁹³IrN₈].

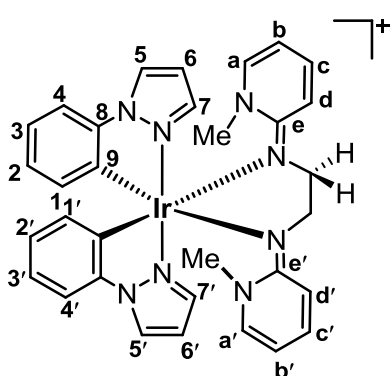
Synthesis of *p*-3.32



Complex *p*-3.32 was prepared from dimer **2.15a** (70 mg, 0.068 mmol), [*p*-HPYE₃]**I** (49.01 mg 0.149 mmol), and NaOMe (8.2 mg, 0.149 mmol) in MeOH (7 ml). After work up, After work up gave *p*-3.32 as pale yellow solid (81 mg, 69%). See appendix **Table 5** for X-Ray crystal data. ¹H NMR (500MHz, CD₂Cl₂, 298 K): δ 8.19(1H, d, $J = 2.7$ Hz, H_{5A}), 8.12(1H, d, $J = 2.7$ Hz, H_{5B}), 7.85(1H, dt, $J = 7.7, 1.6$ Hz, H_h), 7.71(1H, d, $J = 5.7$ Hz, H_j),

7.67(1H, d, $J = 7.8$ Hz, H_g), 7.50(1H, d, $J = 2.2$ Hz, H_{7A}), 7.34(1H, dd, $J =$ Hz, H_{4A}), 7.24(1H, dd, $J = 7.8, 1.0$ Hz, H_{4B}), 7.17(1H, dd, $J = 7.8, 2.0$ Hz, H_b), 7.09(1H, t, $J = 6.4$ Hz, H_i), 7.03(1H, dt, $J = 7.7, 1.3$ Hz, H_{3A}), 6.95-6.91(1H, m, H_{3B}), 6.90(1H, d, $J = 2.2$ Hz, H_{7B}), 6.78(2H, tt, $J = 7.4, 1.4$ Hz, H_{2A, 2B}), 6.65(1H, br. d, $J = 8.94$, Hz, H_a), 6.64-6.61(2H, m, H_{6A, c}), 6.59(1H, t, $J = 1.0$ Hz, 1 H_{6B}), 6.46(1H, dd, $J = 7.9, 2.8$ Hz, H_d), 6.29(1H, dd, $J = 7.5, 1.3$ Hz, H_{1B}), 6.14(1H, dd, $J = 7.4, 1.2$ Hz, H_{1A}), 5.06(1H, d, $J = 19.4$ Hz, H_g), 4.85(1H, d, $J = 19.4$ Hz, H_h), 3.47(3H, s, H_{NMe}). ¹³C NMR (125 MHz, CD₂Cl₂, 298K): δ 164.7(C_e), 162.4(C_f), 149.9(C_j), 143.6(C_{9A/9B}), 143.2(C_{9A/9B}), 140.2(C_{7A}), 140.0(C_b), 138.4(C_h), 137.8(C_a), 137.7(C_{7B}), 134.6(C_{1B}), 134.5(C_{8A/8B}), 133.7(C_{1A}), 133.5 (C_{8A/8B}), 127.2 (C_{5A/5B}), 127.0(C_{2A/2B}), 126.8(C_{5A/5B}), 126.6(C_{2A/2B}), 124.5(C_i), 123.2(C_{3A}), 122.4(C_g), 115.4(C_c), 112.1(C_{4A}), 111.8(C_{4B}), 108.3(C_{6A}), 108.1(C_{6B}), 107.6(C_d), 60.3(C_{CH2}), 43.4(C_{NMe}). Carbon (C_{3B}) peak was not observed my be overlapping with others peaks. HRMS (FAB): m/z 678.1950 [678.1957 calculated for C₃₀H₂₇¹⁹³IrN₇].

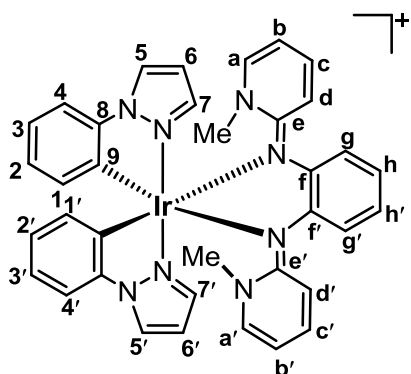
Synthesis of *o*-3.30



Complex *o*-3.30 was prepared from **2.51a** (80 mg, 0.078 mmol) and *o*-PYE₁ (41.5 mg, 0.171 mmol) and KPF₆ (38.7 mg, 0.210 mmol). After work up, gave *o*-3.30 as a brown-yellow solid (86 mg, 64%), see appendix **Table 6** for X-Ray crystal data. ¹H NMR (500MHz, CD₂Cl₂, 298 K): δ 8.09 (2H, d, $J = 1.0$ Hz, H_{7,7'}), 7.89(2H, d, $J = 1.0$ Hz, H_{5,5'}), 7.06(2H, br t, $J = 7.0$ Hz, H_{c, c'}), 6.97(2H, br d, $J = 7.9$ Hz, H_{4,4'}), 6.89(2H, dt, $J = 7.2, 1.0$ Hz, H_{3,3'}), 6.72(2H, t, $J = 2.4$ Hz, H_{6,6'}), 6.65(2H, br d, $J = 5.6$ Hz, H_{a, a'}), 6.61(2H, dt, $J = 6.9, 0.5$ Hz, H_{2, 2'}), 6.50(2H, br d, $J = 8.7$ Hz, H_{d, d'}), 6.20-6.14(4H, m, H_{1,1', b, b'}), 3.85(2H, br d, $J = 7.4$ Hz, H_{CH}), 3.27 (6H, s, H_{NMe}), 3.21(1H, br d, $J = 8.7$ Hz, H_{CH2}). ¹³C NMR(125 MHz, CD₂Cl₂, 298 K): δ 143.41(C_{quat.}), 140.1(C_{5,5'}), 139.66(C_{7,7'}), 136.3(C_{c, c'}), 126.0(C_{2,2'}), 125.2(C_{a, a'}), 122.4(C_{3,3'}), 110.4 (C_{4,4'}), 109.5(C_{1,1'}), 108.8(C_{b, b'}), 108.0(C_{d, d'}), 107.9(C_{6,6'}), 54.3(C_{CH2}), 44.27(C_{NMe}). one C-H carbon and two quaternary carbon peaks were not observed. This my be overlapping with others peaks. HRMS (FAB): m/z 721.2400 [721.2379 calculated for C₃₂H₃₂¹⁹³IrN₈].

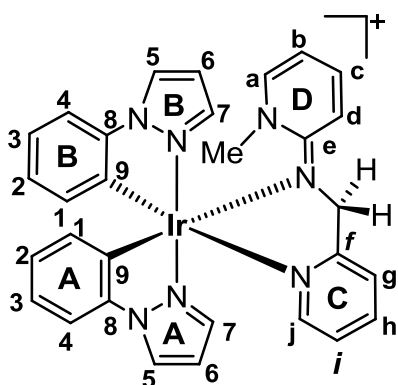
Synthesis of *o*-3.31

Complex *o*-3.31 was prepared from **2.15a** (70 mg, 0.068 mmol) and *o*-PYE₂ (43.4 mg, 0.149 mmol) and KPF₆ (27.6 mg, 0.149 mmol). After work up, gave *o*-3.31 as a dark red



solid (68 mg, 65%), see appendix **Table 6** for X-Ray crystal data. ^1H NMR (500MHz, CD_2Cl_2 , 298 K): δ 7.83(2H, d, $J = 2.6$ Hz, $\text{H}_{5,5'}$), 7.79(2H, d, $J = 1.8$ Hz, $\text{H}_{7,7'}$), 7.04-6.99(2H, m, $\text{H}_{c, c'}$), 6.94(2H, br d, $J = 7.7$ Hz, $\text{H}_{4,4'}$), 6.90-6.85(4H, m, $\text{H}_a, a', 3,3'$), 6.74-6.69(4H, m, H_g, g', h, h'), 6.63(2H, d, $J = 9.1$ Hz, $\text{H}_{d, d'}$), 6.6-6.56(4H, m, $\text{H}_{2,2',6,6'}$), 6.41(2H, t, $J = 6.3$ Hz, $\text{H}_{b, b'}$), 6.18(2H, d, $J = 7.4$ Hz, $\text{H}_{1,1'}$), 3.40(6H, s, H_{NMe}). ^{13}C NMR (126MHz, CD_2Cl_2 , 298 K): δ 166.2 ($\text{C}_{e, e'}$), 149.9($\text{C}_{f, f'}$), 143.4($\text{C}_{9,9'}$), 138.8($_{5,5'}$), 138.6($\text{C}_{c, c'}$), 136.5($\text{C}_{1,1'}$), 130.0($\text{C}_{8,8'}$), 126.6($\text{C}_{a, a'/3,3'}$), 126.2($\text{C}_{2,2',6,6'}$), 125.8($\text{C}_{7,7'}$), 122.7($\text{C}_{a, a'/3,3'}$), 122.2($\text{C}_{g, g'/h, h'}$), 121.6($\text{C}_{d, d'}$), 120.8($\text{C}_{g, g'/h, h'}$), 113.0($\text{C}_{b, b'}$), 110.7($\text{C}_{4,4'}$), 108.2($\text{C}_{2,2',6,6'}$), 44.1(C_{NMe}). HRMS (ASAP): m/z 769.2386 [769.2379 calculated for $\text{C}_{32}\text{H}_{32}^{193}\text{IrN}_8$].

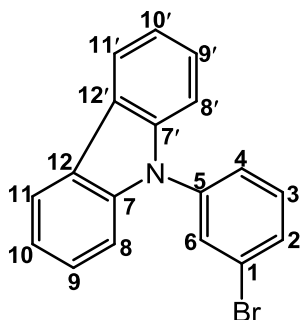
Synthesis of *o*-3.32



Using the general procedure for cationic complexes, complex *o*-3.32 was prepared from **2.15a** (70 mg, 0.068 mmol) and *o*-PYE₃ (31.2 mg, 0.157mmol) and KPF₆ (31.1 mg, 0.163 mmol) and after work, gave *o*-3.32 as a yellow solid (69 mg, 62%), see appendix **Table 6** for X-Ray crystal data. ^1H NMR (500 MHz, CD_2Cl_2 , 298 K): δ 8.23(1H, dd, $J = 2.9, 0.5$ Hz, H_{5A}), 7.90(1H, d, $J = 2.9$ Hz, H_{5B}), 7.87(1H, dt, $J = 7.7, 1.6$ Hz, H_h), 7.78(1H, dd, $J = 2.3, 0.5$ Hz, H_{7A}), 7.67(1H, d, $J = 7.4$ Hz, H_g), 7.63(1H, dd, $J = 5.6, 0.7$ Hz, H_j), 7.35(1H, dd, $J = 7.9, 1.1$ Hz, H_{4B}), 7.23(1H, dd, $J = 2.3, 0.5$ Hz, H_{7B}), 7.21-7.18(1H, m, H_c), 7.10(1H, t, $J = 6.6$ Hz, H_i), 7.01(1H, dd, $J = 7.6, 1.0$ Hz, H_{3B}), 6.97(1H, dd, $J = 8.2, 1.2$ Hz, H_{4A}), 6.90 (1H, dt, $J = 1.3, 7.6$ Hz, H_{3A}), 6.77(1H, dd, $J = 1.7, 6.6$ Hz, H_a), 6.72-6.69(3H, m, $\text{H}_{2A, 6A, 2B}$), 6.60(1H, t, $J = 2.5$ Hz, H_{6B}), 6.56(1H, d, $J = 9.0$ Hz, H_d), 6.36(1H, dd, $J = 7.5, 1.0$ Hz, H_{1A}), 6.23(1H, dt, $J = 6.7, 1.2$ Hz, H_b), 6.10(1H, dd, $J = 7.6, 1.0$ Hz, H_{1B}), 5.17(1H, d, $J = 17.1$ Hz, H_{CH}), 4.70 (1H, d, $J = 17.2$ Hz, H_{CH}), 3.32 (3H, s, H_{NMe}). ^{13}C NMR (126MHz, CD_2Cl_2 , 298 K): δ 166.7(C_e), 165.5(C_i), 149.2(C_k), 143.5(C_{8B}), 143.3(C_{9B}), 140.5(C_a), 140.1(C_{7B}), 139.3(C_{7A}), 139.0(C_c), 138.8(C_m), 135.5(C_{1A}), 134.1(C_{1B}), 132.2(C_{9A}), 128.88(C_{8A}), 127.5(C_{5B}), 126.8(C_{5A}), 126.7($\text{C}_{2A/6A/2B}$), 126.0(C_l), 124.7(C_{3B}), 123.3(C_{3A}), 123.0(C_j), 122.5 ($\text{C}_{2A/6A/2B}$), 115.6(C_d), 112.0 (C_{4B}), 110.8(C_{4A}), 109.8(C_b), 108.5($\text{C}_{2A/6A/2B}$), 108.4(C_{6B}), 59.6(C_f), 44.0(C_{NMe}). HRMS (ASAP): m/z : 678.1976 [678.1957 calculated for $\text{C}_{30}\text{H}_{27}^{193}\text{IrN}_7$].

5.4 Data for compounds in chapter four

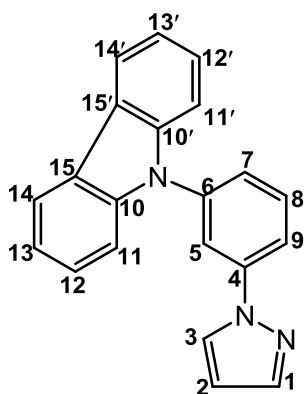
9-(3-Bromophenyl)-9H-carbazole



The compound was synthesized using a procedure similar to that employed in literature.¹¹ A mixture of 1-Bromo-3-iodobenzene (1000 mg, 3.53 mmol), carbazoles (393.5 mg, 2.36 mmol), Cu₂O (67.5 mg, 0.471 mmol), and Cs₂CO₃ (1536 mg, 4.71 mmol) in dry MeCN (13 ml) was allowed to react under nitrogen atmosphere at 110° C for overnight.

After this time the solvent was removed *in vacuo* leaving behind a solid which was dissolved in DCM (40 ml) and passed through celite. The filtrate was added to brine (10 ml) and extracted three times with dichloromethane (3×10 ml), and dried over MgSO₄. The solvent was removed by rotary evaporation and the desired product was Purification by flash chromatography on a silica gel, (petroleum ether, 100%): a colourless oil, 701 mg, 92%. ¹H NMR (500 MHz, CDCl₃, 298 K): δ 8.18 (2H, d, *J* = 7.75 Hz, H_{carbazole}), 7.79(1H, t, *J* = 1.79 Hz, H₆), 7.64(1H, dd, *J* = 1.39, 7.75, Hz, H₄), 7.58-7.55(1H, m, H₃), 7.52(1H, d, *J* = 7.9 Hz, H₂), 7.47-7.44(4H, m, H_{carbazole}), 7.34 (2H, ddd, *J* = 7.7, 6.0, 1.9 Hz, H_{carbazole}). ¹³C NMR (126 MHz, 500 MHz, CDCl₃, 298.0 K): δ 140.6(2C_{quat}), 139.2(2C_{quat}), 131.1(C_{CH}), 130.5(C_{CH}), 130.2(C_{CH}), 126.2(2C_{CH}), 125.8(C_{CH}), 125.7(2C_{CH}), 123.6(C_{quat}), 123.2(C_{quat}), 120.4(C_{CH}), 120.3(C_{CH}), 109.6(2C_{CH}). HRMS (ASAP): [M+H]⁺ *m/z* 322.0231[322.0231 calculated for C₁₈H₁₃BrN]. The data are consistent with the literature.¹¹

Ligand Hppz_b:



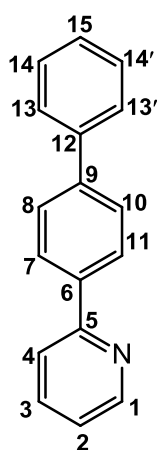
The compound **Hppz_b** was synthesized using a procedure similar to that employed in literature.¹¹ 9-(3-Bromophenyl)-9H-carbazole (662mg, 2.06 mmol), (Hppz) (210 mg, 3.08 mmol), Cu₂O (59 mg, 0.41 mmol, 20%), and Cs₂CO₃ (1676mg, 5.14 mmol) in dry MeCN (12 ml) was allowed to react under nitrogen atmosphere at 110° C for overnight. After this time the solvent was removed *in vacuo* leaving behind a solid which was dissolved in DCM (30 ml) and passed through celite. The filtrate was added to brine (20 ml) and extracted three times with dichloromethane (3×20 ml), and dried over MgSO₄. The solvent was removed by rotary evaporation, the product was isolated by short column chromatography on a silica gel, eluting with 20% ethyl acetate in petroleum ether, to give the desired product as

colourless oil, 420mg, 66%. ^1H NMR (500 MHz, CDCl_3 , 298.0 K): δ 8.08(2H, br.d, $J = 7.7$ Hz, $\text{H}_{\text{carbazole}}$), 7.88(1H, br. d, $J = 9.5$ Hz, $\text{H}_{3,9}$), 7.74(1H, br.d, $J = 7.9$ Hz, H_5), 7.67(1H, s, H_1), 7.61(1H, t, $J = 7.95$ Hz, H_8), 7.43-7.33(5H, m, $\text{H}_7, 4_{\text{carbazole}}$), 7.23(2H, br. t, $J = 7.03$ Hz, $\text{H}_{\text{carbazole}}$), 6.42(1H, br. s, H_2). ^{13}C NMR (126 MHz, CDCl_3 , 298.0 K): δ 141.6(C_{quat}), 141.5(C_{CH}), 140.7(2 C_{quat}), 139.0 (C_{quat}), 130.9(C_{ph}), 126.8($\text{C}_{\text{carbazole}}$), 126.1($\text{C}_{\text{carbazole}}$), 124.8(C_{CH}), 123.5(2 C_{quat}), 120.4 (2 $\text{C}_{\text{carbazole}}$), 120.2(2 $\text{C}_{\text{carbazole}}$), 117.9(C_3), 117.8(C_{ph}), 109.8(2 $\text{C}_{\text{carbazole}}$), 108.1(C_2). HRMS (ASAP): $[\text{M}+\text{H}]^+$, m/z 310.1347[310.1344 calculated for $\text{C}_{21}\text{H}_{16}\text{N}_3$].

General Procedure for the Suzuki Reaction of 2-bromopyridine with Arylboronic Acids:

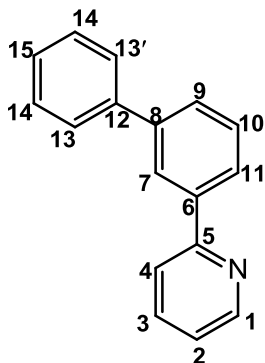
The ligands (L_1 and L_2) were synthesized using a procedure similar to that employed in literature¹² A mixture of 2-bromopyridine (1 mmol equiv.), arylboronic acids (1.5 mmol equiv), $\text{Pd}(\text{OAc})_2$ (10% mmol), potassium phosphate tribasic monohydrate (3 mmol equiv), respectively, the mixture was dissolved in isopropanol/water (1:1) (10-15 ml). The reaction mixture was allowed to stirred at 80 °C in air for 3-8h. After this time, the reaction mixture was cooled to room temperature and the solvent was removed by rotary evaporation. The remaining solid was dissolved in dichloromethane and washed with water (2×20 ml) and brine (2×20 ml), the organic layer was collected, and dried over MgSO_4 . The product was isolated by short chromatography on a silica gel, eluting with 20% ethyl acetate in petroleum ether to give the desired product

Ligand Hppy_b:



A mixture of 2-bromopyridine (500 mg, 3.16 mmol), 4-Biphenylboronic acid, (4.74 mmol), $\text{Pd}(\text{OAc})_2$ (71 mg, 0.316 mmol-10%), potassium phosphate tribasic monohydrate (2180mg, 9.49-mmol), and after work up gave **Hppy_b** as white solid, 547 mg, 73%. ^1H NMR (500 MHz, CDCl_3 , 298.0 K): δ 8.70(1H, d, $J = 4.57$ Hz, H_1), 8.08-8.05(2H, m, Hz, $\text{H}_7, 11$), 7.76-7.73(2H, m, $\text{H}_{3,4}$), 7.72-7.69(2H, m, $\text{H}_8, 10$), 7.66-7.64(2H, m, $\text{H}_{13, 13'}$), 7.47-7.43(2H, m, $\text{H}_{14, 14'}$), 7.36(1H, br. t, $J = 7.3$ Hz, H_{15}), 7.24-7.20(1H, m, H_2). ^{13}C NMR(126 MHz, CDCl_3 , 298.0 K): δ 157.1(C_{quat}), 149.7(C_1), 141.7(C_{quat}), 140.6(C_{quat}), 138.3(C_{quat}), 136.8(C_{CH}), 128.9(C_{CH}), 128.2(C_{CH}), 127.7(C_{CH}), 127.6(C_{CH}), 127.5(C_{CH}), 127.3(C_{CH}), 127.1(C_{CH}), 126.8(C_{CH}), 126.7(C_{CH}), 122.2(C_{CH}), 120.5(C_{CH}). HRMS (ASAP): $[\text{M}+\text{H}]^+$ m/z 232.1128 [232.1126 calculated for $\text{C}_{17}\text{H}_{14}\text{N}$]. The data are consistent with the literature.¹²

Ligand Hppy_c:

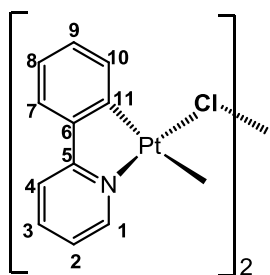


A mixture of 2-bromopyridine (700 mg, 4.43 mmol), 3-Biphenylboronic acid, (1316 mg, 6.64 mmol), Pd(OAc)₂ (99 mg, 0.44 mmol-10%), base (3050 mg, 13.3 mmol), and after work up gave **Hppy_c** as a colourless oil, 621 mg, 61%. ¹H NMR (500 MHz, CDCl₃, 298.0 K): δ 8.63(1H, d, *J* = 4.6 Hz, H₁), 8.15(1H, t, *J* = 1.6 Hz, H₇), 7.88(1H, d, *J* = 7.7 Hz, H_{ph}), 7.70-7.67(2H, m, H_{3,4}), 7.61-7.58(2H, m, H_{13,13'}), 7.56 (1H, d, *J* = 7.7 Hz, H_{ph}), 7.46(1H, t, *J* = 7.6 Hz, H_{ph}), 7.39-7.36 (2H, m, H_{14,14'}), 7.28(1H, t, *J* = 7.35 Hz, H₁₅), 7.17-7.15(1H, m, H₂). ¹³C NMR (126 MHz, CDCl₃, 298.0 K): δ ¹³C NMR 157.4(C_{quat}), 149.8(C₁), 141.8(C_{quat}), 141.1(C_{quat}), 140.0(C_{quat}), 136.8(C_{CH}), 129.2(C_{CH}), 128.8(C_{CH}), 127.8(C_{CH}), 127.4(C_{CH}), 127.3(C_{CH}), 127.2(C_{CH}), 125.9(C_{CH}), 125.9(C_{CH}), 122.3(C_{CH}), 120.7(C_{CH}), 114.5(C_{CH}). HRMS (ASAP): [M+H]⁺ *m/z* 232.1125 [232.1126 calculated for C₁₇H₁₄N]. The data are consistent with the literature.¹²

General Procedure for the Synthesis of [Pt(C^N)Cl]₂ Dimers

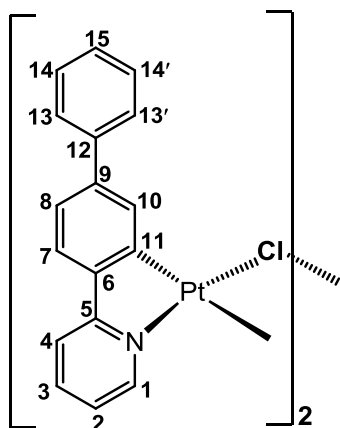
All Pt(II) complexes were synthesized according to the similar procedure.¹³ This involves heating the K₂PtCl₄ salt with 1:1 equiv. of substituted cyclometalating HC^N ligand in a 3:1 mixture of 2-ethoxyethanol and water to 80 °C under N₂ for 16-24 h. Water (10-30 ml) was added to the reaction mixture, and the resulting precipitate was isolated by filtration, washed with water diethyl ether, methanol and chloroform and dried in vacuum to give the desired dimers.

Synthesis of [Pt₂(ppy)₂Cl₂]. 4.13a



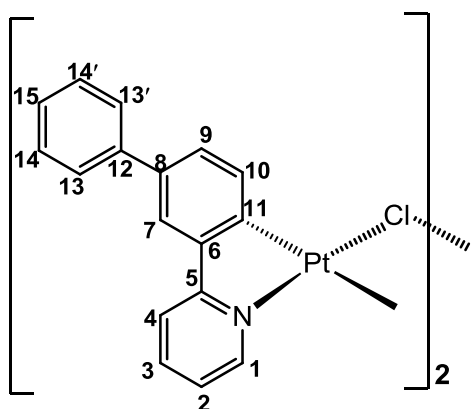
This was prepared from K₂PtCl₄ (200 mg, 0.482 mmol) and 2-phenylpyridine (Hppy) (74.79 mg, 69 μl, 0.482 mmol). After work up gave **4.13a** [Pt(ppy)(μ-Cl)]₂ as yellow crystals, 105 mg, 57%. ¹H NMR (500 MHz, DMSO, 298.0 K): δ 9.49(1H, d, *J* = 5.76 Hz, H₁), 8.22(1H, d, *J* = 7.55 Hz, H₁₀), 8.17-8.13(2H, m, H_{3,4}), 7.79(1H, dd, *J* = 1.3, 7.5 Hz, H₇), 7.52(1H, td, *J* = 1.89, 6.31 Hz, H₂), 7.11-7.21 (2H, m, H_{8,9}). ¹³C NMR (126 MHz, DMSO, 298 K): δ 165.0(C_{quar.}), 149.2(C₁), 144.(C_{quar.}), 141.5(C_{3/4}), 140.1(C_{quar.}), 133.4(C₁₀), 130.0(C_{8/9}), 124.8(C_{8/9}), 124.2(C₇), 122.7(C₂), 119.4(C_{3/4}). The data are consistent with the literature.¹⁴ The ES mass spectrum shows an ion at *m/z* 734 assigned to [Pt(ppy)₂Cl](MeCN)]⁺ confirming the ease of splitting the dimer in the presence of a coordinating solvent *i.e.* MeCN.

Synthesis of [Pt₂(Ph-ppy)₂Cl₂] 4.13b



This was prepared from **K₂PtCl₄** (150 mg, 0.361 mmol) and **L1** (83.47 mg, 0.361 mmol). After work up gave **4.15b** [Pt(ph-ppy)(μ -Cl)]₂. yellow solid 112 mg, 67%. ¹H NMR (500 MHz, DMSO, 298K) δ : 9.49(1H, d, J = 5.3 Hz, H₁) 8.64(1H, d, J = 1.6 Hz, H₁₀), 8.19(1H, br. d, J = 7.5 Hz, H₄), 8.15(1H, br. dd, J = 8.2, 1.1 Hz, H₃), 7.86(1H, d, J = 8.0 Hz, H₇), 7.68(2H, br d, J = 7.3 Hz, H₁₃, 13'), 7.54-7.52(1H, m, H₂), 7.51-7.46(3H, m, H_{8,14,14'}), 7.37(1H, br. t, J = 7.32 Hz, H₁₅). ¹³C NMR (126 MHz, DMSO, 298 K): δ 164.6(C_{quat}), 149.3(C₁), 143.7(C_{quat}), 141.5(C_{3/4}), 141.3(C_{quat}), 140.5(C_{quat}), 140.2(C_{quat}), 131.7(C₁₀), 128.9(2C_{14, 14'}), 128.7(C₈), 127.6(C₁₅), 126.7 (2C_{13/13'}), 124.7(C₇), 123.1(C₂), 119.6(C_{4/3}). The ES mass spectra show ions at m/z 926 due to [Pt₂(C[^]N)₂MeCNCl]⁺

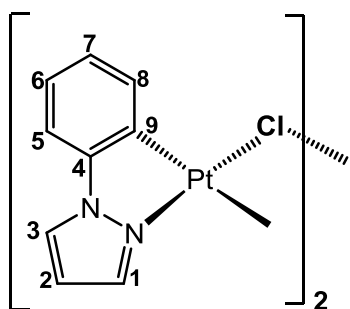
Synthesis of [Pt₂(Ph-ppy)₂Cl₂] 4.13c



This was prepared from **K₂PtCl₄** (170 mg, 0.409 mmol) and **L2** (74.79 mg, 0.409 mmol). After work up gave **4.15c** [Pt(Ph-ppy)(μ -Cl)]₂ as yellow solid, 113 mg, 61%. ¹H NMR (500 MHz, DMSO, 298K) δ 9.52(1H, dd, J = 6.4, 1.4 Hz, H₁), 8.41(1H, d, J = 8.0 Hz, H₄), 8.31(1H, d, J = 8.2 Hz, H₁₀), 8.13(1H, t, J = 7.3 Hz, H₃), 8.09(1H, s, H₇), 7.79(2H, br. d, J = 7.76 Hz, H_{13,13'}), 7.55(1H, t, J = 6.3 Hz, H₂), 7.50-7.46(3H, m, H_{9,14,14'}), 7.37(1H, br. t, J = 7.32 Hz, H₁₅). ¹³C NMR (126 MHz, DMSO, 298 K): δ 164.9(C_{quat}), 149.3(C₁), 145.2(C_{quat}), 141.6(C₃), 139.7(C_{quat}), 139.6 (C_{quat}), 136.8 (C_{quat}), 134.0(C₁₀), 128.8 (C_{9,14,14'}), 128.1(C_{9,14,14'}), 127.2 (C_{13/13'}), 126.8 (C₁₅), 126.3 (C_{13/13'}), 123.1(C_{9,14,14'}), 123.0(C₂), 122.3(C₇), 120.0(C₄). (ES), m/z 885 due to [Pt₂(C[^]N)₂Cl+MeCN]⁺

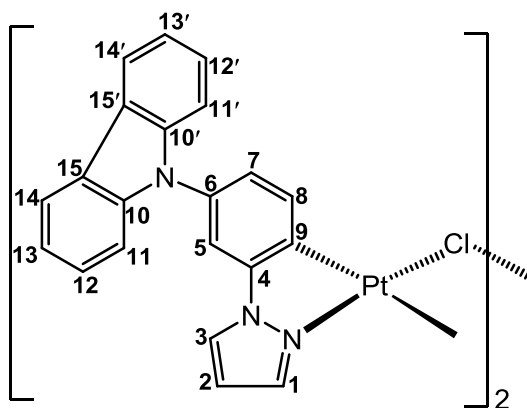
Synthesis of [Pt₂(ppz)₂Cl₂] 4.15a

This was prepared from **K₂PtCl₄** (150 mg, 0.361 mmol) and 1-phenyl-1H-pyrazole (Hppz) (52.11 mg, 48 μ l, 0.361 mmol). and after work up gave **4.15a** [Pt(ppz)(μ -Cl)]₂. as a grey solid 61 mg, 50.2%. ¹H NMR (500 MHz, DMSO, 298K) δ 8.87(1H, d, J = 2.78 Hz, H₃), 8.16(1H, d, J = 1.9 Hz, H₁), 8.13(1H, d, J = 7.2 Hz, H₈), 7.65(1H, d, J = 7.4 Hz,



H₅), 7.21(1H, t, $J = 7.2$ Hz, H₆), 7.02(1H, t, $J = 7.1$ Hz, H₇), 6.82(1H, t, $J = 2.5$ Hz, H₂). ¹³C NMR (126 MHz, DMSO, 298 K): δ 142.8(C₉), 140.3(C₃), 134.0(C₈), 128.8(C₁), 126.0(C₇), 125.2(C₆), 124.6(C₄), 112.0(C₅), 107.7(C₂). HRMS (ASAP): m/z 711[M-Cl]⁺. The data are consistent with the literature.¹⁵

Synthesis of [Pt₂(carbazoles-ppz)₂Cl₂] 4.15b



This was prepared from **K₂PtCl₄** (200 mg, 0.482 mmol) and **L3** (149.1 mg, 0.482 mmol). and after work up gave **4.15b** [Pt(carbazoles-ppz)(μ -Cl)]₂ as a grey solid 124 mg. ¹H NMR (500 MHz, DMSO, 298.0 K): δ 8.97(1H, d, $J = 2.5$ Hz, H₃), 8.42(1H, d, $J = 8.2$ Hz, H₈), 8.25(2H, br. d, $J = 8.0$ Hz, H_{carbazole}), 8.22(1H, d, $J = 2.06$ Hz, H₁),

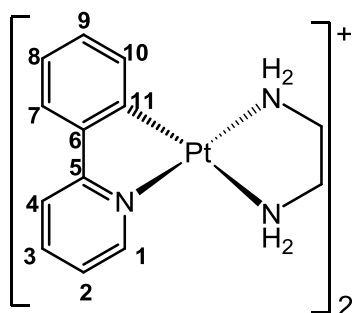
8.03(1H, d, $J = 2.1$ Hz, H₅), 7.47-7.40(4H, m, H_{carbazole}), 7.31-7.27(3H, m, H_{7, 2carbazole}), 6.83(1H t, $J = 2.52$ Hz, H₂). ¹³C NMR (126 MHz, DMSO, 298.0 K): δ 144.2(C_{quat}), 140.8(C_{CH}), 140.2(2C_{quat}), 135.3(C_{CH}), 134.2(C_{quat}), 129.7(C_{CH}), 126.3(2C_{CH}), 124.3(C_{quat}), 124(C_{CH}), 122.6(2C_{quat}), 120.4(2C_{CH}), 120.0(2C_{CH}), 111.0(C_{CH}), 109.8(2C_{CH}), 108.1(C). The (ES), 1083 assigned to [Pt₂(C[^]N)₂(MeCN)Cl]⁺

General Procedure for the Synthesis of [(C[^]N)Pt(N[^]N)]PF₆ Complexes:

It was synthesized by modifying the methodology as reported recently.⁵ In an evacuated shlenck tube, Ethylenediamine (3-3.5 mmol equiv.) was added at room temperature to a stirred solution of appropriate Pt(II) dimers [Pt(C[^]N)Cl]₂ (one mmol equiv), Potassium hexafluorophosphate (2.2-3 mmol equiv) in dry methanol (5-7ml). The mixture was placed under a N₂ atmosphere and the mixture was stirred for 15 mins to overnight at room temperature. After this time, the solvent removed under reduced pressure, leaving behind a solid. This crude solid was washed with water, diethyl ether and chloroform (3×10 ml) respectively and dried in high vacuum to give the desired complexes.

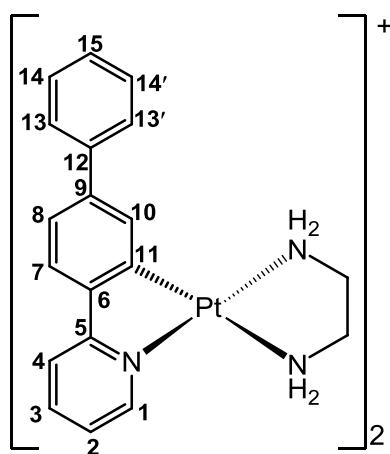
Synthesis of 4.16a

This was prepared from the solution of **4.13a** (70 mg, 0.129 mmol), Ethylenediamine (26 μ l, 0.389 mmol) and KPF₆ (53 mg, 0.285 mmol) and after work up gave **4.16a** as a yellow solid 55 mg, 76%. ¹H NMR (500 MHz, DMSO, 298.0 K): δ 8.58(1H, d, $J = 5.5$ Hz, H₁), 8.10(1H, br. t, $J = 7.32$ Hz, H₃), 8.02-8.06(1H, d, $J = 7.8$ Hz, H₄), 7.70(1H, br. d,



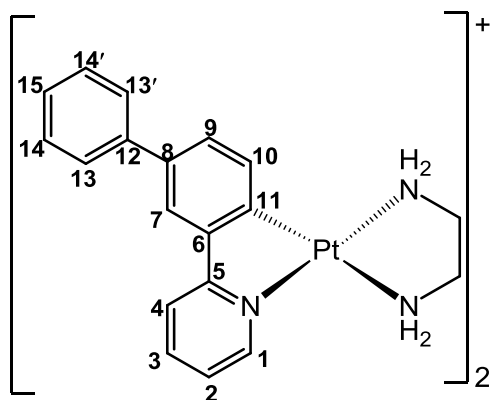
$J = 3.6$ Hz, H_7), 7.37(1H, t, $J = 5.8$ Hz, H_2), 7.27-7.25(1H, m, H_{10}), 7.13-7.10(2H, m, $H_{8,9}$), 6.04(2H, br. s., H_{NH_2}), 5.23(1H, br. s., H_{NH_2}), 2.67(4H, br. s., $H_{CH_2-CH_2}$). ^{13}C NMR (126 MHz, DMSO, 298.0 K): δ 166.4(C_{quat}), 151.0(C_1), 145.0(C_{quat}), 144.1(C_{quat}), 139.9(C_3), 133.6(C_{10}), 129.5($C_{8,9}$), 124.0(C_7), 123.6($C_{8,9}$), 123.2(C_2), 119.4(C_4), 47.8(C_{CH_2}), 43.5(C_{CH_2}). HRMS (ESI): m/z 409.0992[409.0992 calculated for $C_{13}H_{16}N_3^{195}Pt$]. The data are consistent with the literature.¹⁶

Synthesis of 4.16b



This was prepared from the **4.13b** (60 mg 0.065 mmol), Ethylenediamine (10 μ l 0.143 mmol) and KPF_6 (29 mg, 0.156 mmol) and after work up gave **4.16b** as a yellow solid 49 mg, 60%. 1H NMR (500 MHz, DMSO, 298.0 K): δ 8.62(1H, d, $J = 5.3$ Hz, H_1), 8.12(1H, d, $J = 7.3$ Hz, H_4), 8.09(1H, br. d, $J = 7.32$ Hz, H_3), 7.79(1H, br. d, $J = 8$ Hz, H_7), 7.75(2H, br. d, $J = 7.3$ Hz, $H_{13,13'}$), 7.57(1H, br. s, H_{10}), 7.49(2H, t, $J = 7.3$ Hz, $H_{14,14'}$), 7.42(1H, br. t, $J = 7.1$ Hz, H_8), 7.40-7.36(2H, m, $H_2, 15$), 6.16(2H, br. s., H_{NH_2}), 5.30(2H, br. s., H_{NH_2}), 2.71(4H, br. s., $H_{CH_2-CH_2}$). ^{13}C NMR (126 MHz, DMSO, 298.0 K): δ 166.1(C_{quat}), 151.0(C_1), 144.5(C_{quat}), 144.3(C_{quat}), 141.0(C_{quat}), 140.3(C_{quat}), 139.9(C_4), 131.9(C_{10}), 128.8 ($2C_{14,14'}$), 127.6($C_{2/15}$), 126.7($2C_{13,13'}$), 124.3(C_7), 123.2(C_8), 122.1($C_{2/15}$), 119.5(C_3), 47.7 (C_{CH_2}), 43.6(C_{CH_2}). HRMS (ESI): m/z 485.1303[485.1305 calculated for $C_{19}H_{20}N_3^{195}Pt$].

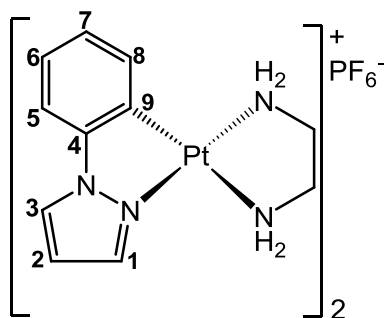
Synthesis of 4.16c



This was prepared from the **4.13c** (60 mg 0.065 mmol), Ethylenediamine (10 μ l, 0.143 mmol) and KPF_6 (29 mg, 0.156 mmol) and after work up gave **4.16c** as yellowish solid 60 mg, 73 %. 1H NMR (500 MHz, DMSO, 298.0 K): δ 8.63(1H, d, $J = 5.26$ Hz, H_1), 8.29(1H, d, $J = 8.0$ Hz, H_4), 8.15(1H, t, $J = 7.2$ Hz, H_3), 8.04(1H, d, $J = 1.6$ Hz, H_7), 7.78(2H, br. d, $J = 7.3$ Hz, $H_{13,13'}$), 7.49-7.46(3H, m, $H_{14,14',9}$), 7.41(1H, t, $J = 6.1$ Hz, H_2),

7.38-7.34(2H, m, H_{10,15}), 6.11(2Hbr. s., H_{NH2}), 5.30(2H, br. s., H_{NH2}), 2.70(4H, br. s., H_{CH2-CH2}) ¹H NMR ¹³C NMR (126 MHz, DMSO, 298.0 K): δ 166.3(C_{quat}), 151.0(C₁), 145.9(C_{quat}), 143.5(C_{quat}), 140.2(C_{quat}), 139.9(C₃), 135.5(C_{quat}), 134.2(C_{10/15}), 128.8(2C_{14,14'/9}), 127.7(C_{14/14'/9}), 127.0(C_{10/15}), 126.2(2C_{13,13'}), 123.4(C₂), 122.0(C₇), 119.8(C₄), 47.9(C_{CH2}), 43.5(C_{CH2}). HRMS (ESI): *m/z* 485.1305 [485.1305 calculated for C₁₉H₂₀N₃¹⁹⁵Pt].

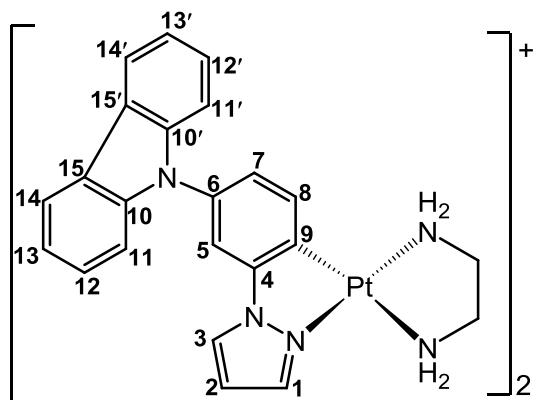
Synthesis of 4.17a



This was prepared from the **4.15a** (80 mg 0,11 mmol), Ethylenediamine (10μl, 0.22 mmol) and KPF₆ (47.3 mg, 0.26 mmol) and after work up gave **4.17a** as a yellow- white solid 70 mg, 60%. ¹H NMR (500 MHz, DMSO, 298.0 K): δ 8.75(1H, d, *J* = 2.5 Hz, H₃), 8.00(1H, d, *J* = 1.8 Hz, H₁), 7.56(1H, d, *J* = 7.3 Hz,

H₅), 7.30(1H, d, *J* = 6.4 Hz, H₈), 7.14(1H, t, *J* = 7.1 Hz, H₆), 7.01(1H, t, *J* = 6.9 Hz, H₇), 6.76(1H, t, *J* = 2.5 Hz, H₂), 6.14(2H, br. s., H_{NH2}), 5.30(2H, br. s., H_{NH2}), 2.66(4H, br. s., H_{CH2-CH2}). ¹H NMR ¹³C NMR (126 MHz, DMSO, 298.0 K): δ 144.0(C_{quat}), 141.4(C₁), 134.6(C₈), 129.0(C_{quat}), 128.0(C₃), 125.4(C₇), 124.0(C₅), 111.4(C₆), 107.8(C₂), 47.5(C_{CH2}), 44.1(C_{CH2}). HRMS (ESI): *m/z* 389.0945 [389.0944 calculated for C₁₁H₁₅N₄¹⁹⁵Pt]. The data are consistent with the literature.¹⁷

Synthesis of 4.17b



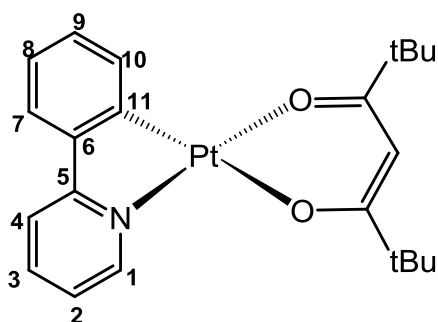
This was prepared from the **4.15b** (60 mg 0,56 mmol), Ethylenediamine (12μl, 0.167 mmol) and KPF₆ (31 mg, 0.167 mmol) and after work up gave **4.17b** as a gray solid 25 mg, 45%. ¹H NMR (400 MHz, CD₃CN, 298.0 K): δ 8.18-8.16(2H, m, H_{3, 8}), 8.15-8.14(1H, m, H_{carbazole}), 7.80(1H, d, *J* = 2.3 Hz, H₁), 7.56(1H, d, *J*

= 1.9 Hz, H₅), 7.44-7.37(5H, m, H_{carbazole}), 7.27(2H, ddd, *J* = 7.8, 5.5, 2.4 Hz, H₇, carbazole), 7.20(1H, dd, *J* = 7.8, 2.0 Hz, H_{carbazole}), 6.60(1H, t, *J* = 2.6 Hz, H₂), 5.03(2H, br. s., H_{NH2}), 4.29(2H, br. s., H_{NH2}), 2.85(4H, br. s., H_{CH2-CH2}). ¹³C NMR (126 MHz, DMSO, 298.0 K): δ 145.1(C_{quat}), 141.6(C₁), 140.6(2C_{quat}), 134.7(C₅), 133.7(C_{quat}), 127.8(C₃), 126.7(C_{quat}), 126.0(2C_{carbazole}), 124.0(C₇), 122.7(2C_{quat}), 120.0(2C_{carbazole}), 119.7(2C_{carbazole}), 110.4(C₈), 109.7(2C_{carbazole}), 107.7(C₂), 47.3(C_{CH2}), 44.0(C_{CH2}). HRMS (ESI): *m/z* 563.1534 [563.1523 calculated for C₂₃H₂₂N₅¹⁹⁵Pt].

General Procedure for the Synthesis of [(C^N)Pt(O[^]O)] Complexes:

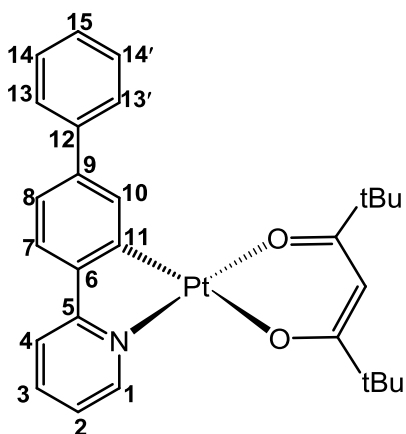
The appropriate dimers Pt(C^N)Cl₂ (one equiv.), dipivaloylmethane (Hdpm) (2.5-3 equiv.) and sodium carbonate (3-4 equiv.) in dry methanol 5-7 ml. the mixture was allowed to react under nitrogen atmosphere for 3–24 hrs at room temperature. After this time the solvent was removed under reduced pressure, and the residue was dissolved in DCM (15-30 ml) and passed through celite. The filtrate was evaporated leaving behind a solid which was isolated and the compounds could be recrystallised from DCM/MeOH

Synthesis of 4.18a



This was prepared from the **4.13a** (60 mg, 0.078 mmol), (Hdpm) (50 μ l, 0.234 mmol) and Na₂CO₃ (99 mg, 0.94 mmol) and after work up gave **4.18a** as yellow solid, 55 mg, 66%. ¹H NMR (500 MHz, CDCl₃, 298.0 K): δ 9.01(1H, d, J = 5.2 Hz, H₁), 7.80(1H, td, J = 7.7, 1.4 Hz, H₃), 7.66(1H, br d, J = 7.6 Hz, H₁₀), 7.62(1H, br d, J = 7.9 Hz, H₃), 7.44(1H, br d, J = 7.4 Hz, H₇), 7.21(1H, br t, J = 6.9 Hz, H₉), 7.10(2H, m, H_{2,8}), 5.81(1H, s, H_{CH}), 1.28 (9H, s, H_{tBu}), 1.27 (9H, s, H_{tBu}). (126 MHz, DMSO, 298.0 K): δ 168.6(C_{quat}), 152.5(C_{quat}), 147.1(C₁), 140.1(C_{quat}), 138.0(C₃), 131.0(C₁₀), 129.3(C₉), 123.4(C_{2/8}), 123.0(C₇), 121.2(C_{2/8}), 118.3(C₄), 93.2(C_{CH}), 51.0(C_{quat}), 28.7(C_{tBu}), 28.4(C_{tBu}). One quaternary carbon was not observed. HRMS (ASAP): [M+H]⁺, m/z 533.1776 [533.1768 calculated for C₂₂H₂₈NO₂¹⁹⁵Pt]. The data are consistent with the literature.¹⁸

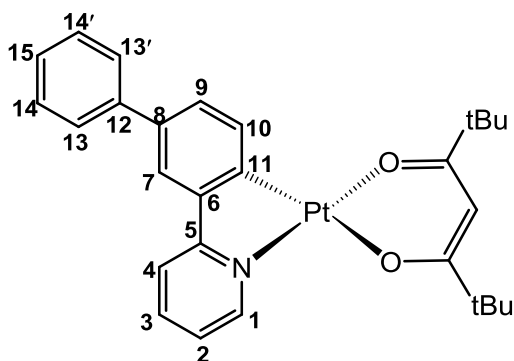
Synthesis of 4.18b



This was prepared from the **4.13b** (70 mg 0.076 mmol), Hdpm (52 μ l, 0.23 mmol) and Na₂CO₃ (73 mg, 0.68 mmol) and after work up gave **4.18b** as yellowish solid 60 mg, 73 %. ¹H NMR (500 MHz, CDCl₃, 298.0 K): δ 9.02(1H, d, J = 5.7 Hz, H₁), 7.89(1H, d, J = 1.2 Hz, H₁₀), 7.81(1H, td, J = 7.5, 1.5 Hz, H₃), 7.73(2H, br. d, J = 7.5 Hz, H_{13,13'}), 7.65(1H, d, J = 7.9 Hz, H₄), 7.52(1H, d, J = 8.0 Hz, H₇), 7.46(2H, br. t, J = 7.6 Hz, H_{14,14'}), 7.39-7.33(2H, m, H_{8,15}), 7.13(1H, t, J = 6.2 Hz, H₂), 5.84(1H, s, H_{CH}), 1.31(9H, s, H_{tBu}), 1.30(9H, s, H_{tBu}). ¹³C NMR (126 MHz, CDCl₃, 298.0 K): δ 146.2(C₁), 142.9 (C_{quat}), 140.7(C_{quat}),

140.5(C_{quat}), 139.3(C_{quat}), 137.0(C₃), 128.2(C₁₀), 127.6(2C_{14,14'}), 126.2(2C_{13,13'}), 126.1(C₇), 122.3(C_{8/15}), 121.4(C_{8/15}), 120.1(C₂), 117.4(C₄), 92.3(C_{CH}), 40.5(C_{quat}), 40.1(C_{quat}), 27.6(C_{tBu}), 27.4(C_{tBu}). One quart. carbon was not observed. HRMS (ASAP): [M+H]⁺, *m/z* 609.2084 [609.2081 calculated for C₂₈H₃₂NO₂¹⁹⁵Pt].

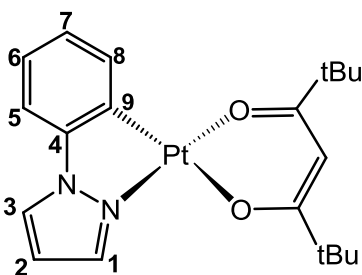
Synthesis of 4.18c



This was prepared from the **4.13c** (52 mg, 0.056 mmol), Hdpm (36 μ l, 0.17 mmol), Na₂CO₃ (72 mg, 0.68 mmol) and after work up, the crude was Purification by flash chromatography on a silica gel (DCM 100%): to gave **4.18c** as yellowish solid 44 mg, 64%. ¹H NMR (500 MHz, CDCl₃, 298.0 K): δ 8.97(1H, br. d, *J* = 5.20 Hz, H₁), 7.74-

7.78(1H, m, H₃), 7.67(1H, br. d, *J* = 7.9, Hz, H₇), 7.64(1H, br. d, *J* = 7.9, Hz, H₄), 7.55-7.60(3H, m, H_{13/13'}, 9), 4.41(1H, dd, *J* = 7.9, 1.7 Hz, H₁₀), 7.39-7.39 (2H, m, H_{14,14'}), 7.26(1H, t, *J* = 7.3, Hz, H₁₅), 7.09-7.05 (1H, m, H₂), 5.76(1H, s, H_{CH}), 1.23(1H, s, H_{tBu}), 1.21(9H, s, H_{tBu}). ¹³C NMR (126 MHz, CDCl₃, 298.0 K): δ 195.1(C_{quat}), 193.8(C_{quat}), 168.4(C_{quat}), 147.2(C₁), 145.2(C_{quat}), 141.9(C_{quat}), 139.4(C_{quat}), 138.0(C₃), 136.5(C_{quat}), 131.4(C₇), 128.7(2C_{14,14'}), 128.3(C₁₀), 126.7(2C_{13/13'}), 126.6(C₁₅), 121.4(C₉), 121.0(C₂), 118.4(C₄), 93.3(C_{CH}) 41.5(C_{C-tBu}), 29.7(C_{C-tBu}), 28.7(C_{tBu}), 28.4(C_{tBu}). The high resolution mass spectrum (ASAP) show [M+H]⁺ *m/z* 609.2091 [609.609.81 calculated for C₂₈H₃₂NO₂¹⁹⁵Pt].

Synthesis of 4.19a

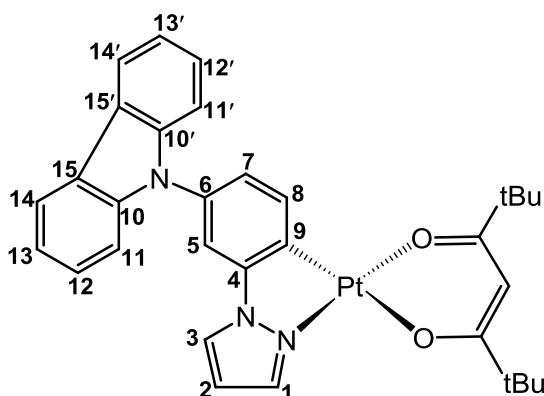


This was prepared from the **4.15a** (60 mg, 0.080 mmol), Hdpm (54 μ l, 0.24 mmol), Na₂CO₃ (77 mg, 0.72 mmol) and after work up gave **4.19a** as greenish solid 52 mg, 61 %. ¹H NMR (500 MHz, CDCl₃, 298.0 K): δ 7.91(1H, d, *J* = 2.78 Hz, H₃), 7.74(1H, d, *J* = 1.99 Hz, H₁), 7.60-7.56(1H, m, H₈), 7.06-7.11(3H, m, H_{5,6,7}), 6.49(1H, t, *J* = 2.38 Hz,

H₂), 5.81(1H, s, H_{CH}), 1.27(9H, s, H_{tBu}), 1.25(9H, s, H_{tBu}). ¹³C NMR (126 MHz, CDCl₃, 298.0 K): δ 144.5(C_{quat}), 137.2(C₁), 132.0(C₈), 125.4(C₃), 125.0(C_{5/6/7}), 123.7(C_{5/6/7}), 123.3(C_{quat}), 109.9(C_{5/6/7}), 106.2(C₂), 93.0(C_{CH}), 41.5(C_{C-tBu}), 41.0(C_{C-tBu}), 28.6(C_{tBu}),

28.2(C_{tBu}). HRMS (ASAP): [M+H]⁺, *m/z* 522.1723[522.1720 calculated for C₂₀H₂₇N₂O₂¹⁹⁵Pt]. The data are consistent with the literature.¹⁹

Synthesis of 4.19b



This was prepared from the **4.15b** (100 mg, 0.093 mmol), Hdpm (60 μ l, 0.28 mmol), Na₂CO₃ (74 mg, 0.69 mmol) and after work up gave **4.19b** as light yellow 60 mg, 49.7%. ¹H NMR (500 MHz, CD₃CN, 298.0 K): δ 8.25(1H, d, *J* = 2.8 Hz, H₃), 8.20(2H, d, *J* = 7.8 Hz, H_{carbazole}), 7.86(1H, d, *J* = 2.1 Hz, H₁), 7.73(1H, d, *J* = 7.7 Hz, H₈), 7.59(1H, d,

J = 1.8 Hz, H₅), 7.45-7.43(4H, m, H_{carbazole}), 7.31-7.28 (3H, m, H_{7, carbazole}), 6.65(1 H, t, *J* = 2.5 Hz, H₂), 5.95(1H, s, H_{CH}), 1.28(9H, s, H^t_{Bu}), 1.27(9H, s, H^t_{Bu}). ¹³C NMR (126 MHz, CDCl₃, 298.0 K): δ 145.6(C_{quat}), 140.7(2C_{quat}), 137.9(C₁), 133.1(C_{quat}), 132.3(C₈), 127.5(C₃), 125.8 (2C_{carbazole}), 123.1(C₇), 122.7(C_{quat}), 120.6(2C_{quat}), 119.9(2C_{carbazole}), 119.6(2C_{carbazole}), 109.7(2C_{carbazole}) 109.6(C₅), 106.8(C₂), 93.0(C_{CH}), 27.5(C_{tBu}), 27.1(C_{tBu}). HRMS (ASAP): [M+H]⁺, *m/z* 687.2318[687.2299 calculated for C₃₂H₃₄N₃O₂¹⁹⁵Pt].

Bibliography

1. F. Wang and A. W. Schwabacher, *Tetrahedron Lett.*, 1999, **40**, 4779-4782.
2. X. Y. Yu, L. Deng, B. Zheng, B. R. Zeng, P. Yi and X. Xu, *Dalton Trans.*, 2014, **43**, 1524-1533.
3. W. S. Yu, C. C. Cheng, Y. M. Cheng, P. C. Wu, Y. H. Song, Y. Chi and P. T. Chou, *J. Am. Chem. Soc.*, 2003, **125**, 10800-10801.
4. M. Pichette Drapeau, T. Ollevier and M. Taillefer, *Chem. Eur. J.*, 2014, **20**, 5231-5236.
5. C. Liu, X. Lv, Y. Xing and J. Qiu, *J. Mater. Chem. C.*, 2015, **3**, 8010-8017.
6. D. L. Davies, M. P. Lowe, K. S. Ryder, K. Singh and S. Singh, *Dalton Trans.*, 2011, **40**, 1028-1030.
7. N. M. Shavaleev, F. Monti, R. Scopelliti, N. Armaroli, M. Grätzel and M. K. Nazeeruddin, *Organometallics*, 2012, **31**, 6288-6296.
8. J. Y. Li, C. Lee, C. Y. Chen, W. L. Lee, R. Ma and C. G. Wu, *Inorg. Chem.*, 2015, **54**, 10483-10489.
9. E. Cristina Souza Brenelli and P. Moran, *The reactivity of some primary amines in SN2Ar reactions with 2- and 4-chloro-1-methylpyridinium ions*, 1989.
10. Q. Shi, R. J. Thatcher, J. Slattery, P. S. Sauari, A. C. Whitwood, P. C. McGowan and R. E. Douthwaite, *Chem. Eur. J.*, 2009, **15**, 11346-11360.
11. F. Chen, N. Liu, E. Ji and B. Dai, *RSC Advances*, 2015, **5**, 51512-51523.
12. S. K. Gurung, S. Thapa, B. Shrestha and R. Giri, *Org. Chem. Front.*, 2015, **2**, 649-653.
13. C. O'Brien, M. Y. Wong, D. B. Cordes, A. M. Z. Slawin and E. Zysman Colman, *Organometallics*, 2015, **34**, 13-22.
14. T. Pawlak, D. Niedzielska, J. Vícha, R. Marek and L. Pazderski, *J. Organomet. Chem.*, 2014, **759**, 58-66.
15. W. Wu, H. Guo, W. Wu, S. Ji and J. Zhao, *Inorg. Chem.*, 2011, **50**, 11446-11460.
16. S. S. Pasha, P. Das, N. P. Rath, D. Bandyopadhyay, N. R. Jana and I. R. Laskar, *Inorg. Chem. Commun.*, 2016, **67**, 107-111.
17. E. A. Katlenok, E. V. Ivanova, M. V. Puzyk and K. P. Balashev, *Optics and Spectroscopy*, 2012, **113**, 279-283.
18. A. F. Henwood, J. Webster, D. Cordes, A. Z. Slawin, D. Jacquemin and E. Zysman-Colman, *RSC Advances*, 2017, **7**, 25566-25574.

19. B. K. T. Batagoda, P. I. Djurovich, S. Bräse and M. E. Thompson, *Polyhedron*, 2016, **116**, 182-188.

Appendix

X-Ray crystal

The X-ray diffraction data were collected on a Bruker APEX 2000 CCD diffractometer using graphite-monochromated Mo-K α radiation, $\lambda = 0.71073 \text{ \AA}$.

Table 1: X-ray data for ppz complexes **2.16aHL₁**, **2.16aHL₂**, **2.16aHL₃**, and **2.17aL₂**

Compound reference	2.16aHL₁	2.16aHL₂	2.16aHL₃	2.17aL₂
Chemical formula	C ₂₆ H ₂₁ F ₆ IrN ₇ P (H ₂ O)	C ₃₀ H ₂₉ F ₆ IrN ₇ P (C ₆ H ₁₄)	(C ₃₂ H ₂₅ F ₆ IrN ₇ P) ₂₂ (CH ₂ Cl ₂) (H ₂ O)	C ₃₀ H ₂₈ Ir N ₇ (CH ₂ Cl ₂)
Formula Mass	786.68	910.94	1792.46	763.72
Temperature/K	150(2)	150(2)	150(2)	150(2)
Crystal system	Orthorhombic	Orthorhombic	Monoclinic	Orthorhombic
Space group	Pbca	Fdd2	P2(1)/n	Pbca
a/ \AA	10.379(4)	26.346(4)	19.438(3)	17.859(3)
b/ \AA	16.873(6)	53.628(7)	16.341(3)	16.147(3)
c/ \AA	30.938(11)	9.5813(13)	21.309(4)	21.284(3)
α / $^\circ$	90	90	90	90
β / $^\circ$	90	90	106.081(3)	90
γ / $^\circ$	90	90	90	90
U/ \AA^3	5418(3)	13537(3)	6504.0(19)	6137.8(16)
No. of formula units per unit cell, Z	8	16	4	8
Density (calc.) Mg/m ³	1.929	1.788	1.831	1.653
Abs. coefficient/mm ⁻¹	5.065	4.066	4.310	4.558
F(000)	3056	7264	3504	3008
Crystal size mm	0.18 x 0.17 x 0.08	0.29 x 0.14 x 0.06	0.16 x 0.15 x 0.09	0.24x0.16x 0.09
Theta range $^\circ$	2.36 to 26.00	1.72 to 26.00	1.26 to 26.00	1.91 to 26.00
Index ranges	-12<=h<=12, -20<=k<=20, -38<=l<=38	-32<=h<=32, -66<=k<=66, -11<=l<=11	-23<=h<=23, -17<=k<=20, -26<=l<=18	-21<=h<=22, -19<=k<=19, -26<=l<=25
No. of reflections measured	40184	26207	33347	46125
No. of independent reflections	5327 [R(int) = 0.1309]	6648 [R(int) = 0.0930]	12730 [R(int) = 0.0791]	6029 [R(int) = 0.1289]
Data / restraints / parameters	5327 / 0 / 370	6648 / 7 / 409	12730 / 0 / 880	6029 / 0 / 370
Goodness-of-fit, F ²	0.894	1.032	0.833	0.946
Final R indices [I>2 σ (I)]	R1 = 0.0460, wR2 = 0.0740	R1 = 0.0537, wR2 = 0.1345	R1 = 0.0441, wR2 = 0.0678	R1 = 0.0461, wR2 = 0.0900
R indices (all data)	R1 = 0.1025, wR2 = 0.0854	R1 = 0.0623, wR2 = 0.1388	R1 = 0.0760, wR2 = 0.0748	R1 = 0.0848, wR2 = 0.1004
Largest diff. peak and hole e. \AA^{-3}	1.279 and -0.782	1.683 and -2.254	1.395 and -1.101	1.337 and -1.148

Table 2: X-ray data for ppy complexes **2.16cHL₁**, **2.16cHL₂**, **2.16cHL₃**, and **2.17cL₃** .

Compound reference	2.16cHL₁	2.16cHL₂	2.16cHL₃	2.17cL₃
Chemical formula	C ₃₀ H ₂₃ F ₆ IrN ₅ P (H ₂ O)	(C ₃₄ H ₃₁ F ₆ IrN ₅ P) ₂ (C ₆ H ₁₂) ₂ (H ₂ O)(3H)	C ₃₆ H ₂₇ F ₆ Ir N ₅ P (CHCl ₃) ₂ (H ₂ O)	(C ₃₆ H ₂₆ IrN ₅) ₄ (CH ₂ Cl ₂) ₇
Formula Mass	808.72	1883.98	1123.55	3477.75
Temperature/K	150(2)	150(2)	150(2)	150(2)
Crystal system	Orthorhombic	Triclinic	Monoclinic	Monoclinic
Space group	Pbca	P-1	P2(1)/n	P2(1)/n
a/Å	10.7474(16)	11.648(5)	15.389(3)	15.196(3)
b/Å	17.421(3)	16.487(7)	14.072(2)	10.3751(19)
c/Å	31.295	19.704(9)	19.607(3)	21.860(4)
α/°	90	91.865(7)	90	90
β/°	90	100.706(7)	94.216(3)	99.262(4)
γ/°	90	93.332(7)	90	90
U/Å ³	5859.5(15)	3708(3)	4234.6(12)	3401.5(11)
No. of formula units per unit cell, Z	8	2	4	1
Density (calc.) Mg/m ³	1.833	1.687	1.762	1.698
Abs. coefficient/mm ⁻¹	4.684	3.713	3.634	4.236
F(000)	3152	1884	2200	1710
Crystal size mm	0.15 x 0.09 x 0.04	0.24 x 0.16 x 0.04	0.22 x 0.12 x 0.05	0.18 x 0.14 x 0.10
Theta range°	2.30 to 26.00	1.66 to 26.00	1.63 to 26.00	1.52 to 26.00
Index ranges	-13<=h<=12, -21<=k<=21, -38<=l<=38	-14<=h<=14, -20<=k<=20, -24<=l<=24	-18<=h<=18, -17<=k<=17, -24<=l<=24	18<=h<=18, -12<=k<=12, -26<=l<=26
No. of reflections measured	43518	28454	32497	25993
No. of independent reflections	5755 [R(int) = 0.0989]	14329 [R(int) = 0.0779]	8309 [R(int) = 0.0845]	6688 [R(int) = 0.1505]
Data / restraints / parameters	5755 / 0 / 397	14329 / 5 / 862	8309 / 0 / 442	6688 / 0 / 433
Goodness-of-fit, F ²	0.977	0.911	0.943	0.896
Final R indices [I>2σ(I)]	R1 = 0.0414, wR2 = 0.0762	R1 = 0.0553, wR2 = 0.1140	R1 = 0.0417, wR2 = 0.0888	R1 = 0.0589, wR2 = 0.0953
R indices (all data)	R1 = 0.0876, wR2 = 0.0864	R1 = 0.0933, wR2 = 0.1231	R1 = 0.0570, wR2 = 0.0922	R1 = 0.1170, wR2 = 0.1085
Largest diff. peak and hole e.Å ⁻³	0.918 and -0.811	3.711 and -1.840	1.199 and -0.675	2.056 and -1.148

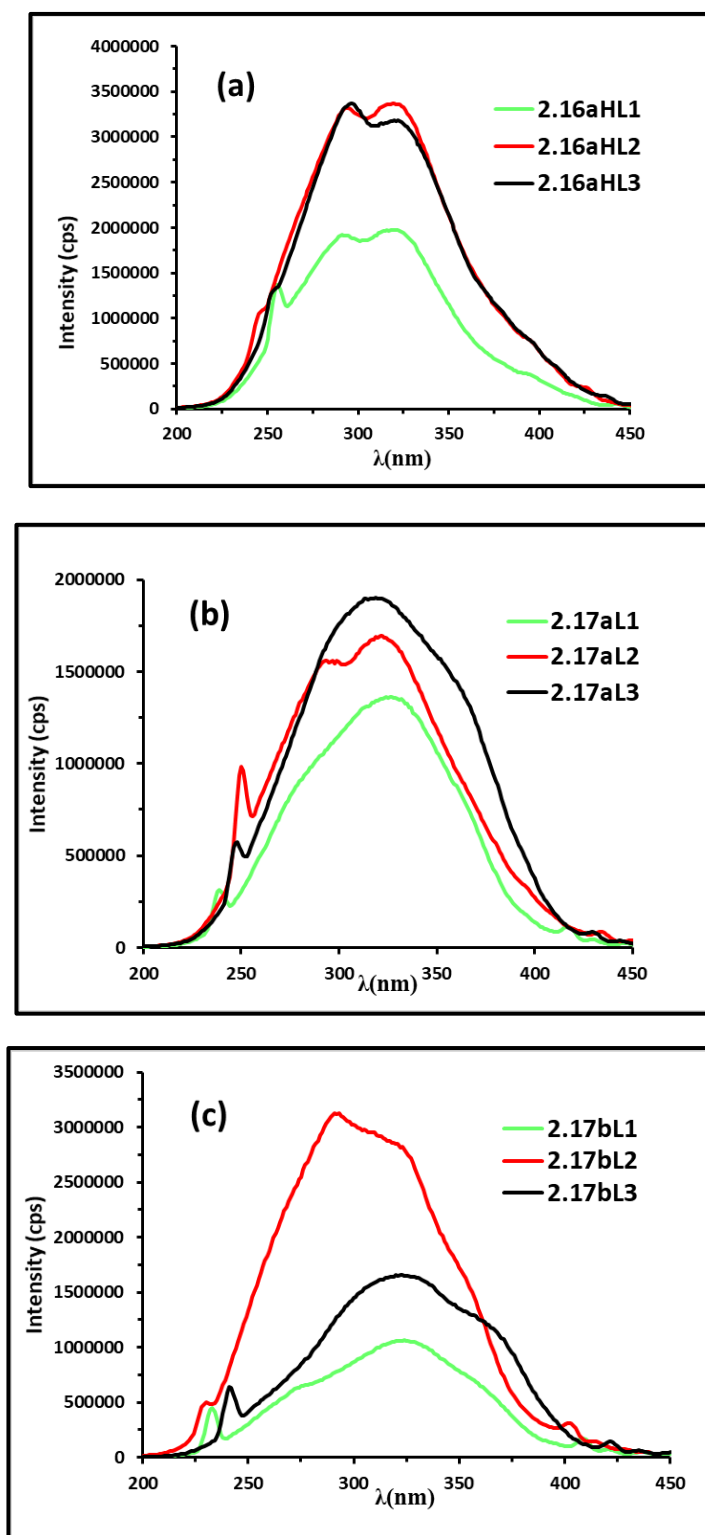


Figure 1: Excitation spectra of (a) cationic ppz complexes **2.16aHL**₁₋₃, (b) neutral ppz complexes **2.17aL**₁₋₃, and (c) neutral ppz-CF₃ complexes **2.17bL**₁₋₃ in MeCN at 0.02(—) and 0.2(- - -)mM.

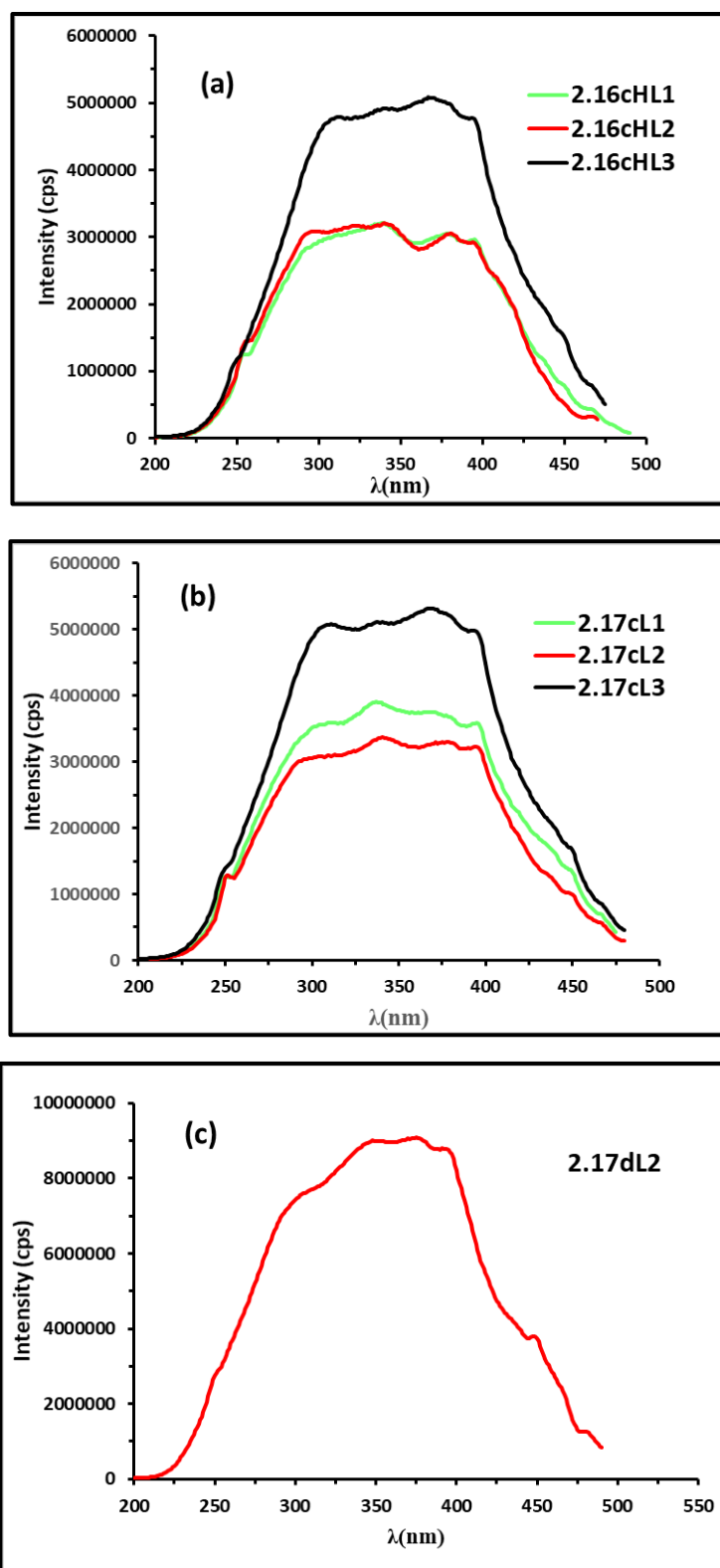
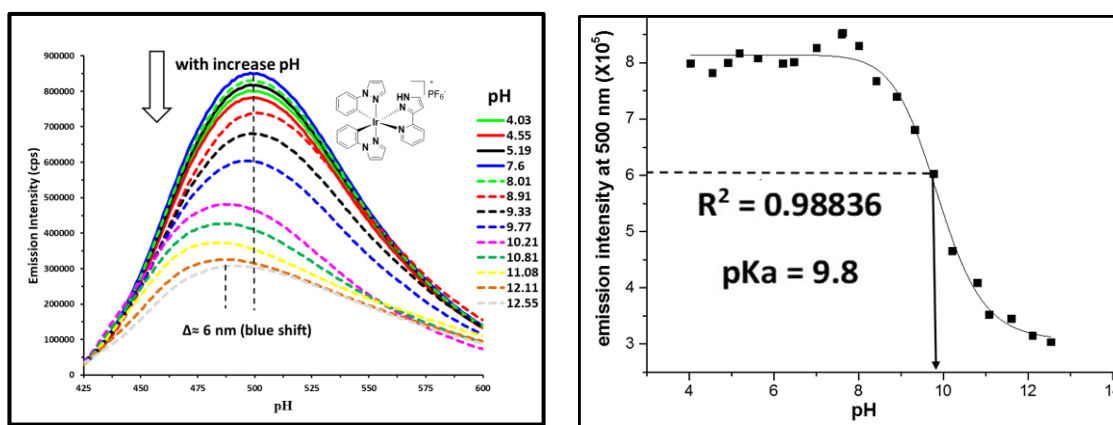


Figure 2: Excitation spectra of (a) cationic ppy complexes **2.16cHL**₁₋₃, (b) neutral ppy complexes **2.17cL**₁₋₃, and (c) neutral ppy- CF_3 complexes **2.17dL**₂ in MeCN at 0.02(—) and 0.2(- - -)mM.



A(i)

A(ii)

Figure 3: **A(i).** Emission titration spectra of complex **2.16aHL₁** (0.02mM) at various pH values in MeCN/H₂O (1:9), with the addition of 0.1 M HCl(—) and NaOH(---), respectively in air excitation at 324 nm. **A(ii).** A plot of emission intensity of complex **2.16aHL₁** against different pH.

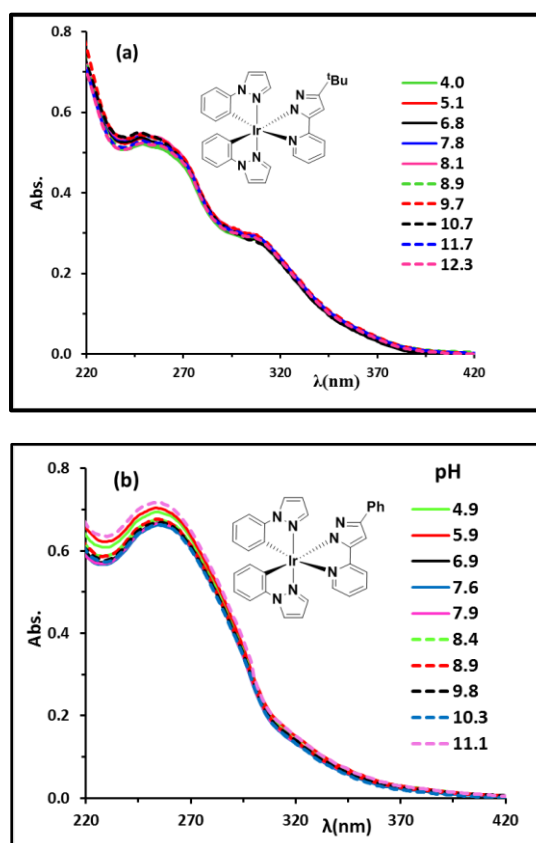


Figure 4: Changes in UV-vis spectra of complexes **a: 2.17aL₂** and **b: 2.17aL₃** (0.02mM) at various pH values in MeCN/H₂O (1:9), with the addition of 0.1 M HCl(—) and 0.1 M NaOH(---) at RT.

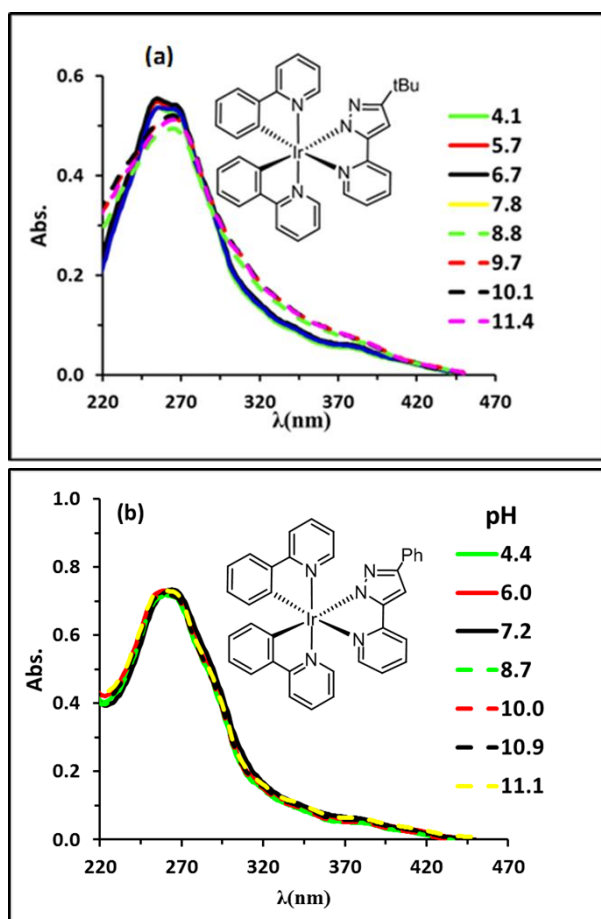


Figure 5: Changes in UV-vis spectra of complexes **a: 2.17cL₂** and **b: 2.17cL₃** (0.02mM) at various pH values in MeCN/H₂O (1:9), with the addition of 0.1 M HCl(—) and 0.1 M NaOH(- -) at RT.

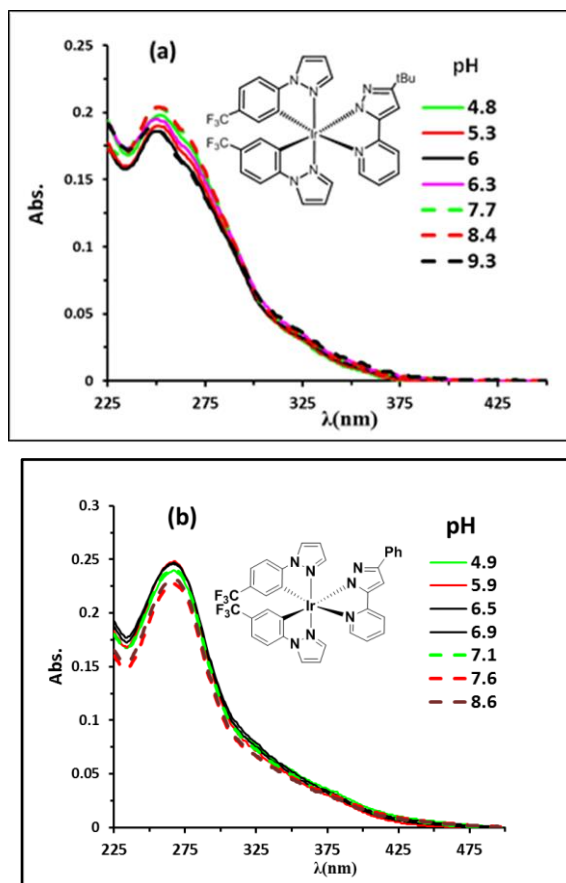


Figure 6: Changes in

UV-vis spectra of complexes **a: 2.17bL₂** at (0.005 mM) and **b: 2.17bL₃** (0.02mM) at various pH values in MeCN/H₂O (1:9) with the addition of 0.1 M HCl(—) and 0.1 M NaOH(- - -) at RT.

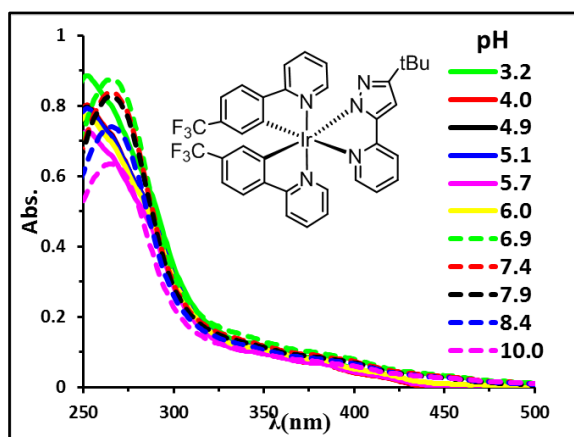


Figure 7: Selected absorbance spectra of complex **2.17dL₂** (0.02mM) at various pH values in MeCN/H₂O (1:9), with the addition of 0.1 M HCl(—) and 0.1 M NaOH (- - -) at RT.

Table 3. Bond lengths [\AA] and angles [$^\circ$] for [*p*-H₂PYE₁]₂

Bond lengths	[\AA]	Angles	[$^\circ$]	angles	[$^\circ$]
N(1)-C(1)	1.354(4)	C(1)-N(1)-C(5)	119.2(3)	N(1)-C(6)-H(6B)	109.5
N(1)-C(5)	1.356(4)	C(1)-N(1)-C(6)	120.6(3)	H(6A)-C(6)-H(6B)	109.5
N(1)-C(6)	1.468(4)	C(5)-N(1)-C(6)	120.2(3)	N(1)-C(6)-H(6C)	109.5
N(2)-C(3)	1.326(4)	C(3)-N(2)-C(7)	125.5(3)	H(6A)-C(6)-H(6C)	109.5
N(2)-C(7)	1.455(4)	C(3)-N(2)-H(2B)	119.3	H(6B)-C(6)-H(6C)	109.5
N(2)-H(2B)	0.7754	C(7)-N(2)-H(2B)	115.0	N(2)-C(7)-C(7)#1	113.2(2)
C(1)-C(2)	1.360(5)	N(1)-C(1)-C(2)	122.2(3)	N(2)-C(7)-H(7A)	108.9
C(1)-H(1)	0.9500	N(1)-C(1)-H(1)	118.9	C(7)#1-C(7)-H(7A)	108.9
C(2)-C(3)	1.421(5)	C(2)-C(1)-H(1)	118.9	N(2)-C(7)-H(7B)	108.9
C(2)-H(2)	0.9500	C(1)-C(2)-C(3)	119.8(3)	C(7)#1-C(7)-H(7B)	108.9
C(3)-C(4)	1.414(5)	C(1)-C(2)-H(2)	120.1	H(7A)-C(7)-H(7B)	107.8
C(4)-C(5)	1.360(5)	C(3)-C(2)-H(2)	120.1	H(1A)-O(1)-H(1B)	106.6
C(4)-H(4)	0.9500	N(2)-C(3)-C(4)	120.0(3)		
C(5)-H(5)	0.9500	N(2)-C(3)-C(2)	123.3(3)		
C(6)-H(6A)	0.9800	C(4)-C(3)-C(2)	116.6(3)		
C(6)-H(6B)	0.9800	C(5)-C(4)-C(3)	120.4(3)		
C(6)-H(6C)	0.9800	C(5)-C(4)-H(4)	119.8		
C(7)-C(7)#1	1.511(6)	C(3)-C(4)-H(4)	119.8		
C(7)-H(7A)	0.9900	N(1)-C(5)-C(4)	121.7(3)		
C(7)-H(7B)	0.9900	N(1)-C(5)-H(5)	119.2		
O(1)-H(1A)	0.7919	C(4)-C(5)-H(5)	119.2		
O(1)-H(1B)	0.8291	N(1)-C(6)-H(6A)	109.5		

Table 4. Bond lengths [Å] and angles [°] for *o*-PYE₂

Bond lengths	[Å]	Angles	[°]	angles	[°]
N(1)-C(5)	1.368(2)	C(5)-N(1)-C(1)	122.09(14)	N(4)-C(12)-C(13)	114.92(14)
N(1)-C(1)	1.3994(19)	C(5)-N(1)-C(17)	120.49(13)	C(14)-C(13)-C(12)	122.24(17)
N(1)-C(17)	1.455(2)	C(1)-N(1)-C(17)	117.42(12)	C(14)-C(13)-H(13)	118.9
N(2)-C(1)	1.2964(19)	C(1)-N(2)-C(6)	118.13(13)	C(12)-C(13)-H(13)	118.9
N(2)-C(6)	1.4162(19)	C(12)-N(3)-C(11)	118.03(13)	C(13)-C(14)-C(15)	120.2(2)
N(3)-C(12)	1.2944(19)	C(5)-N(1)-C(1)	122.09(14)	C(13)-C(14)-H(14)	119.9
N(3)-C(11)	1.4207(19)	C(16)-N(4)-C(12)	121.82(16)	C(15)-C(14)-H(14)	119.9
N(4)-C(16)	1.369(2)	C(16)-N(4)-C(18)	120.32(15)	C(16)-C(15)-C(14)	118.60(18)
N(4)-C(12)	1.4030(19)	C(12)-N(4)-C(18)	117.84(14)	C(16)-C(15)-H(15)	120.7
N(4)-C(18)	1.451(2)	N(2)-C(1)-N(1)	116.62(14)	C(14)-C(15)-H(15)	120.7
C(1)-C(2)	1.431(2)	N(2)-C(1)-C(2)	128.27(14)	C(15)-C(16)-N(4)	122.16(18)
C(2)-C(3)	1.352(2)	N(1)-C(1)-C(2)	115.10(13)	C(15)-C(16)-H(16)	118.9
C(2)-H(2)	0.9500	C(3)-C(2)-C(1)	121.76(16)	N(4)-C(16)-H(16)	118.9
C(3)-C(4)	1.411(2)	C(3)-C(2)-H(2)	119.1	N(1)-C(17)-H(17A)	109.5
C(3)-H(3)	0.9500	C(1)-C(2)-H(2)	119.1	N(1)-C(17)-H(17B)	109.5
C(4)-C(5)	1.342(2)	C(2)-C(3)-C(4)	120.60(17)		
C(4)-H(4)	0.9500	C(2)-C(3)-H(3)	119.7		
C(5)-H(5)	0.9500	C(4)-C(3)-H(3)	119.7		
C(6)-C(7)	1.395(2)	C(5)-C(4)-C(3)	118.39(16)		
C(6)-C(11)	1.406(2)	C(5)-C(4)-H(4)	120.8		
C(7)-C(8)	1.384(2)	C(3)-C(4)-H(4)	120.8		
C(7)-H(7)	0.9500	C(4)-C(5)-N(1)	122.03(16)		
C(8)-C(9)	1.378(2)	C(4)-C(5)-H(5)	119.0		
C(8)-H(8)	0.9500	N(1)-C(5)-H(5)	119.0		
C(9)-C(10)	1.383(2)	C(7)-C(6)-C(11)	118.76(14)		
C(9)-H(9)	0.9500	C(7)-C(6)-N(2)	120.40(14)		
C(10)-C(11)	1.393(2)	C(11)-C(6)-N(2)	120.62(14)		
C(10)-H(10)	0.9500	C(8)-C(7)-C(6)	121.56(14)		
C(12)-C(13)	1.430(2)	C(8)-C(7)-H(7)	119.2		
C(13)-C(14)	1.349(2)	C(6)-C(7)-H(7)	119.2		
C(13)-H(13)	0.9500	C(9)-C(8)-C(7)	119.70(15)		
C(14)-C(15)	1.413(3)	C(9)-C(8)-H(8)	120.1		
C(14)-H(14)	0.9500	C(7)-C(8)-H(8)	120.1		
C(15)-C(16)	1.338(3)	C(8)-C(9)-C(10)	119.51(15)		
C(15)-H(15)	0.9500	C(8)-C(9)-H(9)	120.2		
C(16)-H(16)	0.9500	C(10)-C(9)-H(9)	120.2		
C(17)-H(17A)	0.9800	C(9)-C(10)-C(11)	121.84(15)		
C(17)-H(17B)	0.9800	C(9)-C(10)-H(10)	119.1		
C(17)-H(17C)	0.9800	C(11)-C(10)-H(10)	119.1		
C(18)-H(18A)	0.9800	C(10)-C(11)-C(6)	118.62(14)		
C(18)-H(18B)	0.9800	C(10)-C(11)-N(3)	118.12(14)		
C(18)-H(18C)	0.9800	C(6)-C(11)-N(3)	123.07(13)		
C(17)-H(17A)	0.9800	N(3)-C(12)-N(4)	117.07(15)		
C(15)-H(15)	0.9500	N(3)-C(12)-C(13)	127.98(14)		

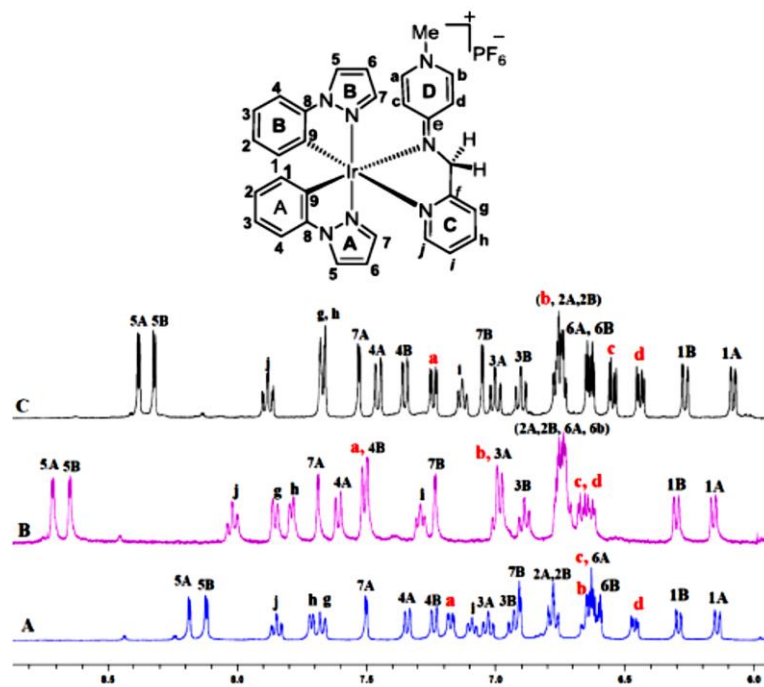


Figure 8. Section of the ^1H NMR spectrum (500 MHz, 298K) of complex *p*-3.32; (A) in CD_2Cl_2 , (B) in $(\text{CD}_3)_2\text{CO}$ and (C) in CD_3CN (500 MHz, at room temperature)

Table 5: X-ray data for *para*-PYE Ir(III) complexes *p*-3.30, and *p*-3.32

Compound reference	<i>p</i> -3.30	<i>p</i> -3.31	<i>p</i> -3.32
Chemical formula	C ₃₂ H ₃₂ F ₆ IrN ₈ P (CH ₂ Cl ₂)	No data	C ₃₀ H ₂₇ F ₆ IrN ₇ P (CHCl ₃) ₂
Formula Mass	950.75		1061.49
Temperature/K	150(2)		150(2)
Crystal system	Orthorhombic		Orthorhombic
Space group	Pca2(1)		P2(1)2(1)2(1)
a/Å	22.742(6)		12.268(4)
b/Å	9.060(2)		13.234(4)
c/Å	17.582(4)		24.876(8)
α/°	90		90
β/°	90°		90
γ/°	90°		90
U/Å ³	3622.7(15)		4039(2)
No. of formula units per unit cell, Z	4		4
Density (calc.)/Mg/m ³	1.743		1.746
Abs. coefficient/mm ⁻¹	3.945		3.804
F(000)	1872		2072
Crystal size/mm ³	0.18 x 0.15 x 0.09		0.36 x 0.06 x 0.04
Theta range for data collection/°	1.79 to 26.00		1.64 to 26.00
Index ranges	-28<=h<=27, -11<=k<=11, -21<=l<=21		-15<=h<=15, -16<=k<=16, -30<=l<=30
No. of reflections collected	26795		31788
No. of independent reflections	7091 [R(int) = 0.0833]		7919 [R(int) = 0.1334]
Data / restraints / parameters	7091 / 22 / 498		7919 / 4 / 506
Goodness-of-fit, F2	0.888		0.869
Final R indices [I>2σ(I)]	R1 = 0.0402, wR2 = 0.0752		R1 = 0.0526, wR2 = 0.0781
R indices (all data)	R1 = 0.0581, wR2 = 0.0791		R1 = 0.0879, wR2 = 0.0861
Largest diff. peak and hole e.Å ⁻³	2.099 and -0.455		1.301 and -1.202

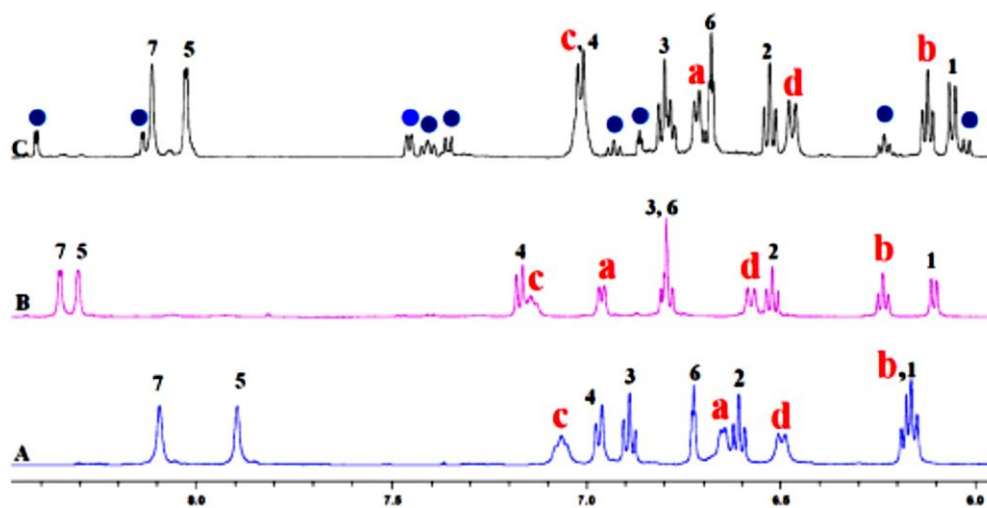


Figure 9 Section of the ^1H NMR spectrum (500 MHz, 298K) of complex *o*-3.30; (A) in CD_2Cl_2 , (B) in $(\text{CD}_3)_2\text{CO}$ and (C) in CD_3CN at RT, (●) is the second species.

Table 6: X-ray data for *ortho*-PYE Ir(III) complexes *o*-3.30, *o*-3.31 and *o*-3.32

Compound reference	<i>o</i> -3.30	<i>o</i> -3.31	<i>o</i> -3.32
Empirical formula	C ₃₂ H ₃₂ F ₆ IrN ₈ P (CHCl ₃) ₂	C ₃₆ H ₃₂ F ₆ IrN ₈ P	C ₃₀ H ₂₇ F ₆ IrN ₇ P 1.25(CH ₂ Cl ₂)
Formula weight	1104.56	913.87	928.91
Temperature/K	150(2)	150(2)	150(2) K
Crystal system	Monoclinic	Monoclinic	Monoclinic
Space group	P2(1)/c	P2(1)/c	P2(1)/c
a/Å	14.708(4)	13.528(3)	13.702(7)
b/Å	16.518(5)	14.225(4)	15.661(8)
c/Å	17.913(5)	17.904(5)	16.031(8)
α/°	90°	90	90°
β/°	109.066(6)	96.528(5)	96.330(10)
γ/°	90	90	90
Volume /Å ³	4113(2)	3423.1(15)	3419(3)
No. of formula units per unit cell, Z	4	4	4
Density (calc.) Mg/m ³	1.784	1.773	1.805
Absorption coefficient/ mm ⁻¹	3.740	4.021	4.215
F(000)	2168	1800	1818
Crystal size/mm ³	0.18 x 0.10 x 0.09	0.21 x 0.12 x 0.05	0.23 x 0.08 x 0.06
Theta range for data collection/ °	1.72 to 26.00	1.52 to 26.00	1.50 to 26.00
Index ranges	-17<=h<=18, -20<=k<=19, -22<=l<=22	-16<=h<=16, -17<=k<=17, -22<=l<=21	-16<=h<=16, -19<=k<=19, -19<=l<=19
No. of reflections collected	31877	26509	26377
No. of independent reflections	8081 [R(int) = 0.1605]	6729 [R(int) = 0.1583]	6711 [R(int) = 0.0926]
Data / restraints / parameters	8081 / 546 / 543	6729 / 12 / 471	6711 / 49 / 425
Goodness-of-fit, F2	0.782	0.750	0.916
Final R indices [I>2sigma(I)]	R1 = 0.0537, wR2 = 0.0824	R1 = 0.0509, wR2 = 0.0773	R1 = 0.0428, wR2 = 0.0863
R indices (all data)	R1 = 0.1095, wR2 = 0.0942	R1 = 0.0925, wR2 = 0.0864	R1 = 0.0640, wR2 = 0.0909
Largest diff. peak and hole/e.Å ⁻³	1.457 and -1.867	1.271 and -1.405	1.336 and -0.923

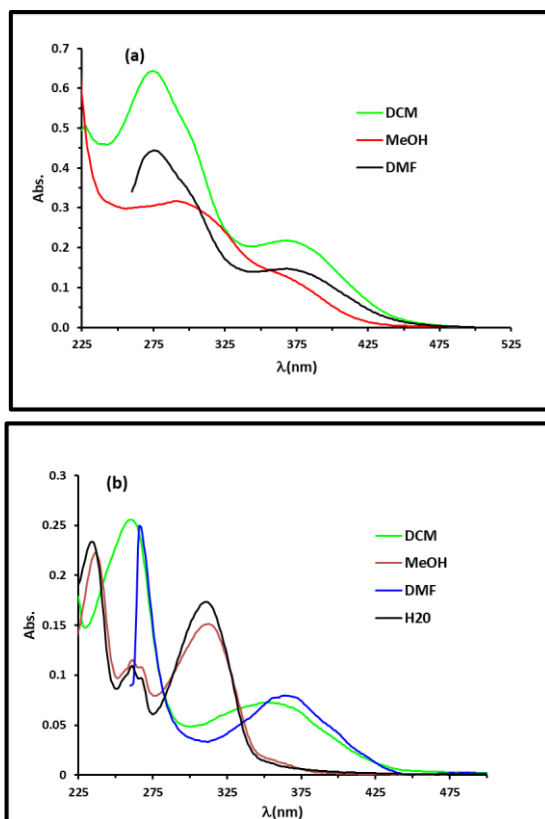


Figure 10: Absorption spectra of compounds **a:** *o*-PYE₂ and **b:** *o*-PYE₃ at 0.02 mM in different solvents.

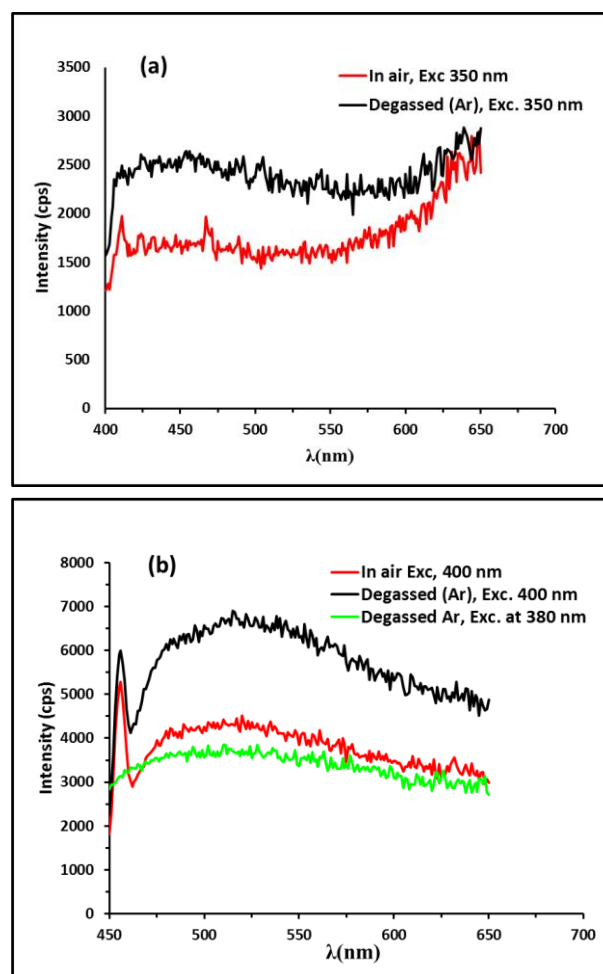


Figure 11: Emission spectra of complexes (a). *p-3.30* and (b). *p-3.31* in DCM at 0.02 mM at RT.

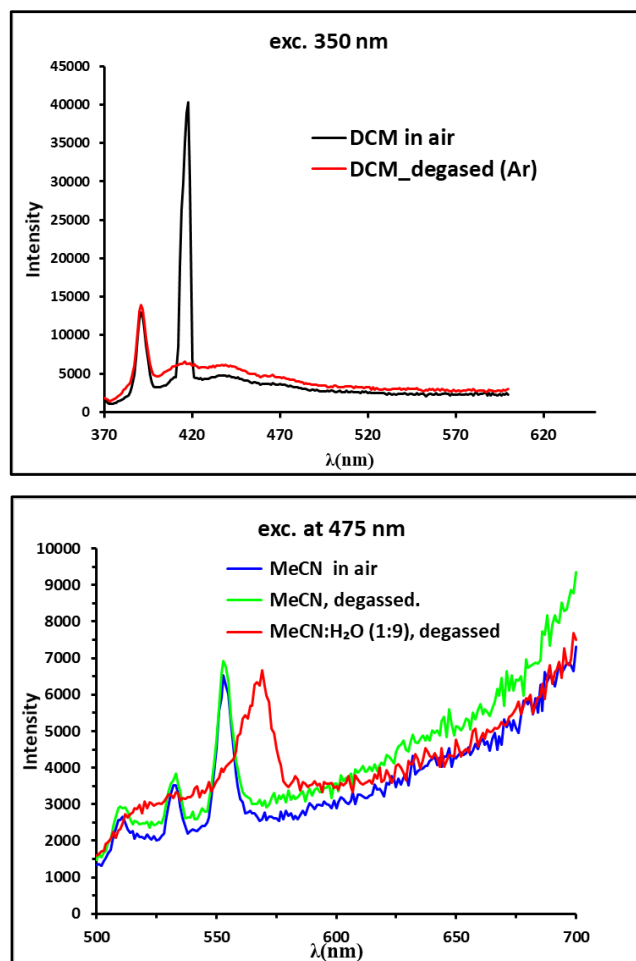


Figure 12.: Emission spectra of complex *o*-3.31 in different solvents at (0.02mM) at RT.

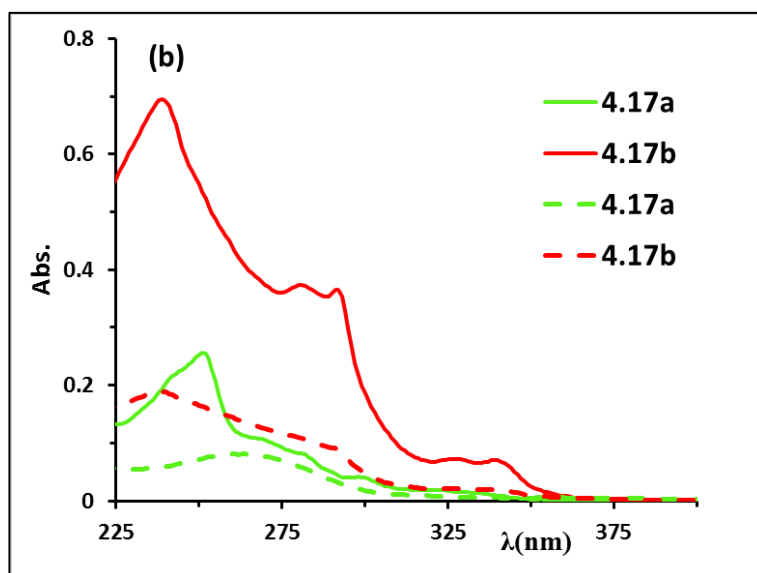
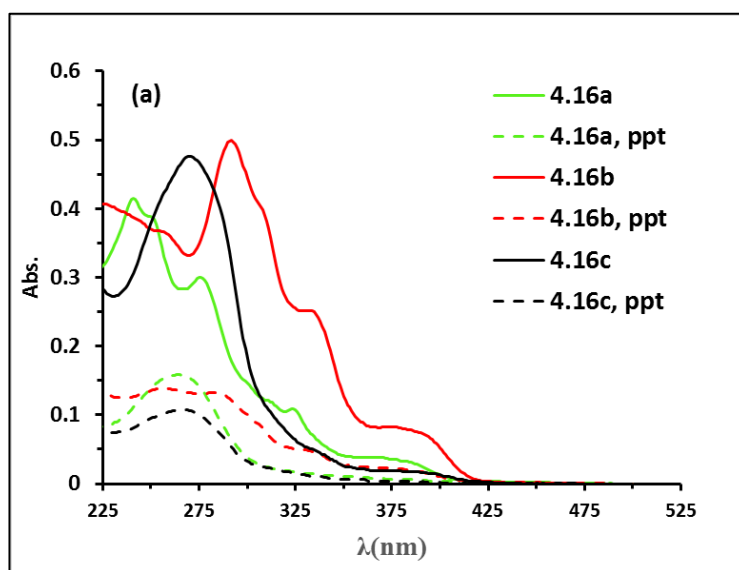


Figure 13: Absorption spectra of [Pt(C^N)(en)]PF₆ (a). 4.16a-c and (b) 4.17a-b in solution at 0.02 mM MeCN (—) and in MeCN/Et₂O 1/9 (ppt) at RT

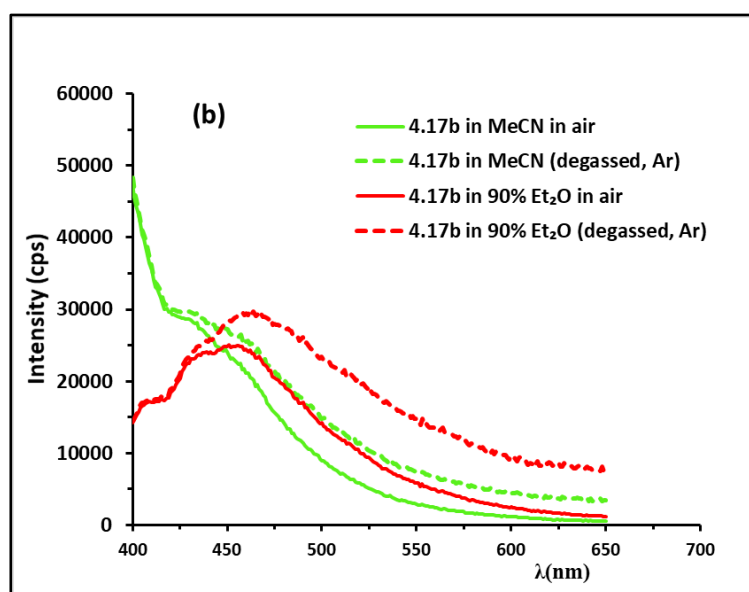
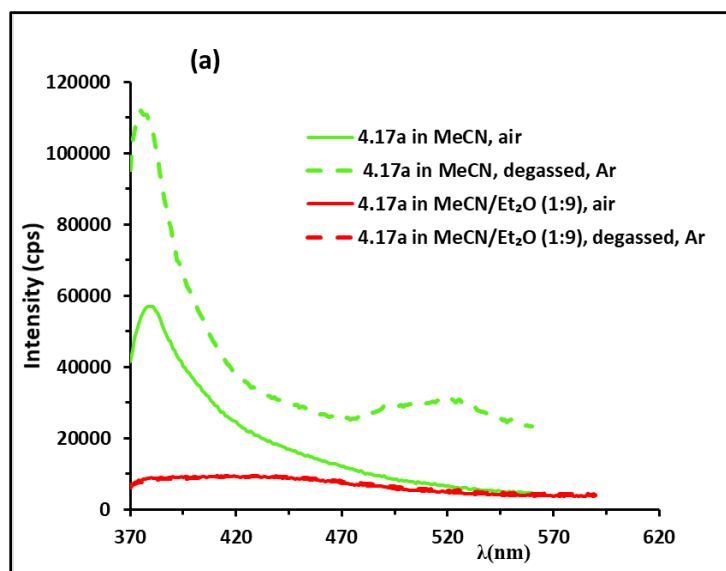


Figure 14: Emission spectra of (a). **4.17a** and (b). **4.17b** in 0% and 90% Et₂O in MeCN at 0.02 mM (λ_{ex} 300 nm for **4.17a** and 340 nm for **4.17b**)

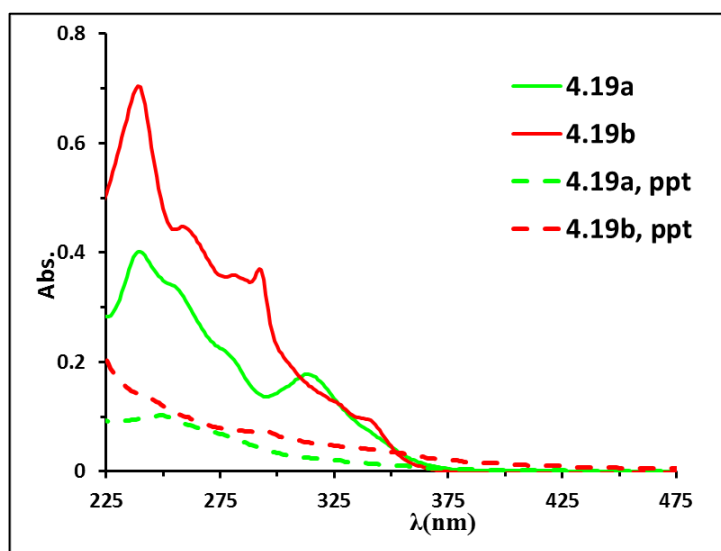
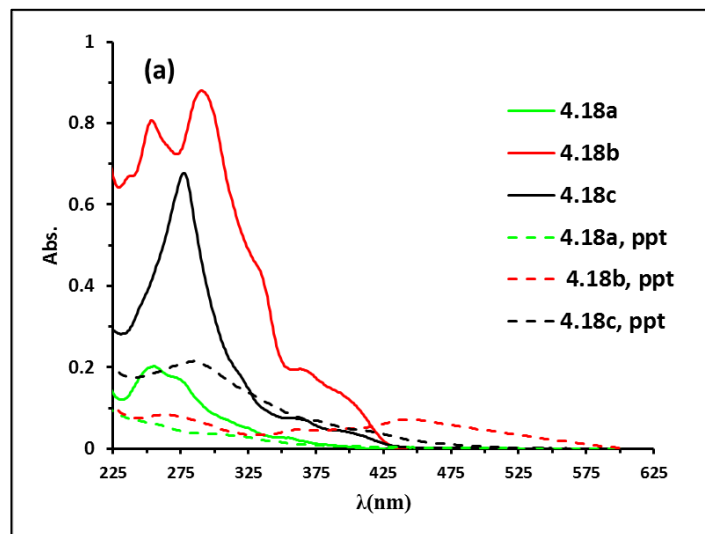


Figure 15: Absorption spectra of [Pt(C^N)(dpm)] (a). 4.18a-c and (b). 4.19a-b in solution at 0.02 mM MeCN (—) and in MeCN/H₂O 1/9 (ppt) at RT